Mapping and Assessing Tidal Marsh Condition Via Multispectral Imaging

Authors and Affiliations:

Brittany P. Wilburn[1], Joshua Moody[1], Mihaela Enache[1], Kirk Raper[1], Metthea Yepsen[1], Lori Lester[1], William Smith[2], Steven Jacobus[2], David DuMont[3], Kevin Blythe[4], Molly VanWieren[4], Charles Schutte[5]

[1]NJDEP, Division of Science and Research
[2]NJDEP, Bureau of GIS
[3]NJDEP, Climate Resilience Planning
[4]NJDEP, Fish and Wildlife, Office of Fish and Wildlife Information Systems
[5]Rowan University

Project Manager: Brittany Wilburn

July 2024

State of New Jersey
Phil Murphy, Governor

Department of Environmental Protection
Shawn M. LaTourette, Commissioner

Division of Science & Research
Nicholas A. Procopio, Ph.D., Director

Visit the DSR website:
https://dep.nj.gov/dsr

Acknowledgements

This project was made possible through NJDEP Division of Science and Research Funding. This study grew to include a network of scientists whose support and expertise drove this project. Metthea Yepsen, Kirk Raper, and Lori Lester, Ph.D. of the NJDEP Division of Science and Research (DSR) were instrumental to this project's inception and focus as co-PIs. Joshua Moody, Ph.D. (DSR) also provided significant support in shaping the project's focus through adaptation of the field collection design and analysis. William Smith and Steven Jacobus of the NJDEP Bureau of GIS (BGIS) provided the crux of the project through drone permitting, training, imagery collection, analysis, and management, with support from David DuMont (NJDEP Climate Resilience Planning), Kevin Blythe (NJDEP Fish and Wildlife, Office of Fish and Wildlife Information Systems; FW), and Molly VanWieren (FW). Diatom community analysis could not have been done without Mihaela Enache, Ph.D. (DSR), who provided field and data analysis support. Additional field and design support came from Maite Whitley, DSR's first SPARK intern. With the DSR funding, we were able to partner with Charles Schutte, Ph.D., of Rowan University, who was instrumental in the completion of this project (contract #SR22-013). Charles Schutte, Ph.D. additionally mentored and included Kriish Hate, who was part of both Rowan University as an undergraduate research assistant and NDJEP DSR through the SPARK internship, and Omar Selim, a second Rowan University undergraduate research assistant. Further support came from the US Fish and Wildlife Service from Joseph Smith, Ph.D., who provided assistance with permitting and project site selection. Lastly, significant project site selection and field assistance came from the Jacques Cousteau National Estuarine Research Reserve, specifically from Gregg Sacowicz, Andrea Habeck, Patricia McHugh, and Christopher Menke.

Recommended Citation

Please cite as: Wilburn, B. P., Moody, J., Enache, M., Raper, K., Yepsen, M., Lester, L., Smith, W., Jacobus, S., DuMont, D., Blythe, K., VanWieren, M., Schutte, C. (2024). Mapping and Assessing Tidal Marsh Condition Via Multispectral Imaging. New Jersey Department of Environmental Protection. Trenton, NJ. 210 pg. Available at dep.nj.gov/dsr.

Executive Summary

Within New Jersey, there are approximately 66,000 hectares of tidal saltwater wetlands. These wetlands are integral to the health and well-being of the residents that live within these coastal areas, as they provide a number of invaluable ecosystem services, including: carbon sequestration (Were et al., 2019), coastal storm energy reduction (Rezaie et al., 2020), flood water storage (Rezaie et al., 2020), water quality enhancement (Fisher and Acreman, 2004), and traditional and cultural significance (Pedersen et al., 2019). However, New Jersey has lost a significant portion of its coastal habitat as a result of climate change and other anthropogenic factors, such as reduced hydrological function from agricultural ditching (Smith et al., 2022). A first step to intervene in these losses is to determine vulnerable habitat as quickly, accurately, and efficiently as possible, in order to prioritize areas of marsh for protection or enhancement.

Currently, multispectral imagery is used to assess crop health, and although there has been a large increase in the use of drone technology in the scientific community due to its wide and flexible applicability, there yet remains to be a standard protocol by which wetland conditions are analyzed using drone imagery. Appropriate protection and restoration efforts require understanding their spatial and temporal vulnerability. Field-based evaluation methods can be costly and time-consuming. Drones represent an opportunity to assess large areas efficiently. The goals of this effort were:

1. Evaluate the use of multispectral drones for the delineation of high and low marsh vegetation communities;
2. Investigate the use of drone-based multispectral imagery to identify conditions that can lead to high marsh pond expansion and vegetation loss by evaluating relationships between soil and porewater chemistry, vegetation, and multispectral indices; and
3. Identify and describe relationships between diatom communities and soil sulfide concentrations.

For this project, a DJI Phantom 4 Multispectral drone was used to collect multispectral images for wetland condition assessment and a DJI Phantom 4 Pro drone was used to collect higher resolution photos for wetland habitat delineation and video for reference and documentation. Data collection began within nine zones of the two salt marsh sites in July and August 2022. Post flight data processing took place over Fall and Winter 2022, including the formation of orthomosaic imagery, spectral band extraction, calculation and summarization of vegetation indices, object-based image analysis with machine learning, and thematic accuracy assessments. Drone imagery was then compared to on-the-ground collected data to determine correlations among spectral signatures, vegetation, and soil parameters. Diatom samples were additionally collected to better understand the health condition of the selected salt marshes, as diatoms have proven to be accurate indicators of nutrients, pollution, and salinity in tidal wetlands (Desianti et al. 2019).

This report includes the following deliverables:

1. A Quality Assurance Project Plan (QAPP) written and approved prior to commencement of research,
2. A procedural report developed on using multispectral drones to delineate habitat,

3. A report on the potential of multispectral drone monitoring to act as a proxy for on-the-ground traditional monitoring methods,
4. A report on the use of diatoms to identify sulfide concentrations in tidal wetland soils, and
5. Outreach products, including intern independent project summaries and presentation abstracts given on the project at local and regional conferences.

The multispectral imagery was successful for high and low marsh habitat delineation to a 7.6-cm (3-inch) resolution. Post-processing results were able to identify a variety of salt marsh species, but the process was not able to be fully automated and required varying levels of site-specific effort, especially concerning differentiation between various mixed-species combinations. Regarding salt marsh condition, we were unable to produce predictive relationships between the multispectral indices and various porewater and soil metrices. Although data showed that some relationships may exist, the sampling size and variability within many of the metrics were too low for conclusive modeling results. Additionally, we found the timing of drone flights relative to the position of the sun and tide was greatly important for interpreting reflectance while minimizing shadowing. Our monitoring plan took these potential effects into account, but the time it took to collect the photos resulted in greater variability in water presence than anticipated. Additionally, the variability in vegetation, soil, and porewater metrics were lower than expected, likely due to influence of the tidal magnitude and geomorphology of the sites driving these levels at a scale greater than our sampling strata (i.e., site location, expanding vs stable ponds, and distance of plot from pond). While these relationships were largely statistically insignificant, we did find useful relationships among the vegetation, chemistry, and diatom communities that can be used to inform our future efforts. Percent cover had a strong negative relationship associated with both pH and oxidation/reduction potential (ORP). Additionally, the multispectral indices (MSIs) showed some strong correlations with a variety of metrics, such as soil penetration depth, depth of water table, pH, sulfides, and sulfate depletion. Unfortunately, low R^2 values indicated that the models were either lacking the appropriate sample size or that there may be other undetermined confounding variables. One significant relationship between the non-photosynthetic index (NPV) and ammonia warrants further evaluation with an enhanced study design to capture varying levels of vegetation cover and direction of growth (i.e., establishing or degrading) along a nutrient gradient. Some issues associated with the collection of the multispectral data, such as the presence of vegetation shadows and the lack of a standardized atmospheric correction methodology, may have affected the results of this effort. But as they have been identified and discussed, future efforts could aim to address them more directly.

In conclusion, this effort represents a move forward in the evaluation of the use of drones to identify coastal wetland health and trajectories. Although drones are used in many regions to delineate various wetland vegetation communities, there is a lack of understanding regarding their appropriate use for assessing wetland health. This study aimed to find links between features identifiable by the drone (i.e., vegetation) that reflect unobservable conditions that drive coastal wetland health (i.e., soil and porewater parameters). If successful, this method would allow for the identification of areas of wetland decline prior to the stage where the vegetation community goes into decline. The results presented here help inform future efforts by narrowing the field of required data by identifying some key relationships and refining the employed methodology to account for some of the confounding variability measured here. Future efforts would continue to benefit from a diverse, multi-disciplinary team comprised of wetland ecologists, geospatial information scientists, drone pilots, and biogeochemists.

Contents

List of Figures

List of Tables

Chapter 1: Introduction

Authors: Brittany P. Wilburn[1], Joshua Moody[1], Metthea Yepsen[1]

[1] NJDEP, Division of Science and Research

Increasing the resilience of New Jersey's tidal wetlands to sea-level rise is of utmost importance. Tidal wetlands provide a myriad of ecosystem services, from cleaning water to buffering coastal developments from storms (NJDEP, 2007; Mitsch & Gosselink, 2015). NJ has more than 300,000 acres of tidal wetlands, including 66,000 hectares of salt marsh, most of which are owned and managed by the State. Traditional field methods for assessing tidal wetland condition are often time- and resource-intensive. The NJDEP Division of Science and Research (NJDEP-DSR) and Fish and Wildlife (NJDEP-FW) are looking for efficient, cost-effective ways to map plant communities and assess the health of tidal wetlands.

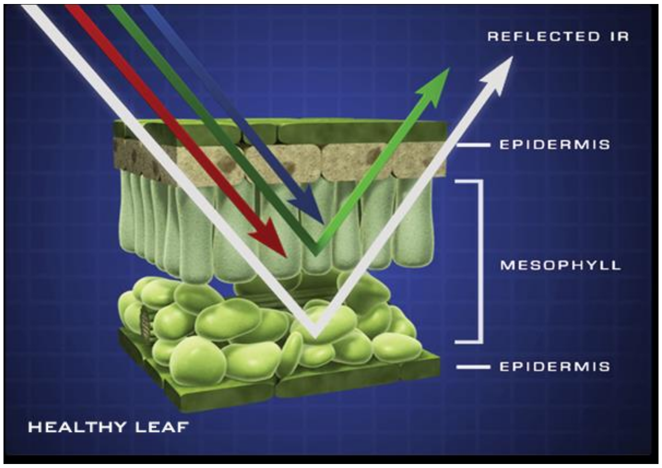

Figure 1.1. Absorption of red and blue light and reflectance of green and infrared light by a healthy leaf's chlorophyll. (Image by Jeff Carns in NOAA, 2010).

Remote sensing of wetland plant health has been done for decades from satellite sensors measuring the wavelengths of light absorbed and reflected by green plants (Guo et al., 2017; NOAA, 2010; Tiner et al., 2015). Chlorophyll in plant leaves strongly absorbs wavelengths of visible red and blue lights while reflecting visible green and invisible near-infrared wavelengths (Figure 1.1). Using these spectral properties, spectral indices (or mathematical calculations derived from imagery pixel values from two or more spectral bands) have been created to measure specific vegetation characteristics through imagery across landscapes. Traditionally, satellite imagery has been used to evaluate vegetation characteristics for larger landscapes. However, the coarse spatial resolution of freely available satellite imagery makes it suitable for larger scale mapping and would not be able to display the variability in plant communities and habitat, which would require at least m^2-scale resolution to map. Additionally, while high resolution (cm^2- or m^2-scale) satellite imagery is available, it is often expensive and may not be available during ideal time periods due to cloud interference, tidal inundation, or other factors. In contrast, drones can collect imagery at the spatial resolution required to assess wetland plant community health and even isolate individual plants while reducing costs and providing flexibility in site coverage and optimal timing.

Landscapes can be modeled using drones by creating orthomosaics and digital surface models (DSMs) from overlapping images using a photogrammetry technique called Structure from Motion. These products are derived from point clouds of data generated from the imagery, containing longitudinal, latitudinal, and elevational coordinates as well as Red-, Green-, and Blue-color (RGB) information (plus other variations of light waves, depending on the type of sensors with which the drone is equipped). This high data density allows for high resolution (cm^2-scale) two-dimensional maps and three-dimensional models to be created for large expanses of landscape and to indicate the relative density and health of vegetation. This data is often analyzed in spatial visualization programs, such as ArcGIS Pro (Environmental Systems Research Institute, Redlands, CA), using color filters and spectral indices. The outputs from these indices provide an opportunity for quantitatively evaluating landscape-level vegetation communities.

Scope of Work

The two overarching research goals of this project were to evaluate the use of multispectral drones for:

1. Delineating low and high marsh habitats, and
2. Evaluating relative salt marsh condition.

Therefore, this report has been organized to reflect these investigations and outcomes, integrating the various deliverables where most appropriate.

Although there has been a large increase in the use of drone technology in the scientific community due to its wide and flexible applicability, there is not a standard protocol by which wetland conditions are analyzed using drone imagery. In this report, we will detail the following methods:

1. The creation of orthomosaics, vegetation indices, classified rasters, and accuracy assessments;
2. The evaluation of salt marsh conditions based on our suite of metrics; and
3. The collection of vegetation, soil, and diatom community parameters.

In order to determine how correlated the multispectral drone imagery was to salt marsh condition, we validated the results derived from processed drone imagery using traditional field methods for assessing and understanding tidal wetland health. This includes measuring soil properties (e.g., porewater salinity, porewater pH, oxidation/reduction potential (ORP), porewater sulfides/sulfates, porewater chloride concentrations, and an index of bearing capacity), and determining diatom assemblages. Diatoms have proven to be accurate indicators of nutrients, pollution, and salinity in tidal wetlands (Desianti et al. 2019). Diatom species composition may also be a valuable indicator of phytotoxic sulfide concentrations in the soil. Since both diatoms and *in situ* measurements of sulfides are already proposed as a part of this project, we took advantage of this opportunity to evaluate if diatoms could be used as a proxy for sulfides.

Timeline

This project took place over a two-year period from March 2022 to March 2024. During the first year, we determined our preliminary methods, selected locations for the study, and performed an initial testing of data collection and analysis. The two salt marshes selected for this study included the Great Bay Boulevard Marsh on the Tuckerton Peninsula and a portion of E.B. Forsythe National Wildlife Refuge to the northeast of Tuckerton Peninsula (Figure 1.2). These marshes are known to be in degrading states due to increased sea-level rise and anthropogenic stress. In Summer 2022, drone flights took place with coincident collection of *Spartina patens* and *S. alterniflora* characteristics, soil and porewater parameters, and diatom samples. Through Fall 2022 to Spring 2023, collected data was summarized and analyzed, looking for correlations between on-the-ground measurements and multispectral signals. For the Summer 2023 data collection, we adapted our methods to have a more specific focus on *S. patens* in stable and unstable portions of the two marshes. Additionally, drone imagery collection and analysis methods were further refined during this portion of the study. Fall 2023 to Spring 2024 was allocated for final analysis of ground measurements and drone spectra. Quarterly progress can be seen in Figure 1.3, and a detailed task list can be found in Table 1.1.

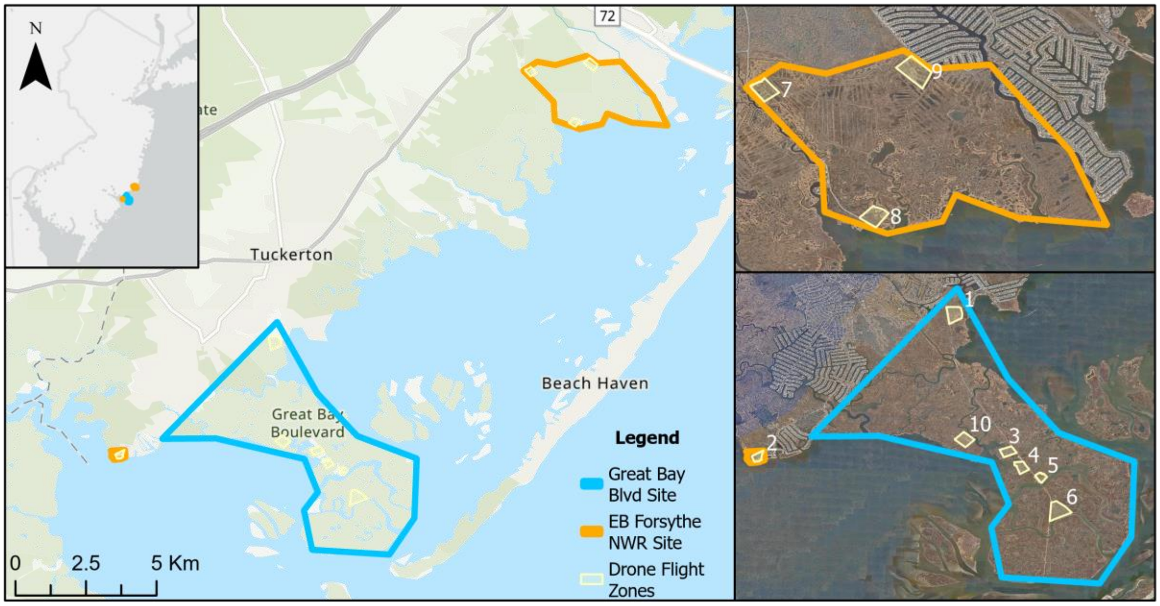

Figure 1.2. Map of selected sites within E. B. Forsythe National Wildlife Refuge and Great Bay Boulevard.

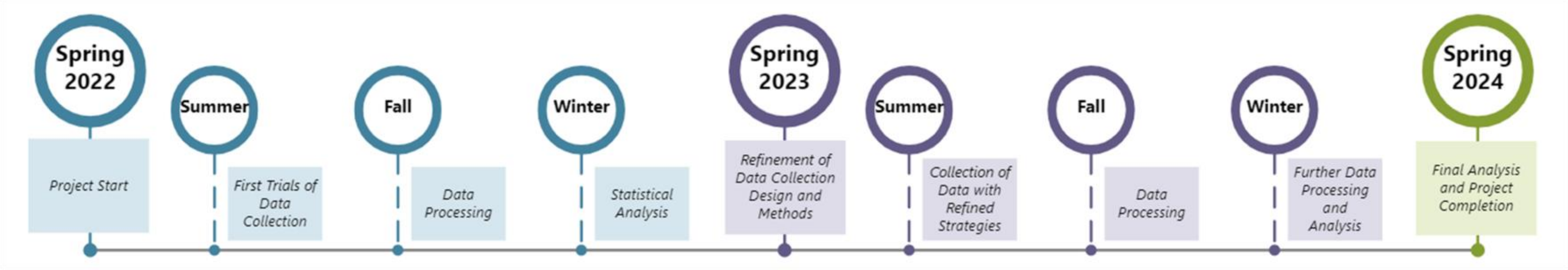

Figure 1.3. Quarterly progress of project from Spring 2022 to Spring 2024.

Table 1.1. Detailed monthly task progress and completion of project. Colors correspond to each 12-month period.

	2022										**2023**												**2024**					
Task	***M***	***A***	***M***	***J***	***J***	***A***	***S***	***O***	***N***	***D***	***J***	***F***	***M***	***A***	***M***	***J***	***J***	***A***	***S***	***O***	***N***	***D***	***J***	***F***	***M***	***A***	***M***	***J***
Planning																												
Project Design	x	x	x																									
QAPP			x	x	x																							
Permit Paperwork			x	x										x	x													
Equipment Purchase				x	x										x													
Field Work																												
Practice Drone Flights				x	x	x																						
Site Scouting & Practice				x	x	x										x	x											
Drone Imagery Collection						x	x										x	x										
Soil & Diatom Collection						x	x										x	x										
On-the ground Surveys						x	x										x	x										
Analysis																												
Lab Analysis - Soils							x	x	x									x	x	x	x	x	x	x	x			
Lab Analysis - Diatoms							x	x	x									x	x	x	x	x	x	x	x	x		
Field Data QAQC							x	x	x									x	x	x			x					
Orthomosaics Formed							x	x	x	x								x	x	x								
Imagery Indices Calculated										x	x												x	x				
Raster Classification											x	x	x	x										x	x			
Accuracy Assessments											x	x	x	x	x									x	x			
Geospatial Data Finalized															x										x	x		
Write Up																												
Methodologies Written								x	x	x																x	x	
Methodologies Refined													x	x	x								x	x	x			
Final Products Delivered																												x

Deliverables & Report Organization

This report has been organized to create a linear narrative around the goals and scope of the project.

This report includes the following deliverables:

1. A Quality Assurance Project Plan (QAPP) written and approved prior to commencement of research,
2. A procedural report developed on using multispectral drones to delineate habitat,
3. A report on the potential of multispectral drone monitoring to act as a proxy for on-the-ground traditional monitoring methods,
4. A report on the use of diatoms to identify sulfide concentrations in tidal wetland soils, and
5. Outreach products, including intern independent project summaries and presentation abstracts given on the project at local and regional conferences.

The deliverables have been organized into the following chapters:

- Chapter 2: Quality Assurance
    - Deliverable 1: QAPP
- Chapter 3: Evaluating the use of multispectral drone for the delineation of low and high marsh communities.
    - Deliverable 2: A procedural report for using multispectral drones to map habitats
- Chapter 4: Evaluating the use of a multispectral drone to delineate the relative condition of high marsh habitat.
    - Deliverable 3: A report on the potential of multispectral drone monitoring to act as a proxy for on-the-ground traditional monitoring methods
- Chapter 5: Relationships between diatom communities and sulfide concentrations in two salt marshes of New Jersey
    - Deliverable 4: A report on the use of diatoms to identify sulfide concentrations in tidal wetlands soils
- Chapter 6: Outreach
    - Deliverable 5: Outreach products, including intern independent project summaries and presentation abstracts given on the project at local and regional conferences.

Following the task descriptions and deliverables, Chapter 7 additionally offers our final conclusions and recommendations for future projects.

Chapter 2: Quality Assurance

Authors: Brittany P. Wilburn[1], Metthea Yepsen[1], Kirk Raper[1], Mihaela Enache[1], Lori Lester[1], Charles Schutte[2], Steven Jacobus[3], William Smith[3], Kevin Blythe[4], Molly VanWieren[4]

[1] NJDEP, Division of Science and Research
[2] Rowan University
[3] NJDEP, Bureau of GIS - DOIT
[4] NJDEP, Fish and Wildlife, Office of Fish and Wildlife Information Systems

Objective: Produce a quality assurance project plan (QAPP) for examining salt marshes of known condition with multispectral drones and cross-compare with traditional on-the-ground methods.

Approach: A series of meetings were held with research partners throughout the region to select potential study sites and to determine key factors to consider for flying multispectral drones in salt marsh habitats. Due to interest in the future use of detailed drone imagery for habitat evaluation, sites were selected at Great Bay Boulevard Marsh on the Tuckerton Peninsula and a portion of E.B. Forsythe National Wildlife Refuge to the northeast of Tuckerton Peninsula. These marshes have a significant amount of prior research examining the condition of the salt marsh and the impacting forces on these habitats. It is well known that these two marshes are in a degrading state due to sea-level rise and additional anthropogenic impacts, making these sites ideal locations for testing the capabilities of the drone to pick up on salt marsh vegetation stress signals. Additional meetings were held to determine methods of vegetation characterization, soil and porewater collection and analysis, and diatom sample collection and analysis. Once decided, methodologies were compiled into a QAPP for final quality assurance approval.

The QAPP can be found in Appendix A.

Responsibilities and Deliverables: The NJDEP-DSR 1) organized meetings, 2) determined project partners and sites, 3) and oversaw completion of a QAPP (*Deliverable 1*).

The NJDEP-FW, NJDEP Bureau of Geospatial Information Systems (NDJEP-BGIS), and Rowan University supported completion of the QAPP with methodology supplementation and review.

Chapter 3: Evaluating the use of multispectral drones for the delineation of low and high marsh communities

Authors: William Smith[1], Steven Jacobus[1], David DuMont[2], Kevin Blythe[3], Molly VanWieren[3], Brittany P. Wilburn[4]

[1] NJDEP, Bureau of GIS - DOIT
[2] NJDEP, Climate Resilience
[3] NJDEP, Fish and Wildlife, Office of Fish and Wildlife Information Systems
[4] NJDEP, Division of Science and Research

Objective: Establish a procedure for flying a Phantom 4 Pro Multispectral drone, and process, classify, and analyze the collected data as it relates to salt marsh habitat delineation.

Approach: Following the QAPP and permit approvals, flight plans were established for one zone of Great Bay Boulevard marsh for a pre-data collection test run in July 2022. Finding that our selected methods were acceptable, imagery collection began within nine zones of the two salt marsh sites in August 2022. Post flight data processing took place over Fall and Winter 2022, including formation of orthomosaic imagery, spectral band extraction, calculation and summarization of vegetation indices, object-based image analysis with machine learning, and thematic accuracy assessments.

In the 2023 field season, methods were adapted to focus primarily on *S. patens*. Flyovers were conducted using only the multispectral drone in 2023 within four zones, one of which was a newly added zone that was not a part of 2022's data collection. Vegetation was delineated following the same methods as 2022 in order to provide a final assessment of methods. A final procedural report with flight and processing guidelines, future recommendations, and notes on limitations of the data and processing steps is reported here.

Supplementary results can be found in Appendices B-E.

Responsibilities and Deliverables: The NJDEP-DSR 1) oversaw completion of a QAPP (*Deliverable 1*), 2) oversaw project permitting, 3) conducted some of the research, 4) conducted the statistical analysis of vegetation, soil, and spectral signatures, and 5) assisted with report edits.

The NJDEP-BGIS and NJDEP-FW 1) produced drone flight plans, 2) retrieved drone flight permits, 3) conducted drone imagery collection, 4) processed and classified drone imagery, and 5) wrote a procedural report for future multispectral drone flights (*Deliverable 2*).

Title: Evaluating the use of multispectral drones for the delineation of low and high marsh communities: procedural report

Authors: William Smith[1], Steven Jacobus[1], David DuMont[2], Kevin Blythe[3], Molly VanWieren[3], Brittany P. Wilburn[4]

[1] NJDEP, Bureau of GIS - DOIT
[2] NJDEP, Climate Resilience
[3] NJDEP, Fish and Wildlife, Office of Fish and Wildlife Information Systems
[4] NJDEP, Division of Science and Research

I. Image Acquisition

I.i. Flight Planning

For this project, a DJI Phantom 4 Multispectral drone (Figure 3.1) was used to collect multispectral images and a DJI Phantom 4 Pro drone was used to collect higher resolution photos and video for reference and documentation. The Phantom 4 Multispectral drone is equipped with six 1/2.9” CMOS sensors, including one red-, green-, blue-sensor (RGB) for visible light imaging and five monochrome sensors for multispectral imaging. Each sensor has 2.08 MP, the five monochrome sensors capture Blue: 450 nm ± 16 nm; Green: 560 nm ± 16 nm; Red: 650 nm ± 16 nm; Red edge (RE): 730 nm ± 16 nm; Near-infrared (NIR): 840 nm ± 26 nm images. The Phantom 4 Pro is equipped with a 1-inch 20 MP CMOS RGB sensor.

Figure 3.1. DJI Phantom 4 Pro multispectral drone in flight.

A test flight was conducted on 21 July 2022, at Great Bay Boulevard Wildlife Management Area to determine flight specifications and speed of the drone flights. Data collection was then performed in July and August to capture the peak biomass season at nine zones – Zones 1-6 in the Great Bay Boulevard Wildlife Management Area and Zones 7-9 in the Edwin B Forsythe National Wildlife Refuge (Figure 3.2). In 2023 only four zones were flown, three repeat (Zones 1, 8, and 9) and one new zone (Zone 10) in the Great Bay Boulevard Wildlife Management Area and two repeated in the Edwin B Forsythe National Wildlife. Flights were planned to coincide with the field data collection requiring multiple flights on multiple days. In 2022, all nine sites were mapped using both drones. In 2023, the four sites were only mapped using the Phantom 4 Multispectral drone.

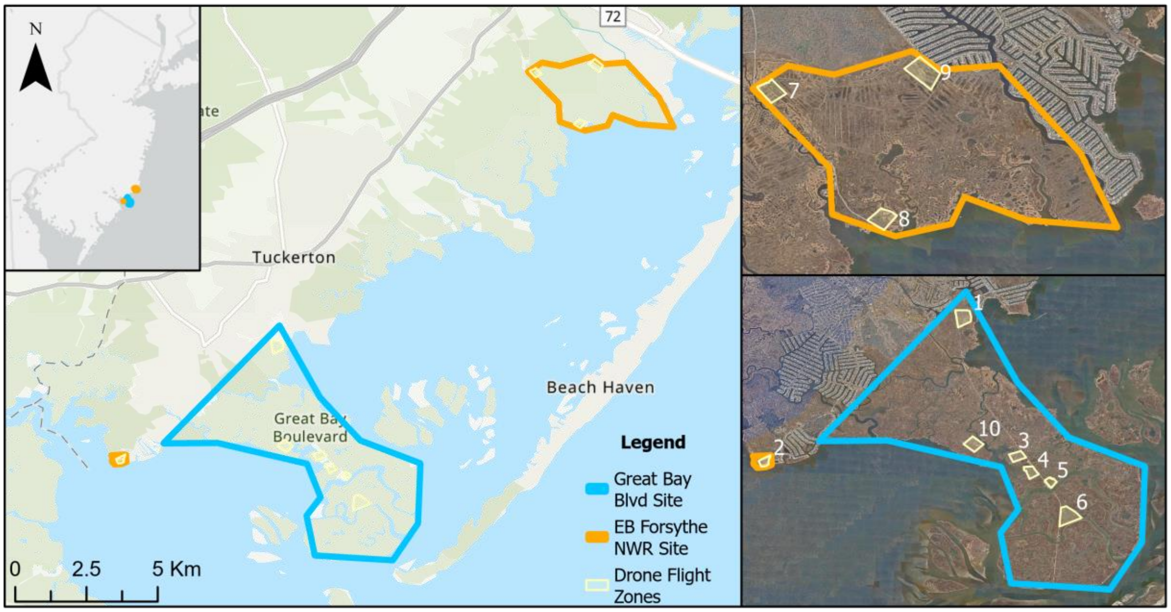

Figure 3.2. Map of drone flight zones in Great Bay Boulevard Wildlife Management Area (GBB) and E. B. Forsythe National Wildlife Refuge (Forsythe). Zones 1-9 were flown in 2022, and Zones 1, 8, 9, and 10 were flown in 2023.

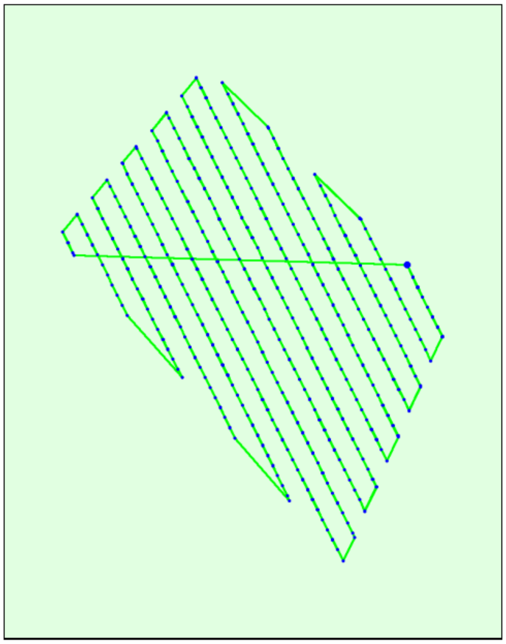

Figure 3.3. Example of the lawnmower pattern of the drone flights. The blue dots are the image collection points, and the green line is the flight path starting at the big blue dot.

Since the marsh aeras are flat without much change in elevation the mapping flights were flown in a lawnmower pattern (Figure 3.3). Mapping flights with the Phantom 4 Multispectral were programed using the DJI Ground Station Pro operating software to fly at 80 M with an 80% front and 70% side photo overlap. Mapping flights with the Phantom were programed using the Pix4D Capture software to fly at 80 M with an 80% front and 80% side overlap.

Ground control points (GCPs) were used for greater accuracy in lining up the processed orthomosaics. Five GCPs were used for each site. Taking into consideration the shape and accessibility of each site the GCPs were placed as close to the four principle corners and center of the site and their location surveyed.

In 2022, two to four study plots of approximately 100 m^2 per Zone were set up to collect further data within. Multispectral data for the 2022 plots was taken from the multispectral orthomosaic produced for the site. In 2023, the study plots were reduced to nine 1 m^2 plots per Zone. These were too small to accurately derive multispectral data from the orthomosaic, so the P4 Multispectral drone was flown over each plot at a low altitude approximately 3 to 5 m and two sets of photos were taken at each site and the better of the two used to create a composite photo including the five multispectral bands.

I.ii. Image Processing

Mapping photos collected in 2022 were processed using ESRI Drone2Map V2.3 software. Images from the P4 Multispectral were adjusted to produce a ground sampling distance of 3 inches and used to create a RGB Orthomosaic (Figure 3.4a), a Multispectral Orthomosaic including Blue, Green, Red, Red Edge and Near Infrared bands (Figure 3.4b), a digital surface model (Figure 3.4c), a digital terrain model (Figure 3.4d), a point cloud (Figure 3.4e), and mesh (Figure 3.4f). Images from the P4P were used for

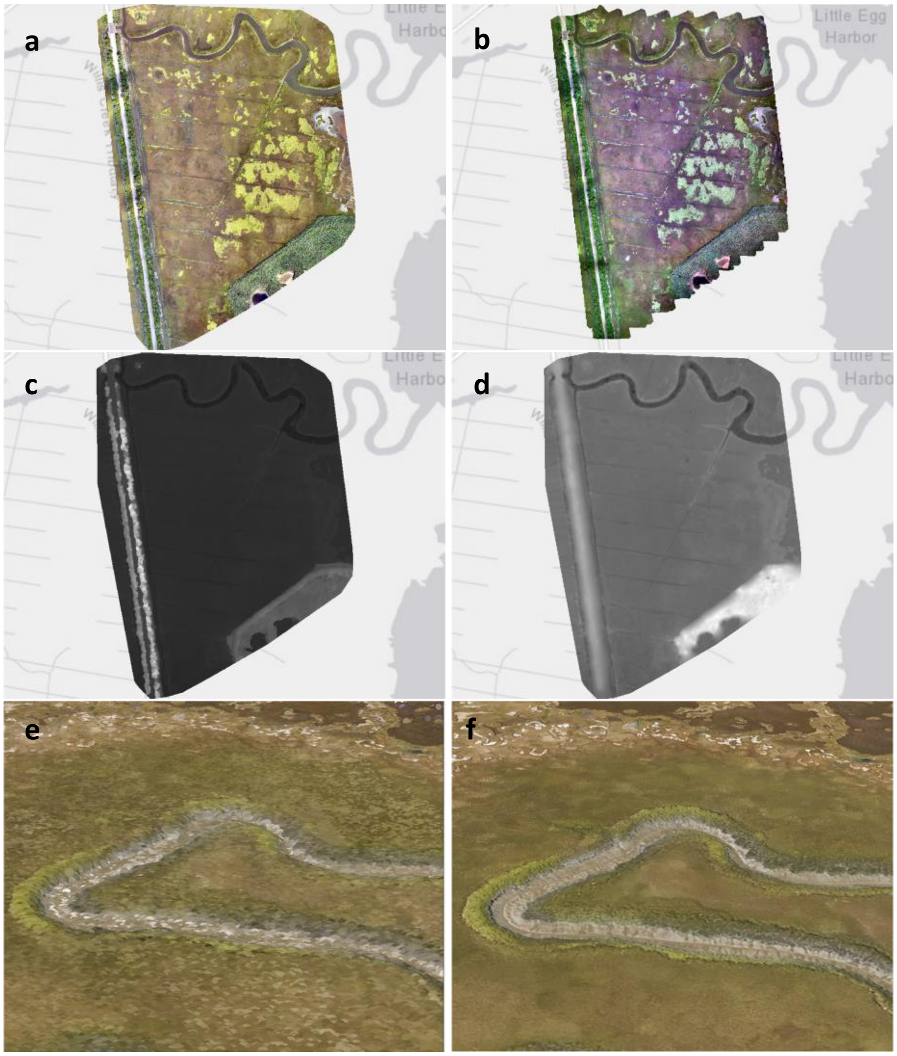

Figure 3.4. Examples of (a) RGB orthomosaic, (b) RGB + RE + NIR orthomosaic, (c) Digital Surface Model (DSM), (d) Digital Terrain Model (DTM), (e) point cloud, and (f) mesh of Zone 1 in 2022.

reference/promotion and included an RGB Orthomosaic, a digital surface model, a digital terrain model, a point cloud and mesh, and photos/video.

Mapping photos collected in 2023 from the P4 Multispectral were processed using Esri Drone2Map v2023. The images were used to create an RGB Orthomosaic and a Multispectral Ortho including RGB, RE, and NIR bands. The P4P was only used to collect photos and video. The individual sets of images taken in 2023 of the 1 m^2 plots were processed in Esri ArcGIS Pro software to first align the images and then combine them into a composite image with all bands.

II. Habitat Delineation Through Image Classification

II.i. General Overview

The purpose of this chapter is to document the concepts and methodology used to generate the classified raster datasets and plot summary statistics used for this project. The criteria and schema are also outlined to describe the parameters of each workflow. ESRI's ArcGIS Pro 3.x software (Environmental Systems Research Institute, Redlands, CA) was used to run all tools involved in this process.

The classified raster datasets were derived from a series of processing steps to classify, edit, and assess the accuracy of features on the marsh. This starts with defining the classification schema to define the possible classes and their reference codes. The primary focus of the image classification was to extract vegetation species, water features, and bare ground features that are commonly present on the marsh, throughout each study zone. Subcategories, or subclasses, were added to differentiate species and coverage types within each category. A classification model was generated depicting these features on the marsh using a supervised classification schema and a machine learning algorithm.

Each zone also contained plots and subplots that were part of a large-scale assessment. Within each plot, vegetation indices were used to calculate different metrics to describe the health of the vegetation within that area. Many subplots were also added to provide additional analysis within the plots. These metrics were then integrated into other field samples data that are covered in Chapter 4.

II.ii. Habitat Classification Schema

As a first step, defining the classification schema for the classified model dictates the following geoprocessing steps' complexity and detail. With the schema defined, the segmentation and training samples become tailored to these class codes in order to properly display the features in question on the marsh. The image classification schema for this project was broken down into five main categories. The main categories included "Vegetation," "Bare Ground," "Water," "Wrack," and "Other (Debris, Coverage, Structures)." The "Vegetation," "Bare Ground," and "Water" categories contained several subcategories, or subclasses, to differentiate the several species or geographic features that are prominent within the zones. Each main category and subcategory were given a unique class code based on the level of detail needed to classify that feature (Table 3.1). Classifying various vegetation species, commonly found water

Table 3.1. Classification schema as it was created to train and edit the classified data model.

Class Names	Class Code
Vegetation	**100**
Spartina alterniflora - Short Form	101
Spartina alterniflora - Tall Form	102
Spartina patens	103
Distichlis spicata	104
Phragmites	105
Other Veg	106
Bare Ground	**200**
Bare Soil	201
Salt Pannes	202
Water	**300**
Creek/Stream	301
Ponds	302
Open Water	303
Wrack	**400**
Other (Debris, Coverage, Structures)	**500**

features, and bare ground features were the main focus of the classification schema. The other main classes cover other less prominent or rare features. The level of detail needed to classify each feature is reflected in the complexity of each main category and their corresponding subcategories.

The “Vegetation” main category was divided into five species subclasses including “*Spartina alterniflora* – Short Form,” “*Spartina alterniflora* – Tall Form,” “*Spartina patens*,” “*Distichlis spicata*,” and “*Phragmites*.” “*Spartina alterniflora* – Short Form” and “*Spartina alterniflora* – Tall Form” were distinguished from each other based on several factors, including texture of vegetation canopy, color, and proximity to creeks and ponds. Short form tended to have a more consistent canopy texture, creating a smoothing of vegetation height, whereas tall form patches were darker green in color (or brown if mud-covered, demonstrating increased saturation and more like to be tall form) and sometimes exhibited shadows within the vegetation patch due to a decreased culm density and bending. Additionally, tall form was found in areas of the marsh that were close to creek and pond edges, while short form dominated the marsh platform away from waterbodies. In order to assist with distinguishing short form vs. tall form, DSMs were used to examine the canopy height. “*Distichlis spicata*” was distinguished from “*Spartina patens*” by primarily texture and color. “*Distichlis spicata*” tended to be slightly darker green than “*Spartina patens*”, had a slightly spiky texture, did not exhibit the wavy growth of “*Spartina patens*”. A sixth subclass, “Other Veg,” was used as a general category for trees, shrubs, and other minor plants that are not included in the other classes, and whose coverage was not consistent or significant in each zone. This class covers up to approximately 5% of a zone's coverage if it is present in the zone. The "Bare Ground" main category was subdivided into "Bare Soil," for general bare soil areas, and "Salt Pannes," for bare ground areas where salt was left behind when water evaporated or receded. The "Water" main category was subdivided into "Creek/Stream," "Ponds," and "Open Water" to cover the hydrographic features present on the marsh.

The fourth main category, "Wrack," was used to classify dead marsh plant stems and leaves that are washed up on the marsh and obscure other features in the imagery. The fifth category, "Other (Debris, Coverage, Structures)," serves to classify any additional non-vegetative features that are on the marsh that are not covered by the other classes. This includes debris that washed up on the marsh like signs, buoys, decks, or boats. If the debris or structure was small enough, the underlying class was used instead. For areas that are too obstructed, these categories serve as a way to represent the features on the marsh at a large mapping scale and avoid misrepresentation in the dataset. This class also includes other landscape coverages not being evaluated, but are present within the zone boundary, including the small area of beach found in Zone 2 (Figure 3.5). Like the "Other Veg" subclass, the "Other (Debris, Coverage, Structures)" class's coverage is not consistent across each zone and covers up to approximately 2% of the total coverage of a zone, if it is present at all.

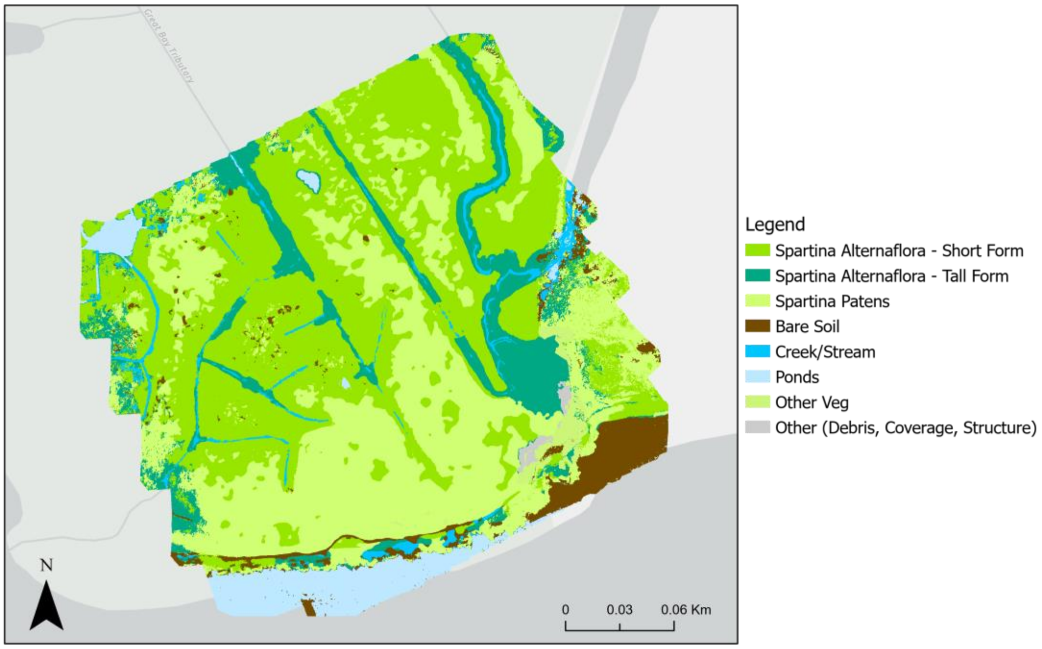

Figure 3.5. Example of classification from Zone 2 in 2023.

II.iii. Image Segmentation

With the use of image segmentation techniques, the detail of the 3-inch multispectral orthomosaic imagery is reduced to reflect similarities in the spectral information, texture, and color (ESRI, n.d. b). Similar, spatially adjacent pixels are grouped into image objects (Green et al., 2017). These complex, detailed features are divided into simplified, characteristically significant objects to detect edges between unique objects and spectrally homogenous zones (Green et al., 2017). The texture of the segmented ortho-imagery is used to delineate heterogeneous areas from homogenous ones (Green et al., 2017). The parameters are balanced based on the classification schema defined previously. The most complex classification main category, "Vegetation," reduces detail within each subcategory while also preserving boundaries and detail without merging neighboring classes together. An example of this is to blend the "*Spartina alterniflora* – Short Form" class so that variability in texture blends together. This species can be found in muddy or dry soils and various places across each zone. Image segmentation blends this variability into similar object neighborhoods. The bushy or leafy texture of another vegetation class is also removed with segmentation to simplify the object neighborhood. Depending on how the image segmentation parameters are prioritized, there are many different versions of the output segmented image. Segmenting the ortho-imagery allows the training samples to better train the classification algorithm and removes complexity in the image classification model.

In addition to the segmentation of the RGB ortho-imagery, the color NIR imagery was also segmented to assist the classification model. Much like segmenting the RGB ortho-imagery, the color NIR imagery generalizes areas and reduces the amount of detail using the NIR, red, and green bands. However, similarities in the reflectance of these bands were shown to cause misclassifications in some areas despite the training sample data. An example of this is a muddy "Bare Ground" class being misclassified as a "Water" class, the "Stream/Creek" class being misclassified as "Pond" or vice versa. Some textures of short form *Spartina alterniflora* were also confused for tall form *Spartina alterniflora*, bare soil, or vice versa (Figure 3.6). Ultimately, segmenting the color NIR imagery provided additional spectral objects and additional ancillary information in the classification model and QC review.

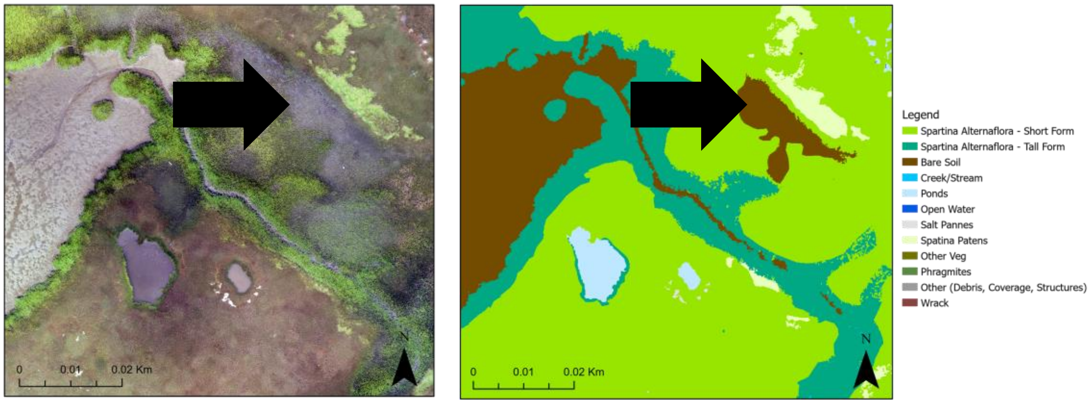

Figure 3.6. Example of misclassification of muddy S. alterniflora as bare soil in a pre-corrected classification of Zone 3.

II.iv. Training Data

To aid the supervised classification model, training data were collected throughout each zone. Each training sample was drawn on the map, representing each class individually (Figure 3.7). The number of training samples, their size, and placement depends largely on the coverage of the feature each class represents on the marsh. Each training sample represents each class exclusively without extending into the other classes. Other criteria for each training sample include completeness, spectral homogeneity,

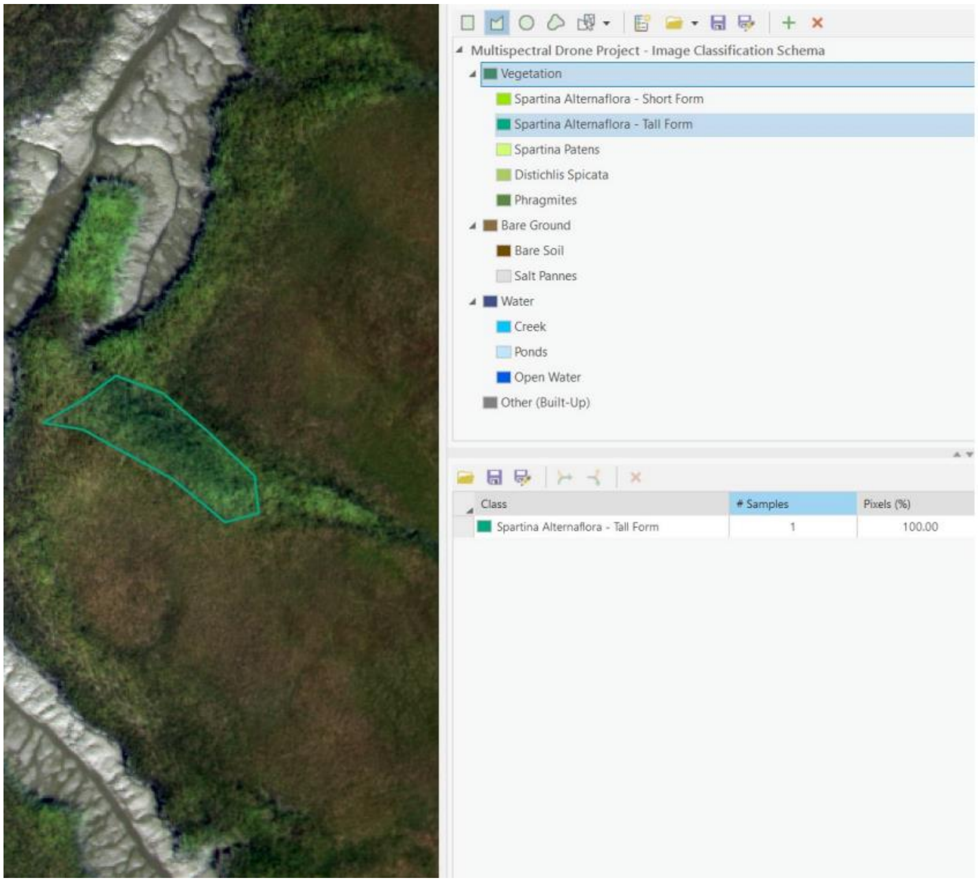

- Multispectral Drone Project - Image Classification Schema
  - Vegetation
    - Spartina Alternaflora - Short Form
    - Spartina Alternaflora - Tall Form
    - Spartina Patens
    - Distichlis Spicata
    - Phragmites
  - Bare Ground
    - Bare Soil
    - Salt Pannes
  - Water
    - Creek
    - Ponds
    - Open Water
  - Other (Built-Up)

Class	# Samples	Pixels (%)
Spartina Alternaflora - Tall Form	1	100.00

Figure 3.7. Example of a polygon drawn for a training dataset that includes only S. alterniflora tall form.

project-wide distribution, accurate, cost effective, and consistent (Congalton and Green, 2019). Depending on the coverage, the training sample size ranged between 15 to 25 samples for each class in each zone. The number of samples were less for classes that were scarce or localized.

The complexity of the class also dictated the number of training samples. For example, short form *Spartina alterniflora* was found in abundance in each zone. Some of these areas were in muddy or dry soils, around other species of vegetation, or near a water source. Conversely, *Spartina patens* was found sparsely in Zone 6, for example, but abundant in Zone 7. *Spartina patens* coverage and uniformity also impacted the number of training samples used to represent this class in the classification model. Training the model to recognize the various textures and spectral signatures of each class impacted the classification model's output.

II.v. Image Classification

The supervised classification model used the datasets derived from the multispectral orthomosaic to classify the features on the marsh based on the classification schema stated previously. Utilizing the training samples to train the model, the supervised classification scheme resembled manual interpretation, whereas an unsupervised classification scheme relied on the statistical clustering of pixels to classify features (Congalton and Green, 2019). This classification scheme incorporated the segmented ortho-imagery and the training samples with a machine learning algorithm to classify the features on the marsh. The segmented color near-infrared ortho-imagery was also used as an ancillary dataset to assist the classification. Incorporating the color infrared ortho-imagery was shown to reduce noise and improve misclassified areas in brief preliminary tests.

By incorporating it into the supervised classification method, the machine learning algorithm mined the imagery’s spectral information and created linkages between the classes and other variables involved in the model (Congalton and Green, 2019). These linkages are then used to classify the other areas of the imagery based on the training samples and supporting datasets. Based on a brief, early testing period, the Support Vector Machine (SVM) algorithm was preferred over other available models due to its ability to reduce noise in the classified model and provided a better initial output. This algorithm could be used with very large images and is less susceptible to using an unbalanced samples size among classes in the classified model (ESRI, n.d. a). This is preferred as an imbalanced design may skew the classification toward classes with more representation or larger area in the model (Congalton and Green, 2019).

In addition to generating the optimal datasets to train and classify the marsh, the parameters of the “Classify” geoprocessing tool must also be considered when producing the initial classified raster. Depending on the quality of all data involved (segmented ortho-imagery, training samples, and the segmented color infrared ortho-imagery), the quality of the initial output will vary. Misclassified noise and features can be introduced into the model and will need to be reviewed and edited for better thematic accuracy.

III. QA/QC of Classified Habitat Maps

III.i. Data Review and Refinement

With the initial classified raster generated, each classified image was inspected for data quality and thematic accuracy. Based on quality of the segmented image, training data, and the segmented color infrared image, each zone required different amounts of editing before reaching a final product. Depending on the quality of the data going into the model and the complexity of features on the marsh, several areas could be misclassified based on similar spectral detail, texture, or color. However, products were reviewed by multiple team members to attempt to determine accurate classifications prior to finalization.

Although the accuracy of the dataset of output model may be adequate, how the data are represented within each zone is a key aspect of the final data product’s thematic accuracy. Rounds of editing were done based on manual photo interpretation and inspection of the classified model. The misclassified areas were manually reclassified to represent the correct class on the marsh. This group of errors largely pertained to broad areas that were confused by the classification model and its components. Feature boundaries may be intact with misclassifications within the feature, or parts of or whole features may be represented as the wrong class. Misclassified noise may also be introduced into the model as small clusters or scattered single pixels. The data were refined with clean-up routines to better represent the features on the marsh and improve their thematic accuracy. Additional editing was done to ensure data accuracy and cartographic representation.

III.ii Thematic Accuracy Assessment

Each of the 13 classified rasters underwent a thematic accuracy assessment using confusion matrices (ESRI, 2021) before being finalized as a data product. An overall accuracy of 90% was selected as the baseline minimum overall accuracy standard. Each accuracy assessment was based on computing the total number of accuracy points by multiplying 50 times the number of classes represented in the classified raster (Congalton and Green, 2019). This number is the basis for how many points are needed to conduct the accuracy assessment. Each zone contained a varying number of classes but were largely dominated by the "*Spartina alterniflora* – Short Form" class. The "*Spartina patens*" and "*Spartina alterniflora* – Tall Form" classes made the next most abundant classes, although their coverage varied from zone to zone. "*Phragmites*" was only found minimally, and the coverage varied. The "Pond," "Stream/Creek," and "Open Water" classes also had varying coverage depending on the hydrography of the zone. The "Bare Ground" subclasses, "Bare Soil" and "Salt Pannes," were found considerably less than the other classes mentioned. Some zones had minimal coverage, if at all.

Each of the checkpoints were reviewed and verified using an attribute field for the classified value and ground truthing value ("Classified" and "GrndTruth," respectively). Once the checkpoints were verified on the map, an error matrix was created for that zone, displaying how the classified data matched with the reference data. The error matrix displays various statistics to describe different aspects of the thematic accuracy of the data using the producer's accuracy, user's accuracy, overall accuracy, and kappa score by comparing each class to another. The producer's accuracy measures the error in omission by dividing each correctly classified sample category by the respective reference data column total (Story and Congalton, 1986). The user's accuracy measures errors in commission (over inclusion as part of a class) by dividing the number of correctly classified sample category by the respective classified sample row totals (Story and Congalton, 1986). The kappa score measures the agreement between the reference and classified data (NV5 Geospatial Solutions, Inc., n.d.).

The overall accuracy provides an overall statistic for the entire dataset without taking each category into account. Each dataset exceeds the 90% minimum overall accuracy standard, with the highest being Zone 5 with 98.66%. Table 3.2 displays the overall accuracy for each of the zones, the collection years, and the total number of checkpoints calculated using GIS software. While having a high overall accuracy is required for these datasets, the other metrics provide more information on the weaknesses of the dataset. Error matrices are found in Appendix C.

Table 3.2. The overall thematic accuracy of each classified raster model.

Site	Zone	Year	Checkpoints	Overall Accuracy
Great Bay Boulevard	Zone 1	2022	420	97.14%
		2023	477	98.11%
	Zone 2	2022	438	96.80%
	Zone 3	2022	640	96.25%
	Zone 4	2022	483	98.55%
	Zone 5	2022	372	98.66%
	Zone 6	2022	537	94.60%
Forsythe	Zone 7	2022	476	94.96%
	Zone 8	2022	376	95.74%
		2023	488	96.31%
	Zone 9	2022	370	96.76%
		2023	423	95.98%
	Zone 10	2023	369	94.58%

IV. Multispectral Vegetation Indices

Several areas around each zone were chosen for small scale analysis. These areas, called plots, were marked out in the field with spray chalk so they were clearly visible in the multispectral drone imagery used for the assessment. The corners of the plots were recorded with real-time kinematric (RTK) GPS and were reconstructed digitally using ArcGIS software. Plots contained four subplots that were also recorded with RTK GPS and buffered with a ½ meter radius. Additional characteristics were added as attributes to describe the species and conditions present within the plots and subplots.

Vegetation indices (VIs) were used to assess the health of the vegetation within these areas. Four vegetation indices were calculated using the individual bands from the 3-inch multispectral orthomosaic imagery collected by a Phantom 4 Multispectral drone. ESRI's ArcGIS Pro 3.x software (Environmental Systems Research Institute, Redlands, CA) was used to run all tools involved in this process. These indices included the normalized difference vegetation index (NDVI), green normalized difference vegetation index (GNDVI), normalized difference red edge index (NDRE), and the non-photosynthetic vegetation index (NPV). Using the equations displayed in Table 3.3, each vegetation index was generated to display the features' ability to reflect or absorb wavelengths of light in the red, green, blue, red edge, and near infrared spectrums. Depending on the type of feature, this ability to reflect or absorb light can suggest different characteristics about vegetation health, surface composition, or qualities of water features.

Using the plot boundaries, subplot boundaries, and vegetation indices, geoprocessing tools were run to generate statistics for each plot and subplot. These statistics included mean, median, standard deviation, minimum, maximum, and range. Additional tables are available in “Appendix D: Plot Summary Results” and “Appendix E: Multispectral Imaging SOP Subplot Summary Results.” Other health trends emerged when integrated with sample data collected by field staff to provide a more complete picture of the health of the vegetation in the plots and subplots.

Table 3.3. Vegetation Index acronyms, band components, and equation.

Name	Acronym	Bands	Equation
Normalized Difference Vegetation Index	NDVI	Near Infrared, Red	(NIR - Red) / (NIR + Red)
Green Normalized Difference Vegetation Index	GNDVI	Near Infrared, Green	(NIR - Green) / (NIR + Green)
Normalized Difference Red Edge Index	NDRE	Near Infrared, Red Edge	(NIR - RE) / (NIR + RE)
Non-Photosynthetic Vegetation	NPV	Blue, Green	(Blue - Green) / (Blue + Green)

V. Conclusions & Limitations

V.i. Habitat Delineation

1. Raw outputs from the classification model were inadequate for exact class area calculation. Although the initial output of the classification model represents the marsh and its features with some degree of accuracy, misclassified noise was scattered throughout the zone. The output raster also did not provide a cartographic representation of the marsh. This noise was displayed as scattered single pixels or very small clusters based on miscalculations in the image classification model. Several geoprocessing steps were needed before the final classified data products were produced to eliminate this problem. Cleanup routines removed this misclassified noise to better represent the marsh, in addition to correcting misclassified codes in classified raster model. Other misclassified data in the initial classified raster output had to do with the model misclassifying features with similar spectral information. This included muddy soils being classified as shallow ponds or streams or vice versa. *Spartina alterniflora* also showed inconsistencies in some instances with differing textures in the imagery.
2. In some areas, the coverage transitions between class codes made it difficult to discern the correct species. These areas blended in some areas, making it difficult to properly train or edit. An example of this was with short form and tall form *Spartina alterniflora* along streams. Some areas were clear but were difficult to discern in other cases based on other textures, colors, and location each species occupies. Other, more mixed areas were also difficult to classify because of a species’ sparseness. In these areas, it was reclassified based on the dominate class code with the other

class code delineated where coverage is more consistent. An example of this was in several zones with sparse *Spartina patens*. There were several areas in Zones 2, 7, and 8 where sparse *Spartina patens* was mixed with short form *Spartina alterniflora*. Although the *Spartina patens* was not as dense as other areas where it is well established, the texture and spectral detail of the vegetation did not match that of short form *Spartina alterniflora*, either. However, Zones 2 and 7 were only collected in 2022. In Zones collected in both 2022 and 2023, some of these areas were an indication that *S. patens* coverage was expanding; with 2023 showing denser and well-established growth. Due to our classification schema, mixed areas were avoided when creating training sample data for the imagine classification model. Having 3-inch resolution imagery helped fix class coverage issues because we were able to digitize minute details in the imagery that would not be possible with the lower resolution of publicly available imagery datasets. Having multispectral imagery, vegetation indices, and a digital surface model may help differentiate between species, but some issues may still persist in the classified raster. The color infrared imagery served as an additional ancillary dataset to clean up the classified model and helped as an ancillary dataset during review.

3. The final classified data products were based on photo interpretation and what is clearly visible in the imagery. Additional field reconnaissance and verification were not conducted to verify certain characteristics of the marsh. Additional hydrography data were not collected or delineated within each Zone. “Streams/Creeks” and “Ponds” were sometimes obscured by overhanging vegetation. Because of this, the amount of coverage each of the classes cover may be more than what is represented in the dataset and data tables. Streams may seem segmented in various areas if the watercourse is narrow enough to be covered by vegetative classes on both sides of the stream bank. Features could also be obstructed by tall trees, shrubs, shadows, or other vegetation species if heavily mixed on the marsh. The primary prerogative of this mapping effort was to delineate vegetative species in a quick yet accurate way. While training the image classification model and editing the classified output, noting the characteristics of the features, how the features are orientated, and how it relates to other features on the marsh helped determine the appropriate class. Additional fieldwork would be recommended to verify the dimensions of stream networks or other features on the marsh, should those details be needed.
4. The data products were classified based on the classification schema outlined previously in this chapter. The classification schema focused on representing the coverage of each class but relied on the vegetation indices to provide additional health characteristics. Change from 2022 to 2023 was denoted as a change from one class code to another. The classification schema did not include other characteristics like density (sparse or dense), health (healthy or thatched/unhealthy), hydrology (hydric or dry soils), if there was die-off, or other characteristics. Some of these additional characteristics would have required additional fieldwork and extensive testing that were outside of the scope of this project. Changes to water levels due to tides or recent weather events provided different coverage for Zones that were collected in 2022 and 2023. Streams with less water or different amounts of water accumulated along mudflats may reflected a categorical change in the classified raster, although it did not resemble a physical change to the marsh.

However, erosional and depositional processes or vegetation die-off would denote a categorical change and a physical change to the marsh.

V.ii. Multispectral Indices

The plot and subplot summary statistics provided a quick and efficient way of obtaining the mean, median, standard deviation, minimum, maximum, and range of each of the NDVI, GNDVI, NDRE, and NPV multispectral indices. Geoprocessing tools covered the workflow without needing any additional calculations or programming. Although not used to generate cartographic maps, the values of each plot and subplot were used in arranged tables and graphs. The main purpose of the plot and subplot summaries were to generate vegetation health metrics to be integrated with other field sample data.

References

Congalton, R. G., & Green, K. (2019). *Assessing the Accuracy of Remotely Sensed Data: Principles and Practices, Third Edition* (3rd ed.). CRC Press. https://doi.org/10.1201/9780429052729

ESRI. (2021). *Compute Confusion Matrix*. Compute Confusion Matrix. https://desktop.arcgis.com/en/arcmap/latest/tools/spatial-analyst-toolbox/compute-confusion-matrix.htm

ESRI. (n.d. a). *Classify*. Classify. Retrieved April 15, 2024, from https://pro.arcgis.com/en/pro-app/latest/help/analysis/image-analyst/classify.htm NV5 Geospatial Solutions, Inc. (n.d.). *Calculate Confusion Matrices*. Calculate Confusion Matrices. Retrieved April 15, 2024, from https://www.nv5geospatialsoftware.com/docs/CalculatingConfusionMatrices.html

ESRI. (n.d. b). *Segmentation*. Segmentation. Retrieved April 15, 2024, from https://pro.arcgis.com/en/pro-app/latest/help/analysis/image-analyst/segmentation.htm

Green, K., Congalton, R. G., & Tukman, M. (2017). *Imagery and GIS: best practices for extracting information from imagery*. Esri Press.

NV5 Geospatial Solutions, Inc. (n.d.). *Calculate Confusion Matrices*. Calculate Confusion Matrices. Retrieved April 15, 2024, from https://www.nv5geospatialsoftware.com/docs/CalculatingConfusionMatrices.html

Story, M., & Congalton, R. G. (1986). *Accuracy assessment: a user's perspective*. *52*(3), 397–399. https://www.asprs.org/wp-content/uploads/pers/1986journal/mar/1986_mar_397-399.pdf

Chapter 4: Evaluating the use of multispectral drones to delineate the relative condition of high marsh habitat.

Authors: Brittany P. Wilburn[1], Joshua Moody[1], Charles Schutte[2], Metthea Yepsen[1], Steven Jacobus[3], William Smith[3], Kirk Raper[1], Kriish Hate[1,2], Lori Lester[1], Kevin Blythe[4], Molly VanWieren[4]

[1] NJDEP, Division of Science and Research
[2] Rowan University
[3] NJDEP, Bureau of GIS - DOIT
[4] NJDEP, Fish and Wildlife, Office of Fish and Wildlife Information Systems

Objective: Determine the applicability and efficacy of multispectral drone monitoring of salt marsh condition in place of or in supplement to traditional on-the-ground field measurements.

Approach: Utilizing the processed drone imagery, spectral signatures were compared to vegetation, soil, and porewater characteristics to determine if drone spectra could act as a proxy for on-the-ground measurements of salt marsh condition. For the first year of data collection (in 2022), a factorial design was used to evaluate qualitatively defined “healthy” and “unhealthy” units of *Spartina patens* (representing high marsh) and *Spartina alterniflora* (low marsh) at both Great Bay Boulevard Wildlife Management Area (GBB) and E. B. Forsythe National Wildlife Refuge (Forsythe) salt marshes. A total of 32 plots (each 100 m^2 in area) were selected and surveyed among nine drone flight zones across the two salt marshes. Within each plot, four subplots were chosen as representatives of the larger plot for points of sample collection for soil and porewater. Spectral responses of these subplots were then used to determine if vegetation, soil, and spectral signatures were correlated. Initial analyses demonstrated some connections between multispectral indices and soil parameters, but some spectral signatures were masked by shadows of *S. patens* canopy structure and the robustness of *S. alterniflora*. Therefore, an adapted study design was utilized the following year in 2023.

In 2023, using historic imagery of Great Bay Boulevard and Forsythe marshes, we selected two zones in the GBB and Forsythe marshes each that fit into “stable” or “unstable” categories (four zones in total). “Unstable” was defined by a combination of reduction of *S. patens* habitat over time from visual assessment of aerial imagery and *in situ* evaluation of the distribution and density patterns of the vegetation, expansion of marsh platform ponds over time, and/or presence of ditching. “Stable” was defined by contiguous habitat without ditching, a constant or growing expanse of *S. patens*, and/or unchanging diameter of present ponds. Within each of the four zones, three ponds were selected as points of reference for three transects. Along each transect, a 1 m^2 plot of *S. patens* was established within 5 m distance from the pond edge, and a second 1 m^2 plot of *S. patens* was established within a 10-20 m distance from pond edge. At each of these plots, similar vegetation, soil, and porewater characterization and sampling as 2022 occurred. Furthermore, multispectral drone images were taken of each plot at lower elevations and close to solar noon in an attempt to reduce shadowing effects.

A draft manuscript is included in this chapter, which is intended to be revised and submitted for publication to an appropriate peer-reviewed scientific journal. This draft may undergo minor or significant edits prior to submission, as such many portions to the draft manuscript may appear verbatim in the submission version of the article.

Responsibilities and Deliverables: The NJDEP-DSR 1) oversaw project design, 2) oversaw permit retrieval, 3) conducted portions of the field research, 4) performed the statistical analyses, and 5) led manuscript writing and editing (*Deliverable 3*).

The NJDEP-BGIS 1) produced drone flight plans, 2) retrieved drone flight permits, 3) conducted drone imagery collection, 4) processed and classified drone imagery, and 5) supported manuscript writing and review (*Deliverable 3*).

The NJDEP-FW 1) provided the multispectral drone, 2) participated in drone imagery collection, and 3) processed and classified drone imagery (*Deliverable 3*).

Rowan University 1) conducted soil and porewater sampling and analysis and 2) supported manuscript writing and review (*Deliverable 3*).

Title: Investigating the potential of multispectral drone analysis as a proxy for traditional on-the-ground monitoring of salt marsh condition

Authors: Brittany P. Wilburn[1], Joshua Moody[1], Charles Schutte[2], Metthea Yepsen[1], Steven Jacobus[3], William Smith[3], Kirk Raper[1], Kriish Hate[1,2], Lori Lester[1], Kevin Blythe[4], Molly VanWieren[4]

[1]NJDEP, Division of Science and Research
[2]Rowan University
[3]NJDEP, Bureau of GIS - DOIT
[4]NJDEP, Fish and Wildlife, Office of Fish and Wildlife Information Systems

Abstract

Coastal wetlands in New Jersey provide a myriad of important ecologic and economic services including habitat, flood protection, and carbon storage. Alterations on the landscape from climate change, sea-level rise, and direct anthropogenic sources have accelerated wetland loss, and there is a need for increased efficiency in identifying spatiotemporal wetland vulnerability to identify and prioritize appropriate intervention activities. Historically, wetland assessment required *in situ* evaluation of a variety of biogeochemical parameters which can be costly, time consuming, and inadvertently destructive of the habitat we want to protect. Due to expenses and temporal considerations, such as tidal cycles, associated with satellite-based imagery and with the continued development and increasing affordability of remotely operated vehicles and environmental sensors, there is increased opportunity to collect remotely sensed data locally across vast areas with lower effort. Multispectral imagery has been used successfully for agricultural applications and can provide a variety of information related to wetland health, including biomass density, phenotypic stage, growth associated with high nitrogen, and non-photosynthetic features such as soil and dead vegetation. The goals of this study were to evaluate if drone-sourced multispectral data could be used to detect early signs of vegetation stress in hydrologically impacted salt marshes.

To evaluate relationships between multispectral indices (MSIs) and various ecologic variables, vegetation, soil, porewater, and multispectral imagery data were collected in 2022 and 2023 at multiple locations within two NJ salt marshes, with experimental design varying by year. Overall, in 2022, *S. patens* plots were more acidic and oxidized, and displayed lower porewater ammonia and sulfide concentrations than their *S. alterniflora* counterparts, which aligned with unstable values reported in the literature. However, none of these chemical parameters were able to significantly predict MSI values. Although the 2023 *S. patens* plots showed some variability among the porewater and soil metrics, again, there were no substantial predictive relations between them and any of the MSIs. The one significant relationship between porewater ammonia and the Non-Photosynthetic Vegetation index (NPV) explained only 23.5% of the MSI variance and requires further evaluation to determine the pre-predictive capacity of NPV for porewater ammonia levels. It is probable that the variability in vegetation, soil, and porewater metrics

were lower than expected, likely due to influence of the tidal magnitude and geomorphology of the sites driving these levels at a scale greater than our sampling strata (i.e., site location, expanding vs stable ponds, and distance of plot from pond). While these experiments were unable to directly tie MSIs to the underlying chemical conditions of these marshes, they do inform us of potential routes of future research including greater spatial dispersion of study sites, an increase in sampling plots per study site, and a reduction for the need of particular strata such as distance from ponds within the study sites.

Introduction

Within New Jersey, there are approximately 66,000 hectares of tidal saltwater wetlands. These wetlands are integral to the health and well-being of over 7 million residents that live within these coastal areas (NOAA Office for Coastal Management, 2024), as they provide a number of invaluable ecosystem services, including: carbon sequestration (Were et al., 2019), coastal storm energy reduction (Rezaie et al., 2020), flood water storage (Rezaie et al., 2020), water quality enhancement (Fisher and Acreman, 2004), and traditional and cultural significance (Pedersen et al., 2019). However, New Jersey has lost a significant portion of its coastal habitat as a result of climate change and other anthropogenic factors, such as reduced hydrological function from agricultural ditching (Smith et al., 2022). A first step to intervene these losses is to determine vulnerable habitat as quickly, accurately, and efficiently as possible, in order to prioritize areas of marsh for protection or enhancement.

There is a significant push within the Mid-Atlantic region to enhance the current monitoring methods of salt marsh condition. This is largely due to the exacerbated relative rates of sea-level rise within this region from a combined effect of loss of marsh elevation from subsidence, directional oceanic currents towards the region, and glacial isostatic rebound (Horton et al., 2018; Kopp et al., 2019). As such, within the 20th century, New Jersey currently experiences relative rates of sea-level rise between 4 to 5 mm yr^{-1} (Haaf et al., 2022) compared to the global average rate of 1.1 to 1.9 mm yr^{-1} (Horton et al., 2018). With these high rates of sea-level rise, loss of salt marsh habitat is expected to be subsequently increased due to increased inundation times, vegetation die-off, and destabilization of the underlying peat matrix (Chambers et al., 2019; Nicholls et al., 1999; Watson et al., 2017). Research has shown that stressed marshes with increased saturation tend to have elevated soil concentrations of ammonia and sulfide, which are known to be phytotoxic (Lamers et al., 2013; van Katwijk et al., 1997). Declines in vegetation biomass result in a decreased sediment trapping capacity aboveground (Kirwan et al., 2010) and a belowground loss of elevation building capacity through decreased root production and increased biomass metabolism (Langley et al., 2009), exacerbating vulnerability to sea-level rise. Because initial signs of stress may be within underlying marsh soil layers, the declining health of a marsh may be gradual. This decline of healthy marsh conditions may not be apparent until it is too late (Kearney et al., 1988; Kearney et al., 2002); therefore, close monitoring of the coastal soils and vegetation is necessary to determine changing health conditions and wetland vulnerability to sea-level rise. However, current *in situ* monitoring methods can be too time consuming and costly to effectively evaluate landscape trends at the detail necessary to effectively mitigate the impacts of sea-level rise (Finlayson and Spiers, 1999). Additionally, traditional on-the-ground methods of monitoring may inadvertently cause negative effects to vegetative health, as it requires traversing across vulnerable landscapes in order to extract the survey data. With the enhancement of technology, monitoring efforts are becoming more digitalized, with many researchers turning towards supplementing their data with remote sensing (e.g., Ganju et al., 2017).

Remote sensing, particularly with the use of satellites, has been used for decades to determine larger trends in habitat condition across wetlands (Ozemsi and Bauer, 2002). However, the typical resolution of satellite imagery ranges from 5 to > 30 m/pixel, which is too granular to effectively capture many valuable landscape features, such as tidal channels or at-risk vegetation patches. While high resolution satellite imagery (i.e., between 1 to 3 meters per pixel) is available, costs associated with general acquisition and for images that meet specific tidal conditions required for remote vegetation evaluation, such as at low tide, are often costly compared to lower resolution imagery. Therefore, for monitoring efforts with a restricted budget, satellite imagery may not offer the data needed to make informed decisions on wetland health condition.

Small unmanned aerial vehicles (or, more colloquially, “drones”) may offer the high-resolution, low-cost solution needed to examine stressors to salt marsh habitat, including vulnerabilities to sea-level rise. Commercially available drones at a cost of less than $5000 are able to achieve high resolution imagery of <0.5 meter per pixel, and after the initial purchase, additional costs related to maintenance are typically low. Customizations can be added to the drone, such as a variety of camera lenses, chemical and vapor sensors, LiDAR, or RTK GPS, to allow for additional data collection during a single flight (Shaw et al., 2021; Turner et al., 2016; Van Alphen et al., 2024). Most drones are equipped with camera lenses that detect visible light, which includes a combination of red, green, and blue (R, G, and B, respectively) wavelengths. Multispectral drones have camera lenses that detect additional wavelengths that are outside the visible range, such as near infrared and red edge (NIR and RE, respectively). The NIR and RE wavelengths have been found to significantly correlate with vegetation condition, as they can be used to detect concentrations of chlorophyll, nitrogen, and moisture (De Castro et al., 2021; Ramsey and Rangoonwala, 2005; Zhang et al., 2019). These connections are determined through correlations of these physiological properties to band indices, which are algebraically derived values from the grouping of wavelengths per pixel. The use of vegetation indices to characterize vegetation health has become a more conventional tactic as it offers a potential method of standardization and comparison amongst landscapes.

The normalized difference vegetation index (NDVI) is commonly used to estimate biomass and density through chlorophyll reflectance (Doughty and Cavanaugh, 2019). Furthermore, NDVI can distinguish between vegetation species due to their varying spectral response patterns related to chlorophyll concentrations (Sun et al., 2016). Other vegetation indices have been developed to discern additional attributes of vegetation, such as the normalized difference red edge vegetation index (NDRE), the green normalized difference vegetation index (GNDVI), and the non-photosynthetic vegetation index (NPV), although these are less commonly used in salt marshes. Similar to NDVI, the NDRE can detect differences in chlorophyll content but is more sensitive to nitrogen concentrations (Boiarskii, 2019). The GNDVI has been developed to further characterize vegetation health at different phenological stages and is particularly successful in providing insight into nitrogen content (De Souza et al., 2020). The NPV is useful in delineating bare soil and dead vegetation by focusing on wavelengths not associated with photosynthetic activity (Baena et al., 2017). A drone equipped with a multispectral camera is able to detect each of the wavelengths necessary to calculate the above-mentioned vegetation indices within one flight, making it a promising tool for characterizing wetland vegetation in depth.

Individual wavelengths can further be analyzed to assist classification and characterization of the marsh platform. Several studies have shown that species can be distinguished from each other based on the range of reflectance of specific individual wavelengths (Artigas and Yang, 2006; Paz-Kagan et al., 2019; Ramsey and Rangoonwala, 2005). Additionally, specific wavelengths can be utilized to identify abiotic components of the marsh platform. For example, near infrared wavelengths are greatly absorbed by water, resulting in a lack of reflectance in areas submerged by water (Mondejar and Tongco, 2019). This attribute can be applied for separation of land and water classifications but poses an additional challenge for classifying coastal wetlands, where water may not be fully drained from the marsh platform. To avoid the obscuration of underlying vegetation by water, timing of multispectral image collection is crucial and should be done at low tide. Therefore, drones offer the greatest flexibility in collecting spectral data across large areas at specific timepoints (e.g., tidal cycles, vegetation emergence, or senescence times of year).

With a variety of easily accessible drone options available, the use of drones in coastal wetland monitoring has significantly increased over the past decade. However, it is still unclear if drone-sourced data can be used to supplant traditional on-the-ground monitoring methods, rather than supplement. If multispectral data were able to be used *in lieu* of *in situ* data, there would need to be clear, significant relationships between the respective multispectral index (MSI), and the target metric of interest (e.g., ammonia, sulfate, sulfide, etc.). The goals of this study were to:

1. Distinguish early signs of high and low marsh vegetation stress in hydrologically impacted salt marshes using traditional field and lab-based methods and
2. Determine if a multispectral drone can detect similar findings as traditional monitoring methods through the use of vegetation indices.

Methods

Site Description

Two salt marshes on the eastern coast of New Jersey were selected for this study: Great Bay Boulevard Wildlife Management Area (GBB) on the Tuckerton Peninsula and a portion of E.B. Forsythe National Wildlife Refuge (Forsythe) salt marsh at the northern end of Little Egg Harbor near Cedar Creek (Figure 4.1). Because these two sites are areas of high interest for wetland management in the context of rising sea-levels, both marshes have been studied extensively, providing a robust background dataset useful for interpreting the results of this study. The average tidal range of GBB is approximately 90 cm, while Forsythe has a range of approximately 50 cm. Both sites are predominantly *Spartina alterniflora* marshes, with some high elevation areas dominated by *S. patens*. Additional species present include *Phragmites australis*, *Iva fructescens*, *Distichlis spicata*, *Limonium carolinianum*, and *Salicornia* spp. Portions of both marshes have been affected by historic agricultural ditching and open marsh water management (OMWM) ponds for mosquito control, resulting in significant shifts in hydrology and, therefore, vegetation cover. The Tuckerton Peninsula is separated down the center by the Great Bay Boulevard, resulting in two separate marshes divided by berms dominated by *P. australis*. While both GBB and Forsythe are located behind NJ's Atlantic coast barrier islands, the GBB site is adjacent to the Great Bay inlet between barrier islands resulting in more intense tidal energy at the southwestern end of the marsh. Within both marshes, lower elevations that experience longer flooding periods are dominated by *S. alterniflora*, while *S. patens* can only be found in clusters at the highest elevations. As a result of increased flooding from sea-level rise

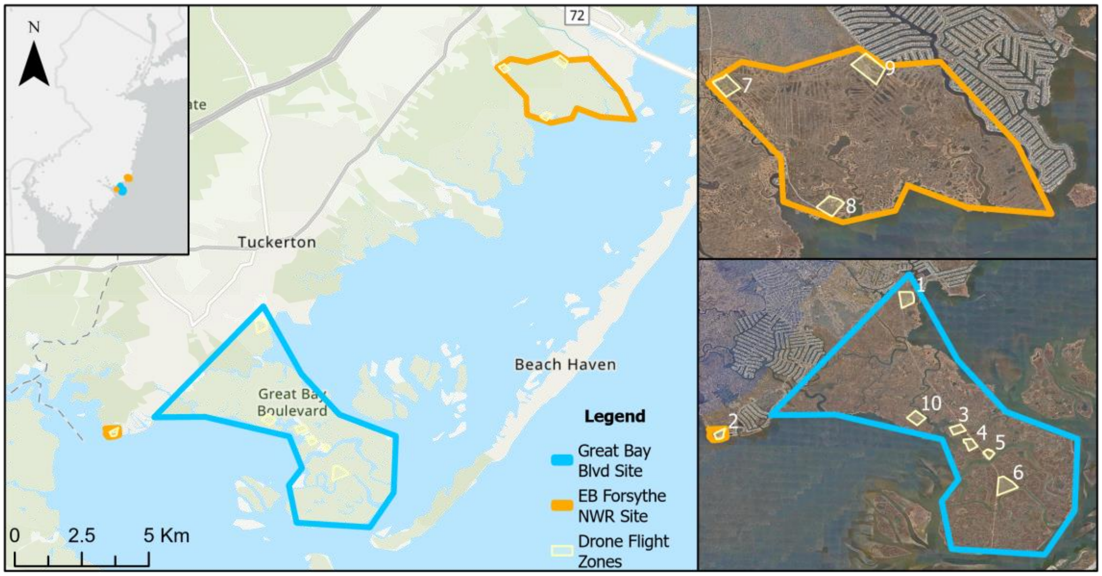

Figure 4.1. Map of salt marshes of interest in the Great Bay Boulevard (GBB, blue polygon) Wetland Management Area and E.B. Forsythe National Wildlife Refuge (orange polygon) for the 2022 and 2023 multispectral, vegetation, and chemistry surveys. In 2022, zones 1-9 were examined, and in 2023, only zones 1 and 10 in GBB and zones 8 and 9 in Forsythe were examined.

and anthropogenic hydrological disturbances, habitat suitable for *S. patens* has been greatly reduced across both marshes.

Vegetation Characterization

2022 Surveys

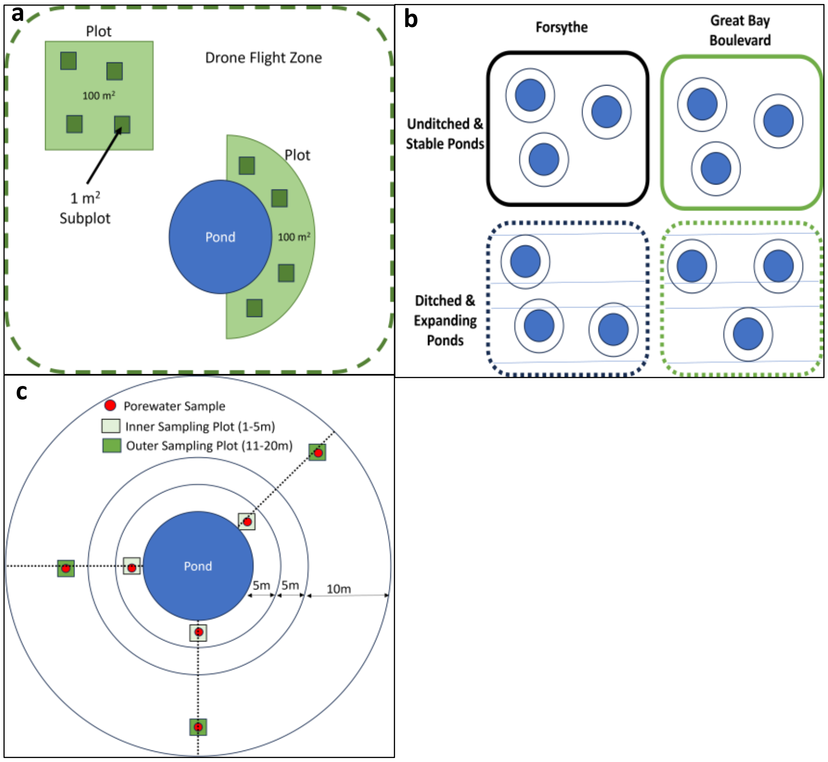

Figure 4.2. Sampling design for the 2022 (a) and 2023 (b &c) field sampling efforts. 2022 plots (a) were selected according to vegetation type and apparent health quality. Additionally, in some cases where vegetation close to ponds seemed to represent poor health condition, a crescent shaped plot was formed around the edge of the pond. In the 2023 design, three ponds were selected in a high (unditched with stable bond boundaries) and low (ditched with unstable pond boundaries) condition area in both the Forsythe and Great Bay Blvd (GBB) sites (b, n=12, ponds varied by two conditions in two sites, replicated in triplicate). Transects were drawn from each pond and a 1 m^2 plot was established within 5 m and within 11-20 m of each pond edge (c, n=2 plots transect^{-1}).

Surveys of GBB and Forsythe took place during the late summer peak vegetation growing season in both 2022 and 2023. In 2022, a factorial design was used to evaluate the relationship between qualitatively defined “healthy” and “unhealthy” units of *S. patens* (representing high marsh) and *S. alterniflora* (low marsh) in both GBB and Forsythe salt marshes (Figures 4.1 and 4.2a) to commonly used multispectral indices. Indices evaluated included normalized difference vegetation index (NDVI), green normalized difference vegetation index (GNDVI), normalized difference red edge (NDRE), and non-photosynthetic vegetation index (NPV). Areas selected for vegetation, chemistry, and drone surveys were designated as “drone flight zones” (herein, referred to as “zones”). Within GBB, five zones were selected, and four zones were selected in Forsythe. Zones were selected based on presence of vegetation cover, accessibility, and clear line of sight for the drone flights. These factors resulted in more suitable zones in GBB compared to Forsythe. One zone of Forsythe (Zone 2) was spatially closer to the GBB and, in analysis, was considered as part of the GBB zones. One GBB zone (Zone 1) and two Forsythe zones (Zones 7 and 9) had mosquito ditches present, while all others were unditched and without Open Marsh Water Management (OMWM) ponds present. Within each zone, at least two 100 m^2 plots of marsh containing vegetation cover of either healthy or unhealthy *S. alterniflora* or *S. patens* were delineated using temporary spray chalk, chosen for its visibility in drone imagery, as well as surveyed using real-time kinematic (RTK) GPS. A total of 32 plots 100 m^2 in area were selected among the nine drone flight zones for vegetation and chemistry surveys (Figure 4.2a). Within the 100 m^2 plots, dominant and additional species were identified and percent cover of each was estimated. Additionally, four 1 m^2 representative subplots were selected within each plot, where percent cover estimation, stem height measurements, and soil penetration depth measurements were collected. Stem height was measured by randomly grabbing a leaf, pulling it taut, and using a meter stick to measure to the apex of the leaf. Flowers and seedheads were not included in stem height measurements. Soil penetration depth measurements were collected following the bearing capacity procedure outlined in the Mid-Atlantic Tidal Wetland Rapid Assessment Method (version 4.1; Demberger et al., 2017).

2023 Surveys

In 2023, using historic imagery of GBB and Forsythe marshes, we selected two areas in the GBB and Forsythe marshes associated with either the presence of mosquito ditches and expanding salt marsh ponds (“ditched”), or without ditching and where pond boundaries had been stable over the last 30 years (“unditched”, Figures 4.2b & 4.3). Additionally, ditched areas displayed a loss of *S. patens* habitat over time, while *S. patens* habitat in unditched areas displayed a more persistent and contiguous habitat over time. Within each of the four areas, three ponds were selected as points of reference for three transects. Along each transect, at random lengths selected through the use of a bounded random number generator, two 1 m^2 plots were established in *S. patens*

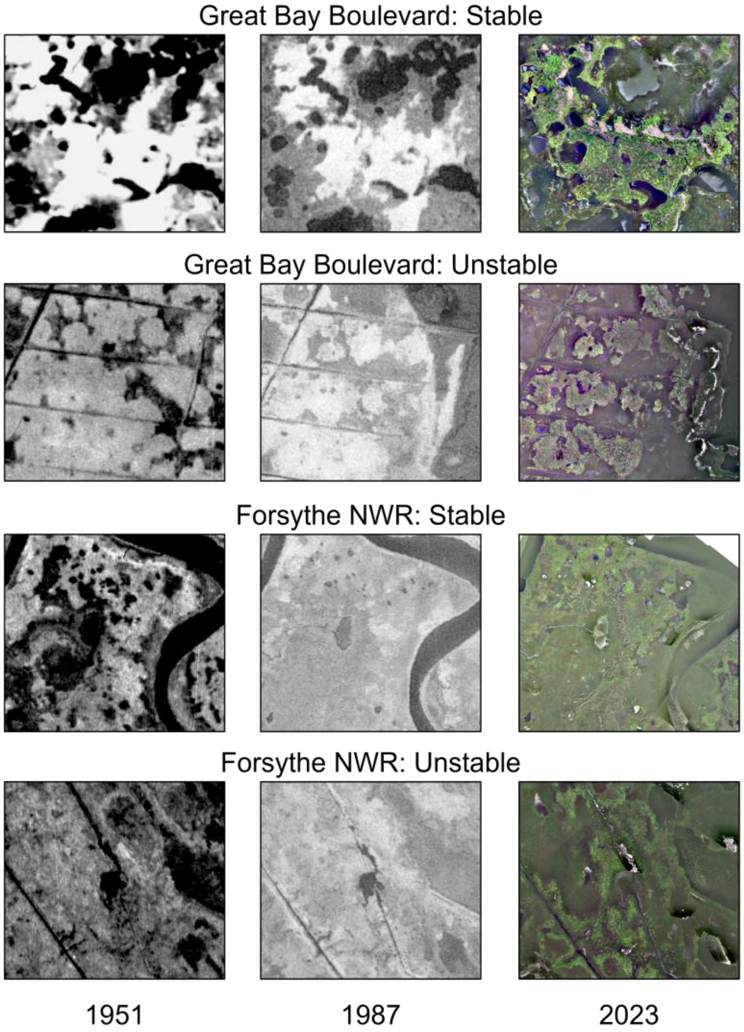

Figure 4.3. NJDEP BGIS satellite (1951, 1987) and drone imagery (2023) of stable and unstable marsh sites in Great Bay Boulevard Wetland Management Area and E. B. Forsythe National Wildlife Refuge selected for study analysis in 2023. Selection of these sites was determined by the change of S. patens cover and pond boundaries from 1951 to 2023.

habitat: one each within 5 m and 11-20 m distance from pond edge (Figure 4.2c). At each of these plots, similar RTK GPS surveying and vegetation measurements as 2022 occurred. This experimental design resulted in three factor levels associated with each plot in the 2023 field data collection effort:

1. Site: “Forsythe” or “GBB”;
2. Condition: “ditched” or “unditched”; and
3. Plot Position: “a” (within 5m) or “b” (within 11-20 m of the associated pond edge).

Soil and Porewater Chemistry

At each subplot (2022) or plot (2023) location, a block of soil (~15 cm wide x ~15 cm long x ~30 cm deep) was removed from the marsh surface to allow access to a fresh, vertical soil profile. All measurements were made 10 cm below the soil surface on the same plane of the hole created in the marsh. Soil temperature was measured by inserting a thermometer directly into the soil on a horizontal plane. Oxidation/reduction potential (ORP) was measured by inserting a sensor into the soil (Extech Instruments ExStik Model RE300 Waterproof ORP meter). Soil pH was measured by inserting a pH sensor (Hanna Instruments Groline Soil pH tester) into the soil. Mean soil chemistry parameters were calculated for each 2022 plot from the measurements made in each subplot within the plot.

Porewater samples were collected from the same location using Rhizon porewater samplers (0.25 mm diameter, 10 cm length, 0.15 µm pore size; Rhizosphere Research Products). Salt marsh porewater samples are often collected from 0–10 cm below the marsh surface where plant roots tend to be the most concentrated (Smith et al., 1979; Bradley & Morris, 1991). In this study, samples were collected from 10 cm below the marsh surface to ensure uniform access to sufficient porewater volume for all samples, even in relatively dry, high elevation marshes. As such, the Rhizon was inserted into the soil horizontally at 10 cm depth. Around 1 mL of porewater was collected into a 12-mL syringe and carefully discarded to rinse the Rhizon and tubing and remove any gas bubbles. Then the syringe was reconnected to the Rhizon and allowed to fill for 1-2 hours. In 2022, even sample volumes from the four subplots within each plot were combined into a single 60-mL syringe to create one composite porewater sample per plot. A composite sampling strategy was used to sample across the spatial heterogeneity within each plot while managing the sample load for the overall project. In 2023, a separate porewater sample was collected and analyzed for each plot. Porewater salinity was measured in the field using a handheld refractometer. The remaining porewater sample was then passed through a 0.2-µm syringe filter with polyethersulfone (PES) membrane into various sample vials for different analyses. For sulfide analysis, 3 mL was dispensed into a 4-mL glass sample vial containing 300 µL of 20% w/v zinc acetate. For chloride and sulfate analysis, 5 mL was dispensed into a 20 mL plastic scintillation vial containing 50 µL of 3.9 N nitric acid. For ammonium analysis, 5 mL was dispensed into a 15-mL centrifuge tube. For conductivity analysis, the remaining volume was collected into a 15-mL centrifuge. All subsamples were kept in a cooler on ice until they were returned to the laboratory, where samples were frozen (ammonium) or refrigerated until analysis.

Sulfide concentrations were measured using the zinc acetate preserved subsample by colorimetric analysis (Cline, 1969). Ammonium concentrations were quantified by colorimetric analysis using a discrete autoanalyzer (Seal AQ300; USEPA Method 350.1, 1993). Chloride and sulfate concentrations were determined via ion chromatography (Schutte et al., 2016). Porewater conductivity was measured using a benchtop conductivity meter (USEPA Method 120.1, 1983).

Multispectral Assessment

Phantom 4 Multispectral drone flights took place in 9 zones in GBB and Forsythe on 8-11 August and 22-25 August, respectively (Figure 4.1). The Phantom 4 Multispectral drone is equipped with six 1/2.9" CMOS sensors, including one RGB sensor for visible light imaging and five monochrome sensors for multispectral imaging. Each sensor has 2.08 MP, the five monochrome sensors capture Blue (B): 450 nm ± 16 nm; Green (G): 560 nm ± 16 nm; Red (R): 650 nm ± 16 nm; Red edge (RE): 730 nm ± 16 nm; Near-infrared (NIR): 840 nm ± 26 nm images. Mapping flights with the Phantom 4 Multispectral were programmed using the DJI Ground Station Pro operating software to fly at 80 m with an 80% front and 70% side photo overlap.

Mapping photos collected with the Phantom 4 Multispectral drone were processed using ESRI Drone2Map software (2022: V2.3; 2023: V2023). Images were adjusted to produce a ground sampling distance of 7.6 cm (3 inches) and used to create a Multispectral Orthomosaic including RGB, RE, and NIR bands. Multispectral indices were calculated using ArcGIS Pro 3.2 (Environmental Systems Research Institute, Redlands, CA) using the Band Arithmetic tool dialog and Raster Calculator (for NPV).

2022 orthomosaic rasters were clipped to the 1 m^2 subplots to generate spatial statistics for each index using the spatial analyst toolbox. In 2023, the drone was flown over each plot for a single, instantaneous photo to create multispectral indices in an effort to reduce the effect of shadows. The 2023 multispectral indices were calculated using the same 2022 methods on each close photo of the 1 m^2 plots, clipping to the edges of the plot within the photos using the flagging as guides.

Statistical Analysis

Statistical analyses were conducted to evaluate the following relationships:

1. Is vegetation cover related to particular soil and porewater parameters, and which multispectral indices related to vegetation percent cover?
2. How do chemical and vegetation parameters vary by the presence of ditching and rapid pond expansion, and could multispectral indices be predicted by a combination of these vegetation stressors?

All statistical calculations were conducted using R (versions 4.1.3 or 4.3.2) open-source statistical software (R Core Team, 2023), and dataset manipulation and summarization were accomplished using the "dplyr" package (v1.0.8). For the 2022 dataset, generalized linear models (R "stats" package v4.1.3) were used to determine the relationship between percent cover, chemical parameters, and multispectral indices due to the non-normality of the data. Percent cover was delineated by species but not health category in order to produce a stronger trend across a range of coverages. A Poisson regression was used for pairwise comparisons of percent cover (as the dependent variable) and chemical parameters (as the independent variables), and a Gaussian link function was applied when comparing multispectral indices (MSIs, as the dependent variables) and percent cover (as the independent variable). Significant models were followed with an ANOVA to determine significance of variables and if they had a significant interaction with site (i.e., Forsythe or GBB). An alpha value of 0.05 was used as the upper threshold in all statistical analyses for determining significance. Elevation measurements were converted into a "position within the tidal prism" metric using tidal datum data from NOAA's Tides & Currents for GBB (station ID: 8534319) and Forsythe at West Creek (station ID: 8533987). At each station, the datums for mean higher high water (MHHW), mean high water, mean tide line, mean low water, and mean lower low water (MLLW) were noted with an estimation of NAVD88 for each site. The elevation of each datum was corrected for sea level rise (datums calculations from 2001) by adding 4mm yr^{-1} (0.013123 ft yr^{-1}) for 22 years, a total increase of 0.289 feet. This was added to each tidal datum, and the elevation of NAVD88 was subtracted from each to produce a current estimate of each datum in 2023 relative to NAVD88 for comparison with *in situ* RTK-GPS collected data. To calculate the position of each sampling plot within the tidal range, the elevation of each plot collected with RTK-GPS (relative to NAVD88) was divided by the calculated position of MHHW per site. Final scores of 1 and 0 indicate that the plot was at MHHW or MLLW, respectively. Values between represent a percentage of distance between MLLW and MHHW.

Following the analysis of the generalized linear models for the 2022 data, and for all 2023 data, a four-step method was applied to each year's dataset to evaluate broader relationships between the MSIs and the vegetation, soil, and porewater metrics. Vegetation, soil, and porewater data are collectively referred to as "ecologic variables" below and were considered the independent variables in this portion of the analysis. As all data were non-linear and did not fit a normal distribution, non-parametric methods and tests were employed.

1) *Evaluation of each ecologic variable:* For each ecologic variable, Kruskal-Wallace tests (R "stats" package version 3.6.2) were employed to determine the presence of statistically significant differences per annual factor level for each ecologic variable within each year (i.e., 2022 factor = site & vegetation health category; 2023 factors = site, condition, & plot). The 'unite' function ("tidyr" package version 1.3.1) was used to combine factor variables into a single variable for testing. Vegetation type and health level were combined into a single factor with four levels in the 2022 data set (healthy and unhealth levels for both *S. alterniflora* and S. *patens).* Site (Forsythe and GBB), Condition (ditched or unditched), and Plot (within 5 m of a pond or 11-20 m from a pond) were combined into a single factor (*n*=8 factor levels) in the 2023 data set. If significant differences were identified, Dunn's Multiple Comparison Test ("dunn.test" version 1.3.6) was used to identify post-hoc differences among factor levels per ecologic metric within each year's data set. Notched boxplots of all ecologic variables across their respective factor levels were produced using the "ggplot2" package. Outliers were identified as data points less than the first quartile minus 1.5x or greater than the third quartile plus 1.5x the interquartile range.
2) *Correlations between MSIs and ecologic variables:* Spearman correlation tests were conducted to evaluate the strength and direction of relationships between the MSIs and all field data using "corrplot" (version 0.92). Correlation matrices were produced and all significant relationships per MSI (*n*=4) were catalogued for advancement to step 3.

3) *Collinearity evaluation:* Mixed-effects linear models were developed for each MSI and their correlated variables from step 2. Collinearity was evaluated for each full MSI model per year using Tolerance and Variance Inflation Factor (VIF) tests in the "olsrr" package (v0.5.3). Tolerance describes the percent of model variability that cannot be explained by other variables, and the VIF measures the inflation of the coefficient of each ecologic variable in the model due to collinearity with other ecological variables. After an initial evaluation of each model, ecologic variables with a Tolerance ≤ 0.4 and a VIF > 3 were removed. Reduced models were subsequently re-run and professional judgment was used to drop additional variables with direct relationships that could produce confounding model results. For example, if the final model included soil ORP and ammonia, ORP was removed as that parameter describes the conditions that facilitate ammonia concentrations. Professional selection prioritized the result (ammonia) over the associated conditioning variable (here, ORP), as there may be other conditions that affect the result variable not accounted for in our dataset. The final model (*MSI ~ ecologic variable 1* ecologic variable 2* … ecologic variable n + 1|effect*) was advanced to step 4.
4) *Model evaluation:* Relationships between MSIs and their remaining correlated ecologic variables were evaluated using full interactive mixed effects models ('lmer' function in the "lme4" package v1.1.32) holding site as a random effect for each year's data set. Each model (per MSI per year) was evaluated against a null model based on lowest Akaike Information Criterion scores (AIC, estimator of relative model quality). A secondary analysis was conducted to confirm the outcome of the initial model comparison using a stepwise regression approach ('step' function, "MASS" package version 7.3-60.0.1). If the addition of ecologic variables did not increase the fit of the null model (greater or equal AIC score), it was concluded that the ecologic variables included in the full model were not suitable predictors for the variability in the associated MSI. If the addition of some ecologic variables resulted in a better fit over the null model (lower AIC score), these variables were included in a secondary model that was subsequently evaluated using ANOVA to check for significant singular and interactive effects. AS this step of the analysis was exploratory and confirmational, all terms with lower AIC scores were included for exploration of significant relationships. Plots for all significant relationships between each MSI and ecologic variables were produced using "ggplot2". All model evaluation statistics, including AIC, step-wide parameter addition scores, and significant outcomes, are reported in the results section.

Results and Discussion

2022 Results and Discussion

Measurements of percent cover, stem height, and penetration depth show that the selection of healthy and unhealthy forms of *S. patens* and *S. alterniflora* were too similar to significantly distinguish within species by health category, except for *S. alterniflora* percent cover (Figure 4.4 and Table 4.1). Healthy *S.*

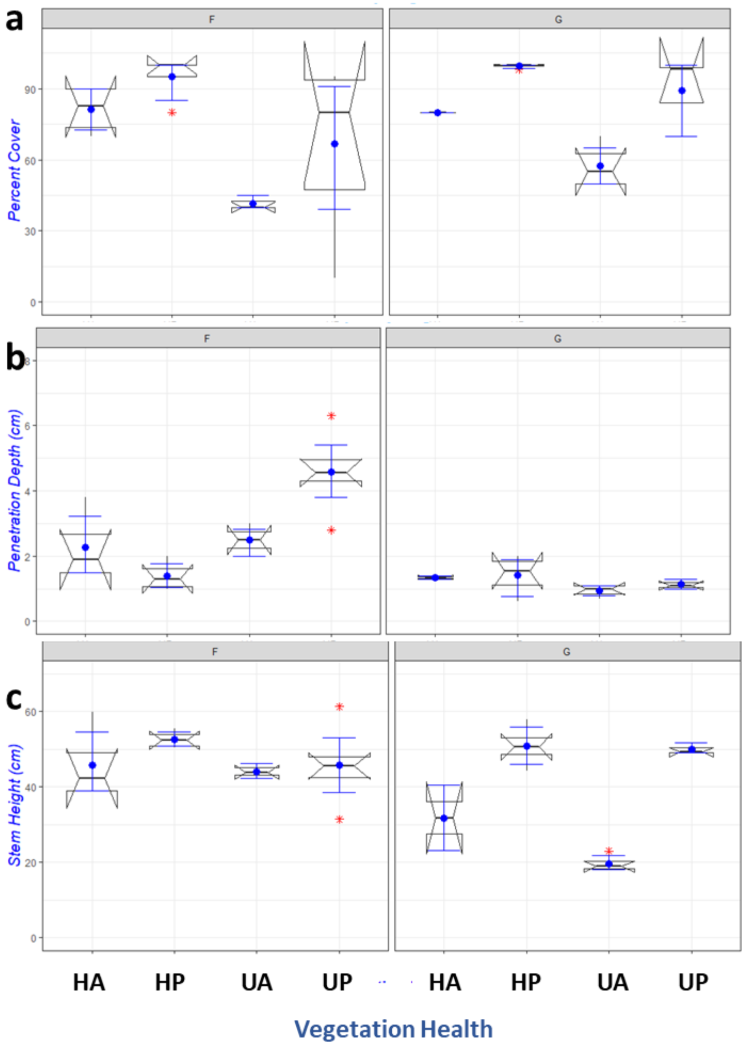

*Figure 4.4. Notched boxplots of total percent cover (a), penetration depth (b), and mean stem height (c) by Site (F= Forsythe, G = Great Bay Blvd) and vegetation health category (HA = healthy S. alterniflora, HP = healthy S. patens, UA= unhealthy S. alterniflora, and UP = unhealthy S. patens). Bounds of box represent the 25% (bottom) and 75% (top) interquartile range, black line near center of notches indicates the median, blue dot identifies the mean, whiskers depict the min and max values, and red stars denote outliers calculated as (min-(1.5*IQR) & max+(1.5*IQR)). IQR = Interquartile Range. The notch displays a confidence interval around the median (+/- 1.58*IQR/sqrt(n)). Notches are used to compare groups. If the notches of two boxes do not overlap, this is an indication that the medians differ. "Ears", or the triangles in the corners of the interquartile range limits denote that the data are either skewed or sample size is low.*

Table 4.1. Results of Kruskal-Wallace and Dunn Multiple Comparison post-hoc tests ("pair-wise difference" column) for vegetation ecologic variables. Pair-wise difference notations are as follows: HA = healthy S. alterniflora, HP = healthy S. patens, UA= unhealthy S. alterniflora, and UP = unhealthy S. patens.

Vegetation Parameter	**Test Type**	X^2	***p*-value**	**Pair-wise Differences**
Percent Cover	Kruskal-Wallis	17.6	$5.27e^{-4}$	All HP:UA (*p*=$8.80e^{-5}$) All HP:UP (*p*=$5.14e^{-2}$)
Stem Height	Kruskal-Wallis	13.6	$3.50e^{-3}$	All HP:UA (*p*=$1.41e^{-3}$)
Penetration Depth	Kruskal-Wallis	22.6	$2.84e^{-4}$	F:G across all plot types

alterniflora plots had a significantly larger mean percent cover (81 ± 3%) compared to unhealthy plots (51 ± 4%), while *S. patens* plots had generally high average cover regardless of health category (85 ± 6.1%).

This difference is likely a result of *S. patens* growing long and thin leaves that have a tendency to create layers of foliage which appear as dense canopy cover. Mean stem height of unhealthy *S. patens* plots was 9% shorter (47 ± 3.0 cm) than healthy *S. patens* stem heights, which averaged 51.8 ± 1.4 cm. In *S. alterniflora* plots, unhealthy stem heights were 27% shorter (30 ± 5.0 cm) than healthy stem heights, which averaged 41.1 ± 4.8 cm. Penetration depth was not found to be statistically different between either vegetation species or health category but was found to be significantly different between the two sites, showing that Forsythe has approximately a 2.4x weaker soil matrix than GBB. Increased penetration depth could be a symptom of increased saturation, resulting in a destabilized soil matrix (Twohig and Stolt, 2011; Wigand et al., 2018).

Chemical parameters largely differed between species within a health category, but not necessarily within a species (Table 4.2, 4.3). Overall, *S. patens* plots were more acidic and oxidized, and had lower ammonia and sulfide concentrations in the porewater. High sulfide and ammonium concentrations have been associated with waterlogged conditions as a result of decreased demand from slower growing and dying vegetation (Ewing et al., 1997; Himmelstein et al., 2021; van Katwijk et al., 1997). The lower concentrations in conjunction with higher ORP suggests that the *S. patens* within the areas we initially labeled as a binary of "healthy" and "unhealthy" could potentially be within the range of "healthy" conditions. Primary categorical differences were found when comparing healthy *S. patens* plots with both healthy and unhealthy *S. alterniflora* plots. Healthy *S. patens* plots had an average ORP of 235 ± 32 mV, while all *S. alterniflora* plots were much more reduced (-52.2 ± 29.5mV). The oxidized conditions of the healthy *S. patens* plots contributed to an average 99.6% decrease in sulfide concentration compared to *S. alterniflora* plots, although variability was high across both species plot types. Additionally, ammonia was significantly greater (by 87%) in unhealthy *S. alterniflora* plots compared to both healthy and unhealthy *S. patens* plots. *S. alterniflora* has a competitive advantage in that it can withstand greater inundation of its roots, allowing the species to grow at lower elevations than *S. patens*. Higher ammonia and sulfide concentrations in *S. alterniflora* plots is somewhat expected due to the increased saturation, but sulfide concentrations can be somewhat controlled and inhibited by *S. alterniflora* aeration of the soil by its roots (Mendelssohn and Morris, 2000). However, these elevated levels of ammonia in the *S. alterniflora* plots are similar to ranges of sulfide and ammonia concentrations in unstable marshes as reported by

Table 4.2. Means ± standard error of the means for each ecologic variable per vegetation health level (i.e., healthy or unhealthy).

Condition	pH	Salinity (ppt)	Conductivity (mS cm^{-1})	ORP (mV)	Ammonia (μmol L^{-1})	Chloride (mmol L^{-1})	Sulfate (mmol L^{-1})	Sulfate Depletion (mmol L^{-1})	Sulfide (μmol L^{-1})	Water Table Depth (cm)
S. alterniflora	**6.12 ± 0.15**	**40.7 ± 2.67**	**55.3 ± 3.18**	**-52.2 ± 29.5**	**133 ± 29.2**	**584 ± 40.8**	**22.9 ± 3.20**	**7.28 ± 2.01**	**12500 ± 2210**	**8.20 ± 2.85**
Healthy	6.13 ± 0.21	38.9 ± 3.75	52.0 ± 4.62	-35.1 ± 50.3	98.6 ± 33.6	540 ± 57.4	20.9 ± 5.24	7.01 ± 3.48	12300 ± 3290	7.75 ± 2.24
Unhealthy	6.12 ± 0.23	42.9 ± 3.94	59.1 ± 4.20	-71.7 ± 29.5	173 ± 47.5	634 ± 56.0	25.2 ± 3.61	7.59 ± 1.99	12700 ± 3150	8.71 ± 5.82
S. patens	**4.45 ± 0.38**	**33.9 ± 2.41**	**43.5 ± 2.14**	**150 ± 37.1**	**21.8 ± 4.2**	**431 ± 24.2**	**29.4 ± 3.84**	**-7.13 ± 2.98**	**1930 ± 973**	**10.5 ± 2.19**
Healthy	3.65 ± 0.26	32.4 ± 3.25	43.5 ± 3.82	235 ± 31.8	15.6 ± 2.22	410 ± 40.6	32.1 ± 5.14	-11.0 ± 3.37	44.9 ± 43.2	14.3 ± 1.56
Unhealthy	5.16 ± 0.61	35.2 ± 3.64	43.6 ± 2.26	73.7 ± 53.6	27.3 ± 7.34	452 ± 27.0	26.7 ± 5.89	-3.31 ± 4.76	3610 ± 1680	7.22 ± 3.64

Table 4.3. Results of Kruskal-Wallace and Dunn Multiple Comparison post-hoc tests ("pair-wise difference" column) for soil ecologic variables. Pair-wise difference notations are as follows: HA = healthy S. alterniflora, HP = healthy S. patens, UA= unhealthy S. alterniflora, and UP = unhealthy S. patens.

Chemical Parameter	X^2	*p*-value	Pairwise Differences
pH	10.5	0.014	All HP:UA (p = 1.70e^{-2})
Salinity	13.1	2.88e^{-4}	F:G across all plot types
Conductivity	8.77	0.033	All HP:UA (p = 2.30e^{-2})
ORP	14.2	0.003	HP:HA (p = 1.50e^{-2}) & UA (p =1.00e^{-3})
Ammonia	13.6	0.004	HP:HA (p = 7.00e^{-3}) & UA (p = 1.00e^{-3})
Chloride	9.10	0.028	All HP:UA (p = 1.10e^{-2})
Sulfate	8.54	0.003	F:G across all plot types
Sulfate Depletion	13.1	0.005	All HP:UA (p = 2.00e^{-3})
Sulfide	15.1	0.002	HP:HA (p = 1.30e^{-3}) & UA (p = 1.00e^{-3})
Water Table Depth	6.82	0.078	F:G across all plot types

Himmelstein et al. (2021), suggesting that areas of these marshes containing *S. alterniflora* may be at a high vulnerability state rather than at an equilibrium.

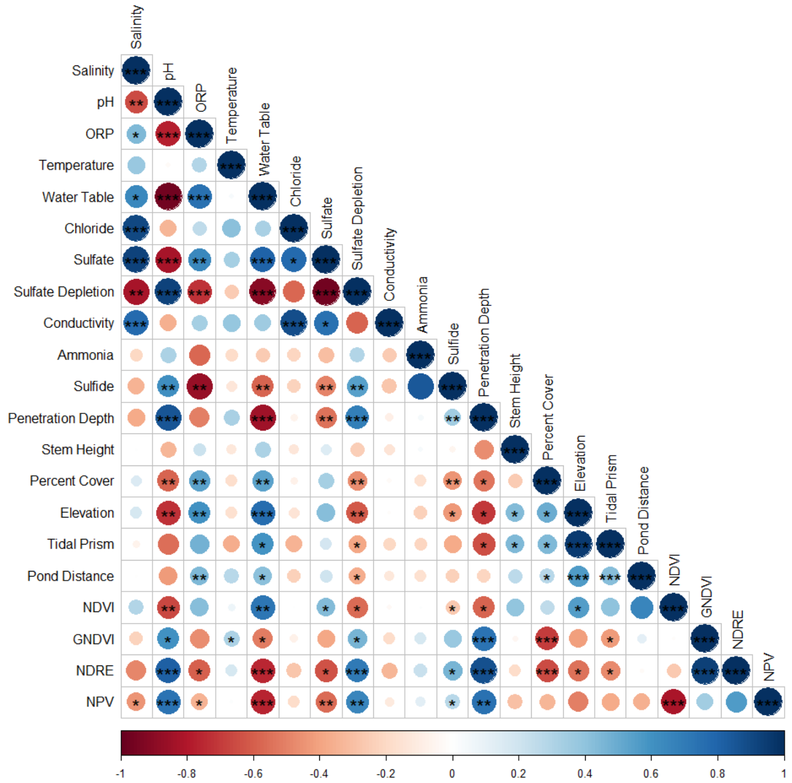

Figure 4.5. Correlation matrix for multispectral indices (MSIs) and ecologic variables from the S. patens 2022 field effort. All parameters are noted along both axes. MSIs are located at the bottom of the y-axis and are fully capitalized. Dot size indicates the strength of the correlation (larger=stronger), and color denotes the direction (blue=positive & red=negative). The number of asterisks describes the strength of the correlation at the following alpha levels: "": p=0.1; "**": p=0.01; and "***": p=0.001.*

Other parameters, including salinity and water table depth, significantly differed between sites but not health status (Table 4.3). Both salinity and water table depth were overall higher in GBB, likely due to differences in geographic positioning between Forsythe and GBB. Forsythe resides within Manahawkin Bay behind barrier islands, resulting in a smaller tidal prism and more freshwater mixing, whereas GBB is positioned at the Great Bay inlet and is more influenced by marine conditions of higher tidal flux and more saline conditions (Kennish, 2001). The shallower water table within Forsythe plots additionally corroborates with our earlier suggestion that Forsythe has a weaker soil matrix as a result of increased saturation.

Results of generalized linear models showed that vegetation percent cover was correlated with multiple chemical parameters, independent of health category, primarily within the *S. patens* plots (Figures 4.5 and 4.6). The strongest regressions were of percent cover against pH and ORP, with an increase in percent cover when there was a decrease in pH and an increase in ORP (Figures 4.7a and 4.7b, respectively, and Table 4.4). An increase in *S. patens* percent cover was additionally correlated with an increase in sulfate and decreases in chloride, sulfate depletion, and sulfide concentrations. While R^2 values were consistently low (<0.30) across all vegetation, these relationships have been reported in literature. Known phytotoxins, sulfides are produced in reduced, non-acidic conditions (Ewing et al., 1997; Lamers et al., 2013). Therefore, a percent cover decrease in *S. patens* is expected under lower ORP, shallower water table (Figure 4.8a and Table 4.4), and more acidic conditions. Additionally, salinity (and, thereby, chloride

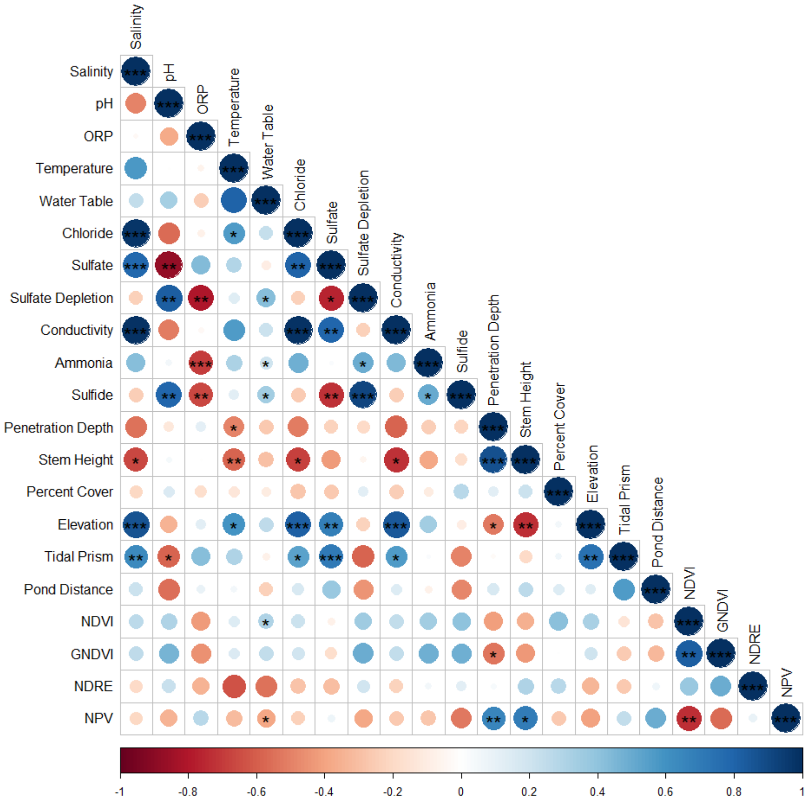

Figure 4.6. Correlation matrix for multispectral indices (MSIs) and ecologic variables from the S. alterniflora 2022 field effort. All parameters are noted along both axes. MSIs are located at the bottom of the y-axis and are fully capitalized. Dot size indicates the strength of the correlation (larger=stronger), and color denotes the direction (blue=positive & red=negative). The number of asterisks describes the strength of the correlation at the following alpha levels: "": p=0.1; "**": p=0.01; and "***": p=0.001.*

concentrations) is another stressor on vegetation, so it is expected that an increase in chloride concentrations would result in a decrease in percent cover (Merino et al., 2010, Figure 4.8b and Table 4.4). The results of *S. alterniflora* regressions all had R^2s below 0.10 and could not be interpreted the same way as *the S. patens* regressions. This is largely due to *S. alterniflora*'s ability as a species to grow in a variety of conditions, despite the presence of stressors, compared to *S. patens* (Bertness, 1991). For example, Wilburn et al. (2024) found that when growing *S. alterniflora* in a range of nutrient concentrations derived from organic material, neither the aboveground nor belowground biomass differed significantly. This finding in conjunction with our study results suggests that percent cover may be more strongly related to soil conditions within the *S. patens* plots rather than *S. alterniflora* plots (Figure 4.9 and Table 4.4).

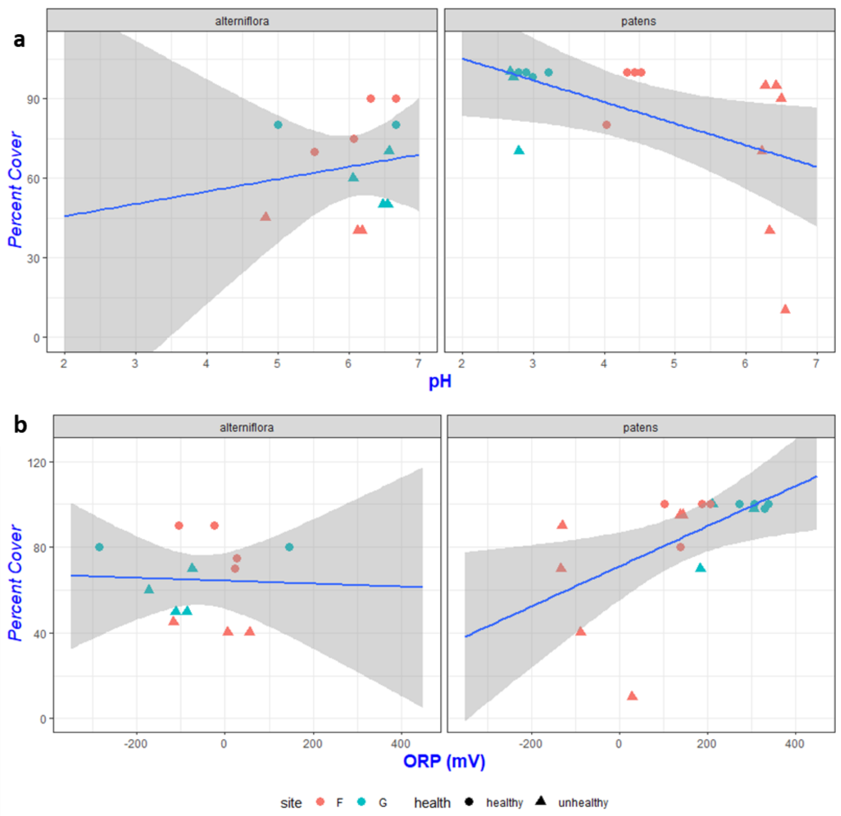

Figure 4.7. Results of the random effects model of the effects of pH (a) and oxidation reduction potential (ORP, b) on vegetation percent cover Site was included as a random effect and is denoted by point color: Forsythe = "F" in red, and Great Bay Blvd = "G" blue. Health condition is displayed as a circle for healthy and as a triangle for unhealth plots. The blue line and grey shaded area depict the linear regression with 95% confidence interval, respectively. Of note, percent cover ranges 0%-100%. Calculated confidence intervals that exceed those bounds were included for transparency but are not values that could be observed in situ.

Table 4.4. Results of generalized linear model regression of relationships between vegetation percent cover by vegetation type (S. alterniflora and S. patens) with two soil (pH & ORP), three porewater (sulfate, sulfate depletion, sulfide), and water table depth metrics. Model p-values are for the full model, not partitioned by vegetation, and R^2 values represent the proportion of the variability in the full model explained by each vegetation component.

Ecologic Variable	***p*-value**	***S. alterniflora* Regression**	***R²***	***S. patens* Regression**	***R²***
pH	0.0063	y = 4.7x + 36	0.02	y = -8.2x + 121	0.26
ORP	2.52e-08	y = -8.5x + 84	0.03	y = 69x - 95	0.26
Sulfate	0.0003	y = -0.36x + 73	0.07	y = 0.56x + 69	0.11
Sulfate Depletion	0.0017	y = 0.29x + 63	0.02	y = -x + 79	0.21
Sulfide	6.23e-07	y = 0.0006x + 58	0.07	y = -0.003x + 90	0.17
Water Table Depth	4.31e-05	y = -0.17x + 66	0.01	y = 1.3x + 71	0.22

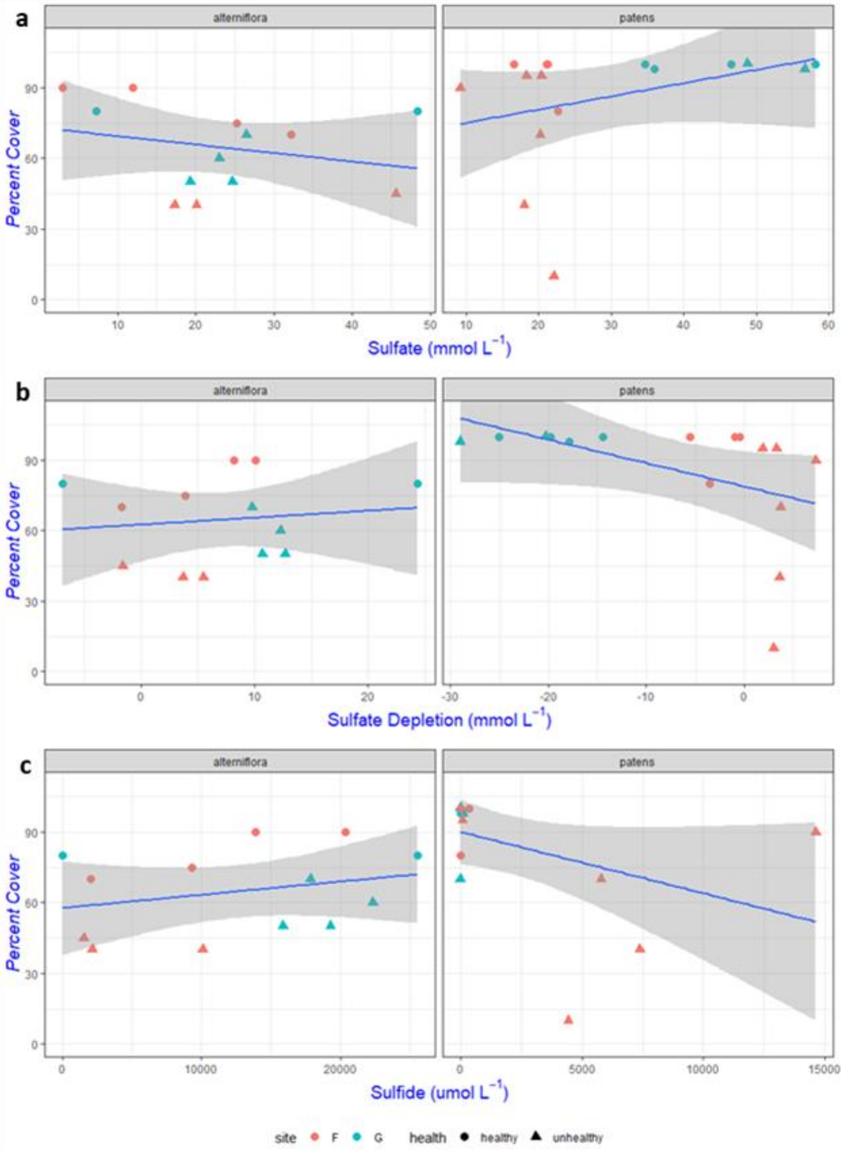

Figure 4.8. Results of the random effects model of the effects of sulfate (a), sulfate depletion (b), and sulfide (c) on vegetation percent cover Site was included as a random effect and is denoted by point color: Forsythe = "F" in red, and Great Bay Blvd = "G" blue. Health condition is displayed as a circle for healthy and as a triangle for unhealth plots. The blue line and grey shaded area depict the linear regression with 95% confidence interval, respectively. Of note, percent cover ranges 0%-100%. Calculated confidence intervals that exceed those bounds were included for transparency but are not values that could be observed in situ.

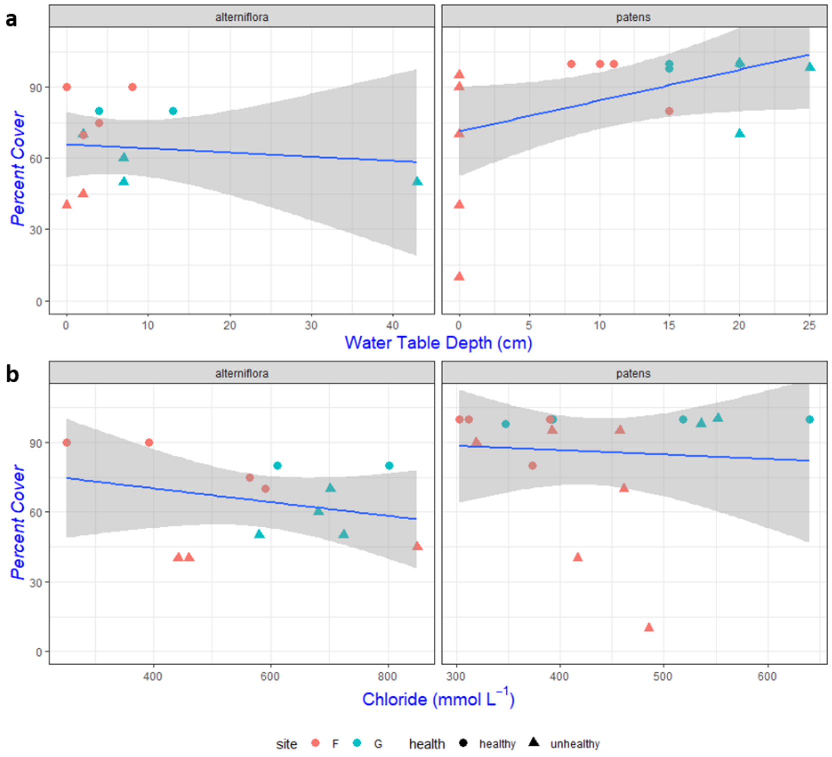

Figure 4.9. Results of the random effects model of the effects of water table depth (a) and chloride (b) on vegetation percent cover Site was included as a random effect and is denoted by point color: Forsythe = "F" in red, and Great Bay Blvd = "G" blue. Health condition is displayed as a circle for healthy and as a triangle for unhealth plots. The blue line and grey shaded area depict the linear regression with 95% confidence interval, respectively. Of note, percent cover ranges 0%-100%. Calculated confidence intervals that exceed those bounds were included for transparency but are not values that could be observed in situ.

Multispectral index (MSI) generalized linear models found a similar pattern as above, where *S. alterniflora* plot percent cover did significantly correlate with MSIs, but *S. patens* plots showed some stronger relationships (Figure 4.10 and Table 4.5). In both *S. alterniflora* and *S. patens* plots, NDVI and NPV models were insignificant with low R^2 values. The GNDVI linear model for *S. patens*, although statistically insignificant, showed that GNDVI decreased as percent cover increased and had an R^2 of 0.46. Only NDRE had a statistically significant model for *S. patens* plots, whereas NDRE decreased, percent cover increased (R^2 = 0.43). Examining the multispectral indices by vegetation health categories, we found significant differences between healthy *S. patens* vs. all *S. alterniflora* plots but not unhealthy *S. patens* plots in GNDVI and NDRE, suggesting that these indices may be beneficial for identifying areas of healthy *S. patens* (Figures 4.11 and 4.12). The GNDVI and NDRE indices have typically been associated with chlorophyll and nitrogen content, where higher values represent increased "greenness" and, thus, healthier vegetation. However, similar to the generalized linear models, healthy *S. patens* plots had lower values of GNDVI and NDRE than unhealthy (Figures 4.11b and 4.12a, respectively, and Table 4.6). We hypothesize that nitrogen uptake is reduced due to increased competition as *S. patens* expands in cover, resulting in a decrease in GNDVI and NDRE values. This also could explain the decrease in ammonia concentrations as percent cover of *S. patens* increases. On the other hand, NDVI was not able to detect any differences among vegetation

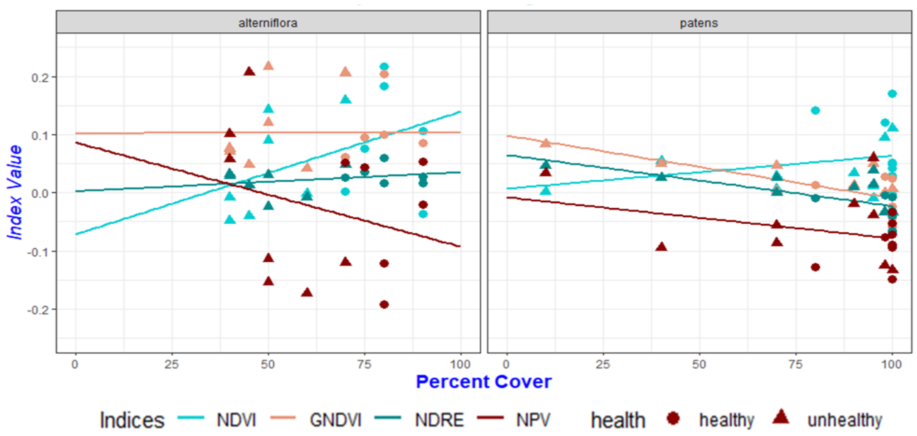

Figure 4.10. Results of generalized liner models for S. alterniflora and S. patens percent cover and each multispectral index: Normalized Difference Vegetation Index (NDVI, light blue), Green Normalized Difference Vegetation Index (GNDVI, pink), Normalized Difference Red Edge index (NDRE, green), and Non-Photosynthetic Vegetation index (NPV, dark red). Shape indicated the health status of each plot: circle = healthy and triangle = unhealthy.

Table 4.5. Results of a generalized linear model regression of relationships between vegetation percent cover by vegetation type (S. alterniflora and S. patens) and the multispectral indices: Normalized Difference Vegetation Index (NDVI), Green Normalized Difference Vegetation Index (GNDVI), Normalized Difference Red Edge index (NDRE), and Non-Photosynthetic Vegetation index (NPV). Model p-values are for the full model, not partitioned by vegetation, and R^2 *values represent the proportion of the variability in the full model explained by each vegetation component.*

Multispectral Index	***p*-value**	***S. alterniflora* Regression**	***R*^{2}**	***S. patens* Regression**	***R*^{2}**
NDVI	0.25	y = 0.002x – 0.07	0.17	y = 0.0006x + 0.007	0.07
GNDVI	0.26	y = 0x + 0.1	0	y = -0.001x – 0.1	0.46
NDRE	0.02	y = 0.0003x + 0.002	0.07	y = -0.0009x + 0.07	0.43
NPV	0.53	y = -0.002x + 0.09	0.07	y = -0.0007x – 0.008	0.1

types, but it did show that GBB had a significantly higher range of NDVI values than Forsythe, suggesting that GBB vegetation contained more chlorophyll and a denser canopy (Figure 4.11a and Table 4.6). Values of NPV varied by both vegetation and site. Forsythe had generally higher values of NPV compared to GBB, and Forsythe *S. alterniflora* plots were higher than *S. patens* plots, suggesting that thatch and bare soil were more visible through the canopy. In GBB, however, NPV values were statistically insignificant from each other, potentially as a result of the denser canopy across the site as suggested by the NDVI (Figure 4.12b and Table 4.6).

In order to determine if multispectral indices could be predicted by ecologic variables aside from percent cover, variables were selected from significant relationships found in non-parametric Spearman correlation matrices (Figures 4.5 and 4.6, and Table 4.7). Linear mixed effects models were only produced for *S. patens* plots due to high variability and lack of relationships found between the multispectral indices and ecologic variables within *S. alterniflora* plots. However, some limited relationships were found within the *S. alterniflora* plots, such as a positive correlation between NDVI and water table depth ($\rho = 0.7$; $p < 0.05$); a negative correlation between GNDVI and penetration depth ($\rho = -0.6$; $p < 0.05$); a negative correlation between NPV and water table depth (ρ = -0.7; p < 0.05); and a positive correlation between NPV and penetration depth (ρ = 0.8; p < 0.01) and stem height (ρ = 0.7; p < 0.05). These relationships were not modeled due to the lack of inclusion of both a vegetation and soil/porewater predictor for any particular multispectral index. Within *S. patens* plots, the NDVI variance could not be explained better than the null model through the inclusion of additional ecologic variables; however, GNDVI, NDRE, and NPV were able to explain the variance of the data better than the null models.

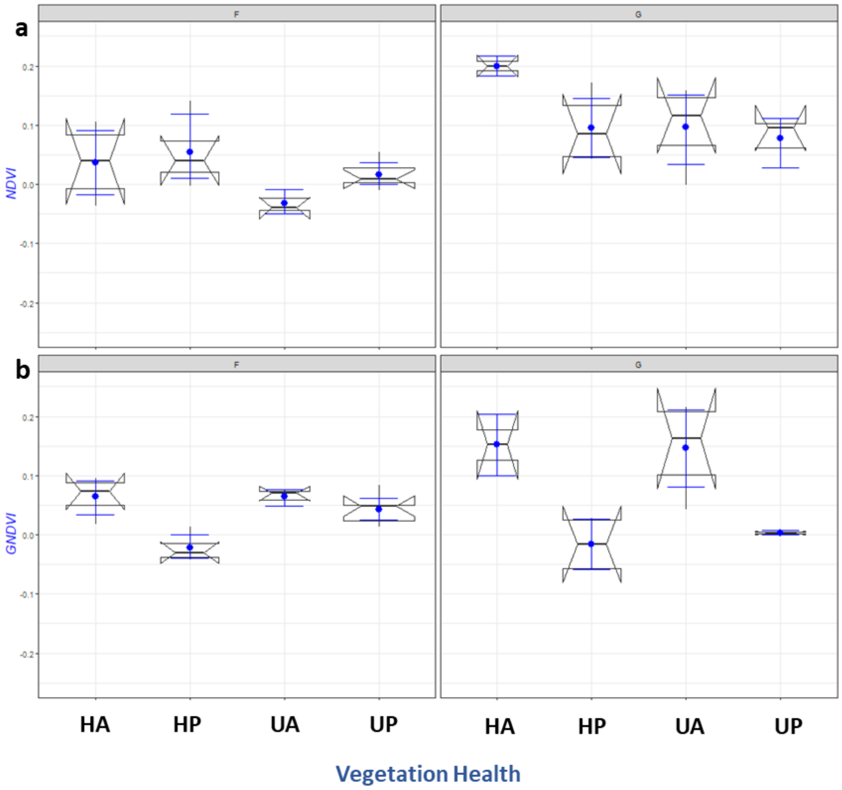

*Figure 4.11. Notched boxplots of Normalized Difference Vegetation (NDVI, a) and the Green Normalized Difference Vegetation (GNDVI, b) multispectral indices. Vegetation health categories are: HA = healthy S. alterniflora, HP = healthy S. patens, UA= unhealthy S. alterniflora, and UP = unhealthy S. patens. Bounds of box represent the 25% (bottom) and 75% (top)m interquartile range, black line near center of notches indicates the median, blue dot identifies the mean, whiskers depict the min and max values, and red stars denote outliers calculated as (min-(1.5*IQR) & max+(1.5*IQR)). IQR = Interquartile Range. The notch displays a confidence interval around the median (+/- 1.58*IQR/sqrt(n)). Notches are used to compare groups. If the notches of two boxes do not overlap, this is an indication that the medians differ. "Ears", or the triangle in the corner of the interquartile range limits denote that the data are either skewed or sample size is low.*

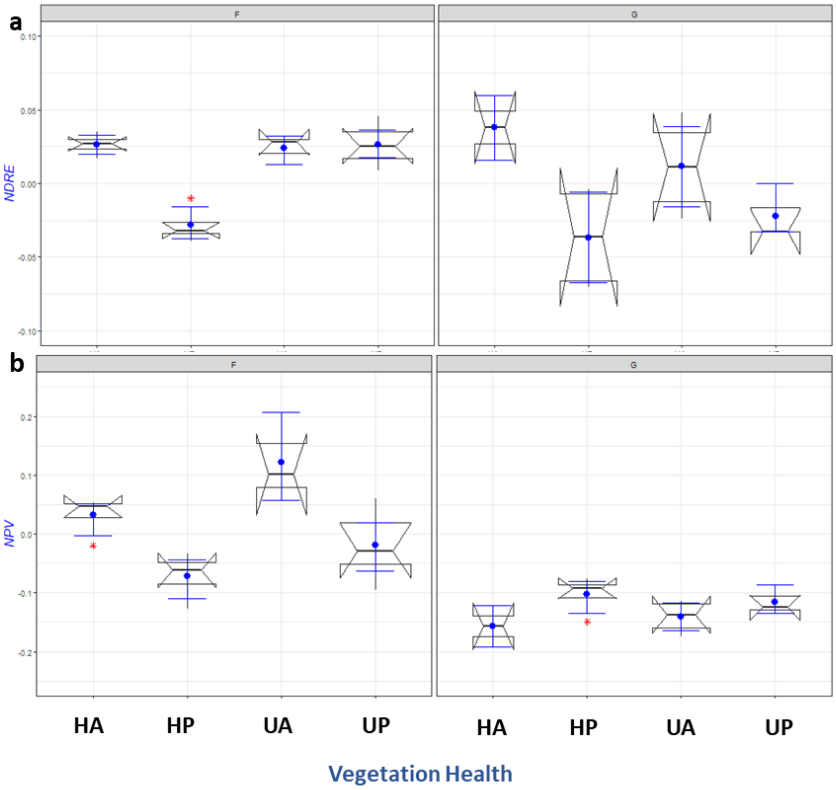

*Figure 4.12. Notched boxplots of the Normalized Difference Red Edge (NDRE, a) and Non-Photosynthetic Vegetation (NPV, b) multispectral indices. Vegetation health categories are: HA = healthy S. alterniflora, HP = healthy S. patens, UA= unhealthy S. alterniflora, and UP = unhealthy S. patens. Bounds of box represent the 25% (bottom) and 75% (top)m interquartile range, black line near center of notches indicates the median, blue dot identifies the mean, whiskers depict the min and max values, and red stars denote outliers calculated as (min-(1.5*IQR) & max+(1.5*IQR)). IQR = Interquartile Range. The notch displays a confidence interval around the median (+/- 1.58*IQR/sqrt(n)). Notches are used to compare groups. If the notches of two boxes do not overlap, this is an indication that the medians differ. "Ears", or the triangle in the corner of the interquartile range limits denote that the data are either skewed or sample size is low.*

Table 4.6. Results of Kruskal-Wallace and Dunn Multiple Comparison post-hoc and ANOVA with Tukey Test of Honestly Significant Differences post-hoc tests ("pair-wise difference" column) for the multispectral indices (MSIs). MSIs= Normalized Difference Vegetation Index (NDVI), Green Normalized Difference Vegetation Index (GNDVI), Normalized Difference Red Edge index (NDRE), and Non-Photosynthetic Vegetation index (NPV). Pair-wise difference notations are as follows: F=Forsythe, G=Great Bay Blvd, HA = healthy S. alterniflora, HP = healthy S. patens, UA= unhealthy S. alterniflora, and UP = unhealthy S. patens.

Vegetation Parameter	**Test Type**	***p*-value**	**Pair-wise Differences**
NDVI	ANOVA	1.19e^{-4}	F:G across all plot types
GNDVI	Kruskal-Wallis	2.87^{-3}	G UA:F HP (p=1.97e-2)
NDRE	ANOVA	1.10e^{-4}	HP:HA (p=9.47e-3) HP:UA (p=2.33e-2) HP:UP (p=4.39e-3)
NPV	ANOVA	4.67e^{-4}	F HA:all G plots (p<8.28e-3) F HP:F UA (p<1.00e-3) F UA:F UP and all G plots (p<5.29e-3) F UP:G HA and G UA plots (p<2.42e-2)

*Table 4.7. Non-parametric Spearman correlation coefficients (ρ) of significant relationships between multispectral indices and chemical, vegetation, and geologic parameters in S. patens plots. Positive ρ values and green shading represent positive relationships, and negative ρ values and orange shading represent negative relationships. Insignificant relationships are denoted by a dash and no shading. Significance level: *, p < 0.05; **, p < 0.01; ***, p < 0.001.*

	NDVI	**GDNVI**	**NDRE**	**NPV**
Ammonia	-	-	-	-
Chloride	-	-	-	-
Conductivity	-	-	-	-
Elevation	0.5*	-	-0.6*	-
ORP	-	-	-0.6*	-0.5*
Penetration Depth	-0.6*	0.8***	0.9***	0.7**
Percent Cover	-	-0.8***	-0.8***	-
pH	-0.6*	0.6*	0.8***	0.8***
Pond Distance	-	-	-	-
Salinity	-	-	-	-0.5*
Stem Height	-	-	-	-
Sulfate	0.6*	-	-0.6*	-
Sulfate Depletion	-0.6*	0.6*	0.8***	-0.6**
Sulfide	-0.5*	-	0.6*	0.5*
Tidal Prism	-	-0.6*	-0.6*	-
Water Table Depth	0.7**	-0.6*	-0.8***	-0.8***

Results from tolerance and variance inflation factor (VIF) analyses were analyzed as described in the statistical analysis section (Step 3 – Collinearity evaluation) to reduce collinearity among initial correlated model variables. Initial model variables, per multispectral index (MSI), were as follows:

1. Green Normalized Difference Vegetation Index (GNDVI): sulfate depletion, percent cover, and tidal prism.
2. Normalized Difference Red Edge (NDRE): sulfate, percent cover, and tidal prism.
3. Normalized Difference Vegetation Index (NDVI): sulfate, sulfide, and elevation.
4. Non-Photosynthetic Vegetation (NPV): sulfide and penetration depth mean.

Removal of collinear variables resulted in only GNDVI and NDRE models containing at least one vegetation and one chemistry metric. Comparison of these reduced models to null models, however, demonstrated that the MSI data could not be significantly explained by the chosen predictors alone. Additionally, none of these models were found to be significantly predictive with or without interactive terms, and, therefore, only serve as comparisons for the 2023 results.

2023 Results & Discussion

The low-flying method for photo collection employed in the 2023 field effort resulted in generally reduced shadowing, but the vegetation morphology itself resulted in unavoidable shadows due to bending and "cow-licked" shapes in the dense vegetation patches. Additionally, photo collection time increased with the lower altitude, resulting in longer collection times for groups of plots and greater variability in sun's position throughout the sampling day. This contributed to additional among-plot shadow variability. Although flying at a lower altitude reduced vegetation-based shadows, it increased sun-shadowing effects. Future efforts can evaluate how to minimize shadow effects through a balance of flight altitude and sampling time.

All ecologic variables had at least one pairwise difference as identified through the Kruskal-Wallace and Dunn pair-wise comparison post-hoc tests (Table 4.8), but there was no evidence that site, condition, and plot position comprehensively influenced any of the ecologic variables, except for elevation and tidal position. Total vegetation and *S. patens* percent cover were strongly correlated (Figure 4.13) as expected since plots were selected with *S. patens* as the dominant vegetation type (Figure 4.14a and 4.14b). Mean stem height did not significantly differ among plots (Table 4.8 and Figure 4.14c). Forsythe ditched plots "a" and "b" had a greater range of *S. patens* cover relative to their range of total percent cover due to the presence of some *S. alterniflora & D. spicata* (Figure 4.14a and 4.14b), which reflect slightly wetter conditions relative to the Forsythe unditched and GBB plots (ditched and unditched).

Stevenson et al. (1986) found that marshes with small tidal ranges are prone to waterlogging, and this may be occurring here due to the low elevations, a shallow water table, and greater access of water to the marsh interior via the ditching. Converting elevation into position in the tidal prism (Figure 4.14e), all ditched sites sat lower than their unditched counterparts, but there were no consistent significant differences between sites at each ditching level (Table 4.8, Figure 4.14e). If the percent cover of *S. patens* was solely driven by elevation and tidal position, we would expect to see greater variability in *S. patens* percent cover at the GBB ditched site where tidal position was lowest (Figures 4.14b and 4.14e). Soil firmness can be influenced by flooding, sediment accumulation, and belowground vegetation structure (Langley et al. 2009, Kirwan and Megonigal 2013). Here, soil penetration depth, an indicator of soil firmness, was correlated with elevation but none of the vegetation parameters (Figures 4.13 and 4.14f). The GBB unditched plots exhibited the lowest penetration depths, indicating firmer conditions, which aligns well with the relatively high elevations and tidal position. But since other sites at higher tidal positions (i.e., Forsythe unditched "a" and "b" plots) displayed greater variability in *S. patens* cover and higher soil penetration, there are likely other variables influencing vegetation cover.

Table 4.8. Results of Kruskal-Wallace and Dunn Multiple Comparison post-hoc tests ("pair-wise difference" column) for all ecologic variables. Italicized rows indicate ecologic variables for which one of the grouping factors resulting in significant differences among all plots of different types. Pair-wise difference notations are as follows: Site is identified as either "G" (Great Bay Blvd) or "F" (Forsythe); Condition is noted as either "D" (ditched) or "U" (unditched); and Plot Position as either "a" (between 1-5m from a pond) or "b" (between 11-20m of a pond).

Ecologic Variable	**Kruskal-Wallace Result**	**Pair-wise Differences**
Total Vegetation Percent Cover	$p<1.027e^{-2}$	GDb:FUa ($p<1.92e^{-2}$)
S. patens Percent Cover	$p<1.080e^{-2}$	GDb:FDa ($p<1.760e^{-2}$)
S. patens Mean Height	$p<1.138e^{-1}$	N/A
Elevation	$p<1.491e^{-10}$	All D:U within each site/plot
Tidal Position	$p<3.447e-^{10}$)	All D:U within each site/plot
Soil Penetration Depth	$p<7.472^{-4}$	GUa:FDa ($p<5.001e^{-4}$) GUa:GDb ($p<2.060e^{-2}$) GUb:FDa ($p<1.311e^{-2}$)
Porewater Sulfate	$p<9.682e^{-5}$	GDa:FDa&b ($p<5.780e^{-4}$) GDa:FUa ($p<4.630e^{-5}$)
Porewater Sulfate Depletion	$p<2.031e^{-6}$	FDa&b:FUa&b ($p<3.210e^{-5}$) FDa&b:GDa&b ($p<1.846e^{-6}$)
Porewater Sulfide	$p<2.363e^{-2}$	GUa:FDa&b ($p<1.315e^{-2}$)
Porewater Ammonia	$p<9.452e^{-4}$	GDa:FDb ($p<3.101e^{-3}$) GDa:FUa ($p<9.201e^{-3}$)
Soil Oxidation/Reduction Potential	$p<7.096e^{-7}$	FDa&b:GUa&b ($p<7.064e^{-7}$) FUa&b:GUa&b ($p<6.974e^{-5}$)
Water Table Depth	$p<9.143e^{-7}$	FDa&b:FUa&b($p<6.548e^{-6}$) FUa&b:GUa ($p<5.548^{-7}$)
Conductivity	$p<2.701e^{-3}$	FUa:GDa ($p<2.613e^{-3}$)
Soil pH	$p<1.963e^{-6}$	FDa&b> all except GUa&b ($p<1.63e^{-2}$)

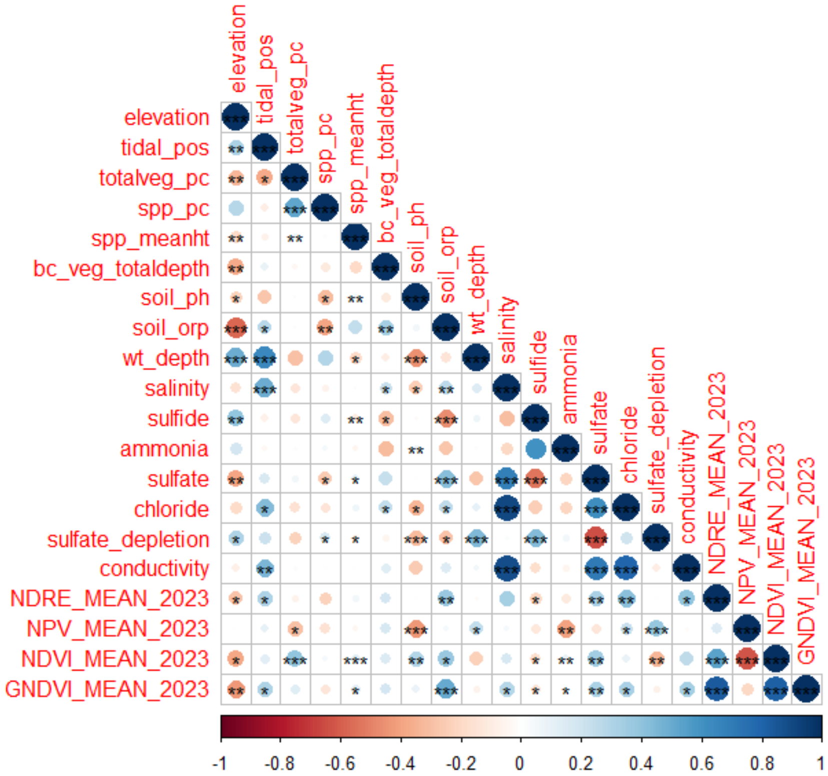

Figure 4.13. Correlation matrix for multispectral indices (MSIs) and ecologic variables from the 2023 field effort. All parameters are noted along both axes. MSIs are located at the bottom of the y-axis and are fully capitalized. Dot size indicates the strength of the correlation (larger=stronger), and color denotes the direction (blue=positive & red=negative). The number of asterisks describes the strength of the correlation at the following alpha levels: "": p=0.1; "**": p=0.01; and "***": p=0.001.*

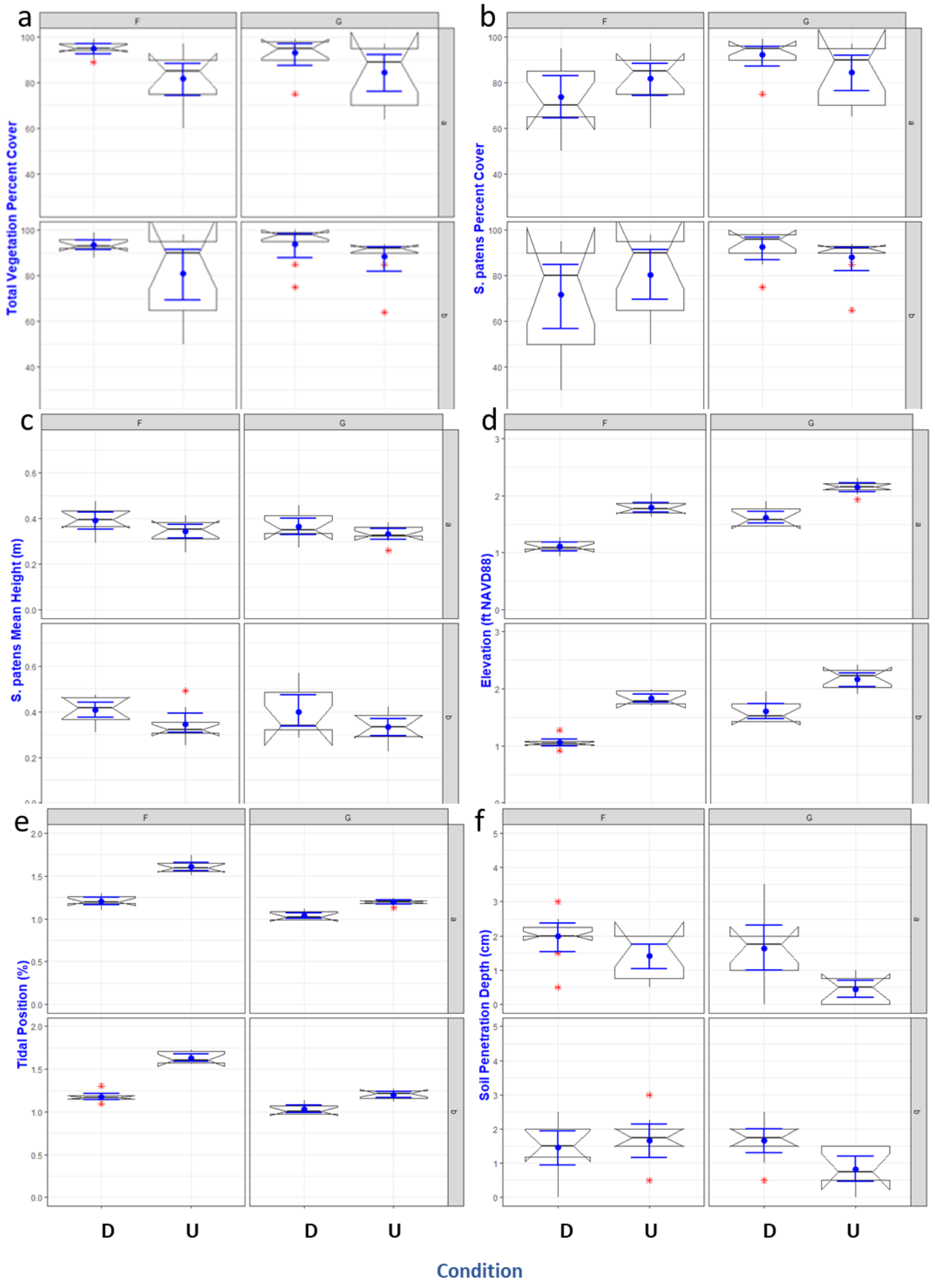

*Figure 4.14. Notched boxplots of total vegetation percent cover (a), S. patens percent cover (b), S. patens mean height (c), elevation (d), tidal position (e), and soil penetration depth (f) by Site (F= Forsythe, G = Great Bay Blvd), Condition (D= ditched, U = unditched), and Plot Position (a= 0-5m from pond, b = 11-20m from pond). Bounds of box represent the 25% (bottom) and 75% (top)m interquartile range, black line near center of notches indicates the median, blue dot identifies the mean, whiskers depict the min and max values, and red stars denote outliers calculated as (min-(1.5*IQR) & max+(1.5*IQR)). IQR = Interquartile Range. The notch displays a confidence interval around the median (+/- 1.58*IQR/sqrt(n)). Notches are used to compare groups. If the notches of two boxes do not overlap, this is an indication that the medians differ. “Ears”, or the triangle in the corner of the interquartile range limits denote that the data are either skewed or sample size is low.*

Differences among soil sulfate, sulfate depletion, sulfide, and ammonia did not follow any consistent pattern among sites, condition, or plots (Figures 4.15a-d and 4.16a-d). Sulfate, sulfide, and sulfate depletion were strongly correlated, but varied in their relationships with soil parameters such as pH and ORP (Figure 4.13). Sulfate depletion was lower in Forsythe ditched and GBB unditched plots relative to Forsythe unditched and GBB ditched plots (Figure 4.15b). Interestingly, the ranges of porewater sulfide reported here largely agree with the values reported in Himmelstein et al. (2021) for their study sites in Blackwater National Wildlife Refuge (MD) as well as results from the 2022 evaluations. There, the higher average sulfide concentrations associated with unstable marshes reflect the upper end of the ranges reported here in the unditched plots. This could indicate that the unditched marshes were not necessarily free of porewater stressors. Additionally, porewater ammonia values reported here are similar to values reported by Himmelstein et al. (2021) for stable marshes. Although there was a greater variability in the

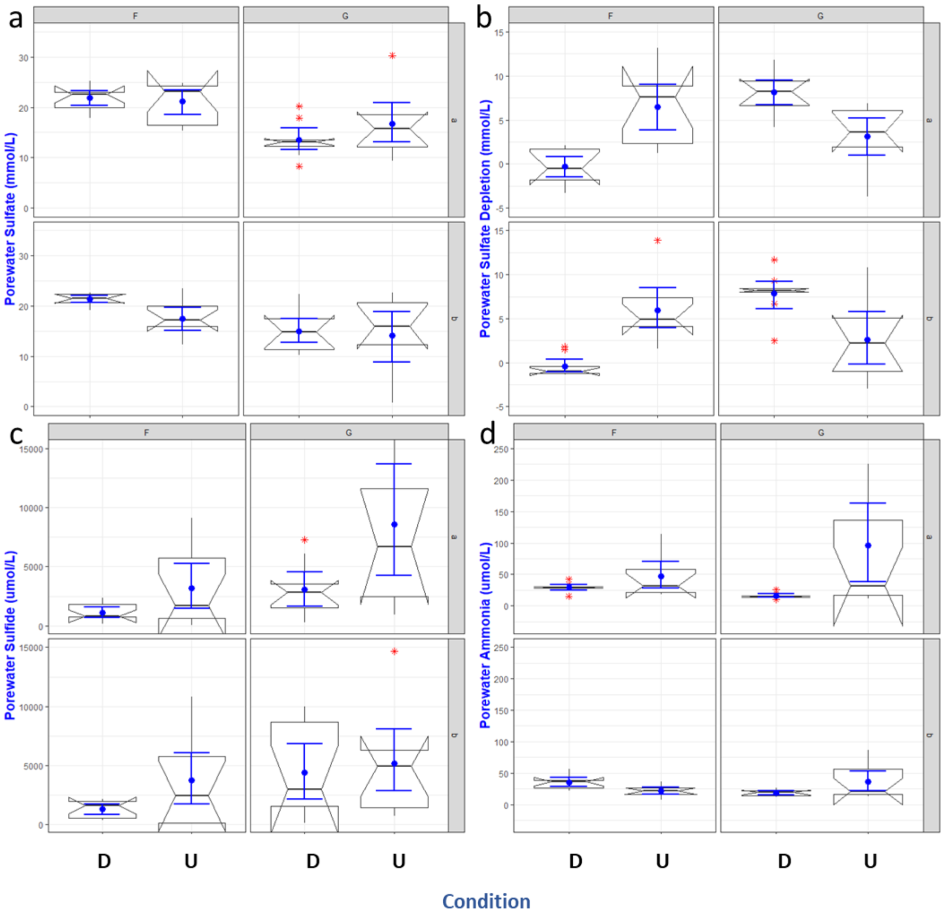

*Figure 4.15. Notched boxplots of porewater sulfate (a), porewater sulfate depletion (b), porewater sulfide (c), and porewater ammonia (d) by Site (F= Forsythe, G = Great Bay Blvd), Condition (D= ditched, U = unditched), and Plot Position (a= 0-5m from pond, b = 11-20m from pond). Bounds of box represent the 25% (bottom) and 75% (top)m interquartile range, black line near center of notches indicates the median, blue dot identifies the mean, whiskers depict the min and max values, and red stars denote outliers calculated as (min-(1.5*IQR) & max+(1.5*IQR)). IQR = Interquartile Range. The notch displays a confidence interval around the median (+/- 1.58*IQR/sqrt(n)). Notches are used to compare groups. If the notches of two boxes do not overlap, this is an indication that the medians differ. "Ears", or the triangle in the corner of the interquartile range limits denote that the data are either skewed or sample size is low.*

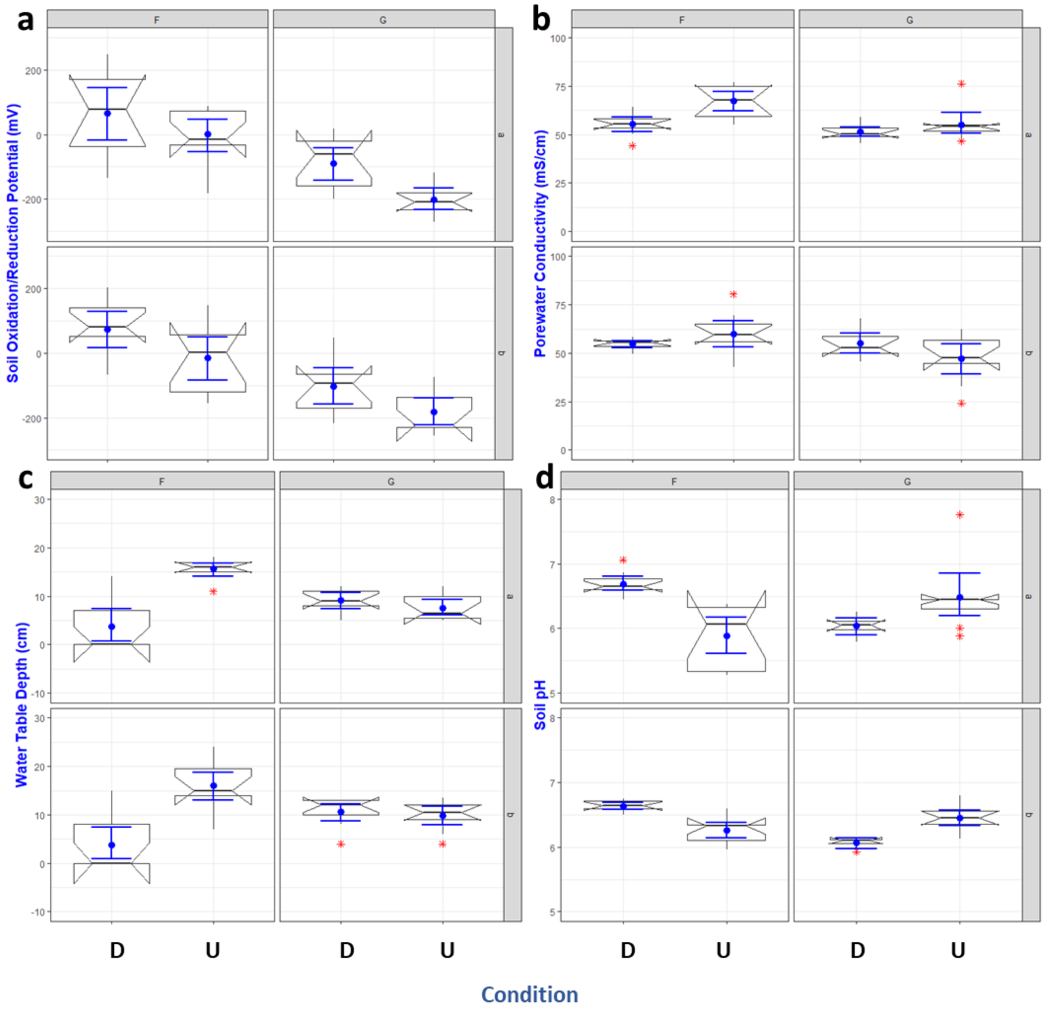

*Figure 4.16. Notched boxplots of oxidation/reduction potential (a), porewater conductivity (b), water table depth (c), & soil pH (d) by Site (F= Forsythe, G = Great Bay Blvd), Condition (D= ditched, U = unditched), and Plot Position (a= 0-5m from pond, b = 11-20m from pond). Bounds of box represent the 25% (bottom) and 75% (top)m interquartile range, black line near center of notches indicates the median, blue dot identifies the mean, whiskers depict the min and max values, and red stars denote outliers calculated as (min-(1.5*IQR) & max+(1.5*IQR)). IQR = Interquartile Range. The notch displays a confidence interval around the median (+/- 1.58*IQR/sqrt(n)). Notches are used to compare groups. If the notches of two boxes do not overlap, this is an indication that the medians differ. "Ears", or the triangle in the corner of the interquartile range limits denote that the data are either skewed or sample size is low.*

GBB unditched plots, there were minimal plot-wise significant differences (Table 4.8 and Figure 4.15d), indicating that ammonia concentrations in our marshes were not necessarily high in 2023. Soil ORP was significantly lower at the GBB unditched plots ("a" and "b") than at both Forsythe ditched and unditched plots (Table 4.8 and Figure 4.16a). As soil ORP measures the tendency for chemicals to gain/lose electrons, in 2023, we can say low ORP corresponds with a higher range of ammonia concentration at the GBB unditched plots (Figure 4.15d). As ammonia is oxidized to nitrate (via nitrite), the nitrogen becomes available for assimilation into the vegetation, although at higher level ammonia toxicity can be present. Interestingly, neither soil ORP nor ammonia were correlated with total vegetation or *S. patens* percent cover (Figure 4.13). The GBB unditched plots were also positioned at relatively higher elevations compared to the other plots (Figure 4.14d) and may be less regularly flooded than their ditched counterpart that displayed a higher range of ORP values. Therefore, there may be other factors or interactions, such as interactive temporal effects between soil chemical parameters and flooding regimes, accounting for the higher range of ammonia, lower ORP, and lack of vegetation cover change at the GBB unditched plots.

Plots for this study were selected to have a visible similarity in *S. patens* cover (Figure 4.14b) but that varied in other factors that are common in NJ marshes – different sites with varying tidal prisms, varying levels of ditching, and distance from intra-marsh ponds. As those factors did not seem to have a consistent effect on the variability of the ecologic variables, further evaluation focused on relationships between the MSIs and the ecologic variables themselves (e.g., can the drone "see" reflectance patterns indicative of soil and porewater differences that can affect vegetation cover). If so, multispectral imagery would be able to detect conditions in high marsh habitat not observable to the eye or through drone-based photography, prior to vegetation die-off. This would allow for the identification of at-risk areas of high marsh, before conditions become dire, to prioritize intervention efforts. Dropping the factor levels, significant correlations between ecologic variables and the MSIs were further evaluated for their predictive capabilities.

Results from tolerance and variance inflation factor (VIF) analyses were analyzed as described in the statistical analysis section (Step 3 – Collinearity evaluation) to reduce collinearity among initial correlated model variables. Initial model variables, per multispectral index (MSI), were as follows:

1. Green Normalized Difference Vegetation Index (GNDVI): elevation, tidal position, *S. patens* mean height, soil ORP, ammonia, sulfate, chloride, and conductivity.
2. Normalized Difference Red Edge (NDRE): elevation, tidal position, soil ORP, sulfate, chloride, and conductivity.
3. Normalized Difference Vegetation Index (NDVI): elevation, total vegetation percent cover, *S. patens* mean height, soil ORP, ammonia, sulfate, and sulfate depletion.
4. Non-Photosynthetic Vegetation (NPV): total vegetation percent cover, *S. patens* mean height, soil ORP, ammonia, chloride, and sulfate depletion.

Although there were many correlations between the ecologic variables and the MSIs (Figure 4.13), collinearity was common. After model reduction, the final vegetation-centric indices (i.e., NDVI & GNDVI) each included a vegetation variable (Table 4.9a and 4.9c) while the non-photosynthetic indices did not (i.e., NDRE & NPV, Table 4.9b and 4.9d). All final tolerances were greater than 0.86 with VIF's less than 1.2 (Table 9). Comparisons of the full GNDVI (Table 4.10a) and NDRE (Table 4.11a) models with their null counterparts, indicated that the additions of variables to the null model did not help explain the variability in their respective response MSI. These results were confirmed using stepwise regression (Table 4.10b for GNDVI & Table 4.11b for NDRE). Therefore, no predictive relationship between the MSI and their correlated ecologic variables was interpreted.

Table 4.9. Final model components per multispectral indices resulting from tolerance (range = 0-1) and variance inflation factor (VIF, range = 0-∞) analysis. GNDVI = Green Normalized Differential Vegetative Index; NDRE = Normalized Difference Red Edge; NDVI = Normalized Difference Vegetation Index; and NPV = Non-Photosynthetic Vegetation. Tolerance & VIF thresholds for final model inclusion were >0.8 & <3, respectively.

a. GNDVI

Variables	Tolerance	VIF
S. patens Mean Height	0.99	1.01
Ammonia	0.98	1.02
Sulfate	0.97	1.03

b. NDRE

Variables	Tolerance	VIF
Tidal Position	0.94	1.06
Sulfate	0.94	1.06

c. NDVI

Variables	Tolerance	VIF
Elevation	0.84	1.19
S. patens Mean Height	0.96	1.04
Ammonia	0.96	1.04
Sulfate	0.87	1.15

d. NPV

Variables	Tolerance	VIF
Total Vegetation Percent Cover	0.98	1.02
Ammonia	0.99	1
Sulfate Depletion	0.98	1.01

The NDVI full model was a significantly better fit for the data than the null model (Table 4.12a). Results were confirmed using a stepwise regression approach that indicated that the inclusion of the sulfate term provided a better fit model, but that the addition of additional terms did not explain enough of the remaining variability to justify the increase in complexity (Table 4.12b). A random effects model was evaluated with sulfate as the independent variable and site (i.e., Forsythe or GBB) as a random grouping variable. Results showed that porewater sulfate was not a significant predictor of NDVI scores ($p > 0.05$), and that the random grouping variable of Site did not explain a significant proportion of the variance (Figure 4.12). Visually represented, there is no discernible pattern in the distribution of data by either Condition (shape) or Site (color), and a wide variety of response values are possible for a sulfate value between 10-25 mmol l^{-1} (Figure 4.17).

The NPV full model was also a significantly better fit for the data than its null counterpart (Table 4.13a). Stepwise regression showed that the inclusion of sulfate depletion, ammonia, total vegetation percent cover, and the interaction between sulfate depletion and total vegetation percent cover comprised a best-fit model (Table 4.13b). Subsequent analysis found both total vegetation percent cover ($p < 0.05$) and ammonia ($p < 0.001$) terms to be significant predictors of NPV (Table 4.13c). As each term was independently significant, separate models

Table 4.10. Results from the GNDVI full and null model comparison (a) and step model verification (b). In "a", reduced indicates the null model, and Full refers to the model that included all correlated terms after Variance Inflation Factor (VIF) and Tolerance testing. In "b", the "+" indicates the addition of a term to the null model on the top line in italics. Lowest Akaike Information Criterion (AIC) score was used to select the best fit model.

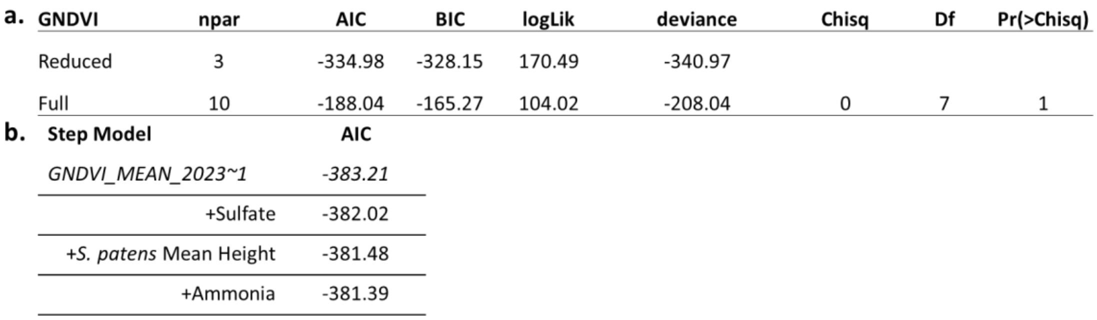

a.

GNDVI	npar	AIC	BIC	logLik	deviance	Chisq	Df	Pr(>Chisq)
Reduced	3	-334.98	-328.15	170.49	-340.97			
Full	10	-188.04	-165.27	104.02	-208.04	0	7	1

b.

Step Model	AIC
GNDVI_MEAN_2023~1	*-383.21*
+Sulfate	-382.02
+*S. patens* Mean Height	-381.48
+Ammonia	-381.39

Table 4.11. Results from the NDRE full and null model comparison (a) and step model verification (b). In "a", reduced indicates the null model, and Full refer to the model that included all correlated terms after Variance Inflation Factor (VIF) and Tolerance testing. In "b", the "+" indicates the addition of a term to the null model on the top line in italics. Lowest Akaike Information Criterion (AIC) score was used to select the best fit model.

a.

NDRE	npar	AIC	BIC	logLik	deviance	Chisq	Df	Pr(>Chisq)
Reduced	3	-334.98	-328.15	170.49	-340.97	NA	NA	NA
Full	6	-332.14	-318.48	172.07	-344.14	3.16	3	3.67E-01

b.

Step Model	AIC
NDRE_MEAN_2023~1	*-543.30*
+Sulfate	-542.68
+Tidal Position	-542.10

Table 4.12. Results from the NDVI full and null model comparison (a) and step model verification (b). In "a", reduced indicates the null model, and Full refer to the model that included all correlated terms after Variance Inflation Factor (VIF) and Tolerance testing (listed in b). In (b), "+" indicates the addition of a term to the null model on the top line in italics. Lowest Akaike Information Criterion (AIC) score was used to select the best fit model in (a), and the appropriate terms for further analysis above the bolded "<none>" in (b).

a.

NDVI	npar	AIC	BIC	logLik	deviance	Chisq	Df	Pr(>Chisq)
Reduced	3	-124.43	-117.60	65.21	-130.43	NA	NA	NA
Full	18	-140.16	-99.18	88.08	-176.16	45.73	15	5.86E-05

b.

Step Model	AIC
NDVI_MEAN_2023~1	*-331.23*
+Sulfate	-333.24
+<none>	**-333.24**
+Elevation	-332.81
+Ammonia	-331.65

were used to evaluate the effects of each independent term on NPV. When isolated, there was no evidence that total vegetation percent cover was a significant predictor of NPV ($p > 0.05$, Figure 4.18), but that ammonia might be ($p < 0.001$, Figure 4.19). As NPV is a non-photosynthetic index, it was unsurprising that the vegetation parameter was ultimately not significant. Increased ammonia stress can reduce vegetation cover, which gives credence to the idea that increased bare ground could indicate high ammonia levels. This was confounded with Himmelstein et al.'s (2021) results showing that the levels of ammonia reported in this study were aligned with values at more stable marsh locations in their study. The GBB unditched plots showed the greatest variability in ammonia (Figure 4.15d) but had a generally high percent cover, although some variability was present (Figure 4.14a and 4.14b). It is plausible that the NPV values were influenced by shadowing in the complex *S. patens* canopy, mistaking them for bare ground.

Regarding ammonia as a predictor variable, although a significant relationship was detected, the R^2 values indicate that the model does not explain more than 23.5% of the variability in the data (Figure 4.19). A significant p and low R^2 values can occur when the independent variable is sufficient to explain more variability than the null model, but the unpredictability in the response variable is not explained well by the model. In this instance, although greater linearity is visible in the data at higher ammonia values, low values are associated with a wide range of NPV values. As the distribution of the porewater ammonia data is highly right-skewed, further evaluation of the effects of porewater ammonia on vegetation cover and NPV values is needed. It is recommended that a controlled field study be conducted that aims to identify sites that comprise a greater distribution of porewater ammonia and percent cover values.

Predictors	*Estimates*	*CI*	*p*
(Intercept)	0.07	-0.02 – 0.16	0.145
sulfate	0.00	-0.00 – 0.01	0.191
Random Effects			
σ^2	0.01		
$\tau_{00\ Site}$	0.00		
ICC	0.05		
N_{Site}	2		
Observations	72		
Marginal R^2 / Conditional R^2	0.028 / 0.078		

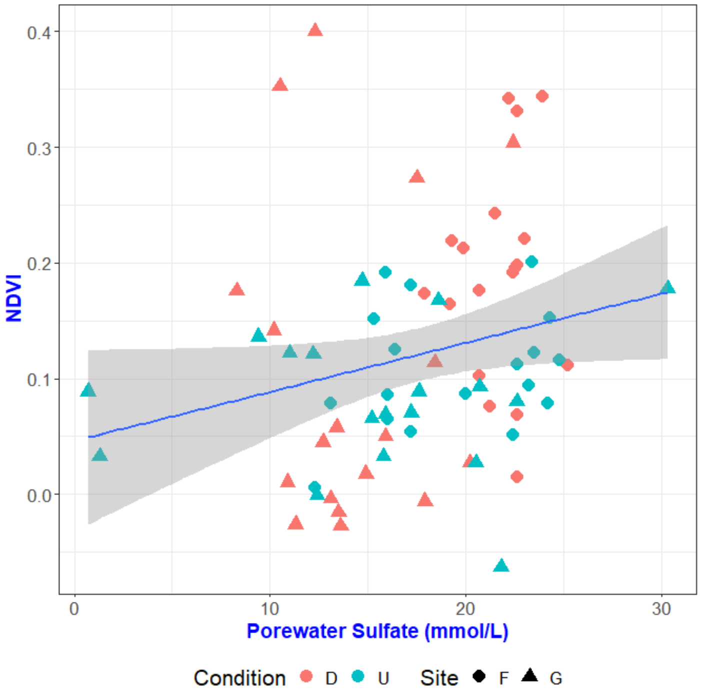

Figure 4.17. Results of the random effects model of the effects of sulfate on Normalized Difference Vegetation Index (NDVI). Site was included as a random effect and is denoted by point shape: Forsythe = "F" as diamonds, and Great Bay Blvd = "G" as triangles. Site condition is displayed as red for ditched ("D") and blue for unditched ("U") locations. The blue line and grey shaded area depict the linear regression with 95% confidence interval, respectively. For the random effects, σ =Variance, τ = between-site variance, ICC = intraclass correlation coefficient which is the proportion of the variance explained by the grouping structure in the population, and N= number of classes in the grouping variable.

Table 4.13. Results from the NPV full and null model comparison (a) and step model verification (b). In "a", reduced indicates the null model, and Full refer to the model that included all correlated terms after Variance Inflation Factor (VIF) and Tolerance testing (listed in b). In (b), "+" indicates the addition of a term to the null model on the top line in italics. Lowest Akaike Information Criterion (AIC) score was used to select the best fit model in (a), and the appropriate terms for further analysis above the bolded "<none>" in (b). ANOVA results for the evaluation of the effects of terms identified in (b) are presented in (c) with noted levels of significance (= p<0.05 & *** = p<0.0001).*

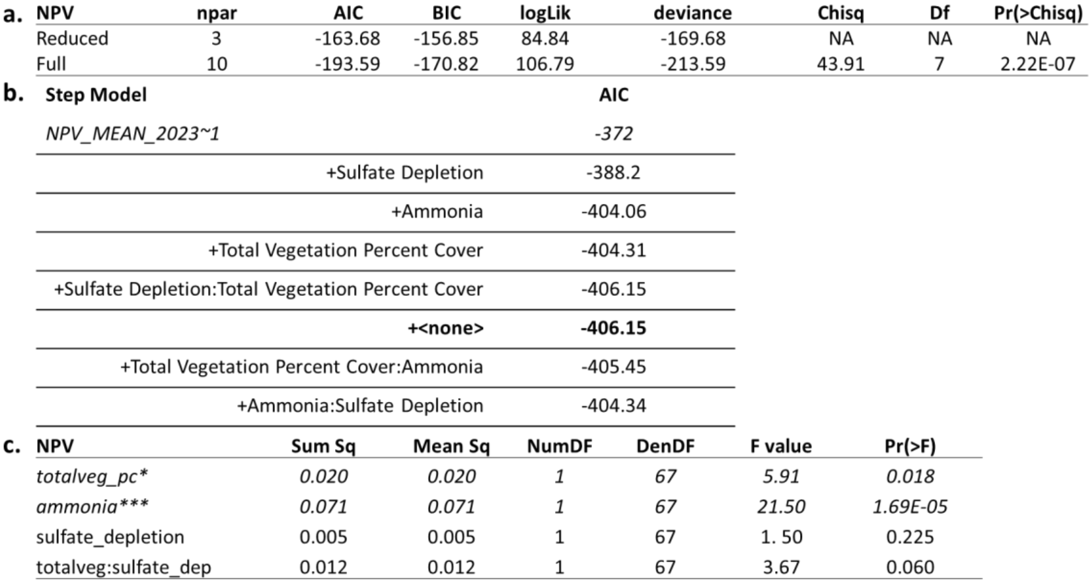

a.

NPV	**npar**	**AIC**	**BIC**	**logLik**	**deviance**	**Chisq**	**Df**	**Pr(>Chisq)**
Reduced	3	-163.68	-156.85	84.84	-169.68	NA	NA	NA
Full	10	-193.59	-170.82	106.79	-213.59	43.91	7	2.22E-07

b.

Step Model	**AIC**
NPV_MEAN_2023~1	*-372*
+Sulfate Depletion	-388.2
+Ammonia	-404.06
+Total Vegetation Percent Cover	-404.31
+Sulfate Depletion:Total Vegetation Percent Cover	-406.15
+<none>	**-406.15**
+Total Vegetation Percent Cover:Ammonia	-405.45
+Ammonia:Sulfate Depletion	-404.34

c.

NPV	**Sum Sq**	**Mean Sq**	**NumDF**	**DenDF**	**F value**	**Pr(>F)**
*totalveg_pc**	*0.020*	*0.020*	*1*	*67*	*5.91*	*0.018*
*ammonia****	*0.071*	*0.071*	*1*	*67*	*21.50*	*1.69E-05*
sulfate_depletion	0.005	0.005	1	67	1. 50	0.225
totalveg:sulfate_dep	0.012	0.012	1	67	3.67	0.060

Predictors	***Estimates***	***CI***	***p***
(Intercept)	-0.05	-0.19 – 0.09	0.496
totalveg pc	-0.00	-0.00 – 0.00	0.129
Random Effects			
σ^2	0.01		
$\tau_{00\ \text{Site}}$	0.00		
ICC	0.04		
N_{Site}	2		
Observations	72		
Marginal R^2 / Conditional R^2	0.031 / 0.072		

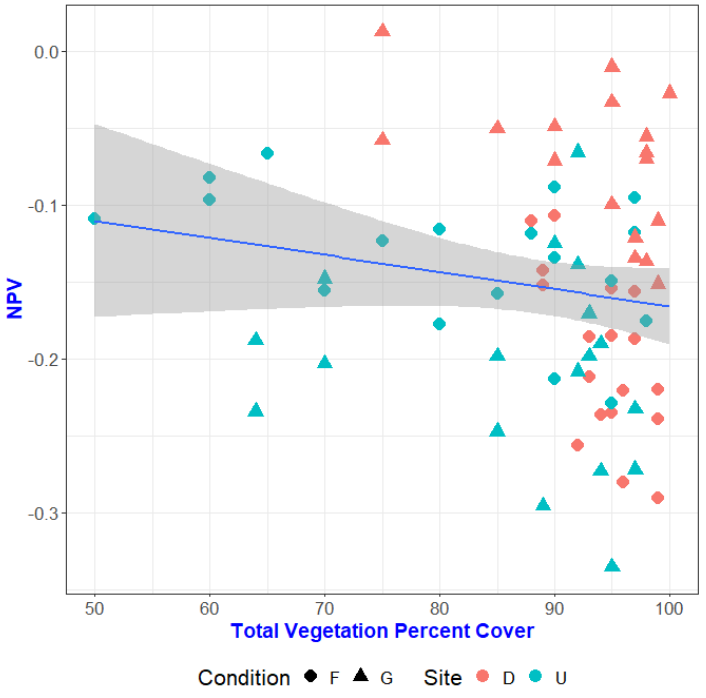

Figure 4.18. Results of the random effects model of the effects of total vegetation percent cover on Non-Photosynthetic Vegetation index (NPV). Site was included as a random effect and is denoted by point shape: Forsythe =”F” as diamonds, and Great Bay Blvd = “G” as triangles. Site condition is displayed as red for ditched (“D”) and blue for unditched (“U”) locations. The blue line and grey shaded area depict the linear regression with 95% confidence interval, respectively. For the random effects, σ =Variance, τ = between-site variance, ICC = intraclass correlation coefficient which is the proportion of the variance explained by the grouping structure in the population, and N= number of classes in the grouping variable.

Predictors	***Estimates***	***CI***	***p***
(Intercept)	-0.13	-0.16 – -0.09	**<0.001**
ammonia	-0.00	-0.00 – -0.00	**<0.001**
Random Effects			
σ^2		0.00	
$\tau_{00\ \mathrm{Site}}$		0.00	
ICC		0.07	
N_{Site}		2	
Observations		72	
Marginal R^2 / Conditional R^2		0.176 / 0.235	

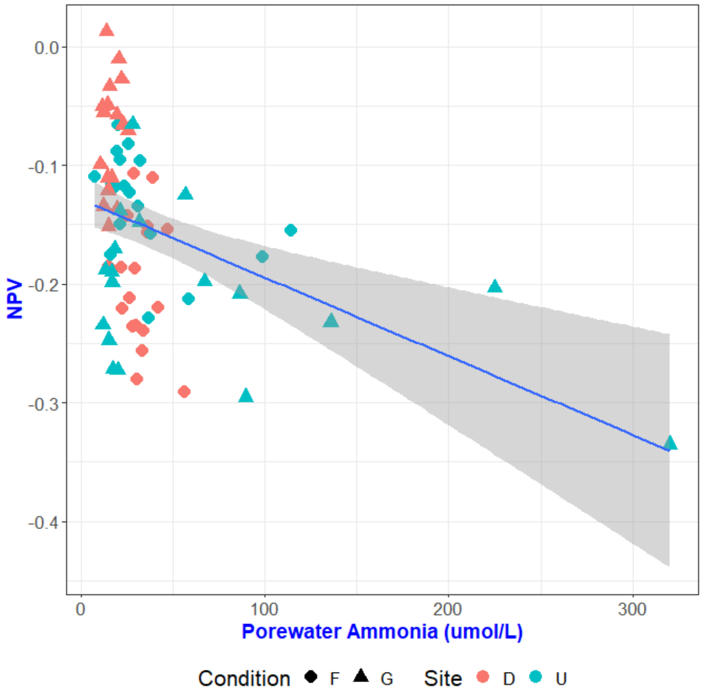

Figure 4.19. Results of the random effects model of the effects of ammonia on Non-Photosynthetic Vegetation index (NPV). Site was included as a random effect and is denoted by point shape: Forsythe ="F" as diamonds, and Great Bay Blvd = "G" as triangles. Site condition is displayed as red for ditched ("D") and blue for unditched ("U") locations. The blue line and grey shaded area depict the linear regression with 95% confidence interval, respectively. For the random effects, σ =Variance, τ = between-site variance, ICC = intraclass correlation coefficient which is the proportion of the variance explained by the grouping structure in the population, and N= number of classes in the grouping variable.

Next Steps

In recent years, many documents have been produced describing methodologies for classifying wetland vegetation communities using drones, but there is little mention in the scientific literature regarding the use of multispectral drones for evaluating salt marsh condition. This may be due to the multi-step relationship identification required for these efforts. First, the drone will need to discern between a variety of vegetation reflection patterns (e.g., reflection partitioning among species and between varying densities of each), and second the observed vegetation differences need to be associated with specific soil or porewater conditions that are influencing the vegetation community. The first step has been well established and reported on in earlier sections of this report. The relationships in the second step have been more difficult to establish. One reason for this is vegetation health and community composition can be influenced by a variety of factors that are interrelated. For example, nutrient enrichment (e.g., ammonia, sulfide) at levels below toxicity thresholds can reduce belowground biomass production resulting in decreased elevation and subsequently vegetation loss (Deegan et al. 2012 & Langley et al. 2009). At toxic levels, vegetation die-off can occur resulting in elevation loss (Watson et al. 2015 & van Katwijk et al. 1997). Under either scenario, a high level of nutrient variability would be associated with similar vegetation community composition (i.e., vegetation percent cover). However, in other instances, enhanced nutrient levels below toxicity can also enhance vegetation production. Under this scenario, a similar concentration of nutrients could be associated with varying levels of vegetation cover, depending on co-factors that may determine if the vegetation density increases or declines because of the enhancement. These types of relationships can confound attempts to identify predictive relationships.

Although no clear, predictive relationships between MSIs and vegetation, soil, and porewater metrics could be established as a result of this effort, progress was made in identifying potential predictor variables and a more appropriate study design. The 2023 field study focused on keeping vegetation community composition relatively constant (single species with high percent cover) and focused on confirming if site, ditching, and distance from ponds played a role. Since the aforementioned factors did not play a consistent role in affecting the levels of ecologic variables, future study designs should focus on other factors. For future field studies aiming to evaluate if drone-sensed data can be used to identify soil and porewater attributes associated with vegetation decline (the proxy metric that the drone can observe), we would recommend planning to vary vegetation cover accounting for directionality – vegetated areas that are stable, expanding, and denuding. Soil and porewater measurements at these locations should reflect greater spatial variability (i.e., >20 m from identified conditions as in this effort) to track gradients across the marsh, especially in areas of expanse and decline. This may help identify combinations and levels of metrics associated with marsh development, persistence, and decline.

References

Artigas, F. J., & Yang, J. (2006). Spectral discrimination of marsh vegetation types in the New Jersey Meadowlands, USA. *Wetlands*, *26*(1), 271–277. https://doi.org/10.1672/0277-5212(2006)26[271:SDOMVT]2.0.CO;2

Baena, S., Moat, J., Whaley, O., & Boyd, D. S. (2017). Identifying species from the air: UAVs and the very high resolution challenge for plant conservation. *PLOS ONE*, *12*(11), e0188714. https://doi.org/10.1371/journal.pone.0188714

Boiarskii, B. (2019). Comparison of NDVI and NDRE indices to detect differences in vegetation and chlorophyll content. *Journal of Mechanics of Continua and Mathematical Sciences*, *spl1*(4). https://doi.org/10.26782/jmcms.spl.4/2019.11.00003

Bradley, P. M., & Morris, J. T. (1991). Relative importance of ion exclusion, secretion and accumulation in *Spartina alterniflora* Loisel. *Journal of Experimental Botany*, *42*(12), 1525–1532. https://doi.org/10.1093/jxb/42.12.1525

Chambers, L. G., Steinmuller, H. E., & Breithaupt, J. L. (2019). Toward a mechanistic understanding of “peat collapse” and its potential contribution to coastal wetland loss. *Ecology*, *100*(7). https://doi.org/10.1002/ecy.2720

Cline, J.D. (1969). Spectrophotometric determination of hydrogen sulfide in natural waters. *Limnology and Oceanography*, 14:454–458. https://doi.org/10.4319/lo.1969.14.3.0454

De Castro, A. I., Shi, Y., Maja, J. M., & Peña, J. M. (2021). UAVs for Vegetation Monitoring: Overview and Recent Scientific Contributions. *Remote Sensing*, *13*(11), 2139. https://doi.org/10.3390/rs13112139

Demberger, S., Haaf, L., Padeletti, A., & Kreeger, D. (2017). *Mid-Atlantic Tidal Rapid Assessment: development of a shoreline change metric to strengthen the MidTRAM shoreline attribute* (PDE Report No. 17–10). Partnership for the Delaware Estuary. https://delawareestuary.s3.amazonaws.com/MidTRAM+4.1+with+Data+Sheets.pdf

De Souza, R., Peña-Fleitas, M. T., Thompson, R. B., Gallardo, M., & Padilla, F. M. (2020). Assessing performance of vegetation indices to estimate nitrogen nutrition index in pepper. *Remote Sensing*, *12*(5), 763. https://doi.org/10.3390/rs12050763

Doughty, C. L., & Cavanaugh, K. C. (2019). Mapping coastal wetland biomass from high resolution unmanned aerial vehicle (UAV) imagery. *Remote Sensing*, *11*(5). https://doi.org/10.3390/rs11050540

Ewing, K., McKee, K. L., & Mendelssohn, I. A. (1997). A field comparison of indicators of sublethal stress in the salt-marsh grass *Spartina patens*. *Estuaries*, *20*(1), 48. https://doi.org/10.2307/1352719

Finlayson, C. M., & Spiers, A. G. (Eds.). (1999). *Global review of wetland resources and priorities for wetland inventory*. Supervising Scientist.

Fisher, J., & Acreman, M. C. (2004). Wetland nutrient removal: a review of the evidence. *Hydrology and Earth System Sciences*, *8*(4), 673–685.

Ganju, N. K., Defne, Z., Kirwan, M. L., Fagherazzi, S., D’Alpaos, A., & Carniello, L. (2017). Spatially integrative metrics reveal hidden vulnerability of microtidal salt marshes. *Nature Communications*, *8*(1), 14156. https://doi.org/10.1038/ncomms14156

Haaf, L., Watson, E. B., Elsey-Quirk, T., Raper, K., Padeletti, A., Maxwell-Doyle, M., Kreeger, D., & Velinsky, D. J. (2022). Sediment accumulation, elevation change, and the vulnerability of tidal marshes in the Delaware Estuary and Barnegat Bay to accelerated sea level rise. *Estuaries and Coasts*, *45*(2), 413–427. https://doi.org/10.1007/s12237-021-00972-9

Himmelstein, J., Vinent, O. D., Temmerman, S., & Kirwan, M. L. (2021). Mechanisms of pond expansion in a rapidly submerging marsh. *Frontiers in Marine Science*, *8*. https://doi.org/10.3389/fmars.2021.704768

Horton, B. P., Kopp, R. E., Garner, A. J., Hay, C. C., Khan, N. S., Roy, K., & Shaw, T. A. (2018). Mapping sea-level change in time, space, and probability. *Annual Review of Environment and Resources*, *43*(1), 481–521. https://doi.org/10.1146/annurev-environ-102017-025826

Kearney, M. S., Grace, R. E., & Stevenson, J. C. (1988). Marsh loss in Nanticoke Estuary, Chesapeake Bay. *Geographical Review*, *78*(2), 205. https://doi.org/10.2307/214178

Kearney, M. S., Rogers, A. S., Townshend, J. R. G., Rizzo, E., Stutzer, D., Stevenson, J. C., & Sundborg, K. (2002). Landsat imagery shows decline of coastal marshes in Chesapeake and Delaware Bays. *Eos, Transactions American Geophysical Union*, *83*(16), 173–178. https://doi.org/10.1029/2002EO000112

Kennish, M. J. (2001). Physical description of the Barnegat Bay—Little Egg Harbor estuarine system. *Journal of Coastal Research*, 13–27. https://www.jstor.org/stable/25736225

Kirwan, M. L., Guntenspergen, G. R., D'Alpaos, A., Morris, J. T., Mudd, S. M., & Temmerman, S. (2010). Limits on the adaptability of coastal marshes to rising sea level. *Geophysical Research Letters*, *37*(23). https://doi.org/10.1029/2010GL045489

Kirwan, M. L., & Megonigal, J. P. (2013). Tidal wetland stability in the face of human impacts and sea-level rise. *Nature*, *504*(7478), 53–60. https://doi.org/10.1038/nature12856

Kopp, R. E., Andrews, C., Broccoli, A., Garner, A., Kreeger, D., Leichenko, R., Lin, N., Little, C., Miller, J. A., Miller, J. K., Miller, K. G., Moss, R., Orton, P., Parris, A., Robinson, D., Sweet, W., Walker, J., Weaver, C. P., White, K., … Auermuller, L. (2019). *New Jersey's Rising Seas and Changing Coastal Storms: Report of the 2019 Science and Technical Advisory Panel*. Rutgers, The State University of New Jersey.

Lamers, L. P. M., Govers, L. L., Janssen, I. C. J. M., Geurts, J. J. M., Van Der Welle, M. E. W., Van Katwijk, M. M., Van Der Heide, T., Roelofs, J. G. M., & Smolders, A. J. P. (2013). Sulfide as a soil phytotoxin—a review. *Frontiers in Plant Science*, *4*. https://doi.org/10.3389/fpls.2013.00268

Langley, J. A., McKee, K. L., Cahoon, D. R., Cherry, J. A., & Megonigal, J. P. (2009). Elevated CO_2 stimulates marsh elevation gain, counterbalancing sea-level rise. *Proceedings of the National Academy of Sciences*, *106*(15), 6182–6186. https://doi.org/10.1073/pnas.0807695106

Merino, J. H., Huval, D., & Nyman, A. J. (2010). Implication of nutrient and salinity interaction on the productivity of Spartina patens. *Wetlands Ecology and Management*, *18*(2), 111–117. https://doi.org/10.1007/s11273-008-9124-4

Mondejar, J. P., & Tongco, A. F. (2019). Near infrared band of Landsat 8 as water index: a case study around Cordova and Lapu-Lapu City, Cebu, Philippines. *Sustainable Environment Research*, *29*(1), 16. https://doi.org/10.1186/s42834-019-0016-5

Muench, A., Elsey-Quirk, T., & Yang, Z. (2019). Competitive reversal between plant species is driven by species-specific tolerance to flooding stress and nutrient acquisition during early marsh succession. *Journal of Applied Ecology*, *56*(9), 2236–2247. https://doi.org/10.1111/1365-2664.13458

Nicholls, R. J., Hoozemans, F. M. J., & Marchand, M. (1999). Increasing flood risk and wetland losses due to global sea-level rise: regional and global analyses. *Global Environmental Change*, *9*, S69–S87. https://doi.org/https://doi.org/10.1016/S0959-3780(99)00019-9

NOAA Office for Coastal Management. (2024). *New Jersey*. https://coast.noaa.gov/states/new-jersey.html

Ozesmi, S. L., & Bauer, M. E. (2002). Satellite remote sensing of wetlands. *Wetlands Ecology and Management*, *10*(5), 381–402. https://doi.org/10.1023/A:1020908432489

Paz-Kagan, T., Silver, M., Panov, N., & Karnieli, A. (2019). Multispectral approach for identifying invasive plant species based on flowering phenology characteristics. *Remote Sensing*, *11*(8), 953. https://doi.org/10.3390/rs11080953

Pedersen, E., Weisner, S. E. B., & Johansson, M. (2019). Wetland areas' direct contributions to residents' well-being entitle them to high cultural ecosystem values. *Science of The Total Environment*, *646*, 1315–1326. https://doi.org/10.1016/j.scitotenv.2018.07.236

R Core Team. (2023). R: A language and environment for statistical computing. https://www.r-project.org/

Ramsey, E., & Rangoonwala, A. (2005). Leaf optical property changes associated with the occurrence of *Spartina alterniflora* dieback in coastal Louisiana related to remote sensing mapping. *Photogrammetric Engineering & Remote Sensing*, *71*(3), 299–311. https://doi.org/10.14358/PERS.71.3.299

Rezaie, A. M., Loerzel, J., & Ferreira, C. M. (2020). Valuing natural habitats for enhancing coastal resilience: Wetlands reduce property damage from storm surge and sea level rise. *PLOS ONE*, *15*(1), e0226275. https://doi.org/10.1371/journal.pone.0226275

Schutte C.A., Wilson, A.M., Evans, T., Moore, W.S., and Joye, S.B. (2016). Methanotrophy controls groundwater methane export from a barrier island. *Geochimica et Cosmochimica Acta* 179, 242-256, doi:10.1016/j.gca.2016.01.022

Shaw, J. T., Shah, A., Yong, H., & Allen, G. (2021). Methods for quantifying methane emissions using unmanned aerial vehicles: a review. *Philosophical Transactions of the Royal Society A: Mathematical, Physical and Engineering Sciences*, *379*(2210), 20200450. https://doi.org/10.1098/rsta.2020.0450

Smith, Katherine K., Ralph E. Good, and Norma F. Good. (1979). Production dynamics for above and belowground components of a New Jersey Spartina alterniflora tidal marsh. *Estuarine and Coastal Marine Science*, 9.2: 189-201.

Stevenson, J. C., Ward, L. G., & Kearney, M. S. (1986). Vertical accretion in marshes with varying rates of sea level rise. In *Estuarine Variability* (pp. 241–259). *Elsevier*. https://doi.org/10.1016/B978-0-12-761890-6.50020-4

Sun, C., Liu, Y., Zhao, S., Zhou, M., Yang, Y., & Li, F. (2016). Classification mapping and species identification of salt marshes based on a short-time interval NDVI time-series from HJ-1 optical imagery. *International Journal of Applied Earth Observation and Geoinformation*, *45*, 27–41. https://doi.org/10.1016/j.jag.2015.10.008

Turner, I. L., Harley, M. D., & Drummond, C. D. (2016). UAVs for coastal surveying. *Coastal Engineering*, *114*, 19–24. https://doi.org/10.1016/j.coastaleng.2016.03.011

Twohig, T. M., & Stolt, M. H. (2011). Soils-based rapid assessment for quantifying changes in salt marsh condition as a result of hydrologic alteration. *Wetlands*, *31*(5), 955–963. https://doi.org/10.1007/s13157-011-0210-7

U.S. EPA. (1993). Method 350.1: Nitrogen, Ammonia (Colorimetric, Automated Phenate) (Revision 2.0). U.S. Environmental Protection Agency, Cincinnati, OH. https://www.epa.gov/sites/default/files/2015-06/documents/epa-350.1.pdf

U.S. EPA. (1982). Method 120.1: Conductance (Specific Conductance, µmhos at 25 °C) by Conductivity Meter. U.S. Environmental Protection Agency, Washington D.C. https://www.epa.gov/sites/default/files/2015-08/documents/method_120-1_1982.pdf

Van Alphen, R., Rains, K. C., Rodgers, M., Malservisi, R., & Dixon, T. H. (2024). UAV-based wetland monitoring: multispectral and lidar fusion with random forest classification. *Drones*, *8*(3), 113. https://doi.org/10.3390/drones8030113

Van Katwijk, M., Vergeer, L., Schmitz, G., & Roelofs, J. (1997). Ammonium toxicity in eelgrass *Zostera marina*. *Marine Ecology Progress Series*, *157*, 159–173. https://doi.org/10.3354/meps157159

Watson, E. B., Wigand, C., Davey, E. W., Andrews, H. M., Bishop, J., & Raposa, K. B. (2017). Wetland loss patterns and inundation-productivity relationships prognosticate widespread salt marsh loss for southern New England. *Estuaries and Coasts*, *40*(3), 662–681. https://doi.org/10.1007/s12237-016-0069-1

Were, D., Kansiime, F., Fetahi, T., Cooper, A., & Jjuuko, C. (2019). Carbon sequestration by wetlands: a critical review of enhancement measures for climate change mitigation. *Earth Systems and Environment*, *3*(2), 327–340. https://doi.org/10.1007/s41748-019-00094-0

Wigand, C., Watson, E. B., Martin, R., Johnson, D. S., Warren, R. S., Hanson, A., Davey, E., Johnson, R., & Deegan, L. (2018). Discontinuities in soil strength contribute to destabilization of nutrient-enriched creeks. *Ecosphere*, *9*(8), e02329. https://doi.org/10.1002/ecs2.2329

Wilburn, B. P., Raper, K., Raposa, K. B., Gray, A. B., Mozdzer, T. J., & Watson, E. B. (2024). Promoting success in thin layer sediment placement: effects of sediment grain size and amendments on salt marsh plant growth and greenhouse gas exchange. *Restoration Ecology*, e14141. https://doi.org/10.1111/rec.14141

Zhang, K., Ge, X., Shen, P., Li, W., Liu, X., Cao, Q., Zhu, Y., Cao, W., & Tian, Y. (2019). Predicting rice grain yield based on dynamic changes in vegetation indexes during early to mid-growth stages. *Remote Sensing*, *11*(4), 387. https://doi.org/10.3390/rs11040387

Chapter 5: Relationships between diatom communities and sulfide concentrations in two salt marshes of New Jersey

Authors: Mihaela Enache[1], Charles Schutte[2], Brittany P. Wilburn[1], Joshua Moody[1], Metthea Yepsen[1], Kriish Hate[1,2]

[1] NJDEP, Division of Science and Research
[2] Rowan University

Objective: Determine if diatom community assemblages can be used as indicators of sulfide concentrations within salt marshes.

Approach: Because sulfide concentrations were collected as part of the soil characterization of the salt marshes in both study years, additional soil samples were collected to be processed for diatom community analysis. Diatoms have been proven to be correlated to several chemical and physical parameters of salt marshes, but no existing study has yet shown that diatom communities could reflect sulfide concentrations. To fill this gap, soil samples were collected from each subplot in 2022 and each plot in 2023 to determine present diatom assemblages. Soil samples were acid treated to remove organic materials, and one slide per sample was prepared for species identification and counting. The resulting assemblages were then compared to soil and porewater chemical parameters collected from the same sampling locations.

A draft manuscript is included in this chapter, which is intended to be revised and submitted for publication to an appropriate peer-reviewed scientific journal. This draft may undergo minor or significant edits prior to submission, as such many portions to the draft manuscript may appear verbatim in the submission version of the article.

Supplementary results can be found in Appendix F.

Responsibilities and Deliverables: The NJDEP-DSR was responsible for collection, processing, and analysis of diatom soil samples.

Rowan University was responsible for collection, processing, and analysis of soil and porewater chemistry.

Both NJDEP-DSR and Rowan University were responsible for final statistical analysis and writing and reviewing a diatom-chemistry focused manuscript (*Deliverable 4*).

Title: Diatoms response to soil and porewater chemistry in New Jersey salt marshes and relationships to vegetation health status

Authors: Mihaela Enache[1], Charles Schutte[2], Brittany P. Wilburn[1], Joshua Moody[1], Metthea Yepsen[1], Kriish Hate[1,2]

[1]NJDEP, Division of Science and Research

[2]Rowan University

Abstract

The relationships between diatom species and porewater chemistry were explored in two salt marshes located in the Tuckerton peninsula’s Great Bay Boulevard Wetland Management Area and E.B. Forsythe National Wildlife Refuge. Diatom samples and porewater chemistry were collected from qualitatively determined healthy and unhealthy vegetated marshes. More than 200 species have been identified. Of these, only a few species, such as *Melosira nummuloides*, *Denticula subtilis*, *Luticola mutica*, and *Nitzscia microcephala,* displayed high abundances of more than 50% relative abundance. Overall, diatom assemblages and porewater chemistry did not reveal strong relationships to marsh vegetation status; however, in healthy *Spartina alterniflora,* higher abundances of *Denticula subtilis* were found, while *Luticola mutica* and *Melosira nummuloides* displayed lowest abundances. The unhealthy *S. alterniflora* and *S. patens* had persistent species of high nutrient lovers, such as *Navicula* and *Nitzschia* species. However, these species also reached high abundances in sites located in the healthy vegetation wetlands. Unconstrained ordination revealed that pH and salinity were the most important environmental factors across the chemistry dataset in determining diatom community assemblages. Canonical Correspondence analyses showed that variations in diatom species composition are significantly related to pH and salinity measurements and diatom species clearly separated high pH from low pH sites within the dataset. This study revealed for the first time the impacts of sediment porewater chemistry on diatom species composition in New Jersey salt marshes, and the potential use of diatom species as a tool to indicate areas degrading due to climate and sea level impacts on wetlands soil characteristics.

Introduction

Wetlands play an essential role in filtering pollutants, storing flood waters, and providing habitats for a diverse and abundant array of fish, wildlife, and plants. From bacteria to eukaryotes, protists, zooplankton, and benthos, there are numerous groups of microorganisms inhabiting the wetlands that also play an essential role in providing food to higher trophic levels. Microorganisms dynamically contribute to soil physico-chemical processes and create surface films that protect the wetlands from tidal erosion impacts. Microorganisms from wetland soils are also sensitive to environmental conditions and can provide potential biological indicators that can help us better understand wetland condition and dynamics (e.g., Astudillo-García et al., 2019; Parmar et al., 2016).

Within these microscopic biological proxies, diatoms have proven to be accurate indicators of nutrients, pollution, and salinity in tidal wetlands. Due to their high diversity, wide distribution and high sensitivity to variation in water and soil characteristics, the use of diatom species in estuaries and coastal wetlands assessment applications has dramatically increased over the last decades (Nelson and Kashima, 1993; Hemphill-Haley, 1995, 1996; Zong and Horton, 1998; Sherrod, 1999; Sawai et al., 2004, 2016; Dura et al., 2016; Desianti et al., 2017, 2019). Diatom species composition varies continuously across different habitat types in salt marsh-dominated coastal ecosystems, and multiple factors interact to determine the diatom community structure along elevation gradients including salinity (Desianti et al., 2017; Wachnicka et al., 2010), tidal inundation (Desianti et al., 2019), sediment grain size (Desianti et al., 2017), sediment organic content (Desianti et al., 2017), nutrient concentrations (Desianti et al., 2019; Underwood et al., 1998), and substrate types (Ribeiro et al., 2013). Compilations of autecological characteristics of coastal diatoms (Denys, 1991; Vos and de Wolf, 1993) from the literature are often employed in environmental assessment or environmental history reconstruction. However, numerical analyses, such as diatom inference models, allow for greater precision than metrics based on expert opinions (Birks, 1995), and they provide statistical assessment of uncertainty associated with ecological inferences. Since 2012, NJDEP has conducted extensive efforts to explore the potential of diatom species as ecological indicators of wetland condition. Recently, Desianti et al. (2017, 2019) successfully developed regional diatom-based models for New Jersey coastal wetlands to assess critical attributes for describing the marshes' state condition, such as salinity, sediment nitrogen content, and tidal inundation. Such diatom inference models are applicable for environmental assessment in the Mid-Atlantic coastal region with large ranges of taxonomic and ecological variations.

Spartina alterniflora and *Spartina patens* are the dominant plants in low elevation and high elevation salt marshes in this region. While these plants are capable of growing roots tens of centimeters into the soil, their roots tend to be most concentrated in the top 10 cm (Bertness and Ellison, 1987; Smith et al., 1979), roughly co-locating them with the diatoms that occupy the soil surface. Both are photosynthetic organisms that rely on energy from sunlight and nutrients from their soil substrate and estuarine waters. As such, both diatom and plant communities are structured in part by gradients in edaphic conditions such as salinity, tidal inundation, and soil and porewater chemistry. For example, the more frequent and longer duration tidal flooding that characterizes low marsh habitat results in more consistently waterlogged soil that is more reduced (having a lower oxidation reduction potential), which is known to inhibit root growth in *S. patens* and may help to maintain the characteristic distribution of *S. patens* in high marsh habitat and *S. alterniflora* in low marsh habitat (Bertness, 1991). *S. alterniflora* tolerance of reduced, waterlogged soil is likely facilitated by its enhanced ability, relative to *S. patens*, to transport oxygen to its roots (Maricle and Lee, 2007). Additionally, due to the abundance of seawater-derived sulfate in coastal wetland porewaters, phytotoxic sulfide can be produced as a byproduct from sulfate reduction, an important pathway for organic matter oxidation (Hines et al., 1989; Howarth, 1979; Howarth and Teal, 1979). Sulfide is toxic to salt marsh plants (Howes et al., 1981) such that its presence in the porewater can be used as an indicator salt marsh health (Himmelstein et al., 2021). Furthermore, in an environment where primary production is typically limited by nitrogen availability, the accumulation of a bioavailable form of inorganic nitrogen like ammonium in the porewater can also be an indicator of poor marsh health (Himmelstein et al., 2021) since plant nitrogen uptake can be inhibited by stressors such as increasing salinity (Bradley and Morris, 1991). While these soil and porewater conditions' effects on salt marsh communities are better understood, there yet remains a gap between these physico-chemical conditions and diatom community assemblages.

The purpose of this study is to explore relationships between diatom species and soil and porewater chemistry in New Jersey salt marshes (Great Bay Boulevard Wildlife Management Area in Tuckerton peninsula and E.B. Forsythe National Wildlife Refuge), with the ultimate goal to utilize diatom species as indicators of wetland vegetation condition. Through this study we are testing the diatom potential to respond to measured soil characteristics and discriminate between marshes of healthy/unhealthy vegetation status, identify areas of vulnerability due to current climate conditions, and in need of protection and remediation.

Methods

Site description

Samples were taken in two different areas in southern New Jersey. The Forsythe National Wildlife Reserve (Forsythe) and a salt marsh on Great Bay Boulevard (GBB) are commonly studied salt marshes, making them suitable for this study. Both areas have segments that have been ditched, with areas of varying degrees of salt marsh loss, and segments that have not experienced ditching, or relative salt marsh loss over time (Figure 5.1). Within both areas, there are large patches of high marsh dominated by *Spartina patens* and low marsh dominated by *Spartina alterniflora*. Therefore, samples were collected from four

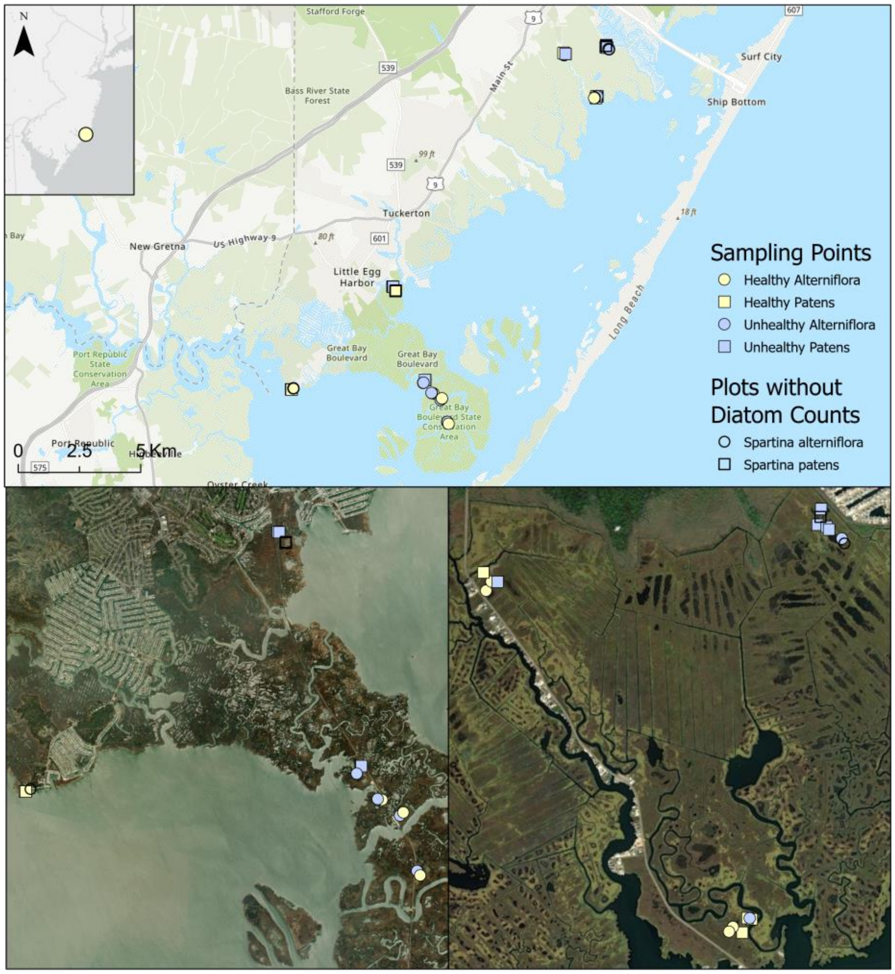

Figure 5.1. Map of the diatom and chemistry sampling points in Great Bay Boulevard Wildlife Management Area (GBB) and E.B. Forsythe National Wildlife Refuge (Forsythe). Plots labelled as healthy are denoted by yellow points; unhealthy plots are denoted by purple points; S. alterniflora dominant plots are circles; S. patens dominant plots are squares. Sampling points where diatoms were not analyzed are represented by hollow points.

marsh health categories: healthy *S. patens*, unhealthy *S. patens*, healthy *S. alterniflora*, and unhealthy *S. alterniflora*.

Sampling design

Samples were collected from 32 plots, each with an area of 100 m^2, distributed between the Forsythe and GBB (Table 5.1). Plots were divided between *Spartina alterniflora* dominated low marshes and *Spartina patens* dominated high marshes. Marsh health was qualitatively assessed based on plant characteristics such as percent cover, stem height, and penetration depth. Within each plot, 4 subsampling points

Table 5.1. Sampling locations and their vegetation health attributes.

Sample ID	Latitude (°)	Longitude (°)	Health Category	Dominant Species	Diatom Counts
Z1P1	39.5768	-74.3438	Unhealthy	*Spartina patens*	X
Z1P2	39.5767	-74.3435	Unhealthy	*Spartina patens*	X
Z1P3	39.5753	-74.3422	Healthy	*Spartina patens*	
Z1P4	39.5751	-74.3423	Healthy	*Spartina patens*	
Z2P5	39.5390	-74.3919	Healthy	*Spartina patens*	X
Z2P6	39.5390	-74.3918	Healthy	*Spartina patens*	X
Z2P7	39.5394	-74.3908	Healthy	*Spartina alterniflora*	
Z3P8	39.5424	-74.3283	Unhealthy	*Spartina patens*	X
Z3P9	39.5413	-74.3291	Unhealthy	*Spartina alterniflora*	X
Z4P10	39.5374	-74.3244	Healthy	*Spartina alterniflora*	X
Z4P11	39.5376	-74.3252	Unhealthy	*Spartina alterniflora*	X
Z5P12	39.5351	-74.3210	Unhealthy	*Spartina alterniflora*	X
Z5P13	39.5356	-74.3204	Healthy	*Spartina alterniflora*	X
Z6P14	39.5270	-74.3179	Unhealthy	*Spartina alterniflora*	X
Z6P15	39.5264	-74.3173	Healthy	*Spartina alterniflora*	X
Z8P2	39.6459	-74.2468	Healthy	*Spartina patens*	X
Z8P3	39.6465	-74.2463	Healthy	*Spartina patens*	X
Z8P4	39.6465	-74.2465	Healthy	*Spartina patens*	X
Z8P5	39.6465	-74.2464	Unhealthy	*Spartina alterniflora*	X
Z8P6	39.6461	-74.2474	Healthy	*Spartina alterniflora*	X
Z8P7	39.6459	-74.2476	Healthy	*Spartina alterniflora*	X
Z7P8	39.6617	-74.2619	Healthy	*Spartina alterniflora*	X
Z7P9	39.6621	-74.2616	Healthy	*Spartina alterniflora*	X
Z7P10	39.6626	-74.2621	Healthy	*Spartina patens*	X
Z7P11	39.6621	-74.2612	Unhealthy	*Spartina patens*	X
Z9P12	39.6653	-74.2419	Unhealthy	*Spartina patens*	X
Z9P13	39.6650	-74.2420	Unhealthy	*Spartina patens*	
Z9P14	39.6646	-74.2421	Unhealthy	*Spartina patens*	X
Z9P15	39.6645	-74.2416	Unhealthy	*Spartina patens*	X
Z9P16	39.6644	-74.2415	Unhealthy	*Spartina patens*	X
Z9P17	39.6640	-74.2407	Unhealthy	*Spartina alterniflora*	X
Z9P18	39.6638	-74.2405	Unhealthy	*Spartina alterniflora*	

representative of health category were selected for detailed diatom and soil and porewater chemistry analyses.

Diatom sampling and analyses

Within each vegetation plot, soil samples were collected from 10x10 cm surface soil plots with approximately 1 cm depth, transported on ice, and stored frozen at NJDEP laboratory until preparation. Upon thawing, samples were carefully homogenized and approximately 1 g sediment was subsampled, treated with HNO_3, and mounted on glass slides following methods described in Charles et al. (2002). Diatom species were identified to the lowest taxonomic level of species and variety using a Differential Interference Contract (DIC)-equipped Leica DM2500 microscope with a Leica DFC3000 G camera. For each slide, up to 300 valves were counted on random transects and extrapolated to provide an estimate of total diversity, with the exception of a few slides that contained very sparse specimens; in these cases, the entire slide was screened. Species identification was based primarily on the New Jersey diatom wetland flora as presented in Desianti et al. (2019) and is available from the NJDEP State Library repository.[1]

Soil measurements

A block of soil (~15 cm wide x ~15 cm long x ~30 cm deep) was removed from the marsh surface to allow access to a fresh, vertical soil profile. All measurements were made 10 cm below the soil surface on the same plane of the hole created in the marsh. Soil temperature was measured by inserting a thermometer directly into the soil on a horizontal plane. Oxidation/reduction potential (ORP) was measured by inserting a sensor into the soil (Extech Instruments ExStik Model RE300 Waterproof ORP meter). Soil pH was measured by inserting a pH sensor (Hanna Instruments Groline Soil pH tester) into the soil.

Porewater sampling

Porewater samples were collected from the same location using Rhizon porewater samplers (0.25 mm diameter, 10 cm length, 0.15 µm pore size; Rhizosphere Research Products). Salt marsh porewater samples are often collected from 0–10 cm below the marsh surface where plant roots tend to be the most concentrated (Smith et al., 1979; Bradley & Morris, 1991). In this study, samples were collected from 10 cm below the marsh surface to ensure uniform access to sufficient porewater volume for all samples, even in relatively dry, high elevation marshes. As such, the Rhizon was inserted into the soil horizontally at 10 cm depth. Around 1 mL of porewater was collected into a 12-mL syringe and carefully discarded to rinse the Rhizon and tubing and remove any gas bubbles. Then the syringe was reconnected to the Rhizon and allowed to fill for 1-2 hours. Even sample volumes from the four subplots within each plot were combined into a single 60-mL syringe to create one composite porewater sample per plot. A composite sampling strategy was used to sample across the spatial heterogeneity within each plot while managing the sample load for the overall project. The salinity of the composite porewater sample was measured in the field using a handheld refractometer. The composite porewater sample was then passed through a 0.2 µm

---

[1] https://hdl.handle.net/10929/68423

syringe filter with polyethersulphone (PES) membrane into various sample vials for different analyses. For sulfide analysis, 3 mL was dispensed into a 4-mL glass sample vial containing 300 µL of 20% (w/v) zinc acetate. For chloride and sulfate analysis, 5 mL was dispensed into a 20-mL plastic scintillation vial containing 50 µL of 3.9 N nitric acid. For ammonium and phosphate analysis, 5 mL was dispensed into a 15-mL centrifuge tube. For conductivity analysis, the remaining volume was collected into a 15-mL centrifuge. All subsamples were kept in a cooler on ice until they were returned to the laboratory where samples were frozen (ammonium) or refrigerated until analysis.

Porewater analysis

Sulfide concentrations were measured using the zinc acetate preserved subsample by colorimetric analysis (Cline, 1969). Ammonium and phosphate concentrations were quantified by colorimetric analysis using a discrete autoanalyzer (Seal AQ300; USEPA Method 350.1, 1993). Chloride and sulfate concentrations were determined via ion chromatography (Schutte et al., 2016). Porewater conductivity was measured using a benchtop conductivity meter (USEPA Method 120.1, 1983).

Data analysis

Ordinations in reduced space were used in this project to provide quantitative information on the relationship among descriptors (species, environmental variables) and sampling sites (Legendre and Legendre, 1998). To estimate the explanatory power of each environmental variable, a series of Canonical Correspondence Analyses (CCA) was performed using each environmental variable as the sole constraining variable. The statistical significance of each variable was assessed using Monte Carlo unrestricted permutation tests involving 999 permutations (ter Braak, 1990). A CCA (and associated Monte Carlo permutation test) with forward selection using all measured environmental variables was carried out to find a minimal set of variables that explain, in a statistical sense, some variance within the biological data. CCA is an ordination method appropriate for species abundance and relative frequency data that have a large number of 0 values (absences of taxa) (Legendre and Legendre, 2012). CCA biplots were produced to represent simultaneously the ordination of samples and diatom species and their relationship to environmental variables. In the ordination diagrams, environmental variables are represented by arrows, the point of which indicates the direction of maximal quantitative variation. Non-constrained Principal Component Analysis was performed to explore variations in pore water chemistry and relationships to sampling sites. All ordinations were performed using Canoco 5 (ter Braak and Šmilauer, 2012). Diatom species and chemistry data were log-transformed with the exception of pH. Species distributions, correlations and mean *t*-test analyses were performed using the JMP v. 14 software (JMP®, SAS Institute Inc., Cary, NC, 1989-2023). Diatom-based reconstructions of salinity, TN, and SWLI were performed using predictive models (transfer functions) published in Desianti et al. (2019).

Results and Discussion

Soil and porewater chemistry

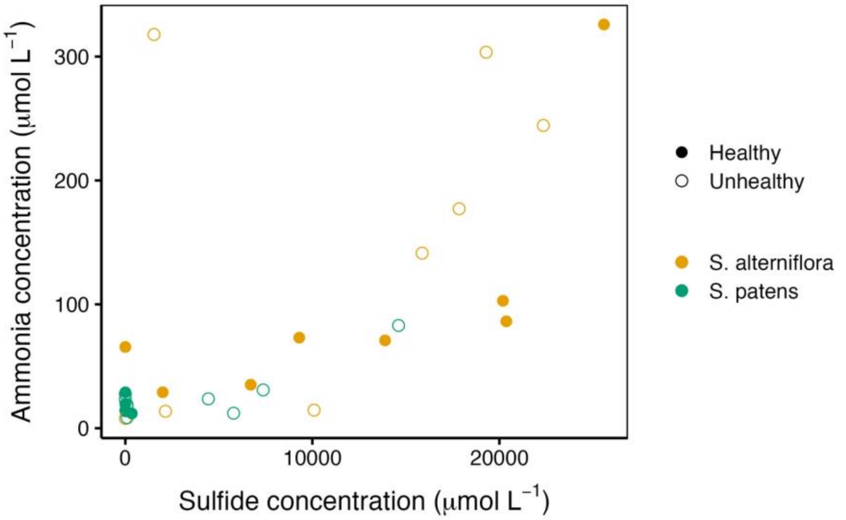

Figure 5.2. Porewater ammonia concentration plotted against porewater sulfide concentration for each marsh type: healthy (filled circle) & unhealthy (open circle). Orange and green circles represent S. alterniflora and S. patens, respectively.

The distribution of soil and porewater chemical parameters across healthy and unhealthy *S. alterniflora* and *S. patens* sites was first explored, and no clear, stand-alone indicators of marsh health were evident (Figures 5.2 and 5.3). However, there were two broad patterns in the chemistry across sites. First, there was a negative relationship between ORP and pH (Figure 5.2), and second, there was a positive correlation between ammonia concentration and sulfide concentration (Figure 5.3).

Healthy *S. patens* sites clustering together at pH < 4.5 and ORP > 100 mV and all *S. alterniflora* sites clustered together at pH > 4.5 and ORP < 210 mV (Figure 5.2). Unhealthy S*. patens* sites, on the other hand, were spread across these two other groups. There are well-documented patterns in soil ORP across salt marsh vegetation zones, with unvegetated soil being very reduced relative to vegetated soil (Howes et al., 1981) and *S. patens* zones being more oxidized than *S. alterniflora* zones (Bertness and Ellison, 1987). Both plants oxidize the soil by translocating oxygen to their root systems to support root metabolism (Maricle and Lee, 2007; Pezeshki et al.,

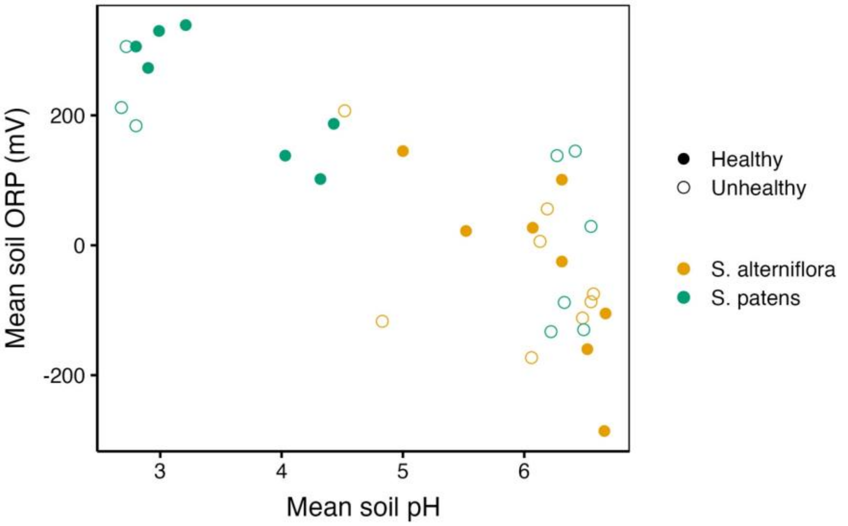

Figure 5.3. Mean soil ORP plotted against mean soil pH for each marsh type: healthy (filled circle) & unhealthy (open circle). Orange and green circles represent S. alterniflora and S. patens, respectively.

1991), but *S. alterniflora* exhibits much more rapid rates of oxygen transport (Maricle and Lee, 2007), which likely helps to maintain the differentiation between *S. patens* dominated high marsh zones and *S. alterniflora* dominated low marsh zones (Bertness, 1991). Transplantation experiments in which *S. patens* was moved into cleared areas of both short- and tall-form *S. alterniflora* demonstrated that *S. patens* did not grow as well in the short-form *S. alterniflora* zone and did not survive in the tall-form *S. alterniflora* zone (Bertness and Ellison, 1987; Bertness, 1991). Therefore, consistently low ORP in an *S. patens* marsh may be an early warning sign of vulnerability to transition from high marsh to low marsh. The fact that we observed overlapping ORP values between healthy and unhealthy *S. patens* sites may be due to short-term variability in edaphic conditions during the one time point that we collected samples or the qualitative way in which sites were designated as healthy or unhealthy.

Sulfide concentrations measured between 0 and 25,600 µM in *S. alterniflora* marshes and between 0 and 14,600 µM in *S. patens* marshes. The median concentration of 12,000 µM in *S. alterniflora* marshes was much higher than the median value of 47 µM in *S. patens* marshes. There was a similar pattern between species in ammonia concentrations, with *S. alterniflora* marshes having a median value of 80 µM and a range of 8–326 µM and *S. patens* marshes having a median value of 18 µM and a range of 8–83 µM. In keeping with our observation of a positive correlation between sulfide and ammonia concentrations across sites, DeLaune et al. (1983) observed decreasing belowground biomass and increasing sulfide and ammonia concentrations with depth in both short- and tall-form *S. alterniflora* marshes of Louisiana and higher ammonia and sulfide concentrations in short-form than tall-form *S. alterniflora*. Himmelstein et al. (2021) observed higher sulfide and ammonia concentrations near the edge of unstable, expanding ponds (6400±800 µM and 161±29 µM respectively) than near stable ponds (3200±500 µM and 97±38 µM, respectively). These values are similar in range to those we observed and indicate the utility of sulfide and ammonia as indicators of marsh health. That said, the variability in ammonia concentrations is similar between *S. patens* marshes with near-zero sulfide concentrations and those with sulfide concentrations greater than 100 µM. This may be because the alternative state for a healthy *S. patens* marsh is a healthy *S. alterniflora* marsh rather than an unvegetated mudflat; if *S. patens* nitrogen uptake is inhibited by stress, the available nitrogen is likely to be taken up by another plant, like *S. alterniflora*, that is in the process of invading.

Relationships between soil pore water parameters were further explored to eliminate redundancies in the environmental data. Significantly ($p \leq 0.05$) correlated environmental variables were identified from a Pearson correlation matrix with Bonferroni adjusted probabilities. Highly correlated pairs were found between chloride, conductivity, and salinity, which is expected given that all these values derive from the salts dissolved in seawater that mix into the estuary. The relationships among the porewater variables (Table 5.2) and the position of the sites with respect to environmental gradients were further explored using a non-constrained PCA ordination based on correlation matrix. The first axis extracts 80% of the data variation (Table 5.3) and variables with highest contribution are pH, sulfide, and sulfate. Chloride, temperature, and conductivity have little contribution to the first axis of the ordination. Variables with small angles between arrows have high positive correlations (e.g., chloride, salinity, conductivity, pH, and sulfate; Figure 5.4). Variables with long arrows have high variance and their proximity to axes determines their relative weight in determining each PCA axis. Salinity and phosphorus contribute to the second ordination axis but absorb a small proportion of the data variation.

Table 5.2. Porewater chemistry data set used in Principal Component Analysis unconstrained ordination. NA's denote samples for which analysis could not be done due to equipment issues.

Sample	Salinity (ppt)	pH	ORP (mV)	Temperature (°C)	Water Table Depth (cm)	Chloride (mmol L^{-1})	Sulfate (mmol L^{-1})	Conductivity (mS cm^{-1})	Ammonia (µmol L^{-1})	Phosphate (µmol L^{-1})	Sulfide (µmol L^{-1})
Z2P5	32	3.0	330	25.6	15	347.6	35.9	40.3	14.7	14.2	0
Z2P6	32	3.2	339	25.6	20	392.9	34.7	40.4	14.4	2.1	0
Z2P7	42	6.3	101	28.2	13	521.7	24.2	52.6	35.1	18.6	6706
Z1P1	51	2.7	212	25.1	20	552.0	48.8	41.4	23.1	4.2	0
Z1P2	47	2.7	306	25.1	25	535.9	56.7	54.1	18.9	25.6	92
Z1P4	43	2.9	273	25.0	20	518.1	46.6	59.0	19.5	12.2	0
Z1P3	49	2.8	306	24.9	15	640.6	58.2	61.5	13.6	5.3	7
Z3P9	50	6.6	-87	27.9	43	724.4	24.7	65.7	141.3	8.9	15869
Z3P8	49	2.8	184	25.9	20	NA	NA	NA	27.6	0.8	0
Z4P11	43	6.1	-173	25.2	7	681.5	23.0	61.8	244.4	10.0	22350
Z4P10	52	5.0	145	25.0	4	802.4	48.4	71.9	65.6	1.0	0
Z5P12	52	6.6	-75	25.0	2	701.6	26.5	67.5	177.2	8.6	17850
Z5P13	43	6.5	-160	24.7	18	582.9	14.9	51.8	102.9	30.5	20190
Z6P14	39	6.5	-112	25.4	7	580.6	19.3	56.3	303.5	11.5	19290
Z6P15	41	6.7	-286	24.8	13	611.4	7.3	56.7	325.9	107.8	25591
Z8P3	22	4.3	102	21.8	11	302.5	21.2	32.2	14.2	1.0	5
Z8P2	28	4.5	207	24.3	10	390.2	21.1	39.6	7.9	1.0	0
Z8P7	45	6.1	27	24.6	4	564.2	25.3	58.4	73.1	5.5	9299
Z8P6	42	5.5	22	25.3	2	590.2	32.2	56.0	29.1	1.3	2001
Z8P4	25	4.4	187	22.8	8	311.3	16.6	34.5	11.9	1.2	347
Z8P5	56	4.8	-117	25.3	2	850.3	45.6	72.9	317.8	2.2	1533
Z9P12	30	6.3	-88	26.3	0	416.8	18.0	41.6	30.9	4.7	7372
Z9P18	30	6.2	56	23.6	0	460.5	20.1	45.7	13.7	1.7	2145
Z9P17	30	6.1	6	24.0	0	442.0	17.3	43.6	14.6	3.3	10091
Z9P16	31	6.4	145	25.3	0	457.4	20.4	47.5	18.0	1.7	86
Z9P15	32	6.6	29	25.5	0	485.4	22.1	47.1	23.7	3.4	4438
Z9P14	24	6.3	138	26.3	0	392.0	18.3	38.8	8.5	2.2	91
Z9P13	31	6.2	-133	22.6	0	461.3	20.2	45.1	12.1	3.8	5788
Z7P11	22	6.5	-130	23.1	0	319.1	9.2	32.9	82.9	3.2	14609
Z7P8	19	6.7	-105	23.8	8	251.9	3.0	27.3	86.3	8.4	20370
Z7P9	27	6.3	-25	25.0	0	391.6	12.0	41.6	70.9	7.8	13889
Z7P10	28	4.0	138	22.1	15	372.9	22.7	40.5	29.0	1.1	0

Table 5.3. Diatom Principal Component results summary.

Statistic	Axis 1	Axis 2	Axis 3	Axis 4
Eigenvalues	0.8041	0.0964	0.0461	0.0203
Explained variation (cumulative)	80.41	90.05	94.66	96.69

Diatom species

Diatoms were represented by more than 200 species in the sampling sites. However, most species had low abundances and sparse occurrences across the dataset.

To reduce the noise of the many 0 (zero) occurrences and to account for the small size of the dataset, species with relative abundances of more than 5% in at least one sample were retained for further analyses. Most species were present in all sampling sites regardless of their vegetation health status. However, *Denticula subtilis* reached higher abundances in healthy *S. alterniflora* sites, while *Luticola mutica*, *Melosira nummuloides* and *Minidiscus* spp. have lowest abundances in these samples. The latter species are mostly characteristic of higher elevation wetlands, which may explain their low abundances in the healthy *S. alteriflora* sites. However, it is notable that *Melosira nummuloides,* a species that also prefers sites with abundant macrophytes, reached highest abundances in an unhealthy *S. alterniflora* site. Another notable feature is that species of *Navicula* and *Nitzschia*, indicators of higher nutrient pollution, were found to be abundant in both healthy and unhealthy vegetation sites with the exception of healthy *S. patens* (Figure 5.5).

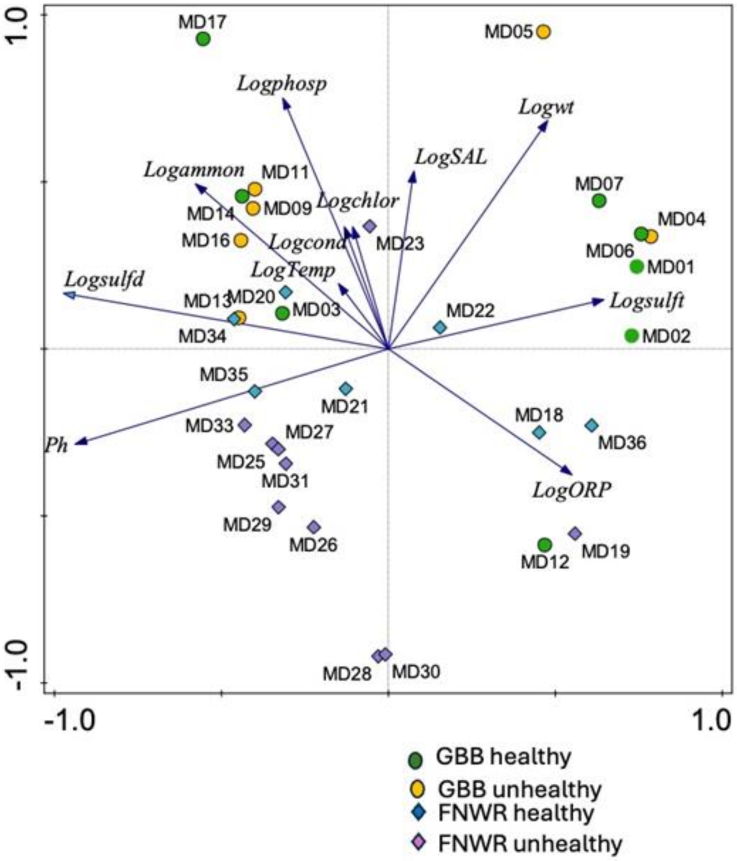

Figure 5.4. Results of a Principle Component Analysis (PCA) showing the importance and correlations between porewater and soil chemistry variables across the study sites GBB = Great Bay Blvd, FNWR = Forsythe National Wildlife Refuge) and their attributed health status (healthy & unhealthy). Sample labels are noted adjacent to each point.

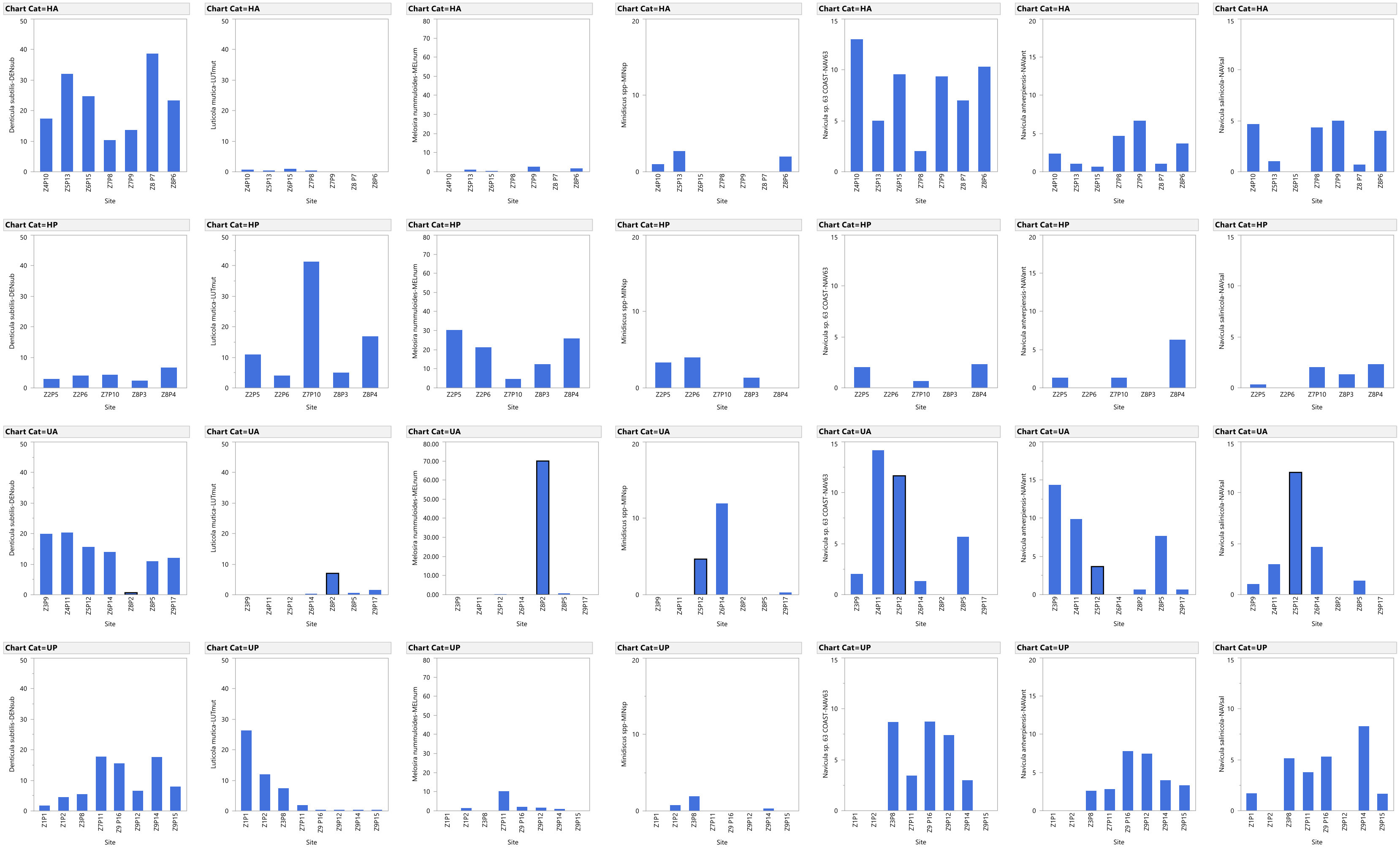

Figure 5.5. Relative abundances of select diatom species in the study sites and their attributed health status of healthy S. alterniflora (HA), healthy S. patens (HP), unhealthy S. alterniflora (UA), and unhealthy S. patens (UP).

Relationships diatom species and porewater chemistry

First, the distribution of diatom species was examined to determine whether linear or unimodal methods are appropriate for the examination of relationships between diatom species and soil porewater chemistry. To this end, the biological dataset (diatom species) was analyzed by Detrended Correspondence Analysis (DCA) to estimate the environmental gradient length. An environmental gradient higher than two standard deviation units is considered appropriate for unimodal methods (Birks, 1995). The diatom species gradient length in our data set was found to be 2.5 SD and unimodal methods were applied for subsequent ordinations.

Canonical Correspondence Analysis (CCA) was performed using a set of four porewater chemistry variables after excluding variables with high correlation and poor contribution to the first PCA axis; 32 diatom species with abundances of more than 5% and presence in at least three samples were included in the analysis. The CCA summary analysis is presented in Table 5.4. The data set comprised 27 samples with both diatom and pore water data available. The forward selection and Monte Carlo testing revealed that pH and salinity were highly significant for explaining a cumulative variation of 32% of diatom species (Table 5.5). These results are remarkable, taking into account the small size of our dataset.

Table 5.5. Canonical Correspondence Analysis (CCA) summary analysis. Total variation is 1.38868, explanatory variables account for 32.2% and adjusted explained variation is 19.3%.

Statistic	Axis 1	Axis 2	Axis 3	Axis 4
Eigenvalues	0.2955	0.0785	0.0449	0.0281
Explained variation (cumulative)	21.28	26.93	30.16	32.19
Pseudo-canonical correlation	0.9212	0.8232	0.7701	0.6035
Explained fitted variation (cumulative)	66.10	83.66	93.70	100.00

Table 5.4. Results of the Canonical Correspondence Analysis (CCA) with forward selection and Monte Carlo testing.

Parameter	% Explained	% Contribution	pseudo-*F*	*p*-value
pH	19.6	60.9	5.9	0.001
Log Salinity	6.4	19.8	2.0	0.006
Log Sulfate	3.5	10.9	1.1	0.342
Log Sulfide	2.7	8.4	0.8	0.642

In freshwater systems, diatom species' high sensitivity to pH is widely known and diatom-based predictive models have been used to reconstruct pH histories in lake sediments and to assess impacts of human activities, especially mining and atmospheric deposition. Relationships between diatom species and freshwater lakes pH have been widely used to explore effects from acid rain during the 1990s (Battarbee, 1984; Charles and Smol, 1990; Dixit et al., 1993; Sebetich and Messaros, 1993) and more recently freshwater wetlands dynamics (Gaiser and Johansen, 2011; Weilhofer and Pan, 2007).

In coastal environments, diatom response to salinity gradients and nutrient concentrations is widely used in bioassessment and paleo environmental studies (e.g., Wachnicka et al., 2011). In NJ coastal environments the effects of salinity and sediment contaminants on diatom species were investigated by Desianti et al. (2017) and Potapova et al. (2015), and diatom assemblages were used to reconstruct the impacts of European settlement on NJ coastal wetlands (Enache and collaborators 2019 NJDEP report[2]). At present, diatom response to soil water pH, sulfide, and sulfate concentrations remains unexplored, mainly because of the obscuring effects due to strong gradients in salinity, nutrients, types of habitat and other factors impacting coastal wetlands dynamics. However, diatom response to pH was found in smaller scale non-coastal wetland investigations. For example, Charles and Brown (2007) explored environmental effects on diatoms in isolated herbaceous wetlands from Florida and soil pH effects were included in the calculation of these isolated wetlands condition indices.

Our investigation, although it included a small dataset, reveals that there is potential in using diatom species as indicators for levels of sulfide and sulfate in wetland soils via their indirect relationships, shown in our data to pH and ORP gradients present in our samples (Figure 5.6 and 5.7). Species of *Navicula* sp. 23, *Seminavis pusilla*, *Planothidium frequentissimum* and *P. delicatulum* (Figure 5.8) clearly display preference for high pH and sulfide by association, while *Paralia sulcata*, *Amphora* sp., and *Cocconeis stauroneiformis* are correlated with low pH/sulfide. Further investigations may be able to more accurately capture the impacts of soil chemistry components on diatom species and ability to reflect the vegetation health status.

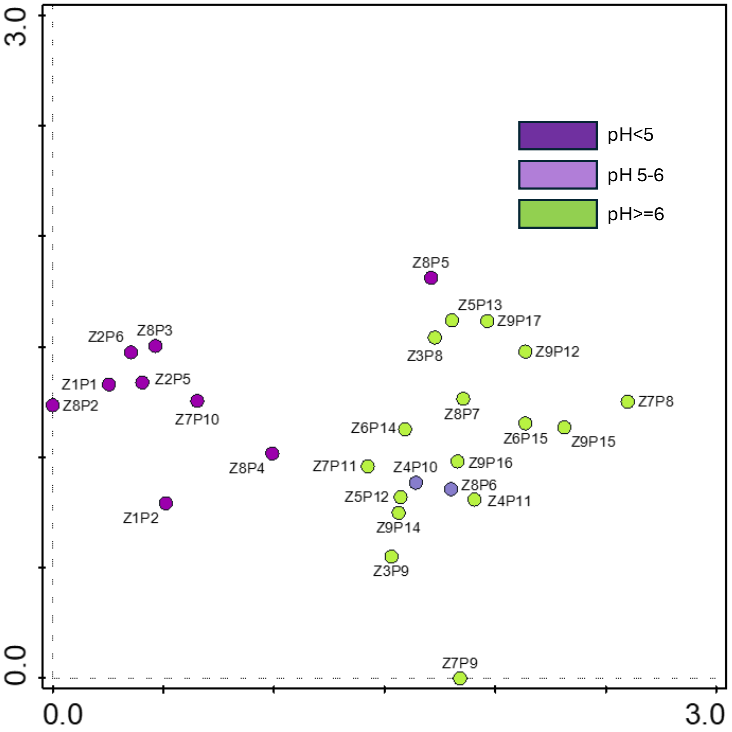

Figure 5.6. Correspondence analysis of diatom species showing distribution across the sampling sites and their respective porewater pH (dark purple = <5, light purple = 5-6, & green = >6). Sample labels are noted in the figure adjacent to each data point.

---

[2] https://hdl.handle.net/10929/68423

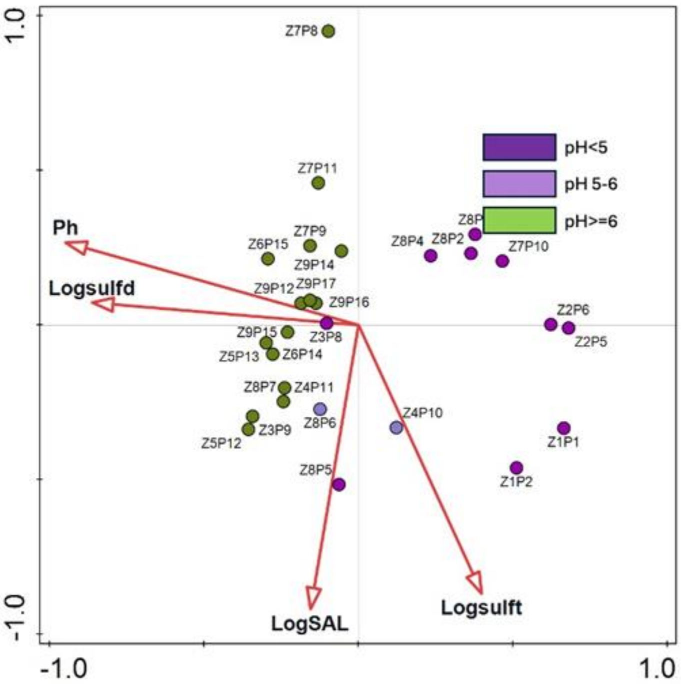

Figure 5.7. Canonical Correspondence Analysis biplot showing the relative position of sampling sites and relationships (red arrows) to pH (Ph), sulfide depletion (Logsulfd), salinity (LogSAL), and sulfate (Logslft). Sites are coded in function of their measured porewater pH. (dark purple = <5, light purple = 5-6, & green = >6). Sample labels are noted in the figure adjacent to each data point.

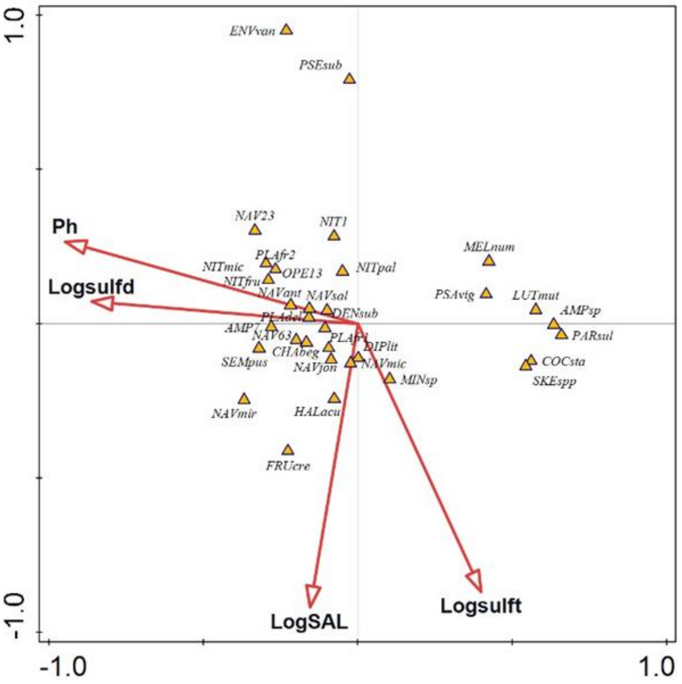

Figure 5.8. Canonical Correspondence Analysis biplot showing the relative position of diatom species and relationships (red arrows) to pH (Ph), sulfide depletion (Logsulfd), salinity (LogSAL), and sulfate (Logslft). Sample labels are noted in the figure adjacent to each data point.

Conclusions and Recommendations

Although this project involved a small dataset, diatoms show statistically significant response to porewater pH and salinity. Although sulfide and sulfate by themselves were not revealed statistically significant, due to their high correlations to pH and salinity respectively, diatom species may also be able to intrinsically indicate variations in these two parameters. As ORP decreases across study sites, sulfide concentrations increase due to more active sulfate reduction and/or slower sulfide oxidation in more reduced soil, and diatoms present in this environment have the potential to indicate wetland degradation. It is very possible that diatom species reveal in fact a response to sulfide concentrations rather than pH, but this relationship is at present obscured due to the strong pH gradient in the pore water chemistry data.

The fact that the diatom species did not clearly discriminate between healthy and unhealthy wetland vegetation may be also due to the fact that diatoms respond also to local variations in marsh elevation, tidal impacts, microhabitat, and hydrology. A larger dataset would be necessary to reveal stronger relationships between diatoms and soil pore water sulfide and increase their ability to indicate healthy or unhealthy marsh areas.

Results of this investigation show that capturing data that covers a wider range of wetland health would be important for generating a more accurate/detailed relationship between diatoms/chemistry/plants. For future marsh vegetation health evaluation, it would be beneficial to include, in addition to visual evaluation, preliminary biogeochemical samples to allow for a more comprehensive condition assessment. Soil ORP would be a particularly useful metric for this type of preliminary assessment because it can be measured quickly and easily in the field and has well-documented relationships with plant species distribution and plant growth. Depending on sedimentation rates, diatom samples would be useful for indicating impacts from adverse pore water chemistry on vegetated marshes covering a wider time scale, of one or possible multiple seasons, in addition to their ability to assess nutrient pollution, salinity changes, and tidal flooding.

References

Astudillo-García, C., Hermans, S. M., Stevenson, B., Buckley, H. L., & Lear, G. (2019). Microbial assemblages and bioindicators as proxies for ecosystem health status: potential and limitations. *Applied Microbiology and Biotechnology*, *103*(16), 6407–6421. https://doi.org/10.1007/s00253-019-09963-0

Bertness, M. D., & Ellison, A. M. (1987). Determinants of Pattern in a New England Salt Marsh Plant Community. *Ecological Monographs*, *57*(2), 129–147. https://doi.org/10.2307/1942621.

Bertness, M. D. (1991). Zonation of Spartina Patens and Spartina Alterniflora in New England Salt Marsh. *Ecology*, *72*(1), 138–148. https://doi.org/10.2307/1938909.

Birks, H. J. B. (n.d.). Quantitative palaeoenvironmental reconstructions. In *Statistical Modelling of Quaternary Science Data* (Technical guide 5, p. 271). Quaternary Research Association. https://www.uib.no/en/rg/EECRG/57871/quantitative-palaeoenvironmental-reconstructions

Bradley, P. M., & Morris, J. T. (1991). The influence of salinity on the kinetics of NH inf4 sup+ uptake in Spartina alterniflora. *Oecologia*, *85*(3), 375–380. https://doi.org/10.1007/BF00320613

Burdick, D. M., & Mendelssohn, I. A. (1990). Relationship Between Anatomical and Metabolic Responses to Soil Waterlogging in the Coastal Grass *Spartina patens*. *Journal of Experimental Botany*, *41*(2), 223–228. https://doi.org/10.1093/jxb/41.2.223

Charles, D. F., & Smol, J. P. (1990). The PIRLA II Project: Regional assessment of lake acidification trends. *SIL Proceedings, 1922-2010*, *24*(1), 474–480. https://doi.org/10.1080/03680770.1989.11898783

Charles, D. F., & Davis, R. S. (2002). *Protocols for the analysis of algal samples collected as part of the U.S. Geological Survey National Water-Quality Assessment Program* (Nos. 02–06). The Academy of Natural Sciences.

Cline, J.D. (1969). Spectrophotometric determination of hydrogen sulfide in natural waters. *Limnology and Oceanography*, 14:454–458. https://doi.org/10.4319/lo.1969.14.3.0454

DeLaune, R. D., Smith, C. J., & Patrick, W. H. (1983). Relationship of Marsh Elevation, Redox Potential, and Sulfide to Spartina alterniflora Productivity. *Soil Science Society of America Journal*, *47*(5), 930–935. https://doi.org/10.2136/sssaj1983.03615995004700050018x.

Denys, L. (1991). *A check-list of the diatoms in the Holocene deposits of the western Belgian coastal plain with a survey of their apparent ecological requirements* (Professional Paper No. 246). Geological Survey of Belgium. http://biblio.naturalsciences.be/rbinspublications/professional-papers-of-the-geological-survey-ofbelgium/pdfs/pp_1991_2_246.pdf/view

Desianti, N., Enache, M. D., Griffiths, M., Biskup, K., Degen, A., DaSilva, M., Millemann, D., Lippincott, L., Watson, E., Gray, A., Nikitina, D., & Potapova, M. (2019). The Potential and Limitations of Diatoms as Environmental Indicators in Mid-Atlantic Coastal Wetlands. *Estuaries and Coasts*, *42*(6), 1440–1458. https://doi.org/10.1007/s12237-019-00603-4

Desianti, N., Potapova, M., Enache, M., Belton, T. J., Velinsky, D. J., Thomas, R., & Mead, J. (2017). Sediment Diatoms as Environmental Indicators in New Jersey Coastal Lagoons. *Journal of Coastal Research*, *78*, 127–140. https://doi.org/10.2112/SI78-011.1

Desianti, N. & Potapova, M. (2019). *Diatom Flora of the New Jersey Coastal Wetlands* (Final Report). New Jersey: NJDEP. https://hdl.handle.net/10929/68423

Dixit, S.S., Cumming, B.F., Birks, H. J. B., Smol, J.P., Kingston, J.C., Uutala, A.J., Charles, D.F., & Camburn, K.E. (1993). Diatom assemblages from Adirondack lakes (New York, USA) and the development of inference models for retrospective environmental assessment. *Journal of Paleolimnology*, *8*(1). https://doi.org/10.1007/BF00210056

Dura, T., Hemphill-Haley, E., Sawai, Y., & Horton, B. P. (2016). The application of diatoms to reconstruct the history of subduction zone earthquakes and tsunamis. *Earth-Science Reviews*, *152*, 181–197. https://doi.org/10.1016/j.earscirev.2015.11.017

Gaiser, E., Wachnicka, A., Ruiz, P., Tobias, F., & Ross, M. (2004). Diatom Indicators of Ecosystem Change in Subtropical Coastal Wetlands. In *Estuarine Indicators* (1st ed., p. 18). CRC Press.

Gaiser, E. E., & Johansen, J. (2000). Freshwater diatoms from Carolina Bays and other isolated wetlands on the Atlantic Coastal Plain of South Carolina, USA, with descriptions of seven taxa new to science. *Diatom Research*, *15*(1), 75–130. https://doi.org/10.1080/0269249X.2000.9705487

Hemphill-Haley, E. (1995). Intertidal diatoms from Willapa Bay, Washington: Applications to studies of small-scale sea-level changes. *Northwest Science* 69(1), 29–45. http://hdl.handle.net/2376/1328.

Hemphill-Haley, E. (1996). Diatoms as an aid in identifying late-Holocene tsunami deposits. *The Holocene*, *6*(4), 439–448. https://doi.org/10.1177/095968369600600406

Himmelstein, J., Vinent, O. D., Temmerman, S., & Kirwan, M. L. (2021). Mechanisms of Pond Expansion in a Rapidly Submerging Marsh. *Frontiers in Marine Science*, *8*. https://doi.org/10.3389/fmars.2021.704768

Hines, M. E., Knollmeyer, S. L., & Tugel, J. B. (1989). Sulfate reduction and other sedimentary biogeochemistry in a northern New England salt marsh. *Limnology and Oceanography*, *34*(3), 578–590. https://doi.org/10.4319/lo.1989.34.3.0578

Howarth, R. W. (1979). Pyrite: Its Rapid Formation in a Salt Marsh and Its Importance in Ecosystem Metabolism. *Science*, *203*(4375), 49–51. https://doi.org/10.1126/science.203.4375.49

Howarth, R. W., & Teal, J. M. (1979). Sulfate reduction in a New England salt marsh1. *Limnology and Oceanography*, *24*(6), 999–1013. https://doi.org/10.4319/lo.1979.24.6.0999

Howes, B. L., Howarth, R. W., Teal, J. M., & Valiela, I. (1981). Oxidation-reduction potentials in a salt marsh: Spatial patterns and interactions with primary production1. *Limnology and Oceanography*, *26*(2), 350–360. https://doi.org/10.4319/lo.1981.26.2.0350

Legendre, P., & Legendre, L. (2012). *Numerical ecology* (Third English edition). Elsevier.

Maricle, B. R., & Lee, R. W. (2007). Root respiration and oxygen flux in salt marsh grasses from different elevational zones. *Marine Biology*, *151*(2), 413–423. https://doi.org/10.1007/s00227-006-0493-z

Mendelssohn, I. A., & McKee, K. L. (1988). Spartina Alterniflora Die-Back in Louisiana: Time-Course Investigation of Soil Waterlogging Effects. *The Journal of Ecology*, *76*(2), 509. https://doi.org/10.2307/2260609

Nelson, A. R., & Kashima, K. (1993). Diatom Zonation in Southern Oregon Tidal Marshes Relative to Vascular Plants, Foraminifera, and Sea Level. *Journal of Coastal Research*, *9*(3), 673–697. https://www.jstor.org/stable/4298122

Parmar, T. K., Rawtani, D., & Agrawal, Y. K. (2016). Bioindicators: the natural indicator of environmental pollution. *Frontiers in Life Science*, *9*(2), 110–118. https://doi.org/10.1080/21553769.2016.1162753

Pezeshki, S. R., Matthews, S. W., & Delaune, R. D. (1991). Root cortex structure and metabolic responses of Spartina patens to soil redox conditions. *Environmental and Experimental Botany*, *31*(1), 91–97. https://doi.org/10.1016/0098-8472(91)90011-C

Ribeiro, L., Brotas, V., Rincé, Y., & Jesus, B. (2013). Structure and diversity of intertidal benthic diatom assemblages in contrasting shores: a case study from the Tagus estuary [1]. *Journal of Phycology*, *49*(2), 258–270. https://doi.org/10.1111/jpy.12031

Sawai, Y., Horton, B. P., & Nagumo, T. (2004). The development of a diatom-based transfer function along the Pacific coast of eastern Hokkaido, northern Japan—an aid in paleoseismic studies of the Kuril subduction zone. *Quaternary Science Reviews*, *23*(23–24), 2467–2483. https://doi.org/10.1016/j.quascirev.2004.05.006

Sawai, Y., Horton, B. P., Kemp, A. C., Hawkes, A. D., Nagumo, T., & Nelson, A. R. (2016). Relationships between diatoms and tidal environments in Oregon and Washington, USA. *Diatom Research*, *31*(1), 17–38. https://doi.org/10.1080/0269249X.2015.1126359

Schutte, C. A., Wilson, A. M., Evans, T., Moore, W. S., & Joye, S. B. (2016). Methanotrophy controls groundwater methane export from a barrier island. *Geochimica et Cosmochimica Acta*, *179*, 242–256. https://doi.org/10.1016/j.gca.2016.01.022

Sherrod, B. L. (1999). Gradient analysis of diatom assemblages in a Puget Sound salt marsh: can such assemblages be used for quantitative paleoecological reconstructions? *Palaeogeography, Palaeoclimatology, Palaeoecology*, *149*(1–4), 213–226. https://doi.org/10.1016/S0031-0182(98)00202-8

Smith, K. K., Good, R. E., & Good, N. F. (1979). Production dynamics for above and belowground components of a New Jersey Spartina alterniflora tidal marsh. *Estuarine and Coastal Marine Science*, *9*(2), 189–201. https://doi.org/10.1016/0302-3524(79)90114-2

ter Braak, C. J. F. (1990). Interpreting canonical correlation analysis through biplots of structure correlations and weights. *Psychometrika*, *55*(3), 519–531. https://doi.org/10.1007/BF02294765

ter Braak, C. J. F., & Smilauer, P. (2012). *Canoco reference manual and user's guide: software for ordination, version 5.0*. Microcomputer Power.

Underwood, G., Phillips, J., & Saunders, K. (1998). Distribution of estuarine benthic diatom species along salinity and nutrient gradients. *European Journal of Phycology*, *33*(2), 173–183. https://doi.org/10.1080/09670269810001736673

U.S. EPA. (1993). Method 350.1: Nitrogen, Ammonia (Colorimetric, Automated Phenate) (Revision 2.0). U.S. Environmental Protection Agency, Cincinnati, OH. https://www.epa.gov/sites/default/files/2015-06/documents/epa-350.1.pdf

U.S. EPA. (1982). Method 120.1: Conductance (Specific Conductance, µmhos at 25 °C) by Conductivity Meter. U.S. Environmental Protection Agency, Washington D.C. https://www.epa.gov/sites/default/files/2015-08/documents/method_120-1_1982.pdf

Vos, P. C., & de Wolf, H. (1993). Diatoms as a tool for reconstructing sedimentary environments in coastal wetlands; methodological aspects. *Hydrobiologia*, *269–270*(1), 285–296. https://doi.org/10.1007/BF00028027

Wachnicka, A., Gaiser, E., Collins, L., Frankovich, T., & Boyer, J. (2010). Distribution of diatoms and development of diatom-based models for inferring salinity and nutrient concentrations in Florida Bay and adjacent coastal wetlands of south Florida (USA). *Estuaries and Coasts*, *33*(5), 1080–1098. https://doi.org/10.1007/s12237-010-9283-4

Wachnicka, A., Gaiser, E., & Boyer, J. (2011). Ecology and distribution of diatoms in Biscayne Bay, Florida (USA): Implications for bioassessment and paleoenvironmental studies. *Ecological Indicators*, *11*(2), 622–632. https://doi.org/10.1016/j.ecolind.2010.08.008

Weilhoefer, C. L., & Pan, Y. (2007). Relationships between diatoms and environmental variables in wetlands in the Willamette Valley, Oregon, USA. *Wetlands*, *27*(3), 668–682. https://doi.org/10.1672/0277-5212(2007)27[668:RBDAEV]2.0.CO;2

Zong, Y., & Horton, B. P. (1998). Diatom zones across intertidal flats and coastal saltmarshes in Britain. *Diatom Research*, *13*(2), 375–394. https://doi.org/10.1080/0269249X.1998.9705456

Chapter 6: Outreach

Authors: Brittany P. Wilburn[1], Joshua Moody[1], Maite Whitley[1], Kriish Hate[1,2]

[1] NJDEP, Division of Science and Research
[2] Rowan University

Objectives: 1) Provide opportunities for early career individuals to network, build professional and research skills, and develop an independent project. 2) Increase public awareness of the need for standardized salt marsh monitoring protocols.

Approach: One internship was provided each summer in 2022 and 2023, as part of the DEP's Spark internship program. The program is a paid 10-week experience in which qualifying interns received the opportunity to work alongside the NJDEP staff, develop professional and research skills, network, and complete an independent research project. The 2022 Spark intern, Maite Whitley, performed a preliminary analysis of pond expansion and vegetation health in ArcGIS to assist in site selection during our first year of the study. Maite now works for the NJDEP Bureau of Coastal Land Use Enforcement as an Environmental Specialist. The 2023 Spark intern, Kriish Hate, conducted a field experiment, examining the effects of pond expansion on denitrification potential. Their methods and results are reported in this chapter.

Additionally, six poster and oral presentations were given as part of this study to a variety of local, regional, and national conferences. When possible, NJDEP interns and Rowan University students participating in this project were provided the opportunity to present this research at conferences.

Further outreach was performed through the production of fact sheets and online posts, through the NJDEP DSR Outreach Team Instagram. The project will additionally be presented at a future internal NJDEP "What's going on in NJ's wetlands?" seminar. Presentations are listed in Table 6.1, and full abstracts can be found in Appendix G.

Responsibilities and Deliverables: The NJDEP-DSR 1) put together the call for internship applications, 2) mentored interns, 3) oversaw intern projects, 4) provided networking and skill-building opportunities for the interns, 5) presented research from this study, and 6) produced fact sheets and online outreach posts (*Deliverable 5*).

The NJDEP-FW gave a presentation on the development of the methodology from this study (*Deliverable 5*).

Rowan University 1) provided opportunities for students to conduct field research and analysis, 2) provided networking and skill-building opportunities for students, and 3) presented research from this study (*Deliverable 5*).

Table 6.1. Summaries of presentations given by members of this project team. Bolded names are the presenters.

Title	Authors	Conference	Presentation Type
"Assessing salt marsh health through soil and pore water chemistry"	**Kriish Hate,** Brittany Wilburn, Metthea Yepsen, Kirk Raper, Lori Lester, Mihaela Enache, Joe Smith, Andrea Habeck, Gregg Sakowicz, and Charles Schutte	Atlantic Estuarine Research Society 2023 Spring Meeting	Oral Presentation
"Linking soil and porewater chemistry with aboveground measurements to assess coastal wetland health"	**Charles Schutte,** Kriish Hate, Brittany Wilburn, Metthea Yepsen, Kirk Raper, Lori Lester, Mihaela Enache, Joe Smith, Andrea Habeck, and Gregg Sakowicz	Society of Wetland Scientists 2023 annual meeting	Oral Presentation
"Developing a Protocol for Using Multispectral Drone Imagery to Study Salt Marsh Vegetation"	**Kevin Blythe,** Brittany Wilburn, Metthea Yepsen, Josh Moody, William Smith, Steven Jacobus, Molly VanWieren, Kirk Raper, David DuMont	Fall Northeast Arc Users Group meeting 2023	Poster
"Assessing salt marsh health through potential denitrification rates and drone multispectral imagery"	**Kriish Hate,** Charles Schutte, Brittany Wilburn, and Joshua Moody	CERF 2023 27th Biennial Conference	Oral Presentation
"Investigating the use of multispectral drones for identifying salt marsh condition"	**Brittany Wilburn,** Joshua Moody, Charles Schutte, Kevin Blythe, William Smith, and Metthea Yepsen	10th Delaware Wetlands Conference 2024	Oral Presentation
"Ditching creates increased oxidation reduction potential in salt marshes"	**Omar Selim,** Joshua Moody, Brittany Wilburn, and Charles Schutte	Atlantic Estuarine Research Society 2024 Spring Meeting	Poster

Maite Whitley, Summer 2022 Intern

Using NDVI to Assess Plant Health: Preliminary Evaluation

Goals and Background

Salt marshes are a mosaic of vegetation species that each have their own tolerances to increased flooding and other stressors related to sea-level rise. As a result, it is necessary to look for hotspots of increased stress signals to help focus restoration or protection efforts. One potential method is to use multispectral imagery to determine concentrations and density of chlorophyll content through the calculation of Normalized Difference Vegetation Index (NDVI), which can be considered a measure of vegetative health. Values of NDVI range in scale of +1 to -1, with +1 representing high amounts of chlorophyll and values around 0 and below are sites of non-living or abiotic features. The goal of this work was to perform a preliminary evaluation of *Spartina alterniflora* and *S. patens* health within the project area of interest. This preliminary work helped provide a landscape context of vegetation health and how much of a difference in reflective properties should be expected between the two species.

Methods

Sentinel-2B satellite imagery from the Copernicus Sentinel-2 Collection 1 MSI Level-1C was utilized for this project[3]. Obtained data had a 10 m resolution and included red- (~665 nm), green- (~560 nm), blue- (~493 nm), and near infrared-bands (~833 nm). The imagery was collected on 11 July 2022 at 3:38 PM which corresponds to just after low tide. ESRI's ArcGIS Pro 3.x software (Environmental Systems Research Institute, Redlands, CA) was used in this analysis. Bands of the imagery were received as separate rasters, and integrated into a single multiband dataset using Composite Bands geoprocessing tool in ArcGIS Pro. To reduce processing time, the multiband raster was then clipped to include only the Forsythe and Great Bay Boulevard portions of the coastline (Figure 6.1). Using the vegetation identification and photographic data from the project site scouting visits, a training dataset was produced of known *S. alterniflora* and *S. patens* points. Training sets were then applied to the K-Nearest Neighbor[4] and Support Vector Machine Learning[5] tools, following

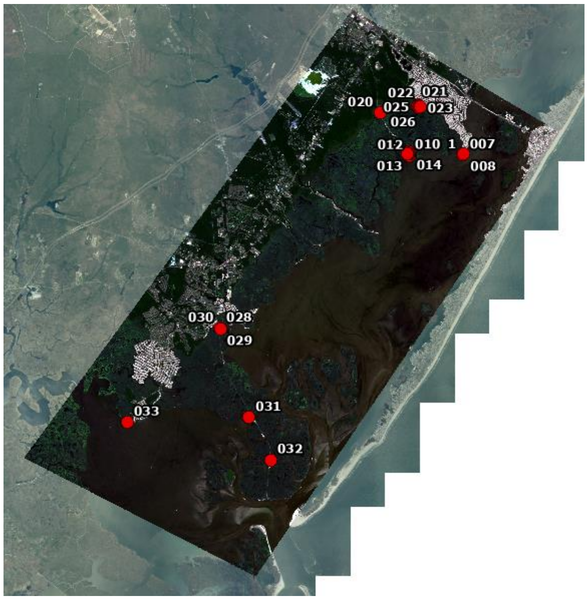

Figure 6.1. Polygon of area of interest used to create a mask on the satellite imagery. Red points are preliminary site locations (selected prior to site confirmation).

---

[3] Metadata can be accessed at https://doi.org/10.5270/S2_-742ikth. Data quality report can be accessed at Data Quality Report (copernicus.eu).

[4] Train K-Nearest Neighbor Classifier (Image Analyst)—ArcGIS Pro | Documentation

[5] Train Support Vector Machine Classifier (Image Analyst)—ArcGIS Pro | Documentation

the classification wizard. Additionally, a third classification following the ISO Cluster method,[6] which is an unsupervised classification. Classification results were assessed visually for accuracy. Support Vector Machine Learning was deemed the most accurate of the three types of classifications tested. In addition to the classification, the built-in NDVI tool was applied to the original multiband raster to produce an overall map of NDVI values. The values of NDVI were extracted for both *S. alterniflora* and *S. patens* using the classified raster.

Results

While the ranges of NDVI values overlapped greatly between the two species, the *S. patens* class had a range that exhibited higher NDVI values, but not reaching a value of 1 (Figure 6.2). *S. alterniflora* demonstrated an overall pattern of higher values more inland and along the back bays compared to the peninsula (Figure 6.3). Similarly, *S. patens* was greatly restricted to interior and back bay marshes and largely not present in areas of low *S. alterniflora* values. This analysis suggests that the Tuckerton

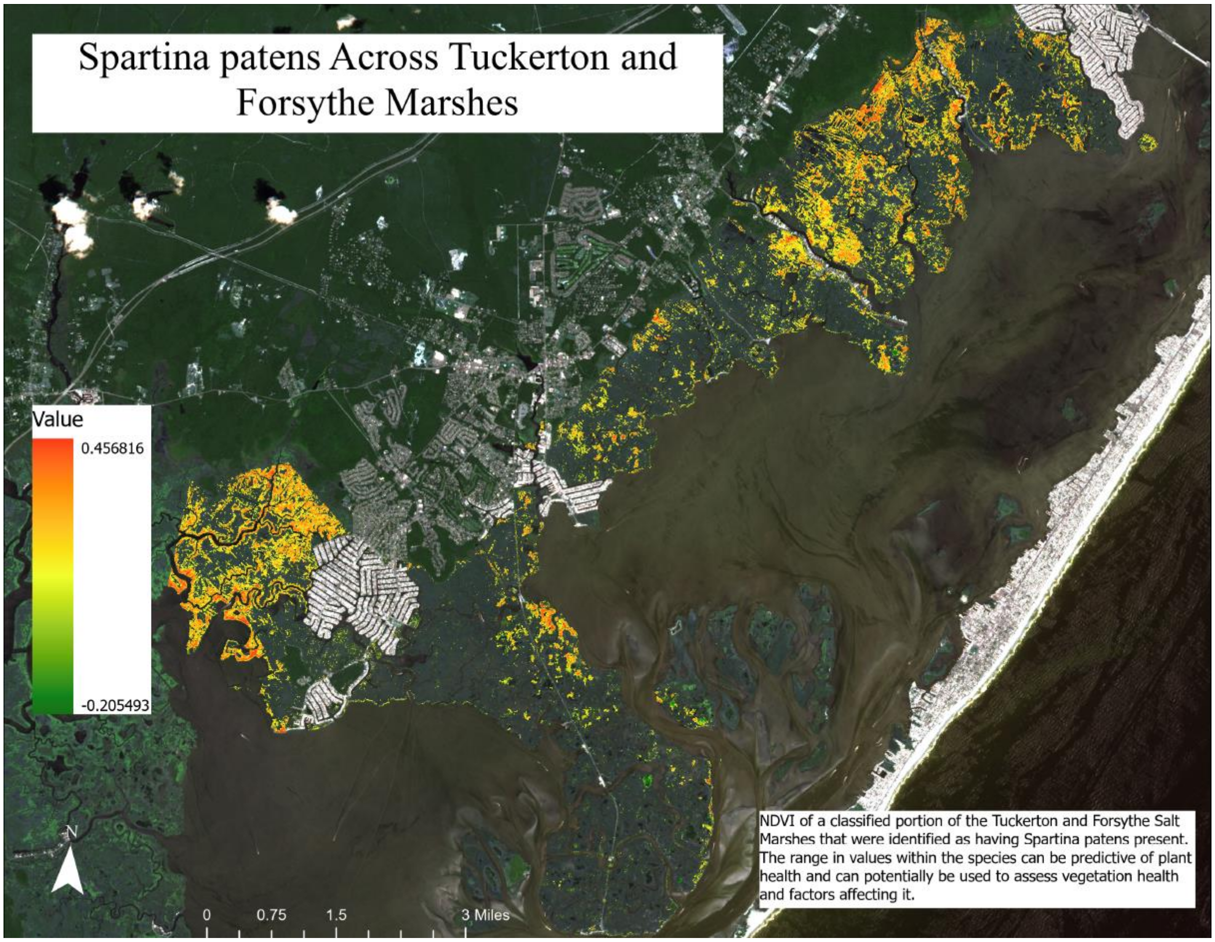

NDVI of a classified portion of the Tuckerton and Forsythe Salt Marshes that were identified as having Spartina patens present. The range in values within the species can be predictive of plant health and can potentially be used to assess vegetation health and factors affecting it.

Figure 6.2. Raster of Spartina patens NDVI values across E.B. Forsythe National Wildlife Refuge and Great Bay Boulevard marsh on Tuckerton Peninsula. Red designates a strong reflectance value, which correlates to higher chlorophyll content. Green is representative of dead, dying, and/or highly stressed vegetation.

---

[6] Train ISO Cluster Classifier (Image Analyst)—ArcGIS Pro | Documentation

peninsula is an area of greater vegetation stress than the surrounding marshes. The *S. alterniflora* community shows a greater range of presence and stress seems to be spatially tied to the peninsula, while the *S. patens* community has potentially had its stress limits exceeded except for larger, intact communities. It is suspected that portions of the community have been extirpated from areas of greater hydrological stress.

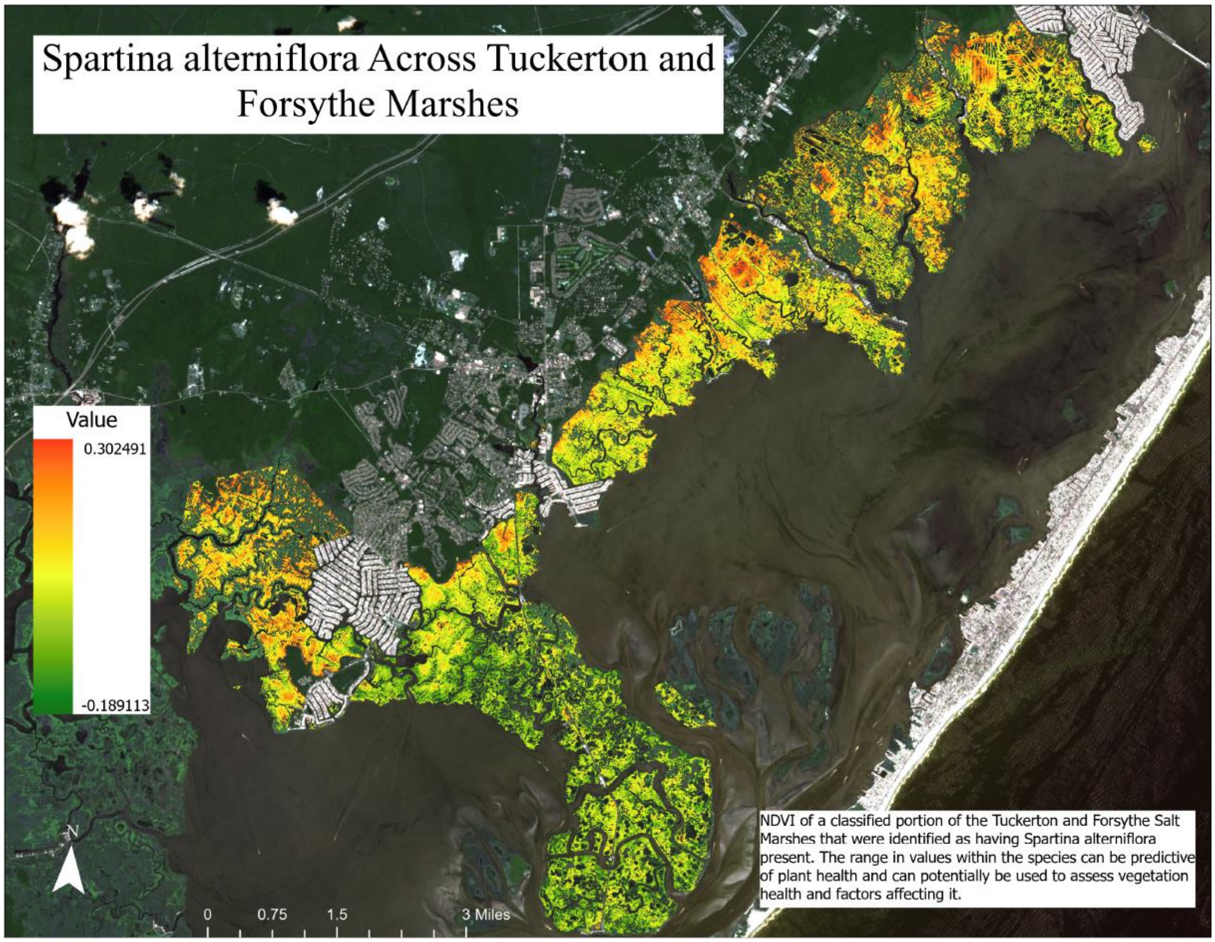

NDVI of a classified portion of the Tuckerton and Forsythe Salt Marshes that were identified as having Spartina alterniflora present. The range in values within the species can be predictive of plant health and can potentially be used to assess vegetation health and factors affecting it.

Figure 6.3. Raster of Spartina alterniflora NDVI values across E.B. Forsythe National Wildlife Refuge and Great Bay Boulevard marsh on Tuckerton Peninsula. Red designates a strong reflectance value, which correlates to higher chlorophyll content. Green is representative of dead, dying, and/or highly stressed vegetation.

Pond Expansion Rates within Tuckerton and Forsythe Salt Marshes

Goals and Background

As sea-level rise increases, the instability of the marsh platform also increases. This instability can potentially be identified through significant changes in the formation of open water habitat over time through pond expansion. While marshes have a natural balance of pond formation, breaching, and replacement by vegetation, significant hydrological changes, such as ditching and sea-level rise influences, can result in the creation of permanent open water habitat. The goal of this project is to determine the rate of pond expansion in select areas of the project prior to field data collection. These rates will provide insight into the overall stability of the marsh platform within both E.B. Forsythe National Wildlife Refuge and Great Bay Boulevard, with more rapid rates of expansion suggesting that the marsh platform may be under higher hydrological stress.

Methods

The Imagery used in this project was Sentinel-2B satellite imagery from the Copernicus Sentinel-2 Collection 1 MSI Level-1C and 1987 and 2002 satellite imagery from NJDEP Bureau of GIS. The most recent imagery was taken in July of 2022, during low tide with a resolution of 10 m. The BGIS satellite imagery to perform the delineation was determined by choosing imagery which appeared to have the finest resolution and visually have minimal differences compared to the 2022 Sentinel imagery. Imagery containing flooding, due to the potential of imagery being taken at high tide, could significantly affect the results and create temporarily “false” ponding and therefore were not good candidates. The best imagery to detect changes in pond growth was determined to be the 1987 and 2002 imagery. The sites chosen for delineation include 3 drone zones in both Tuckerton and Forsythe which had the greatest number of single ponds (Figure 6.4). Some sites had almost no ponds or excessive merging ponds that made delineation difficult and, thus, were not included. Manual digitization of ponds in the recent 2022 imagery initialized which ponds would continue to be digitized and monitored in earlier imagery since there was no pond size requirement determined for digitization. Following the digitization of ponds in 2022 imagery, those same ponds were digitized in the 2002 and 1987 imagery with careful consideration of ponds that may have been a result of flooding or ones that were not recorded in the first set of ponds from 2022. After outlining all ponds from all selected imagery, the area of ponds was calculated in m^2 and summed to find

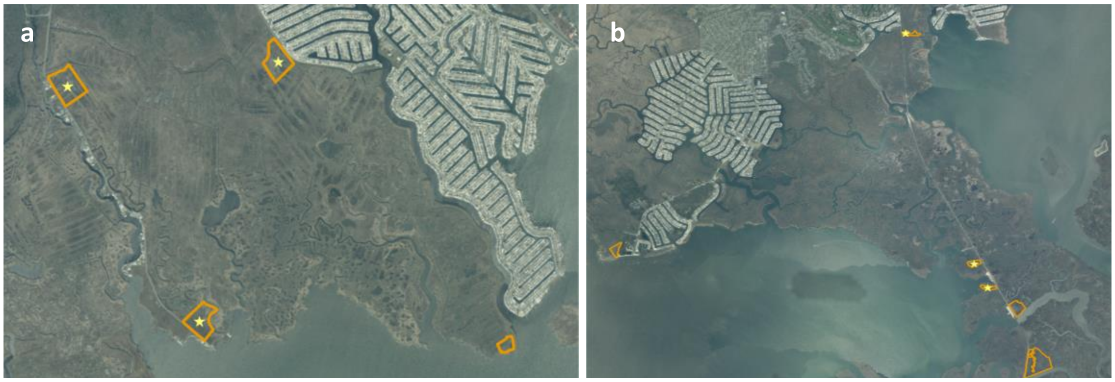

Figure 6.4. Sites selected for pond delineation (denoted by stars) within our drone flight zones in a) E. B. Forsythe National Wildlife Refuge and b) Great Bay Boulevard marsh on Tuckerton Peninsula.

the total area of ponds at each site. After finding the sum in each area (Great Bay Boulevard and Forsythe), the total area of ponds was plugged into a simple rate of change equation: Final (recent) area of ponds – Initial (earlier) divided by change in time. This equation was used for each time step to evaluate a rate from 2022-2002, 2002-1987, and overall change from the time steps, 2022-1987. All 3 rates were then averaged to settle on a single rate.

Results

Over the course of 35 years, the area of ponds within each site went from 2,217.80 m^2 to 11,125.80 m^2 (Figure 6.5). Since the calculations were done using a small portion of the studied salt marshes, this only reflects pond growth on a small-scale and would require more time and dedication in observing ponds throughout the whole area to acquire more precise regional rates. The pond growth rates from 1987-2002 and 2002-2022 are 339.88 m^2 per year and 190.49 m^2 per year, respectively. Over all years, 1987-2022, the growth rate of ponding was 254.51 m^2 per year. All three rates combined show that ponding has increased 261.63 m^2 each year. The areas within Forsythe had the most ponds and the greatest increase in pond area over the years (Figure 6.6). The Great Bay Boulevard ponds seemed to stay consistent and increased at a lower and steadier rate, indicating that the Great Bay Boulevard marshes could be more stable than Forsythe (Figure 6.7). This comparison could help in justifying that the salt marshes at Forsythe respond to the detrimental effects of climate change and sea-level rise more so than Great Bay Boulevard.

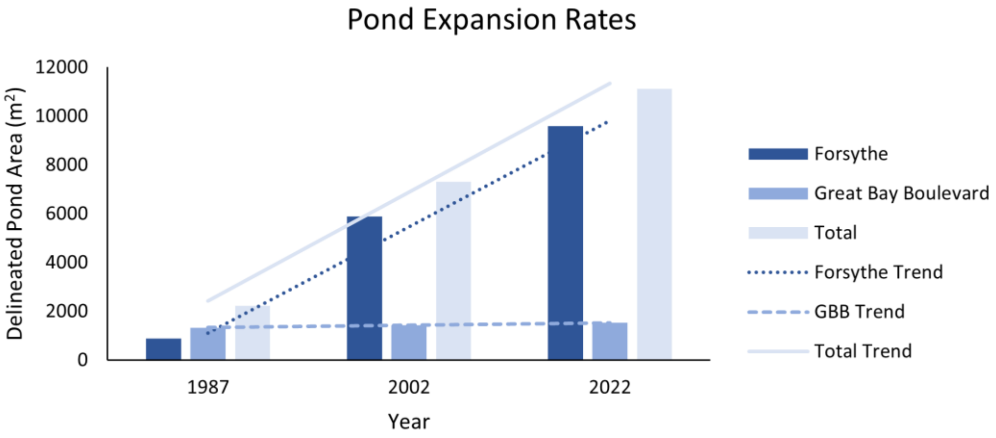

Figure 6.5. Bar graph of pond expansion rates in Forsythe and Great Bay Boulevard salt marshes. Forsythe pond area increased by 8700 m^2 between 1987 to 2022, while Great Bay Boulevard marsh ponds expanded only by 200 m^2.

Additional Recommendations

Resolution Bias is an important factor to consider when delineating ponds to find their area. There were many difficulties in determining the exact boundaries of some ponds due to coarse resolution or unclear differentiation between plants and flooded areas. None of the imagery for this project was resampled but finding a margin error between resolutions was a possibility. Due to the limited metadata about the quality of the imagery in any images available in the DEP toolbar, potential bias in ponding extent may be present due to water obscuring underlying vegetation. In subsequent studies, it is recommended to use imagery of the same type, collected on the same day and time, with the same resolution.

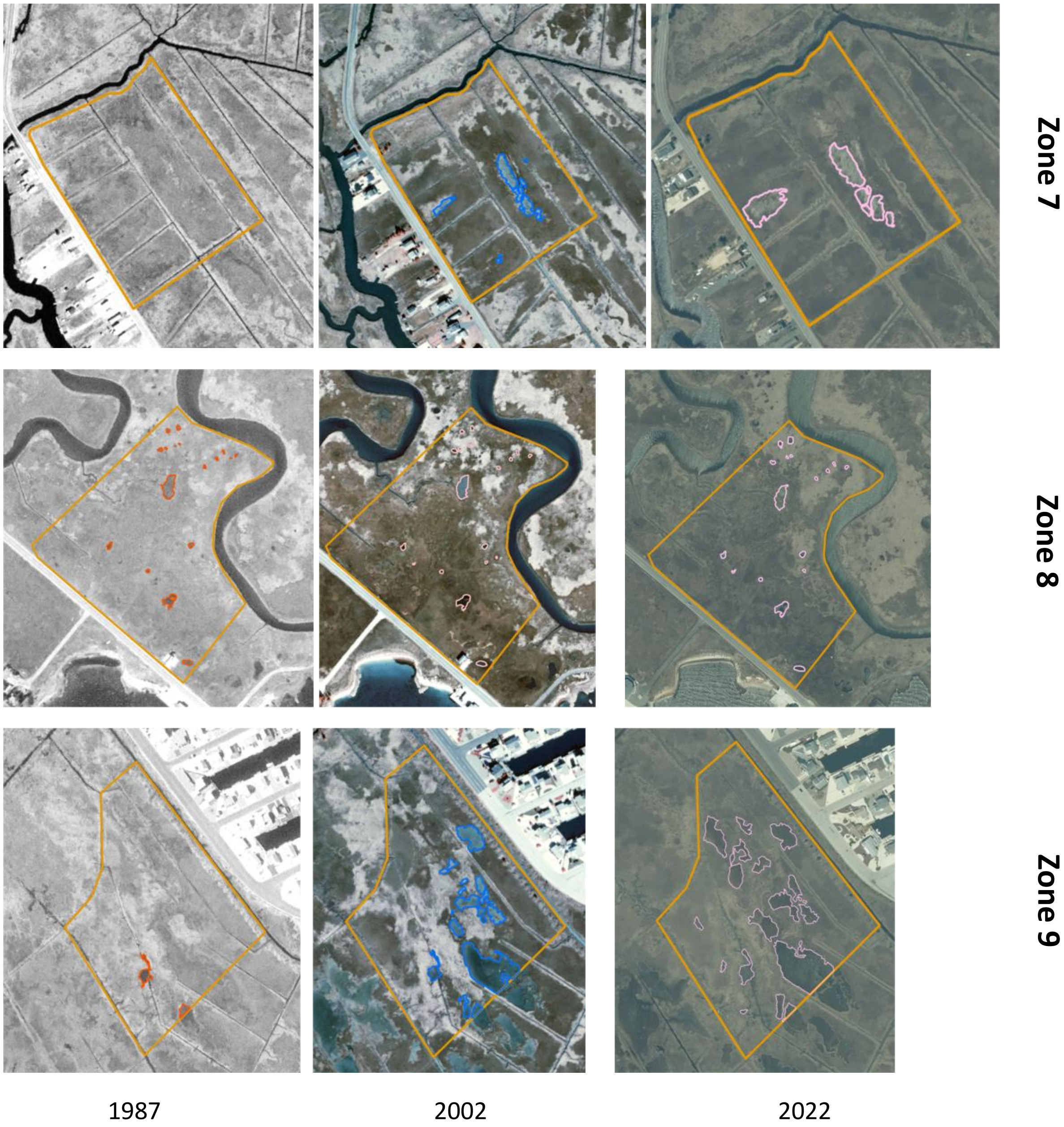

Figure 6.6. Pond delineations at Zones 7, 8, and 9 from 1987 to 2022 at E.B. Forsythe National Wildlife Refuge.

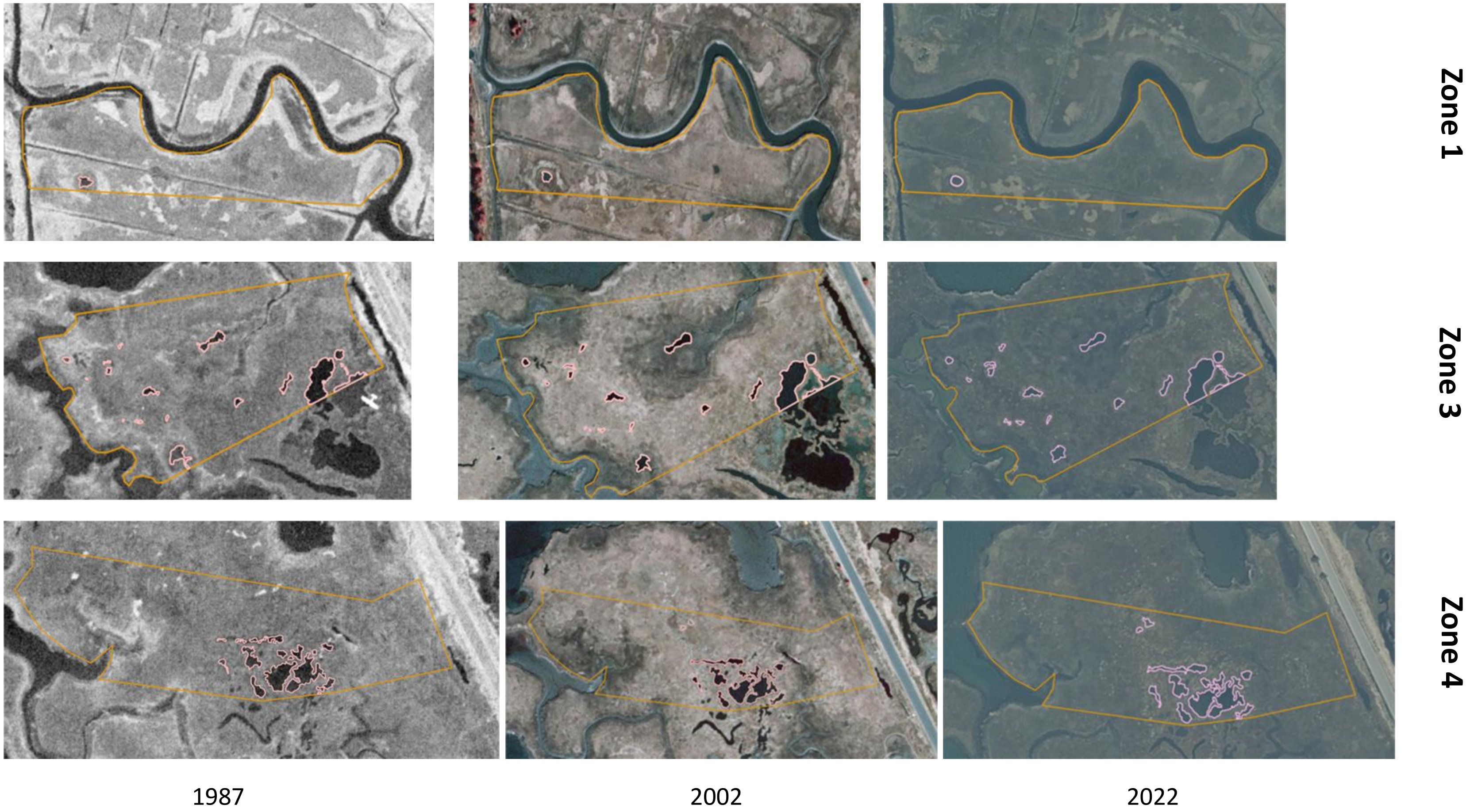

Figure 6.7. Pond delineations at Zones 1, 3, and 4 from 1987 to 2022 at Great Bay Boulevard marsh on the Tuckerton Peninsula.

Kriish Hate, Summer 2023 Intern

Denitrification Process Rates Along a Gradient of Salt Marsh Health

Goals and Background

Salt marshes are essential for providing ecosystem services, including the removal of excess nitrogen. The process of eliminating nitrogen is crucial for preserving water quality and preventing the occurrence of eutrophication in coastal habitats. Salt marshes function as natural filtration systems, employing denitrification and other processes to eliminate excess nitrogen from the water (Craft et al., 1999). This experiment evaluated the influence of historical ditching and distance from both expanding and stable ponds on soil net potential denitrification rates at two salt marsh sites (Great Bay Boulevard Wildlife Management Area [GBB] and Edwin B. Forsythe National Wildlife Refuge [Forsythe]). We hypothesized that potential denitrification rates would be lower in ditched sites compared to unditched sites due to the altered hydrological conditions caused by drainage ditches, which may lead to reduced soil moisture and increased oxygen availability due to ditching, both critical factors influencing denitrification processes (Nyman et al., n.d.). The aim was to determine whether site characteristics such as ditching could predict nitrogen removal capacity, thereby informing targeted restoration efforts to maintain this important ecosystem service (Ooi et al., 2022).

Methods

Soil sampling was conducted along three transects extending from three ponds in four site types: Forsythe ditched, Forsythe unditched, GBB ditched, and GBB unditched. Unditched sites were characterized by stable ponds and *S. patens* habitat, while ditched sites are characterized by expanding ponds and significant loss of *S. patens* habitat. Along each transect, two vegetation plots were established—one in the “Inner” band (1–5 meters) and the other in the “Outer” band (11–20 meters) from the edge of each pond. These plots were utilized for taking metrics such as bearing capacity and percent cover. Denitrification samples were collected within 1 meter adjacent to these vegetation plots. Soil samples were collected within specific bands. A 5 cm x 5 cm x 5 cm deep soil cube was extracted from the top layer of salt marsh soil and any aboveground plant tissue was removed. The soil cube was placed in a sample bag and kept in a cooler on ice until they could be returned to the laboratory and refrigerated. Samples were processed within 24 hours of collection. For each pond, samples collected from the Inner band across the three transects were thoroughly mixed to create a composite sample representing the Inner band for that pond. Similarly, samples collected from the Outer band across the three transects were combined to create a composite sample representing the Outer band for that pond. A composite sampling approach was used to address spatial heterogeneity within each site while maintaining a manageable sample load. Subsequently, the homogenized samples underwent incubation using the acetylene block assay (Sørensen, 1978) to measure net potential denitrification rates. 5 g of soil were placed in 50-mL Erlenmeyer flasks containing 10 mL of salinity-adjusted artificial seawater with 2000 µmol L^{-1} N as nitrate (Schutte et al., 2020). Flasks were purged with pure nitrogen gas and supplemented with 5 mL of acetylene to inhibit nitrous oxide (N_2O) conversion to nitrogen gas (N_2). Incubation occurred at room temperature (21°C), with headspace subsamples collected at 0.5, 1, 2, and 4 hours. Gas samples were injected into nitrogen-purged 10-mL vials and analyzed for N_2O concentrations using a gas chromatograph (Shimadzu GC-2030) with an electron capture detector and headspace autosampler. Net potential denitrification rates were calculated from the linear increase in N_2O concentrations over time and corrected for the dry mass of the soil incubated.

Results

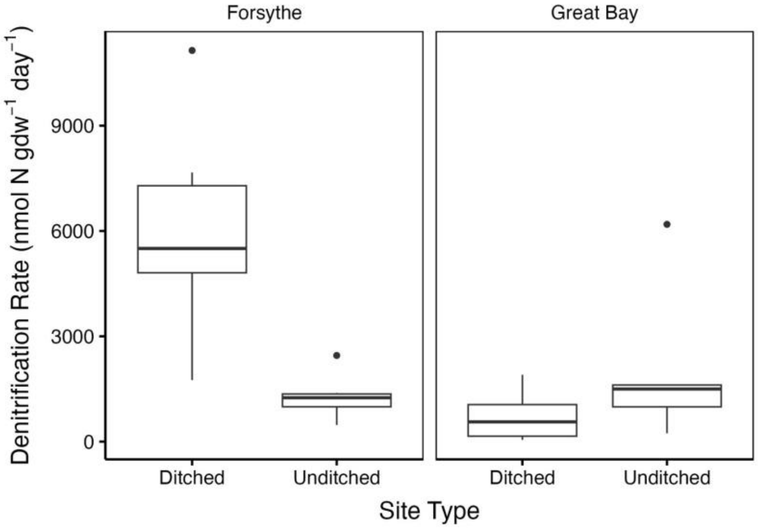

Figure 6.8. Box plot showing net potential denitrification rates across four salt marsh types: Forsythe ditched, Forsythe unditched, Great Bay ditched, and Great Bay unditched.

There were significant differences in net potential denitrification rates between the four site types investigated here (Kruskal-Wallis test, $p = 0.006$, Figure 6.8). Forsythe ditched was significantly different from Forsythe unditched, GBB ditched, and GBB unditched (Dunn's test, $p < 0.045$), with no significant difference among these three (Dunn's test, $p > 0.5$). The median rate of 5500 nmol N gdw^{-1} day^{-1} (Inter Quartile Range [IQR] = 4810–7290 nmol N gdw^{-1} day^{-1}) at Forsythe ditched sites was much higher than the median rate of 1390 (IQR = 821–3040 nmol N gdw^{-1} day^{-1}). Ooi et al. (2022) measured a lower mean denitrification rate of 663 nmol N gdw^{-1} day^{-1} (95% CI = 425–903 nmol N gdw^{-1} day^{-1}) across 20 Connecticut salt marshes. These rates are most similar to those measured at the Forsythe unditched and GBB sites. Mean net potential denitrification rates were higher in the Outer band than they were in the Inner band across all four site types (Figure 6.9), but these differences were not significant (Dunn's test, $p = 1$), likely due to high variation between the three samples within each sample group. Since there were no differences in net potential denitrification rates between the Forsythe ditched, GBB ditched, and GBB unditched site types, these data were pooled together to compare rates between the Inner and Outer bands (Figure 6.10). Even with the larger sample size in each group ($n = 9$), there were no significant differences in net potential denitrification rates between samples collected within 5 meters of a pond edge and those collected 10–15 meters from a pond edge (Wilcoxon test, $p = 0.55$). While ditching and pond stability did not have any discernable influence on denitrification potential as expected, these data demonstrate that denitrification was active across all marsh types regardless of ditching, distance from pond, or pond type. Notably, even marshes adjacent to expanding pond edges exhibited active denitrification potential, indicating that they are still capable of facilitating the nitrogen removal ecosystem service provided by salt marshes. Therefore, denitrification potential may be robust across vegetated portions of highly dynamic salt marsh landscapes, even in areas that are perceived to be low in quality or prone to loss.

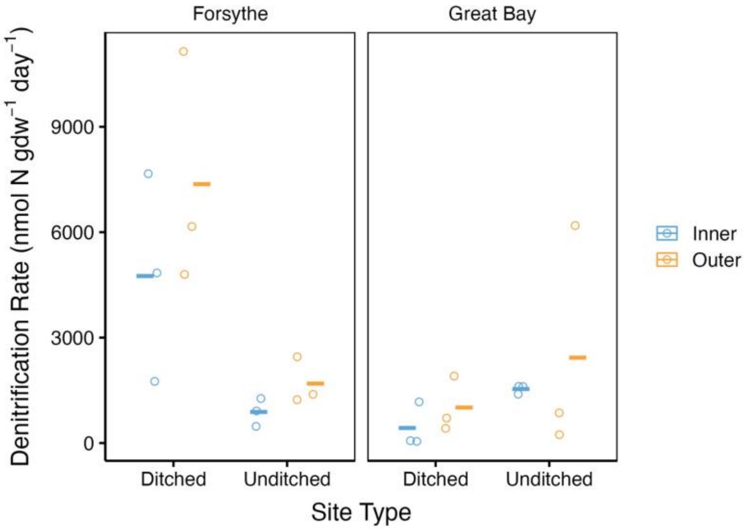

Figure 6.9. Circles represent each individual measurement, and bars represent the mean value of all measurements from the respective site types (Forsythe unditched, Great Bay ditched, Great Bay unditched, and Forsythe ditched).

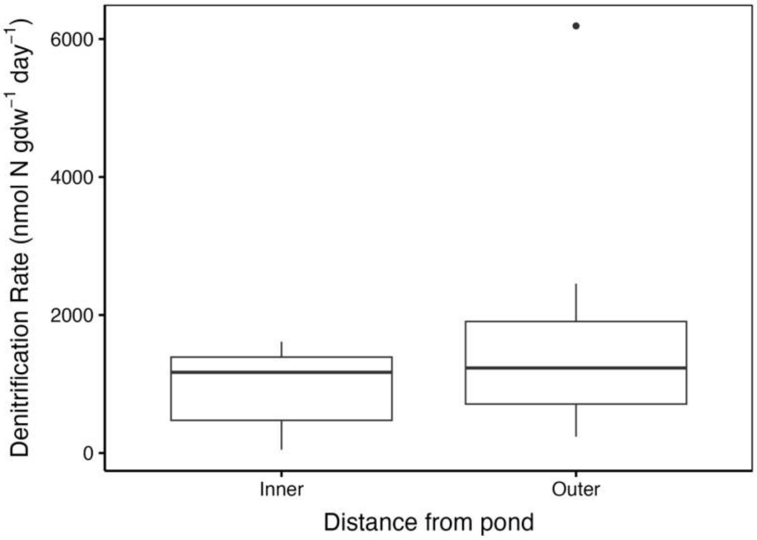

Figure 6.10. Potential denitrification rates across Great Bay (GBB) sites, with Forsythe ditched marshes removed and grouped by the Inner and Outer bands.

References:

Craft, C., Reader, J., Sacco, J. N., & Broome, S. W. (1999). Twenty-Five Years of Ecosystem Development of Constructed Spartina alterniflora (Loisel) Marshes. *Ecological Applications, 9*(4), 1405. https://doi.org/10.2307/2641405

Nyman, J. A., Delaune, R. D., Roberts, H. H., & Patrick, W. H. (n.d.). Relationship between vegetation and soil formation in a rapidly submerging coastal marsh. LSU Scholarly Repository. https://repository.lsu.edu/geo_pubs/1674/

Ooi, S. K., Barry, A., Lawrence, B. A., Elphick, C. S., & Helton, A. M. (2022). Vegetation zones as indicators of denitrification potential in salt marshes. *Ecological Applications, 32*(6). https://doi.org/10.1002/eap.2630

Schutte, C.A., J. M. Marton, A. E. Bernhard, A. E. Giblin, & B. J. Roberts. (2020). No Evidence for Long-term Impacts of Oil Spill Contamination on Salt Marsh Soil Nitrogen Cycling Processes. *Estuaries and Coasts 43*:865 879. https://doi.org/10.1007/s12237-020-00699-z

Sørensen, J. (1978). Denitrification Rates in a Marine Sediment as Measured by the Acetylene Inhibition Technique. *Applied and Environmental Microbiology, 36*(1), 139–143. https://doi.org/10.1128/aem.36.1.139-143.1978

Chapter 7: Final Conclusions and Recommendations

Authors: Brittany P. Wilburn[1], Joshua Moody[1], Mihaela Enache[1], Kirk Raper[1], Charles Schutte[2], Steven Jacobus[3], William Smith[3], Kevin Blythe[4], Molly VanWieren[4]

[1] NJDEP, Division of Science and Research
[2] Rowan University
[3] NJDEP, Bureau of GIS - DOIT
[4] NJDEP, Fish and Wildlife, Office of Fish and Wildlife Information Systems

The DJI Phantom 4 Multispectral drone provides a detailed bird's eye view of the marsh and can measure a wide expanse of useful information. Detailed, 7.6 cm resolution classifications of the salt marsh were successfully created, which can inform future monitoring, estimates of temporal habitat change, and baseline/change maps for habitat enhancement/restoration projects. These high-resolution maps are particularly useful for NJDEP-FW as it could assist in their goals to better conserve saltmarsh sparrow (*Ammodramus caudacutus*), as this species is restricted to nesting only in *S. patens* due to the reduced flooding. Regular monitoring of critical salt marsh habitat by NJDEP-FW could produce necessary trend maps to determine areas of vulnerability within *S. patens*. Future efforts should be made to additionally explore these applications in freshwater wetlands.

Additional insight into the connections between diatom assemblages and soil and porewater chemistry was gained as certain relationships among the vegetation, soil chemistry, and diatom communities were found to be highly correlated. For example, some diatom species were found to be highly correlated with pH and salinity, with potential indirect links to sulfide. We are unaware of these relationships being described within scientific literature, and we intend to continue their exploration in future studies to understand the extent to which diatoms are influenced by these chemical parameters.

However, there are several caveats that restrict the utility of using multispectral drones in salt marsh habitats. As we were unable to definitively correlate the multispectral indices to on the ground measurements, we have several suggestions to enhance future studies in order to establish more specific relationships.

1. ***Greater Geospatial Variability Among Sites and Sampling Plots:*** The inability to identify significant relationships may be directly related to the spatial autocorrelation of the sites and plots. The low variability within many of the metrics suggests that their levels were primarily driven by factors at a scale greater than our sampling resolution. Future efforts may want to distribute sites across NJ, taking advantage of many of our natural gradients (e.g., tidal magnitude difference between Barnegat and Delaware bays, salinity gradients, etc.). Within site, there was little variability between plots at the near (<5m) and far (11-20m) from pond strata levels, indicating that a greater distance between sampling plots per site may be needed. Landscape transects from the marsh edge to the upland may provide a way to standardize plot distribution at a greater scale.

2. ***Greater Number of Sampling Plots:*** In addition to greater site and plot dispersion, a greater number of replicates per site and strata should be employed to ensure a more representative range of natural variability is captured during sampling events.
3. ***Manipulation or Targeted Variability Studies to Ensure Levels of Variability Within Metrics:*** Future studies designed to identify the connection between multispectral indices and on-the-ground metrics should consider a gradient approach. This could be developed by creating experimental plots by trimming vegetation to discrete percent covers or doping plots with standardized amounts of nutrients prior to the growing season. Another option would be to use historical imagery to identify and select study areas to vary by vegetation cover and change directionality – vegetated areas that are stable, expanding, and denuding. Soil and porewater measurements at these locations should reflect greater spatial variability to track gradients across the marsh, especially in areas of expansion and decline. The development of experimental gradients could allow for a greater accounting of the variability associated with specific metrics at discrete levels of various parameters. It would be beneficial to gather data across a wider range of wetland condition/health in order to identify more accurate, detailed, and useful relationships between multispectral indices, aboveground plant metrics, diatom community composition, and soil and porewater chemistry. The wetlands sampled for this study did capture a wide range in soil ORP and porewater ammonia and sulfide concentrations, all of which are mechanistically linked with salt marsh plant species distribution and plant growth. These metrics could be useful for future marsh vegetation health evaluation as a supplement to visual or drone-based evaluation. Soil ORP would be a particularly useful metric for preliminary assessment because it can be measured quickly and easily in the field.
4. ***Novel Multispectral Index Development:*** Other indices or combination of indices may be better able to capture the complexities of marsh landscapes. However, producing a new index requires more time than was allowable for this project timeline. Seasonal flights following phenological timing may additionally assist in producing a new index as it would provide a spectral library to compare against.
5. ***Flight Timing Modification:*** Timing of flights was found to be a difficult variable that resulted in some limitations of the drone imagery. While it is typically recommended to fly a drone at solar noon to reduce shadows, this resulted in imagery that contained strong reflectance from water remaining on the marsh surface despite flying close to low tide. Therefore, we recommend that future flights be conducted 2-3 hours before or after solar noon while aligning with low tide. This should result in the sun hitting the marsh at an oblique angle, allowing the reflection of any water under the vegetation canopy to not be directly reflected towards the drone cameras. Depending on the size of the assessment area, covering large swaths of marshes close to a specific time range will require specific flight altitudes. However, greater flight altitude can result in increased vegetation-sourced shadowing from increased angles within the photos. More guidance is needed in balancing shadow reduction with lower flight altitude and covering large areas in a short duration to minimize shadowing from variable sun angles.
6. ***Including A Reference card for Corrections:*** A reference card for atmospheric correction and reflectance standardization should be used for each flight. The DJI company does not manufacture reference cards for multispectral reflectance correction. Therefore, with each flight with the DJI drones, we have some inherent variability due to differences in weather conditions as flights took

place over several days. We additionally suspect that our multispectral index values are somewhat lower than what can be found in the scientific literature due to this lack of correction. In the future, it is recommended that we purchase a reference card from another company and utilize it to calibrate the sensors of our drones. Calibration of the drone sensors would require a new methodology to be produced but would provide a way to correct for atmospheric interference. This would ensure that our measurements are comparable to other studies.

References

Desianti N., Enache M.D., Griffiths M., Biskup K., Degen A., DaSilva M., Millemann D., Lippincott L., Watson E., Gray A., Nikitina D., Potapova M. (2019). The Potential and Limitations of Diatoms as Environmental Indicators in Mid-Atlantic Coastal Wetlands. Estuaries and Coasts. https://doi.org/10.1007/s12237-019-00603-4

Fisher, J., & Acreman, M. C. (2004). Wetland nutrient removal: a review of the evidence. *Hydrology and Earth System Sciences*, *8*(4), 673–685.

Guo, F., Luo, Y., Nie, W., Xiong, Z., Yang, X., Yan, J., Liu, T., Chen, M., & Chen, Y. (2023). Biochar boosts nitrate removal in constructed wetlands for secondary effluent treatment: Linking nitrate removal to the metabolic pathway of denitrification and biochar properties. *Bioresource Technology*, 129000. https://doi.org/10.1016/j.biortech.2023.129000

Mitsch, W. J., & Gosselink, J. G. (2015). *Wetlands* (Fifth;5th;). John Wiley and Sons, Inc.

National Aeronautics and Space Administration, Science Mission Directorate. (2010). Reflected Near-Infrared Waves. Retrieved April 14, 2022, from NASA Science website: http://science.nasa.gov/ems/08_nearinfraredwaves

New Jersey Department of Environmental Protection (2007). Valuing New Jersey's Natural Capital: An Assessment of the Economic Value of the State's Natural Resources.

Pedersen, E., Weisner, S. E. B., & Johansson, M. (2019). Wetland areas' direct contributions to residents' well-being entitle them to high cultural ecosystem values. *Science of The Total Environment*, *646*, 1315–1326. https://doi.org/10.1016/j.scitotenv.2018.07.236

Rezaie, A. M., Loerzel, J., & Ferreira, C. M. (2020). Valuing natural habitats for enhancing coastal resilience: Wetlands reduce property damage from storm surge and sea level rise. *PLOS ONE*, *15*(1), e0226275. https://doi.org/10.1371/journal.pone.0226275

Smith, J. A. M., Adamowicz, S. C., Wilson, G. M., & Rochlin, I. (2022). "Waffle" pools in ditched salt marshes: assessment, potential causes, and management. *Wetlands Ecology and Management*, *30*(5), 1081–1097. https://doi.org/10.1007/s11273-021-09835-3

Tiner, R., Lang, M., & Klemas, V. (2015). Remote Sensing of Wetlands Applications and Advances. CRC Press.

Were, D., Kansiime, F., Fetahi, T., Cooper, A., & Jjuuko, C. (2019). Carbon Sequestration by Wetlands: A Critical Review of Enhancement Measures for Climate Change Mitigation. *Earth Systems and Environment*, *3*(2), 327–340. https://doi.org/10.1007/s41748-019-00094-0

Appendices

Appendix A: Quality Assurance Project Plan

Appendix B: Mapping and Assessing Tidal Marsh Conditional Via Multispectral Imaging: Multispectral Imaging Standard Operating Procedure

Appendix C: Evaluating the use of multispectral drones for delineation of low and high marsh communities: Error Matrices

Appendix D: Evaluating the use of multispectral drones for delineation of low and high marsh communities: Plot Summary Results

Appendix E: Evaluating the use of multispectral drones for delineation of low and high marsh communities: Subplot Summary Results

Appendix F: Supplementary Information for Chapter 5

Appendix G: Presentation Abstracts

Appendix A: Quality Assurance Project Plan

New Jersey Department of Environmental Protection
Division of Science and Research

Quality Assurance Project Plan (QAPP)

Title Page:

Mapping and Assessing Tidal Marsh Condition Via Multispectral Imaging
March 2022
Brittany Wilburn & Metthea Yepsen
The New Jersey Department of Environmental Protection
Division of Science and Research (DSR)
428 E. State St., 1st Floor
Mail Code 428-01, P.O. Box 420
Trenton, NJ 08625-0420
(609) 940-4008
Brittany.Wilburn@dep.nj.gov
Metthea.Yepsend@dep.nj.gov

NJDEP Project Managers' Names: Brittany Wilburn & Metthea Yepsen

Signatures, Date of Signatures: Brittany P. Wilburn 07/14/2022

Metthea Yepsen 07/14/2022

Project Quality Assurance Officer's Name: Lee Lippincott

Signature, Date of Signature: R. Lee Lippincott 07/07/2022

Project Information Page:

1. **Project Name**: Mapping and Assessing Tidal Marsh Condition Via Multispectral Imaging
2. **Date of Project Initiation**: March 2022
3. **NJDEP Project Managers**: Brittany Wilburn & Metthea Yepsen
4. **Quality Assurance Officer**: Lee Lippincott
5. **Project Description**

    A. **Objective and Scope Statement**: Increasing the resilience of New Jersey's tidal wetlands to sea-level rise is of utmost importance. Tidal wetlands provide a myriad of ecosystem services from cleaning water to buffering coastal developments from storms (NJDEP, 2007; Mitsch & Gosselink, 2015). NJ has more than 300,000 acres of tidal wetlands, most of which are owned and managed by the State. Traditional field methods for assessing tidal wetland condition are often time- and resource-intensive. The NJDEP - Division of Fish and Wildlife (NJDEP-FW), NJDEP – Bureau of Geographic Information Systems (NJDEP – BGIS), Rowan University, Jacques Couteau National Estuarine Research Reserve (JCNERR), and the NJ Tidal Wetlands Monitoring Network (NJTWMN) are looking for efficient, cost-effective ways to map plant communities and assess the health of tidal wetlands.

    Remote sensing of wetland plant health has been done for decades from satellite sensors measuring the wavelengths of light absorbed and reflected by green plants (Guo et al., 2017; NASA, 2010; Tiner et al., 2015). Chlorophyll in plant leaves strongly absorb wavelengths of visible red and blue lights, while reflecting visible green and invisible near-infrared wavelengths (Fig. 1). Using these spectral properties, spectral indices (or mathematical calculations derived from imagery pixel values from two or more spectral bands) have been created to measure specific vegetation characteristics through imagery across landscapes. Traditionally, satellite imagery has been used to evaluate vegetation characteristics for larger landscapes. However, the coarse spatial resolution of available satellite imagery makes it suitable for larger scale mapping and would not be able to display the variability in plant communities and habitat, which would require at least m^2-scale resolution to map. Additionally, while high resolution (cm^2- or m^2-scale) satellite imagery is available, it is often expensive, includes a limited area of coverage, and may not be available during ideal time periods due to cloud interference, tidal inundation, or other factors. In contrast, drones can collect imagery at the spatial resolution required

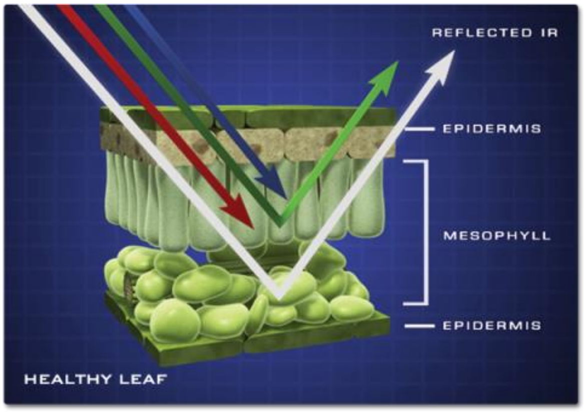

Figure 1. Graphic demonstrating absorbance of red and blue light wavelengths and reflectance of green and infrared light wavelengths in a healthy leaf (image credit: Jeff Carns in NASA, 2010).

to assess wetland plant community health and even isolate individual plants, while reducing costs and providing flexibility in site coverage and optimal timing.

Landscapes can be modelled using drones by creating orthomosaics and digital surface models (DSMs) from overlapping images using a photogrammetry technique called Structure from Motion. These products are derived from point clouds of data generated from the imagery, containing longitudinal, latitudinal, and elevational coordinates as well as Red-, Green-, and Blue-color (RGB) information (plus other variations of light waves, depending on the type of sensors with which the drone is equipped). This high data density allows for high resolution (cm^2-scale) two-dimensional maps and three-dimensional models to be created for large expanses of landscape and to indicate the relative density and health of vegetation. This data is often analyzed in spatial visualization programs, such as ArcGIS Desktop or Pro (Environmental Systems Research Institute, Redlands, CA), ENVI (Exelis Visual Information Systems, Boulder, CO), and eCognition (Trimble Geospatial, Sunnyvale, CA), using color filters and spectral indices. The formulae for selected common multispectral vegetation indices are listed in Table 1. The outputs from these indices provide an opportunity for quantitatively evaluating landscape-level vegetation communities.

Although there has been a large increase in the use of drone technology in the scientific community due to its wide and flexible applicability, there yet remains to be a standard protocol by which wetlands are modeled and analyzed using drone imagery. We propose to develop methods for mapping plant communities and tidal wetland condition using drones equipped with multispectral lenses. We will validate the results derived from processed drone imagery using traditional field methods for assessing and understanding tidal wetland health. This includes measuring soil properties (e.g., porewater salinity, porewater pH, oxidation/reduction potential, porewater sulfides/sulfates, porewater chloride concentrations, and an index of bearing capacity), determining diatom assemblages, and quantifying vegetation characteristics that can be identified with manual techniques and multispectral images (e.g., dominant plant species height, species cover, and total cover). Diatoms have proven to be accurate indicators of nutrients, pollution, and salinity in tidal wetlands (Desianti et al. 2019). Diatom species composition may also be a valuable indicator of sulfide concentrations in the soil. Since both diatoms and *in situ* measurements of sulfides are already proposed as a part of this project, we will take advantage of this opportunity to preliminarily evaluate whether diatoms can be used a proxy for sulfides.

During year one, two marshes – JCNERR’s Great Bay Boulevard Marsh and USFWS’s E.B. Forsythe National Wildlife Refuge – will be assessed. The condition of these sites is known, and many years of environmental data have been collected in them. This will provide a robust background for interpreting imaging results. Year one data will be used to develop and write a draft methods document for mapping plant communities and assessing wetland condition from the multispectral imagery.

For year two, the draft methods will be tested and refined in up to six tidal wetland sites that do not have the benefit of long-term data collection or known condition. These sites will be in areas that are of particular interest to NJDEP-FW or areas where little tidal wetland monitoring has occurred.

B. **Data Usage**:

Drone imagery data will be used to calculate the following metrics for each site:

1) Vegetation Indices (see Table 1)
    a. Normalized Difference Vegetation Index
    b. Green Normalized Difference Vegetation Index
    c. Normalized Difference Red-Edge Index
    d. Enhanced Vegetation Index
    e. Leaf Area Index
    f. Soil Adjusted Vegetation Index
2) % Vegetation Cover
3) Ratio of Vegetated to Unvegetated Area
4) Species Composition and Cover

Table 1. Selected multispectral vegetation indices commonly used for vegetation characterization. VI, vegetation index; NIR, Near-Infrared; RE, Red-Edge; canopy background adjustment factor (L), soil brightness.

Vegetation Index	Acronym of Index	Color Band Formula
Normalized Difference VI	NDVI	$NDVI = \frac{(NIR - Red)}{(NIR + Red)}$
Green Normalized Difference VI	GNDVI	$GNDVI = \frac{(NIR - Green)}{(NIR + Green)}$
Normalized Difference Red-Edge Index	NDRE	$NDRE = \frac{(NIR - RE)}{(NIR + RE)}$
Non-Photosynthetic Vegetation Index	NPV	$NPV = \frac{(Blue - Green)}{(Blue + Green)}$
Enhanced Vegetation Index	EVI	$EVI = 2.5 * \frac{(NIR - Red)}{(NIR + 6 * Red - 7.5 * Blue + 1)}$
Leaf Area Index	LAI	$LAI = 3.618 * EVI - 0.118$
Soil Adjusted Vegetation Index	SAVI	$SAVI = (1 + L) * \frac{(NIR - Red)}{(NIR + Red + L)}$

These data will be combined with field and lab techniques to create a comprehensive classification of the tidal wetland sites. Field and lab measures will additionally include the following for each site:

1) Vegetation Surveys

    a. Maximum height of dominant species
    b. % Cover by Species
    c. % Total Cover
2) Marsh Platform Elevation
3) Edaphic metrics measured *in situ*
    a. Soil pH
    b. Soil oxidation/reduction potential
    c. Bearing capacity
    d. Porewater salinity (refractometer)
4) Edaphic metrics measured *ex situ*
    a. Porewater salinity (YSI)
    b. Porewater sulfide concentration
    c. Porewater chloride concentration
5) Diatom Assemblages

The research questions we are hoping to answer include:

1) Can we distinguish between high marsh and low marsh habitats based on plant species identification using drone imagery?
2) Can we determine signs of significant plant stress indicative of future vegetation die-off using drone imagery?
3) Is there a significant correlation between soil sulfide concentrations and diatom assemblages?

The data we collect during this project will enable rapid assessment of tidal marshes across the State for quick delineation of marsh plant communities and their associated levels of stress and degradation. NJDEP will have an established protocol for future drone modelling and classification of tidal marshes, ensuring that future models created from drone orthomosaics are comparable.

C. **Data Quality Objectives (DQOs)**:

This project falls under **Levels 2** and **3**.

Level 2 Methods development in which there is a new application of a technique or instrument.

Level 3 Methods refinement for potential use in an official protocol or the use of methods that will be used to provide data for a health or ecological assessment.

D. **Monitoring Network Design and Rationale**:

Two sites of known wetland condition will be examined this year (2022) (Fig. 2), and up to six different sites of unknown wetland condition will be examined the following year (2023). The sites of known wetland condition are JCNERR’s Great Bay Boulevard marsh and USFWS’s E.B. Forsythe National Wildlife Refuge. The following factorial design will be used to examine plots within each site: 2 Levels of Marsh Condition (healthy vs degraded) x 2 Levels of Elevation-specific Plant Communities (low marsh *Spartina alterniflora* vs high marsh *Spartina patens*). Plots will be replicated at *n=4* for each treatment combination, for a total of 16 plots at each marsh. This factorial design will allow for variables that include the target plant communities and specific signs of marsh stress to be included in the classification and modelling of marsh habitat and vulnerability.

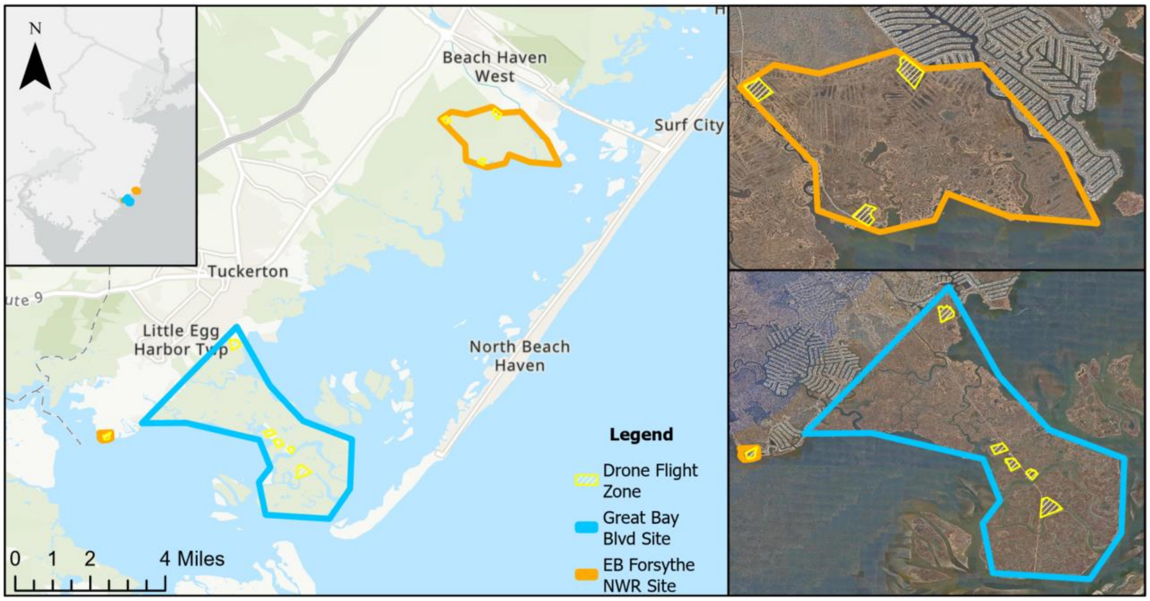

Figure 2. Map of Great Bay Boulevard and E.B. Forsythe National Wildlife Refuge, the two marsh sites of interest for testing the drone and field methods for the 2022 pilot. Plots will be selected within each drone flight zone.

Within each drone flight zone (Figs. 2 and 3), the following metrics will be measured by drone: vegetation indices (Table 1), percent vegetation cover, ratio of vegetated to unvegetated area, and plant species composition and cover. Within the 100 m^2 plot, we will manually determine the dominant species of vegetation, percent vegetation cover, and species composition and cover. At each sub-sample, the following parameters will be measured or collected: bearing capacity, porewater, RTK-GPS elevation, diatom samples, soil pH, soil oxidation/reduction potential, soil temperature, percent vegetation cover, and dominant species. The porewater from each sub-sample will be combined and measured as a composite for sulfate concentration, sulfide concentration, conductivity (as a proxy for salinity), and chloride concentration.

The second year will act as a test of our developed methods and correlations. We will visit up to six coastal wetland sites that do not have extensive long-term monitoring and, therefore, are not well-characterized. The sites will be determined by NJDEP-DSR and NJDEP-FW. The data collection within these sites will follow the same structure as year one.

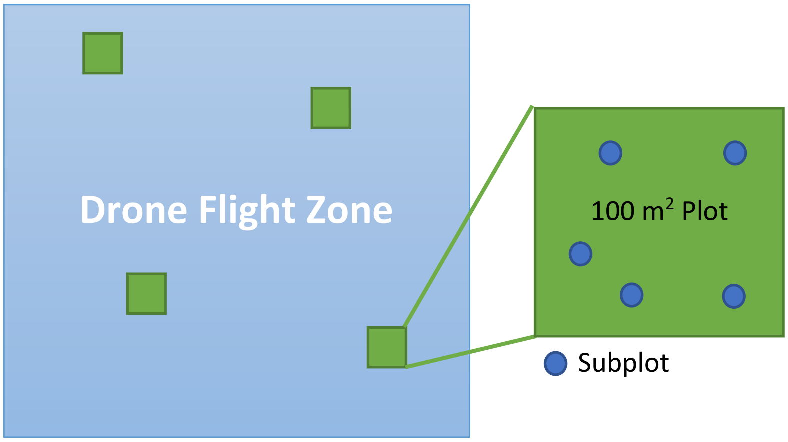

Figure 3. Conceptual diagram of sampling points within plots and sites. The number of plots within the drone flight zone may change depending on local site conditions (e.g., species-specific vegetation cover range, tidal inundation, etc.).

E. **Sampling Procedures**:

Drone Imagery:

Number of team members: Minimum 4

Flight protocol: Two aircraft will be deployed, one to collect multispectral data and one to collect higher resolution RGB mapping photos. Each aircraft will have a minimum crew consisting of a Remote Pilot in Command (RPIC) and a Visual Observer (VO). Flights will be performed using automated flight programs to ensure proper overlap of photos taken.

Safety Measures: RPICs are FAA Certified Remote Pilots and will be following the Federal Aviation Regulations and FAA recommendations to ensure the safety of other aircraft as well as people and property on the ground.

Classification: Drone imagery will undergo segmentation to generalize the imagery. This groups similar pixels based on reflectance signatures and allows for easier classification and manipulation of the imagery. Classification algorithms and spectral indices will be utilized on the segmented image to pull out vegetation characteristics. Multiple classification algorithms, such as Support Vector Machine and Random Forest, will be tested to determine which one will provide the most accurate results based on *in situ* data collection. ArcGIS Pro's (ArcGIS Pro 2022) "Forest-Based Classification and Regression" tool will also be tested to classify the data and predict vegetation communities within the project sites.

Vegetation Surveys:

Number of team members: Between 2 to 3

Survey protocols: Plots (100 m^2 in area) representing the four categories (healthy or unhealthy, high or low marsh) will be staked out and measured for the following characteristics: dominant species plan (NJTWMN, 2021), height of dominant plant species (max 2 species, Quirk et al. 2010), % cover by species (Quirk et al. 2010), and percent total plant cover in plot. Percent total plant cover will be measured as actual estimates rather than by cover classes as this provides a more realistic and comparable value that we can utilize for drone imagery classification.

Plots will be categorized in the field by species presence, hydrogeomorphic features (i.e., nearby creeks and ponds), and plant height, coloration, and density. These factors will be used to determine if the plot is going to be analyzed as a "Healthy Patens", "Healthy Alterniflora", "Unhealthy Patens", or "Unhealthy Alterniflora" plot. Once a plot is estimated to have near homogenous cover with the listed conditions, at least two team members measure out the plot. If the plot is a 10 m x 10 m plot, then a corner is established with a flag and the team members will walk out the plot using field measuring tape, marking each corner with a flag. The team members should remeasure the last edge of the plot to ensure 10 m is achieved. The plot should then be marked with washable spray chalk for better visibility of the plot in the drone imagery. If the plot is estimated to be a rectangle, then similar methods should be used with flexibility on the dimensions of the plot, ensuring that close to 100 m2 is achieved. Finally, if the plot will be along a pond edge or if the vegetation cover is drastically zonated, then the defining edge of the plot (i.e., along the pond or the vegetation change) should be marked with flags and measured with field measuring tape. Then, measuring perpendicular from vegetation barrier across the vegetation plot, measure out equal distances with the field measuring tape to create a near 100 m2 plot (see Fig. 4). Only the outside of the plot should be marked with spray chalk and flags so as not to disrupt the imagery of the inner plot and subplots. These plots will be slightly larger than 100 m2 due to the curvature of the pond or vegetation zone.

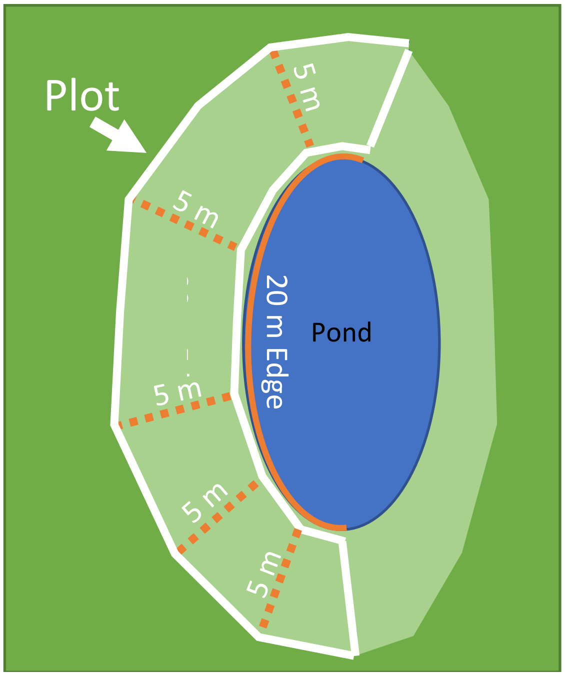

Figure 4. Example of how a plot would be measured and marked around a pond or other curving feature like vegetation zonation.

Bearing Capacity: A capped 2 inch-diameter PVC pipe will be placed within selected sub-sampling points in plots and a standard force will be applied to the pipe using a 7.4 lb slide hammer to assess the belowground stability (Rogerson et al., 2017). After five blows, the penetration depth is used as an index of the strength of the root mat and peat layers.

RTK Elevation Measurements: A real-time kinematic global positioning system (RTK-GPS) will be used to measure survey-grade coordinates and elevations of points of interest in this study, as well as to help characterize the marsh topography. Measurements will be taken at 5 ground control points (GCPs) across the drone flight zone. Additionally, RTK-GPS points will be measured where the ground cover is either 100% *S. alterniflora* or *S. patens* within a 1-meter radius of the measured point, with 6 points of each species type within each drone flight zone, if those species are present. Lastly, measurements will be taken at each sub-sample within each plot. RTK measurements will be processed using the NAD83 horizontal datum and the NAVD88 vertical datum within the NJ State Plane Coordinate System and referenced to a reference point established in situ using a stabilized PVC pipe.

Soil and Porewater Sampling:

Soil sampling protocol: Soil pH and oxidation/reduction potential (ORP) will be measured in the field using *in situ* sensors (Hanna Instruments Groline Soil pH tester and Extech Instruments ExStik Model RE300 Waterproof ORP meter, respectively). Sensors will be inserted to a depth of 2.5 cm (the central depth of porewater extraction, see below) immediately adjacent to each porewater sampling point immediately prior to porewater sampling. Samplers will be trained to collect soil data by C. Schutte.

Porewater sampling and storage protocol: Five Rhizon porewater samplers (0.25 mm diameter, 10 cm length, 0.15 µm pore size; Rhizosphere Research Products) will be haphazardly distributed across each plot and will act as the demarcation of sub-sample points. Rhizons will be inserted vertically into the soil to collect porewater samples across a depth range of 0–10 cm below the marsh surface (Smith et al 1979; Bradley & Morris, 1991). Porewater samples will be collected into 12-mL syringes over 1–2 hours. Porewater from the 5 syringes collected within each plot will be combined into a single 60-mL syringe to generate one composite porewater sample per plot. Two blank samples will be collected from each site, generating a total of 36 samples per project year. Each composite sample will be distributed as follows for standard geochemical analyses (Schutte et al. 2016). One porewater sub-sample will be preserved with nitric acid for subsequent chloride and sulfate analysis via ion chromatography (Schutte et al., 2016). A second porewater sub-sample will be preserved with zinc acetate for subsequent colorimetric sulfide analysis (Cline, 1969). A small sub-sample will be used to estimate the porewater salinity in the field using a refractometer. The remaining composite sample will be returned to the lab for conductivity (USEPA Method 120.1, 1983) analysis. Sub-samples to be measured in the lab will be transported to Rowan University in chilled coolers. Samplers will be trained to collect porewater samples by C. Schutte.

Diatom Sampling: Vegetation will be trimmed from a 10x10 cm plot, and the top 1 cm of soil will be cut and scraped into a sampling bag. Each collection will be taken from within a 0.25 m distance from a soil characterization sub-sample point (see Soil and Porewater Sampling section above, Fig. 3) (Desianti et al., 2019). Samplers will be trained to conduct the diatom sampling by M. Enache.

F. **Sample Custody Procedures**:

Drone Imagery: Multispectral and RGB photos will be recorded on an SD card in the drone. Upon completion of mission, the respective RPIC will download the data to a non-networked computer to check and edit for privacy issues and then process the images into orthomosaic maps and upload them to the OneDrive server for further analysis.

Vegetation Surveys: Data will be collected via field sheets made of Rite In The Rain paper and transferred to the OneDrive server within one week of the field work.

Porewater and Diatom Sampling: Porewater samples will be either measured directly *in situ* or sent to Rowan labs in chilled coolers, depending on the parameter being measured. Soil samples for diatom assemblages will be stored in sealed plastic bags and transported to NJDEP labs in chilled coolers.

Sample custody and analysis progress in all cases will be recorded through a shared document within NJDEP's OneDrive.

G. **Monitoring Sites and Frequency of Sample Collection**:

Year 1

- Great Bay Boulevard, Tuckerton, NJ
    - Dates of Sampling: August 8-11, 2022
    - Types and Locations of Sampling:
        - Drone Imagery across sampling ranges
        - Vegetation Surveys (no physical samples of vegetation will be collected)
            - 16 plots (2 Health-states x 2 Elevation-representative Plant Species x 4 Replications)
        - 18 Porewater Samples
            - 16 composite samples from plots, plus 2 field blanks
        - 16 Diatom Samples
            - All samples will be paired with soil chemistry sub-sample points
- E.B. Forsythe NWR
    - Dates of Sampling: August 22-25, 2022
    - Types and Locations of Sampling: See Great Bay Boulevard sampling plan above

Year 2

- Exact sites TBD
    - Expected Sampling Date: August 2023
    - Expected Types of Sampling: See Great Bay Boulevard sampling plan above

H. **Analytical Procedures**:

Table 2. Porewater Analysis conducted at Rowan University Laboratory

Parameter	Number of Samples	Sample Matrix	Analytical Method	Sample Preservation	Holding Time
Conductivity/ Salinity	32	Water	USEPA Method 120.1	4°C storage	4 weeks
Sulfate concentration	32	Water	Schutte et al., 2016	Nitric acid, pH < 2	Unlimited
Sulfide concentration	32	Water	Cline, 1969	Zinc acetate, 4°C storage	1 week
Chloride concentration	32	Water	Schutte et al., 2016	Nitric acid, pH < 2	Unlimited

Table 3. Diatom Sampling conducted by NJDEP.

Parameter	Number of Samples	Sample Matrix	Analytical Method	Sample Preservation	Holding Time
Diatom	32	Soil	Desianti et al., 2019	-20 °C storage	Unlimited

6. **Data Quality Requirements**:

Drone Methodology: Features to be accurately captured by drone imagery should be no less than the area contained by a pixel within the orthomosaic. This defined area is dependent upon the quality of camera/sensor equipped on the drone, as well as how low the flight takes place. We expect to reach a 2 cm resolution with our drone imagery.

Additionally, for accurate classification we will use training data. Training sample data are drawn throughout the project site to define which image objects belong to each class of the classification scheme. The training sample data should follow consistent guidelines to ensure all defined classes are properly represented, and so they do not introduce error into the classification algorithm. These guidelines include only drawing training sample data in locations that represent one class, each class should have an adequate number of samples across the project area, prioritize areas that provide spectral differences between classes and similarity within classes, samples should be accurately labeled and placed, and should be larger than the minimum mapping unit (Green et al., 2017). The coverage and amount of training samples depends on the coverage and size of the project site.

Porewater Chemistry: Actual method detection limits (marked TBD below) will be calculated using data from the field blank samples.

Table 4. Porewater Chemistry Sampling Limits.

Parameter	Sample Matrix	Detection Limit	Quantitation Limit	Precision	Accuracy
Conductivity	Water	TBD	2 mS/cm	±1%	>99% recovery
Sulfate concentration	Water	TBD	*0.1 mmol/L	*+/- 5%	*95% recovery
Sulfide concentration	Water	TBD	0.03 mg/L	+/- 2% @ 1 mg/L	~97% recovery @ 1 mg/L
Chloride concentration	Water	TBD	*0.1 mmol/L	*+/- 5%	*95% recovery

* Actual quantitation limit, precision, and accuracy will be determined from at least 10 replicate analyses of standards that bracket the sample concentration range in this study. The values here represent minimum acceptable values.

Diatom Correlation: There are no detection limits for diatoms. However, due to their rarity in sandy marsh sediments (Desianti et al., 2019), we will screen one slide per sample for a maximum time of 4 hours to ensure that all diatoms have been counted and identified.

7. Data Quality Assessments

A. Data Representativeness:

The field data collected at these sites will be combined with previously existing monitoring data to produce a robust dataset describing each site. Additionally, the data collected this year (2022) is meant to act as pilot data to configure a model to capture areas of high vegetative stress before plant death. The methods produced from this year's data collection will be evaluated by applying them to other tidal wetland sites of unknown condition.

B. Data Comparability:

As drone technology becomes more accessible, the amount of scientific literature that includes the use of drones for highly resolved landscape mapping has increased (de Castro et al., 2021). However, there lacks a standardized method for mapping a tidal salt marsh, with specific focus on high and low marsh demarcation using plant species. Additionally, this project will establish which spectral indices will be most effective for evaluating such a landscape, as there is currently no standard set of indices used for marsh classification.

The methods selected for this project have all been selected from peer-reviewed publications, standard protocols, and best practices, except for estimating vegetation within plots without using cover classes. However, our estimates of vegetation cover could be converted *post hoc* to cover classes, to ensure comparability with other vegetation surveys.

Marsh vulnerability models have additionally been created before. For example, there is an established Wetland Vulnerability Index that was created for E.B. Forsythe NWR (Defne et al., 2020); however, this index is based on field data that is more cumbersome and time-consuming to collect, as well as imagery obtained through remote sensing and is, thus, at a lower resolution than what we will obtain through drone imaging. Imagery collected from remote sensing via satellites are useful in generally mapping wetland areas, but do not exhibit clear boundaries of different habitats or vegetation due to low resolution and high spectral and temporal variation. Satellite imagery as a method for determining wetland health poses many challenges since it is difficult to account for underlying processes such as hydrology and seasonal inundation (Alvarez-Vanhard et al., 2020). Using drone imagery is promising in filling the gap between in situ field surveys and satellite imagery when identifying plant species and assessing marsh health.

The major nuances of this study will be a standard drone methodology, the combination of field methods and drone technology to create a marsh vulnerability model, classified maps portraying high and low marsh based on vegetation indicators observed through drone imagery, and a potential demonstration of a relationship between diatom assemblages and sulfide concentrations.

8. **Calibration Procedures and Preventative Maintenance**:

Drone Calibration: The drone compass is calibrated on each field day prior to the first flight.

RTK-GPS Calibration: The RTK GPS is maintained with firmware updates. Prior to surveying, the appropriate settings are reviewed and configured for the project to achieve the desired accuracy, including adjustment of the duration (number of satellite positions logged), correctly entering the antenna height, and uploading any reference data to the project file. While surveying, accuracy is validated by regularly checking that the network connection is maintained, the geometric dilution of precision (GDOP) does not exceed a limit of 3.5, and the three-dimensional coordinate quality (3DCQ) remains less than 1.97 inches (5 centimeters). As a quality check, repeat measurements are taken at the beginning and end of the survey, either at marked locations of hard surfaces (e.g., road) if available, or atop temporary stakes driven into the marsh. If permitted and accessible, additional checks will be made at nearby surface elevation tables (SETs), by surveying atop the SET receiver according to the site owners' (JCNERR/USFWS) standard vertical point of precision (VPR).

Redox Calibration: ORP sensors will be calibrated at the beginning and end of each field day.

pH Probe Calibration: pH sensors will undergo a 2-point calibration prior to the first measurement on each field day.

9. **Quality Control Checks**:

Segmentation and Classification: In preparation to generate a classified dataset, the orthomosaic goes through segmentation and training workflow steps. Segmentation "divides an image into relatively homogeneous, characteristically significant, and spatially unique segments or objects" (Green et al., 2017). In order to determine an accurate classification of the segmented image, a training dataset will be used. In this case, the field data collected from each plot will be used as a point of on-the-ground measurement and will be included as training data. Each sub-sample point would be an ideal training data point, which would produce a training data set of at least 80 data points per site (5 sub-samples per plot, 16 plots per site).

Once the data is classified, a thematic accuracy assessment is conducted using random points across the project site, which includes an Error Matrix, Producer's Accuracy, Users Accuracy, and Overall Accuracy as main thematic metrics. The distribution of the random points should be proportionate to the size of each class; for example, if a site contains 10% of the area of the overall project site, that feature will require 10% of the available random check points. The random points contain the class information of the classified image at that location and will be reviewed with reference data (original imagery, field surveys, etc.). The resulting accuracy will be represented using the overall accuracy of the project site.

Porewater Chemistry: Four field blanks will be collected. Internal check standards will be included every 10 samples for all geochemical analyses.

Diatom Assemblages: The 10x10 cm soil samples will each be homogenized to make sure that all diatoms present in the sample will be equally distributed and representative of the sample. Due to their microscopic size (2-100 µm) and high abundance, no replicates are used for these samples.

10. **Documentation, Data Reduction, and Reporting**

    A. **Documentation**:

    All field measurements will be written on Rite In The Rain paper, either as field sheets or within field journals. Following our return to the office, all hand-written data will be transferred to the project's shared OneDrive folder. All digital data, including drone raw imagery, orthomosaics, and classified maps, will additionally be stored within the project's shared OneDrive folder. All diatom count data will be entered in Microsoft Excel spreadsheets containing the following: sample code and date of counting; diatom species name and the # of valves counted for each species. All raw data will be converted to relative abundances. Diatom abundance data will additionally be stored within the project shared OneDrive folder. Lastly, external data from Rowan University labs will be uploaded to the shared OneDrive folder.

    B. **Data Reduction and Reporting**:

    Drone imagery will be consolidated into orthomosaics that will then be classified by vegetation indicators. This classification will be combined with collected field data to build a robust dataset that will be used to create a model of marsh vulnerability. The output of the marsh vulnerability model will include maps demonstrating areas of high and low marsh, as well as points of vegetative stress. The values resulting from the raster formed by the marsh vulnerability model will be the final rating of the marshes. This model will then be fine-tuned using drone imagery collected from other marshes with little to no known health status.

Additionally, the field data will be combined with the diatom assemblages to determine if a relationship exists with the soil sulfites and to create a predictive model if this is the case.

11. **Data Validation**:
    Multiple types of modelling approaches will be used to determine the best form of classification of the drone imagery. Following modelling and classification, the resulting classified maps will be checked against known field data to ensure the maps were classified accurately, and an accuracy assessment will be produced. Additionally, the final marsh vulnerability model will be checked against other known models of the Great Bay Boulevard and E.B. Forsythe NWR, such as the Wetland Vulnerability Index by Defne et al. (2020), to ensure that our model is not skewed.

12. **Performance and Systems Audits**: The principal investigators (Brittany Wilburn, Metthea Yepsen, Lori Lester, Kirk Raper, and Charles Schutte) will review the protocols, field work, and data as it is collected and analyzed to ensure that the project goals and needs are met. Additional guidance from Nick Procopio, NJDEP-FW, NJDEP-BGIS, JCNERR, and NJTWMN will be received during the project to produce outputs that are useful to each organization involved.

13. **References**

ArcGIS Pro. (2022). (Version 2.9.3). Esri Inc. https://www.esri.com/en-us/arcgis/products/arcgis-pro/overview.

Bertness, M.D. and Ellison, A.M. (1987). Determinants of pattern in a New England salt marsh plant community. *Ecological monographs*, 57(2), pp.129-147.

Charles, D.F., Knowles C., and R.S. Davis. (2002). Protocols for the analysis of algal samples collected as part of the U.S. Geological Survey National Water-Quality Assessment Program. The Academy of Natural Sciences, Philadelphia, Report No 02-06

Cline, J.D. (1969). Spectrophotometric determination of hydrogen sulfide in natural waters. *Limnology and Oceanography*, 14:454–458. https://doi.org/10.4319/lo.1969.14.3.0454

Congalton, R. G., & Kass Green. (2019). *Assessing the accuracy of remotely sensed data: principles and practices* (pp. 69–97). CRC Press.

Defne, Z., Aretxabaleta, A.L., Ganju, N.K., Kalra, T.S., Jones, D.K., & Smith, K.E.L. (2020). A geospatially resolved wetland vulnerability index: Synthesis of physical drivers. *PLoS ONE*, 15(1): e0228504. https://doi.org/10.1371/journal.pone.0228504

Desianti N., Enache M.D., Griffiths M., Biskup K., Degen A., DaSilva M., Millemann D., Lippincott L., Watson E., Gray A., Nikitina D., Potapova M. (2019). The Potential and Limitations of Diatoms as Environmental Indicators in Mid-Atlantic Coastal Wetlands. *Estuaries and Coasts*. https://doi.org/10.1007/s12237-019-00603-4

Green, K., Congalton, R. G., & Tukman, M. (2017). *Imagery and GIS best practices for extracting information from imagery* (pp. 278–279, 285–291). Redlands, California Esri Press.USEPA. 2021. National Wetland Condition Assessment 2021: Field Operations Manual. EPA 843-B-21-002. U.S. Environmental Protection Agency, Washington D.C.

Guo, M., Li, J., Sheng, C., Xu, J., & Wu, L. (2017). A Review of Wetland Remote Sensing. Sensors, 17(4), 777. *MDPI AG*. Retrieved from http://dx.doi.org/10.3390/s17040777

Mitsch, W.J., & Gosselink, J.G. (2015). *Wetlands* (5th ed.). Wiley.

Moody, J. 2017. Methods for Shellfish Population Density and Demographics in Living Shoreline Treatments. Partnership for the Delaware Estuary. PDE Method No. 46. 7pp.

National Aeronautics and Space Administration, Science Mission Directorate. (2010). Reflected Near-Infrared Waves. Retrieved April 14, 2022, from NASA Science website: http://science.nasa.gov/ems/08_nearinfraredwaves

New Jersey Department of Environmental Protection (2007). Valuing New Jersey's Natural Capital: An Assessment of the Economic Value of the State's Natural Resources.

Quirk, T., Thomas, R., and Velinsky, D. (2010). SOP # 029 Vegetation: Percent Cover and Height Determination of Vegetation within Quadrats. Academy of Natural Sceinces of Philadelphia - Patrick Center for Environmental Research. Procedure No. P-16-128, Rev. 0 (09/2010).

Rogerson, A, McLaughlin, E & Havens, K (2017), Mid-Atlantic Tidal Wetland Rapid Assessment Method Version 4.1 [online], Delaware Department of Natural Resources and Environmental Control, Division of Water Resources, Dover, DE, Maryland Department of Natural Resources, Riparian and Wetland Restoration Services, Annapolis, MD and Virginia Institute of Marine Science, Centre, Gloucester Point, VA. Available at: http://www.dnrec.delaware.gov/Admin/DelawareWetlands/Documents/Tidal%20Rapid_Protocol%203.0%20Jun10.pdf

Schutte C.A., Wilson, A.M., Evans, T., Moore, W.S., and Joye, S.B. (2016). Methanotrophy controls groundwater methane export from a barrier island. *Geochimica et Cosmochimica Acta* 179, 242-256, doi:10.1016/j.gca.2016.01.022

Smith, Katherine K., Ralph E. Good, and Norma F. Good. (1979). Production dynamics for above and belowground components of a New Jersey Spartina alterniflora tidal marsh. *Estuarine and Coastal Marine Science*, 9.2: 189-201.

Tiner, R., Lang, M., & Klemas, V. (2015). *Remote Sensing of Wetlands Applications and Advances*. Crc Press.

USEPA. (1982). Method 120.1: Conductance (Specific Conductance, µmhos at 25 °C) by Conductivity Meter. U.S. Environmental Protection Agency, Washington D.C.

USEPA. (2021). National Wetland Condition Assessment 2021: Field Operations Manual. EPA 843-B-21-002. U.S. Environmental Protection Agency, Washington D.C.

14. **Project Operations and Responsibility:**

Table 5. Project personnel and respective responsibilities within the project.

Project Personnel	**Organization**	**Project Responsibilities**
Brittany Wilburn	NJDEP – DSR	Principal investigator, Sampling operations (e.g., vegetation surveys, bearing capacity index), Sampling QC, Data processing activities, Data processing QC, Data quality review, Performance evaluation/auditing, Overall QA
Metthea Yepsen	NJDEP – DSR	Principal investigator, Sampling operations (e.g., vegetation surveys, bearing capacity index), Sampling QC, Data processing activities, Data processing QC, Data quality review, Performance evaluation/auditing, Overall QA
Joshua Moody	NJDEP – DSR	Principal investigator, Sampling operations (e.g., vegetation surveys, bearing capacity index), Sampling QC, Data processing activities, Data processing QC, Data quality review, Performance evaluation/auditing, Overall QA
Lori Lester	NJDEP – DSR	Principal investigator, Data processing activities, Data processing QC, Data quality review, Performance evaluation/auditing
Kirk Raper	NJDEP – DSR	Principal investigator, Sampling operations (e.g., elevation surveys), Sampling QC, Data processing activities, Data processing QC, Performance evaluation/auditing
Charles Schutte	Rowan University	Principal investigator, Sampling operations (e.g., soil and porewater sampling), Sampling QC, Laboratory analysis, Laboratory QC, Data processing activities, Data processing QC, Performance evaluation/auditing
Mihaela Enache	NJDEP – DSR	Sampling operations (e.g., diatom sampling), Sampling QC, Laboratory analysis, Laboratory QC, Data processing activities, Data processing QC, Data quality review
Maite Whitley	NJDEP – DSR	Sampling operations (e.g., vegetation surveys, bearing capacity index, elevation surveys, sediment and porewater sampling, diatom sampling), Sampling QC, Data processing activities, Data processing QC, Data quality review
Kriish Hate	NJDEP – DSR	Sampling operations (e.g., vegetation surveys, bearing capacity index, elevation surveys, sediment and porewater sampling, diatom sampling), Sampling QC, Data processing activities, Data processing QC, Data quality review
Steven Jacobus	NJDEP – BGIS	Sampling operations (e.g., drone flights), Sampling QC, Data processing activities (e.g., orthomosaicing of drone imagery), Data processing QC, Data quality review

Table 5 – cont. Project personnel and respective responsibilities within the project.

Project Personnel	**Organization**	**Project Responsibilities**
William Smith	NJDEP – BGIS	Sampling operations (e.g., drone flights), Sampling QC, Data processing activities (e.g., orthomosaicing of drone imagery, classification and modelling), Data processing QC, Data quality review
David DuMont	NJDEP – Climate Resilience	Sampling operations (e.g., drone flights), Sampling QC, Data processing activities (e.g., orthomosaicing of drone imagery, classification and modelling), Data processing QC, Data quality review
Kevin Blythe	NJDEP – Fish & Wildlife (FW)	Sampling operations (e.g., drone flights), Sampling QC, Data processing activities (e.g., orthomosaicing of drone imagery, classification and modelling), Data processing QC, Data quality review
Molly VanWieren	NJDEP – FW	Sampling operations (e.g., drone flights), Sampling QC, Data processing activities (e.g., orthomosaicing of drone imagery, classification and modelling), Data processing QC, Data quality review

Appendix B: Evaluating the use of multispectral drones for delineation of low and high marsh communities: Classifications

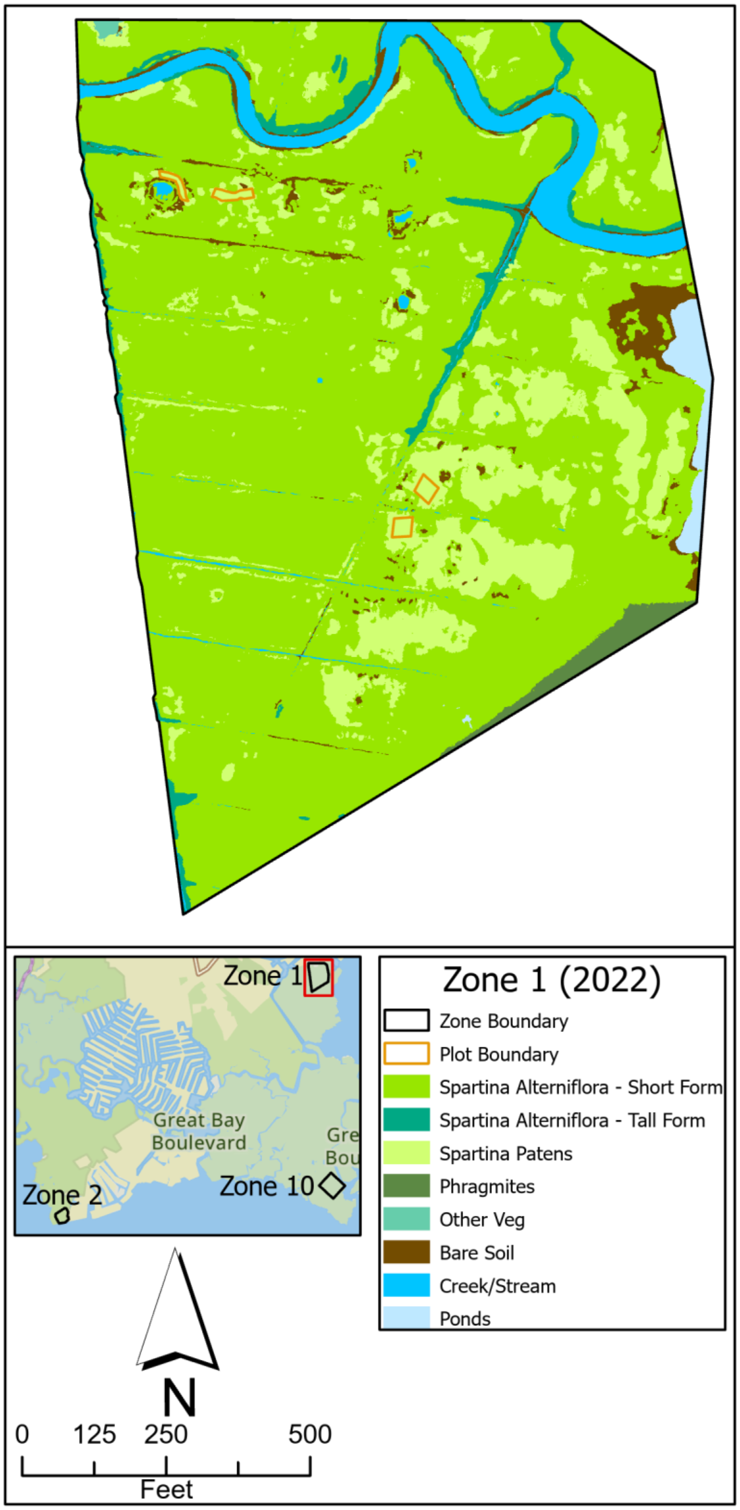
Zone 1
Great Bay Boulevard
Gre
Bou
Zone 2
Zone 10
Zone 1 (2022)
Zone Boundary
Plot Boundary
Spartina Alterniflora - Short Form
Spartina Alterniflora - Tall Form
Spartina Patens
Phragmites
Other Veg
Bare Soil
Creek/Stream
Ponds
N
0
125
250
500
Feet

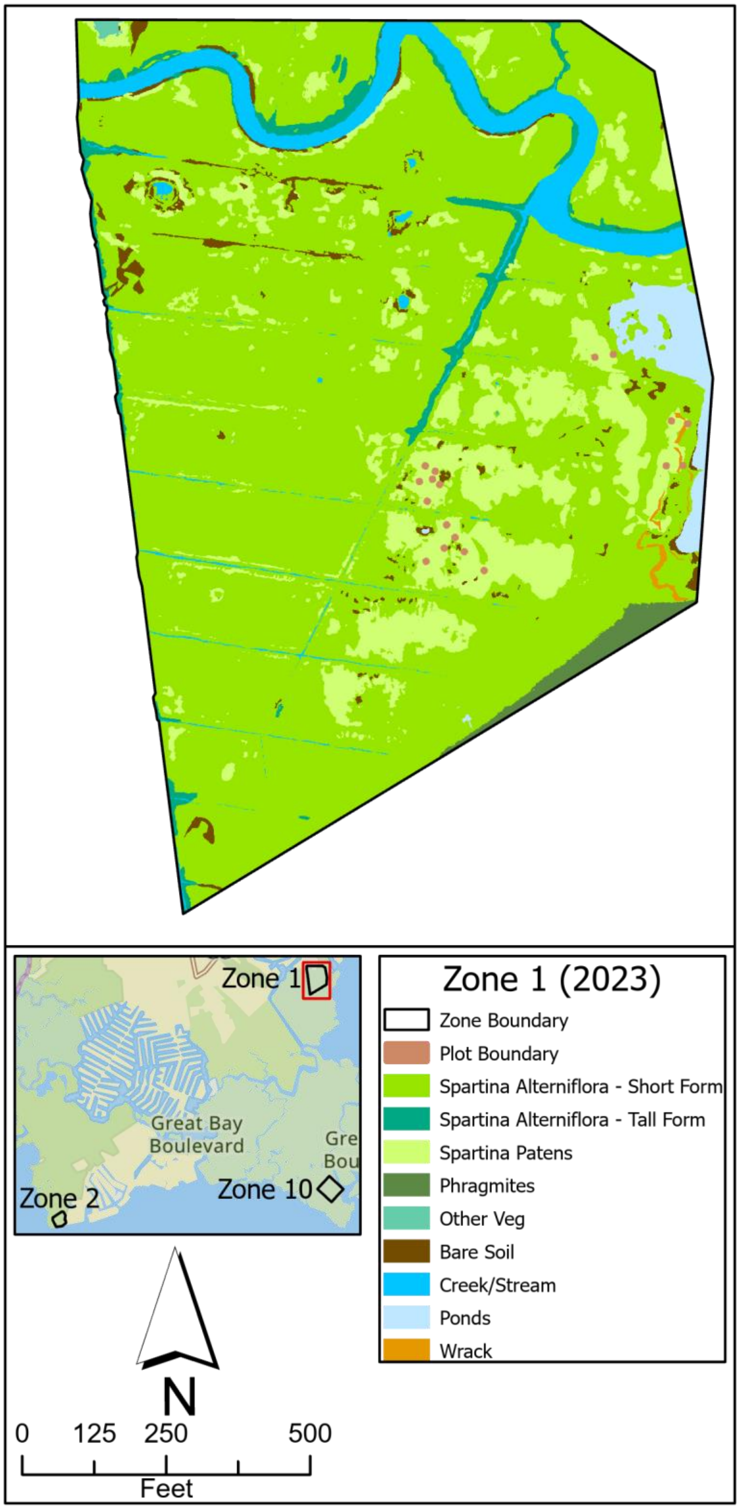
Zone 1
Great Bay Boulevard
Gre Bou
Zone 2
Zone 10
Zone 1 (2023)
Zone Boundary
Plot Boundary
Spartina Alterniflora - Short Form
Spartina Alterniflora - Tall Form
Spartina Patens
Phragmites
Other Veg
Bare Soil
Creek/Stream
Ponds
Wrack
N
0
125
250
500
Feet

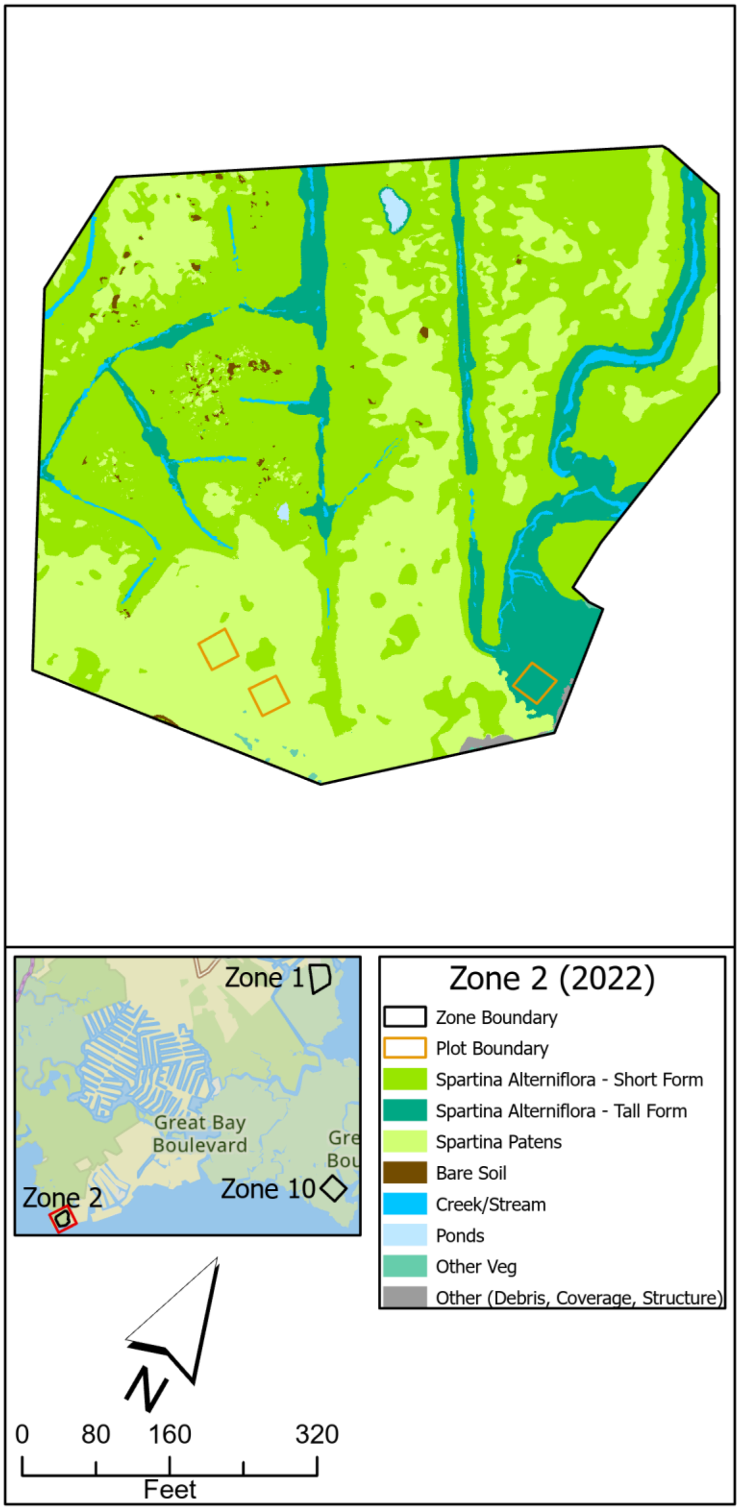
Zone 1
Great Bay Boulevard
Gre
Bou
Zone 2
Zone 10
Zone 2 (2022)
Zone Boundary
Plot Boundary
Spartina Alterniflora - Short Form
Spartina Alterniflora - Tall Form
Spartina Patens
Bare Soil
Creek/Stream
Ponds
Other Veg
Other (Debris, Coverage, Structure)
N
0
80
160
320
Feet

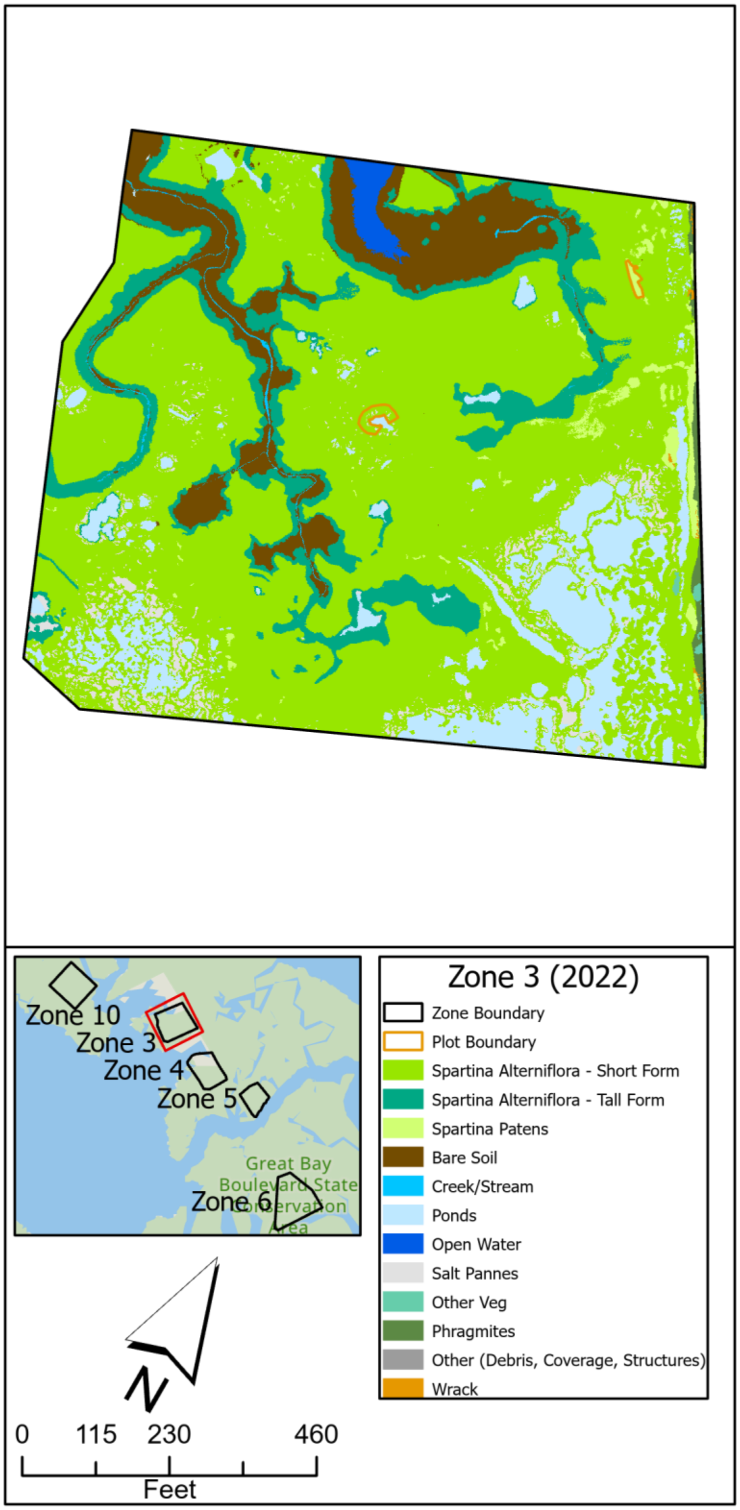
Zone 10
Zone 3
Zone 4
Zone 5
Great Bay Boulevard State Conservation Area
Zone 6
N
0
115
230
460
Feet
Zone 3 (2022)
Zone Boundary
Plot Boundary
Spartina Alterniflora - Short Form
Spartina Alterniflora - Tall Form
Spartina Patens
Bare Soil
Creek/Stream
Ponds
Open Water
Salt Pannes
Other Veg
Phragmites
Other (Debris, Coverage, Structures)
Wrack

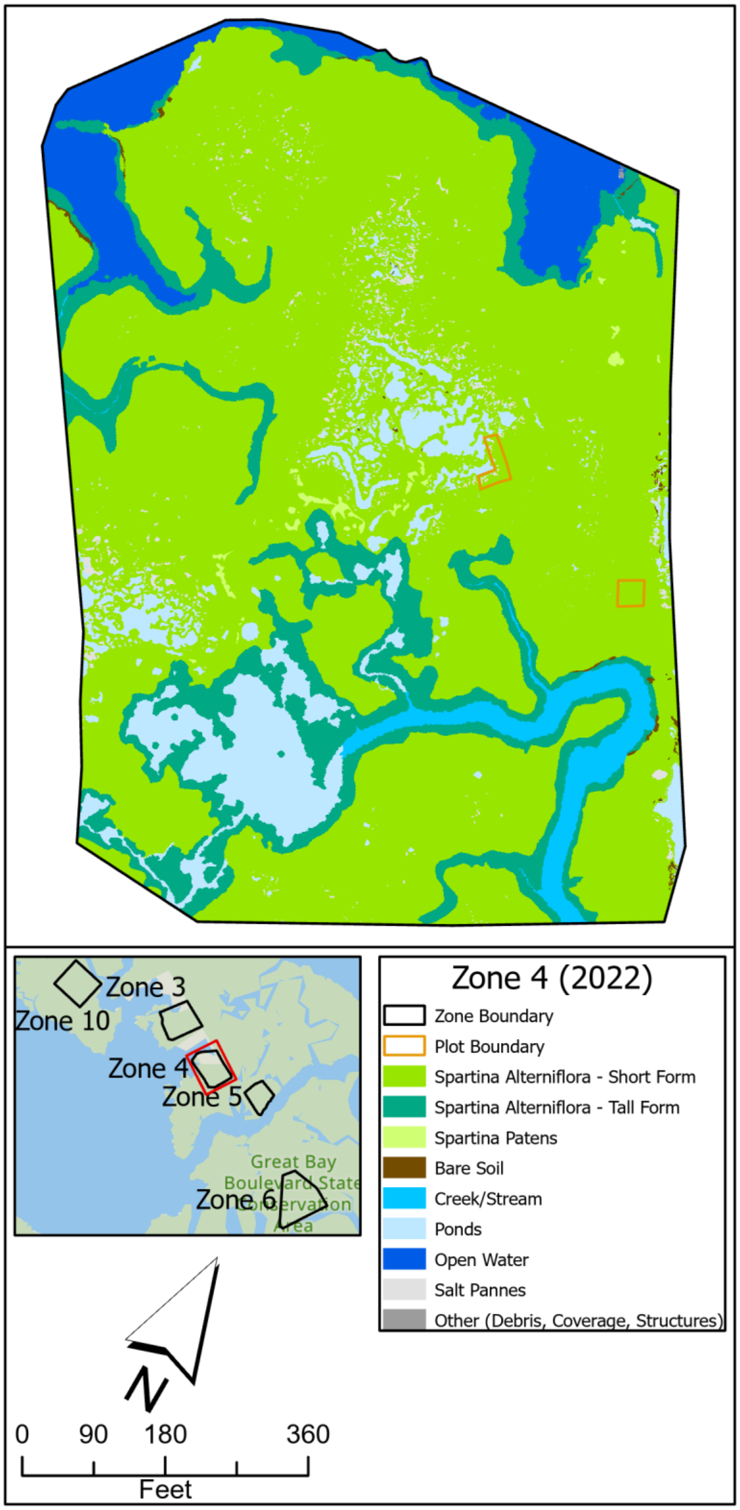
Zone 3
Zone 10
Zone 4
Zone 5
Great Bay Boulevard State Conservation Area
Zone 6
Zone 4 (2022)
Zone Boundary
Plot Boundary
Spartina Alterniflora - Short Form
Spartina Alterniflora - Tall Form
Spartina Patens
Bare Soil
Creek/Stream
Ponds
Open Water
Salt Pannes
Other (Debris, Coverage, Structures)
N
0
90
180
360
Feet

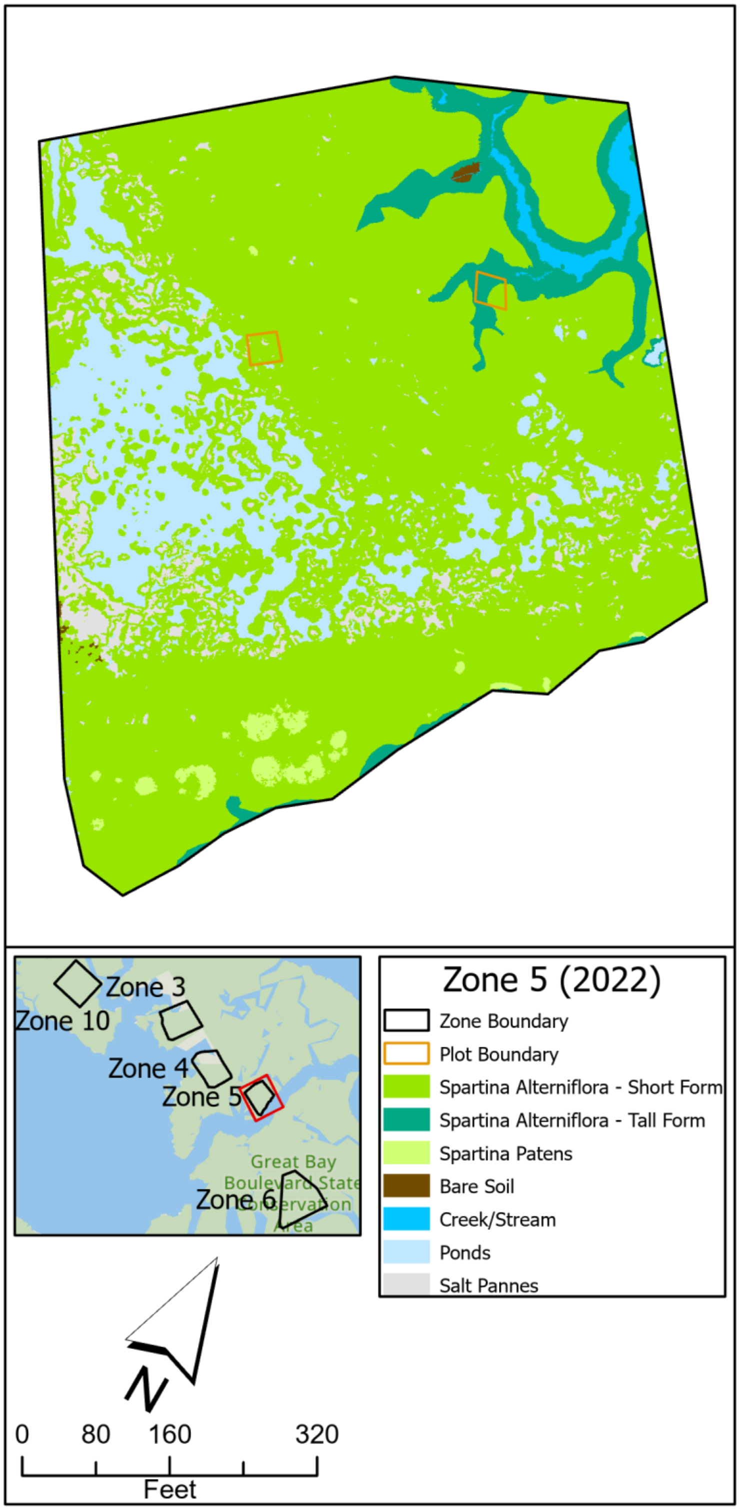
Zone 3
Zone 10
Zone 4
Zone 5
Great Bay Boulevard State Conservation Area
Zone 6
Zone 5 (2022)
Zone Boundary
Plot Boundary
Spartina Alterniflora - Short Form
Spartina Alterniflora - Tall Form
Spartina Patens
Bare Soil
Creek/Stream
Ponds
Salt Pannes
N
0
80
160
320
Feet

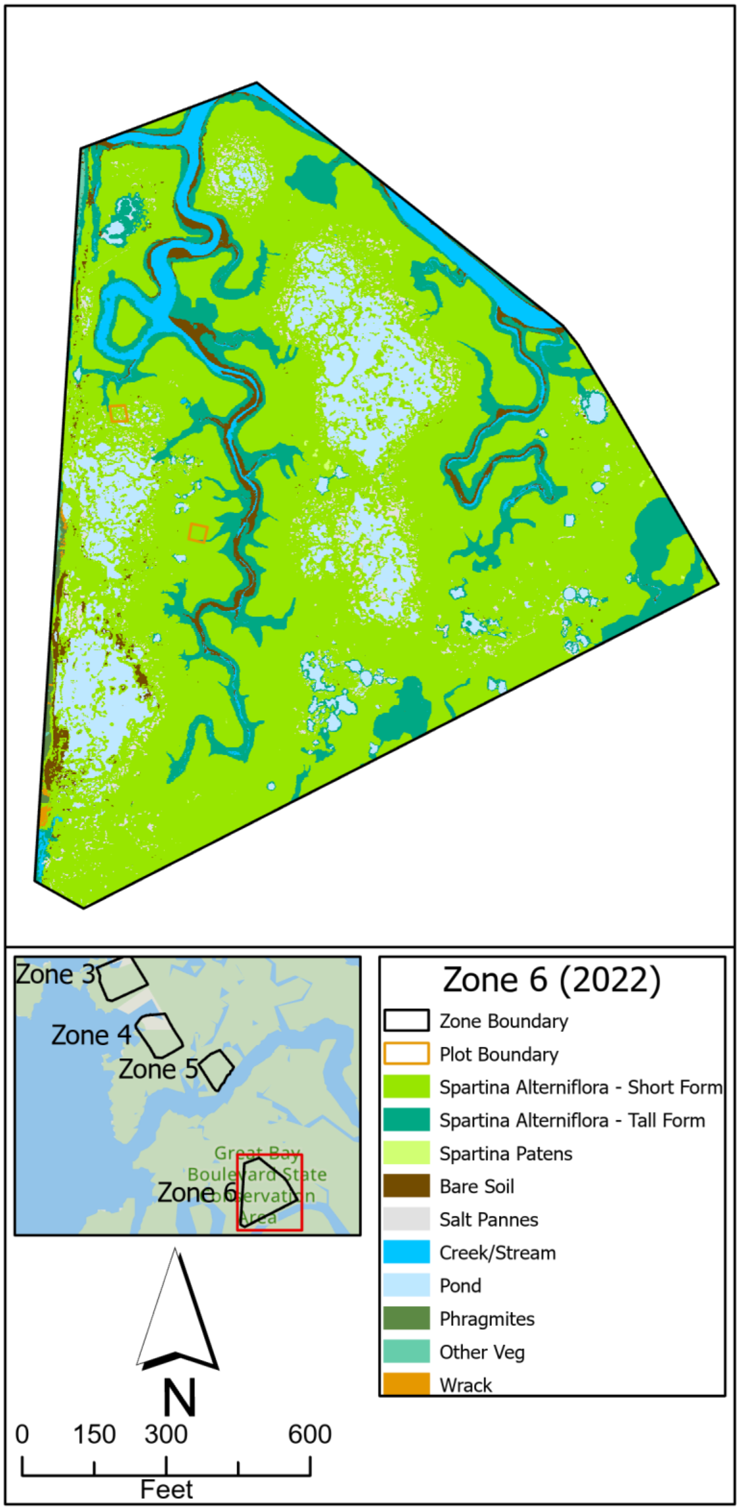
Zone 3
Zone 4
Zone 5
Zone 6
Great Bay Boulevard State Conservation Area
Zone 6 (2022)
Zone Boundary
Plot Boundary
Spartina Alterniflora - Short Form
Spartina Alterniflora - Tall Form
Spartina Patens
Bare Soil
Salt Pannes
Creek/Stream
Pond
Phragmites
Other Veg
Wrack
N
0
150
300
600
Feet

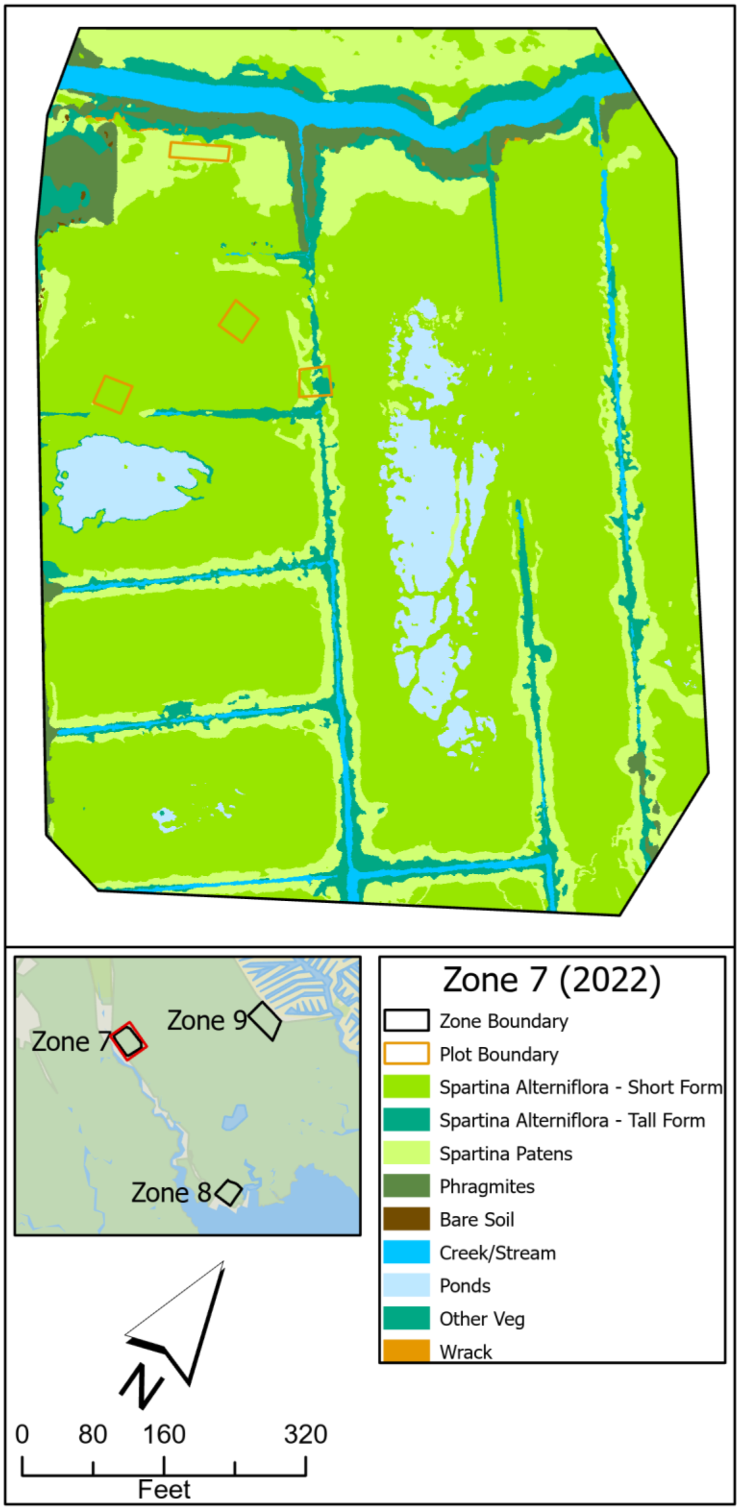
Zone 7
Zone 9
Zone 8
Zone 7 (2022)
Zone Boundary
Plot Boundary
Spartina Alterniflora - Short Form
Spartina Alterniflora - Tall Form
Spartina Patens
Phragmites
Bare Soil
Creek/Stream
Ponds
Other Veg
Wrack
N
0
80
160
320
Feet

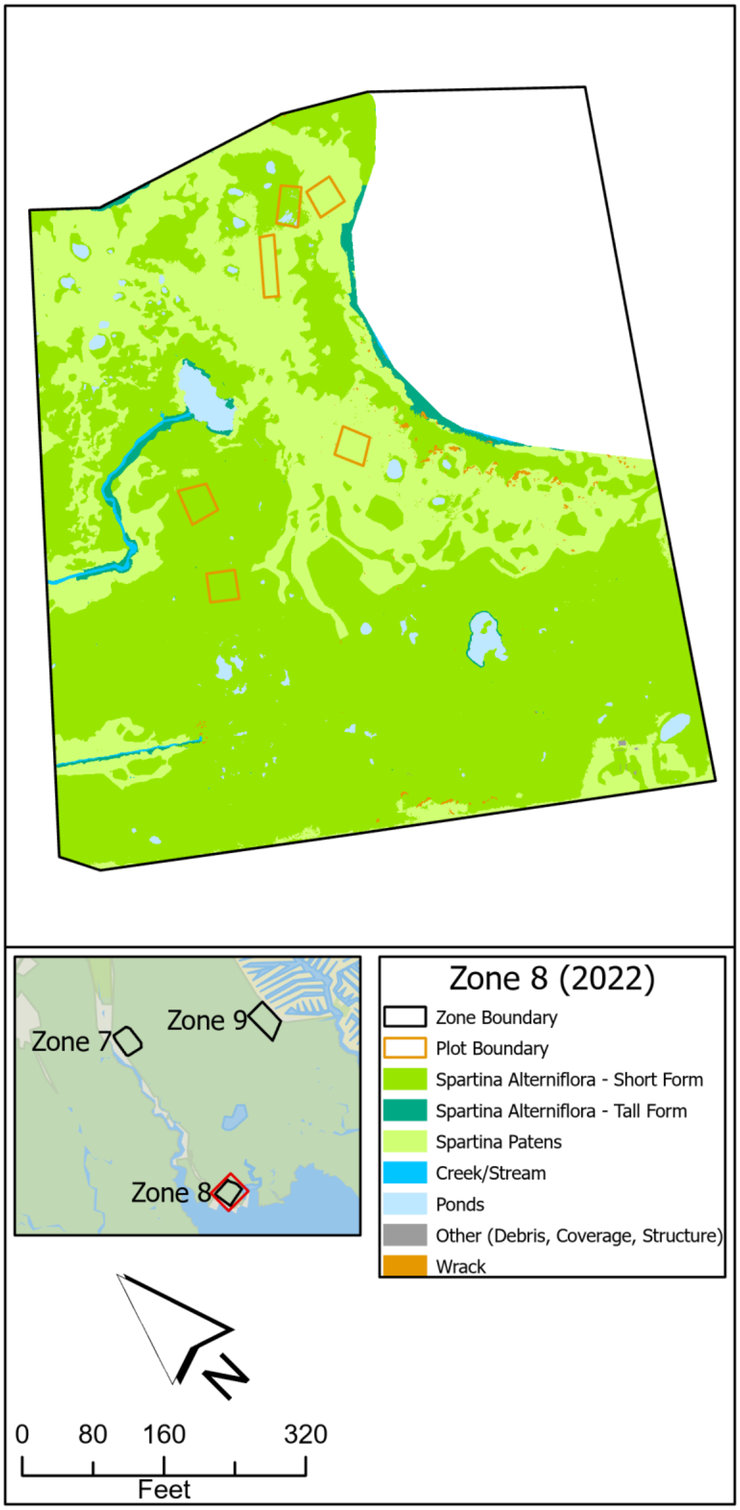
Zone 7
Zone 9
Zone 8
Zone 8 (2022)
Zone Boundary
Plot Boundary
Spartina Alterniflora - Short Form
Spartina Alterniflora - Tall Form
Spartina Patens
Creek/Stream
Ponds
Other (Debris, Coverage, Structure)
Wrack
N
0
80
160
320
Feet

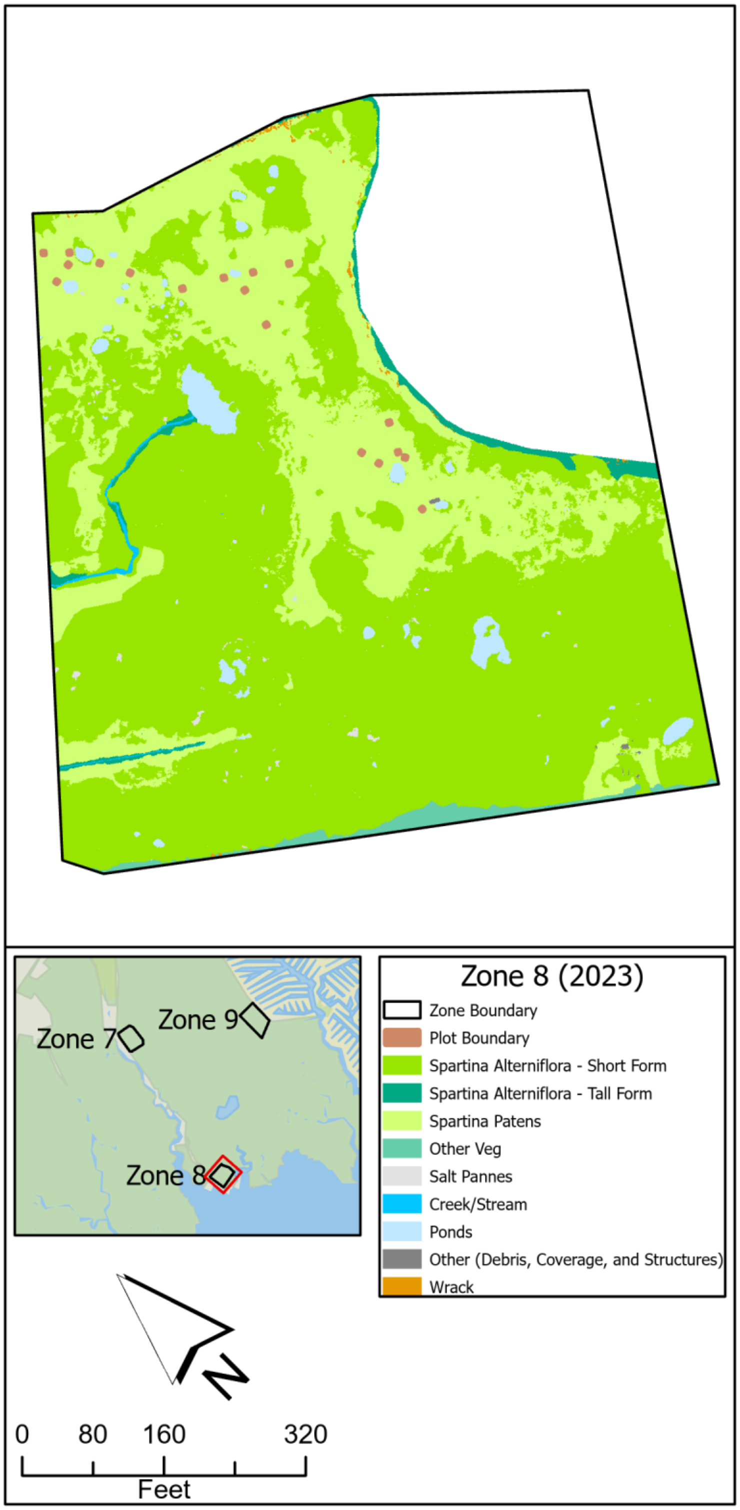
Zone 7
Zone 9
Zone 8
Zone 8 (2023)
Zone Boundary
Plot Boundary
Spartina Alterniflora - Short Form
Spartina Alterniflora - Tall Form
Spartina Patens
Other Veg
Salt Pannes
Creek/Stream
Ponds
Other (Debris, Coverage, and Structures)
Wrack
N
0
80
160
320
Feet

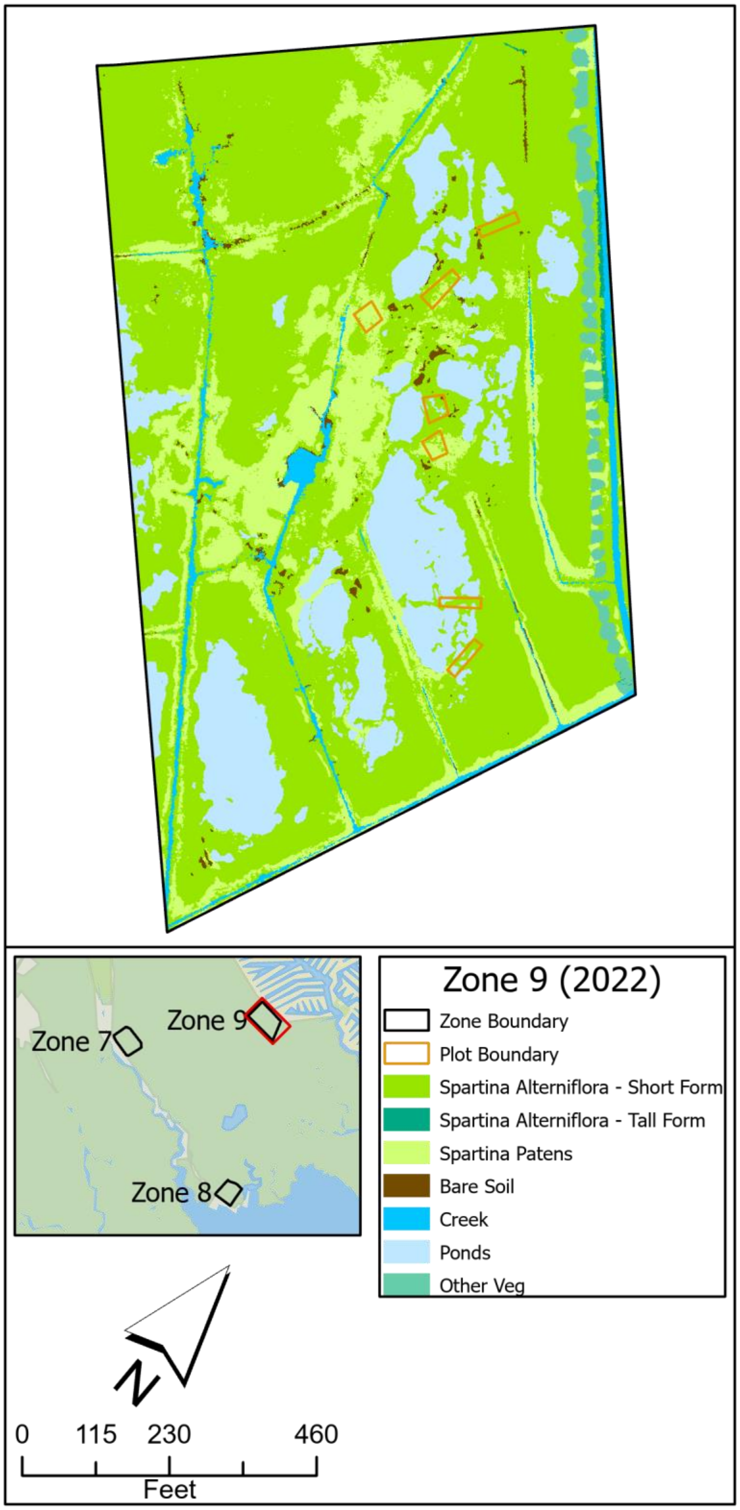
Zone 7
Zone 9
Zone 8
Zone 9 (2022)
Zone Boundary
Plot Boundary
Spartina Alterniflora - Short Form
Spartina Alterniflora - Tall Form
Spartina Patens
Bare Soil
Creek
Ponds
Other Veg
N
0
115
230
460
Feet

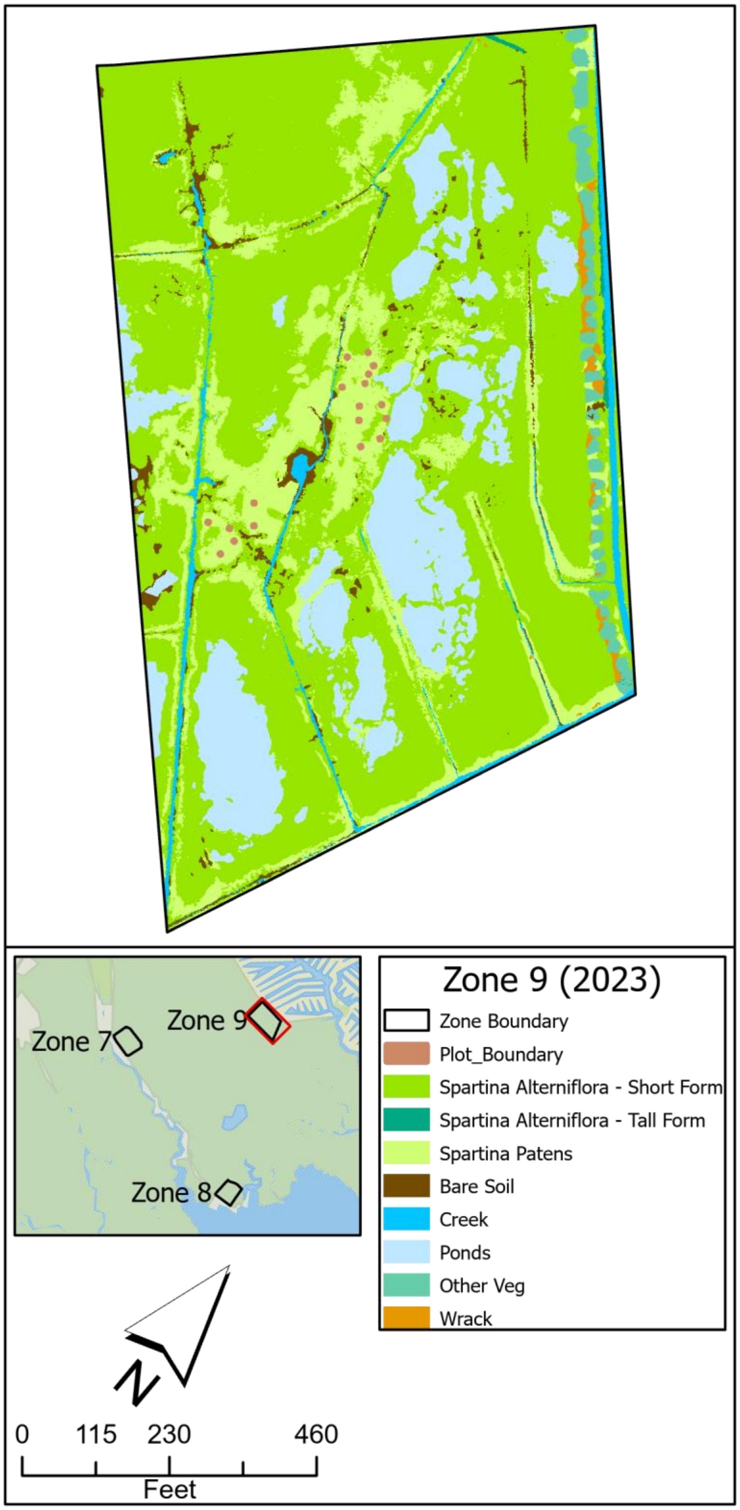
Zone 7
Zone 9
Zone 8
Zone 9 (2023)
Zone Boundary
Plot_Boundary
Spartina Alterniflora - Short Form
Spartina Alterniflora - Tall Form
Spartina Patens
Bare Soil
Creek
Ponds
Other Veg
Wrack
N
0
115
230
460
Feet

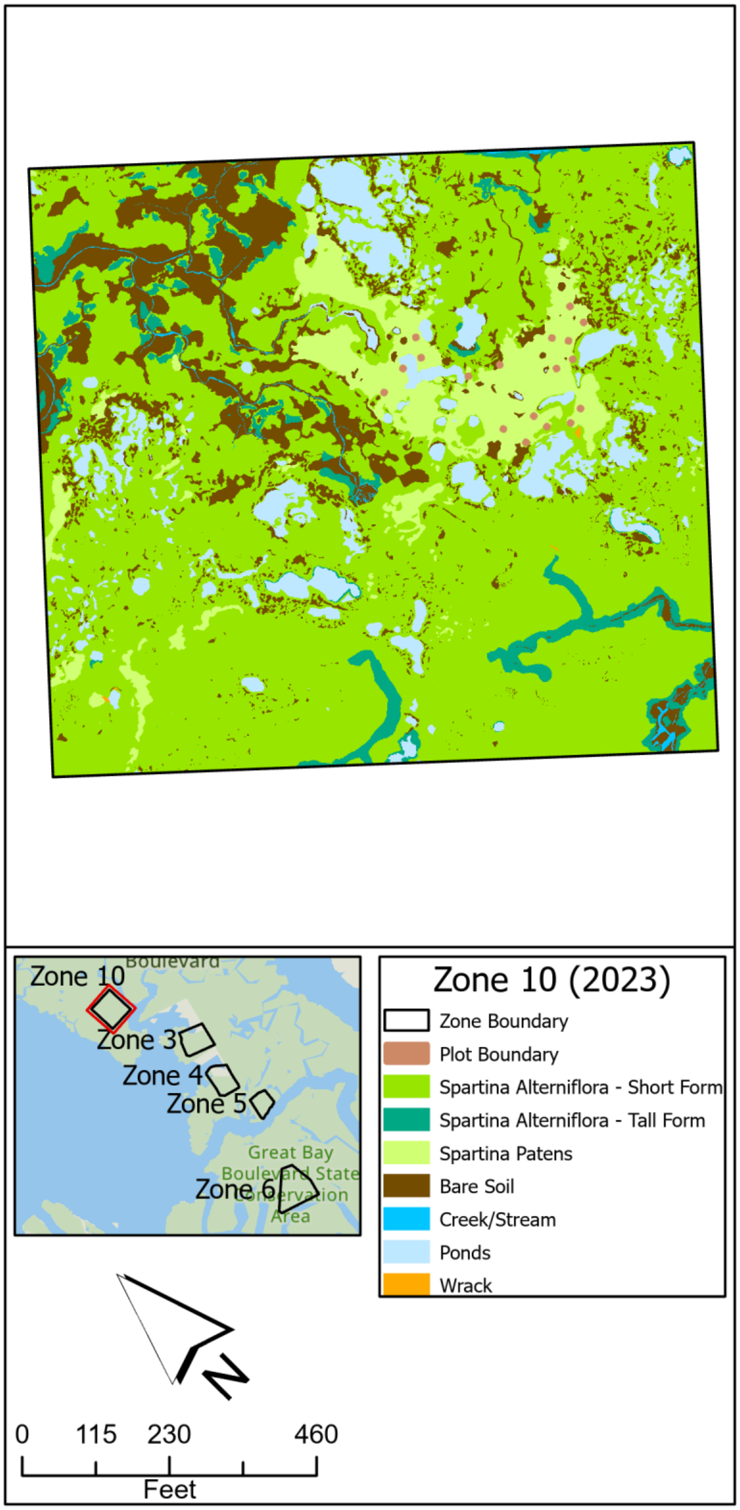
Zone 10 (2023)
Zone Boundary
Plot Boundary
Spartina Alterniflora - Short Form
Spartina Alterniflora - Tall Form
Spartina Patens
Bare Soil
Creek/Stream
Ponds
Wrack
Zone 10
Boulevard
Zone 3
Zone 4
Zone 5
Zone 6
Great Bay Boulevard State Conservation Area
N
0
115
230
460
Feet

Appendix C: Evaluating the use of multispectral drones for delineation of low and high marsh communities: Error Matrices

Zone 1

Zone 1 Error Matrix (2022)

Class Name	***S. alterniflora short form***	***S. alterniflora tall form***	***S. patens***	***Phragmites***	**Other Veg**	**Bare Soil**	**Creek/ Stream**	**Ponds**	**Total Checkpoints**	**User's Accuracy**	**Kappa**
S. alterniflora – short form	297	1	4	0	0	0	0	0	302	98.34%	0
S. alterniflora – tall form	0	10	0	0	0	0	0	0	10	100.00%	0
S. patens	0	0	50	0	0	1	0	0	51	98.04%	0
Phragmites	0	0	0	10	0	0	0	0	10	100.00%	0
Other Veg	2	0	1	0	7	0	0	0	10	70.00%	0
Bare Soil	2	0	0	0	0	8	0	0	10	80.00%	0
Creek/Stream	1	0	0	0	0	0	16	0	17	94.12%	0
Ponds	0	0	0	0	0	0	0	10	10	100.00%	0
Total Checkpoints	302	11	55	10	7	9	16	10	420	0	0
Producer's Accuracy	98.34%	90.91%	90.91%	100.00%	100.00%	88.89%	100.00%	100.00%	0	97.14%	0
Kappa	0	0	0	0	0	0	0	0	0	0	0.938

Zone 1 Error Matrix (2023)												
Class Name	***S. alterniflora* short form**	***S. alterniflora* tall form**	***S. patens***	***Phragmites***	**Other Veg**	**Bare Soil**	**Creek/ Stream**	**Ponds**	**Wrack**	**Total Checkpoints**	**User's Accuracy**	**Kappa**
S. alterniflora – short form	331	1	1	0	0	2	1	0	1	337	98.22%	0
S. alterniflora – tall form	0	11	0	0	0	0	0	0	0	11	100.00%	0
S. patens	0	0	57	0	0	0	0	0	0	57	100.00%	0
Phragmites	0	0	0	10	0	0	0	0	0	10	100.00%	0
Other Veg	1	0	1	0	8	0	0	0	0	10	80.00%	0
Bare Soil	1	0	0	0	0	9	0	0	0	10	90.00%	0
Creek/Stream	0	0	0	0	0	0	22	0	0	22	100.00%	0
Ponds	0	0	0	0	0	0	0	10	0	10	100.00%	0
Wrack	0	0	0	0	0	0	0	0	10	10	100.00%	0
Total Checkpoints	333	12	59	10	8	11	23	10	11	477	0	0
Producer's Accuracy	99.40%	91.67%	96.61%	100.00%	100.00%	81.82%	95.65%	100.00%	90.91%	0	98.11%	0
Kappa	0	0	0	0	0	0	0	0	0	0	0	0.961

Zone 2

Zone 2 Error Matrix (2022)

Class Name	*S. alterniflora short form*	*S. alterniflora tall form*	*S. patens*	Other Veg	Bare Soil	Creek/ Stream	Ponds	Other (Debris, Coverage, Structures)	Total Checkpoints	User's Accuracy	Kappa
S. alterniflora* – *short form	201	0	4	0	1	0	0	0	206	97.57%	0
S. alterniflora* – *tall form	1	40	0	0	0	0	0	0	41	97.56%	0
S. patens	2	0	139	0	0	0	0	0	141	98.58%	0
Other Veg	0	0	0	10	0	0	0	0	10	100.00%	0
Bare Soil	3	0	0	0	7	0	0	0	10	70.00%	0
Creek/Stream	0	1	0	0	0	9	0	0	10	90.00%	0
Ponds	0	1	0	0	0	0	9	0	10	90.00%	0
Other (Debris, Coverage, Structures)	0	0	1	0	0	0	0	9	10	90.00%	0
Total Checkpoints	207	42	144	10	8	9	9	9	438	0	0
Producer's Accuracy	97.10%	95.24%	96.53%	100.00%	87.50%	100.00%	100.00%	100.00%	0	96.80%	0
Kappa	0	0	0	0	0	0	0	0	0	0	0.952

Zone 3

Zone 3 Error Matrix (2022)

Class Name	***S. alterniflora short form***	***S. alterniflora tall form***	***S. patens***	***Phragmites***	**Other Veg**	**Bare Soil**	**Salt Pannes**	**Creek/ Stream**	**Ponds**	**Open Water**	**Wrack**	**Total Checkpoints**	**User's Accuracy**	**Kappa**
S. alterniflora - short form	373	4	1	0	0	2	4	0	0	0	1	385	96.88%	0
S. alterniflora - tall form	1	64	0	0	0	0	0	0	0	0	0	65	98.46%	0
S. patens	0	0	10	0	0	0	0	0	0	0	0	10	100.00%	0
Phragmites	0	0	0	10	0	0	0	0	0	0	0	10	100.00%	0
Other Veg	0	0	0	0	7	0	0	0	0	0	3	10	70.00%	0
Bare Soil	0	0	0	0	0	52	0	0	0	0	0	52	100.00%	0
Salt Pannes	0	0	0	0	0	0	16	0	0	0	0	16	100.00%	0
Creek/Stream	0	1	0	0	0	1	0	8	0	0	0	10	80.00%	0
Ponds	3	0	0	0	0	0	0	0	59	0	0	62	95.16%	0
Open Water	0	0	0	0	0	0	0	0	0	10	0	10	100.00%	0
Wrack	0	0	0	3	0	0	0	0	0	0	7	10	70.00%	0
Total Checkpoints	377	69	11	13	7	55	20	8	59	10	11	640	0	0
Producer's Accuracy	98.94%	92.75%	90.91%	76.92%	100.00%	94.55%	80.00%	100.00%	100.00%	100.00%	63.64%	0	96.25%	0
Kappa	0	0	0	0	0	0	0	0	0	0	0	0	0	0.939

Zone 4

Zone 4 Error Matrix (2022)

Class Name	*S. alterniflora short form*	*S. alterniflora tall form*	*S. patens*	Bare Soil	Salt Pannes	Creek/ Stream	Ponds	Open Water	Other (Debris, Coverage, Structures)	Total Checkpoints	User's Accuracy	Kappa
S. alterniflora – short form	307	1	0	1	0	0	0	0	0	309	99.35%	0
S. alterniflora – tall form	1	59	0	0	0	0	0	0	0	60	98.33%	0
S. patens	0	0	10	0	0	0	0	0	0	10	100.00%	0
Bare Soil	1	0	0	8	0	0	1	0	0	10	80.00%	0
Salt Pannes	2	0	0	0	8	0	0	0	0	10	80.00%	0
Creek/Stream	0	0	0	0	0	12	0	0	0	12	100.00%	0
Ponds	0	0	0	0	0	0	36	0	0	36	100.00%	0
Open Water	0	0	0	0	0	0	0	26	0	26	100.00%	0
Other (Debris, Coverage, Structures)	0	0	0	0	0	0	0	0	10	10	100.00%	0
Total Checkpoints	311	60	10	9	8	12	37	26	10	483	0	0
Producer's Accuracy	98.71%	98.33%	100.00%	88.89%	100.00%	100.00%	97.30%	100.00%	100.00%	0	98.55%	0
Kappa	0	0	0	0	0	0	0	0	0	0	0	0.974

Zone 5

Zone 5 Error Matrix (2022)										
Class Name	***S. alterniflora* short form**	***S. alterniflora* tall form**	***S. patens***	**Bare Soil**	**Salt Pannes**	**Creek/ Stream**	**Ponds**	**Total Checkpoints**	**User's Accuracy**	**Kappa**
***S. alterniflora* – short form**	255	1	0	1	1	0	0	258	98.84%	0
***S. alterniflora* – tall form**	0	19	0	0	0	0	0	19	100.00%	0
S. patens	0	0	10	0	0	0	0	10	100.00%	0
Bare Soil	0	0	0	10	0	0	0	10	100.00%	0
Salt Pannes	0	0	0	0	15	0	0	15	100.00%	0
Creek/Stream	0	2	0	0	0	8	0	10	80.00%	0
Ponds	0	0	0	0	0	0	50	50	100.00%	0
Total Checkpoints	255	22	10	11	16	8	50	372	0	0
Producer's Accuracy	100.00%	86.36%	100.00%	90.91%	93.75%	100.00%	100.00%	0	98.66%	0
Kappa	0	0	0	0	0	0	0	0	0	0.973

Zone 6

Zone 6 Error Matrix (2022)

Class Name	***S. alterniflora short form***	***S. alterniflora tall form***	***S. patens***	***Phragmites***	**Other Veg**	**Bare Soil**	**Salt Pannes**	**Creek/Stream**	**Ponds**	**Wrack**	**Total Checkpoints**	**User's Accuracy**	**Kappa**
S. alterniflora - short form	319	4	0	0	0	1	0	0	4	1	329	96.96%	0
S. alterniflora - tall form	5	64	0	0	0	0	0	0	0	0	69	92.75%	0
S. patens	1	1	7	0	0	1	0	0	0	0	10	70.00%	0
Phragmites	0	1	0	9	0	0	0	0	0	0	10	90.00%	0
Bare Soil	0	0	0	0	0	12	0	1	1	0	14	85.71%	0
Salt Pannes	1	0	0	0	0	3	6	0	0	0	10	60.00%	0
Creek/Stream	0	0	0	0	0	0	0	19	0	0	19	100.00%	0
Ponds	1	0	0	0	0	0	0	0	55	0	56	98.21%	0
Other Veg	0	0	0	1	9	0	0	0	0	0	10	90.00%	0
Wrack	0	0	0	2	0	0	0	0	0	8	10	80.00%	0
Total Checkpoints	327	70	7	12	9	17	6	20	60	9	537	0	0
Producer's Accuracy	97.55%	91.43%	100.00%	75.00%	100.00%	70.59%	100.00%	95.00%	91.67%	88.89%	0	94.60%	0
Kappa	0	0	0	0	0	0	0	0	0	0	0	0	0.909

Zone 7

Zone 7 Error Matrix (2022)												
Class Name	***S. alterniflora short form***	***S. alterniflora tall form***	***S. patens***	***Phragmites***	**Other Veg**	**Bare Soil**	**Creek/ Stream**	**Ponds**	**Wrack**	**Total Checkpoints**	**User's Accuracy**	**Kappa**
S. alterniflora – short form	284	0	2	0	0	0	0	0	0	286	99.30%	0
S. alterniflora – tall form	2	20	1	0	3	0	0	0	0	26	76.92%	0
S. patens	4	1	67	0	0	0	1	0	0	73	91.78%	0
Phragmites	0	0	1	11	2	1	0	0	0	15	73.33%	0
Other Veg	0	0	0	1	9	0	0	0	0	10	90.00%	0
Bare Soil	0	0	1	0	0	9	0	0	0	10	90.00%	0
Creek/Stream	0	3	0	0	0	0	16	0	0	19	84.21%	0
Ponds	0	1	0	0	0	0	0	26	0	27	96.30%	0
Wrack	0	0	0	0	0	0	0	0	10	10	100.00%	0
Total Checkpoints	290	25	72	12	14	10	17	26	10	476	0	0
Producer's Accuracy	97.93%	80.00%	93.06%	91.67%	64.29%	90.00%	94.12%	100.00%	100.00%	0	94.96%	0
Kappa	0	0	0	0	0	0	0	0	0	0	0	0.916

Zone 8

Zone 8 Error Matrix (2022)

Class Name	*S. alterniflora short form*	*S. alterniflora tall form*	*S. patens*	Creek/ Stream	Ponds	Wrack	Other (Debris, Coverage, Structures)	Total Checkpoints	User's Accuracy	Kappa
S. alterniflora – short form	185	0	8	0	0	0	0	193	95.85%	0
S. alterniflora – tall form	0	10	0	0	0	0	0	10	100.00%	0
S. patens	4	0	118	0	0	0	0	122	96.72%	0
Creek/Stream	0	0	0	21	0	0	0	21	100.00%	0
Ponds	0	0	0	0	10	0	0	10	100.00%	0
Wrack	0	0	0	0	0	10	0	10	100.00%	0
Other (Debris, Coverage, Structures)	1	0	2	0	1	0	6	10	60.00%	0
Total Checkpoints	190	10	128	21	11	10	6	376	0	0
Producer's Accuracy	97.37%	100.00%	92.19%	100.00%	90.91%	100.00%	100.00%	0	95.74%	0
Kappa	0	0	0	0	0	0	0	0	0	0.932

Zone 8 Error Matrix (2023)													
Class Name	***S. alterniflora short form***	***S. alterniflora tall form***	***S. patens***	**Other Veg**	**Bare Soil**	**Salt Pannes**	**Creek/ Stream**	**Ponds**	**Wrack**	**Other (Debris, Coverage, Structures)**	**Total Checkpoints**	**User's Accuracy**	**Kappa**
S. alterniflora – short form	237	0	5	0	1	1	0	0	0	0	244	97.13%	0
S. alterniflora – tall form	0	10	0	0	0	0	0	0	0	0	10	100.00%	0
S. patens	8	1	148	0	0	0	0	0	0	0	157	94.27%	0
Other Veg	0	0	0	10	0	0	0	0	0	0	10	100.00%	0
Bare Soil	0	0	0	0	0	0	0	0	0	0	0	0.00%	0
Salt Pannes	0	0	0	0	0	9	0	0	0	1	10	90.00%	0
Creek/Stream	0	0	0	0	1	0	26	0	0	0	27	96.30%	0
Ponds	0	0	0	0	0	0	0	10	0	0	10	100.00%	0
Wrack	0	0	0	0	0	0	0	0	10	0	10	100.00%	0
Other (Debris, Coverage, Structures)	0	0	0	0	0	0	0	0	0	10	10	100.00%	0
Total Checkpoints	245	11	153	10	2	10	26	10	10	11	488	0	0
Producer's Accuracy	96.73%	90.91%	96.73%	100.00%	0.00%	90.00%	100.00%	100.00%	100.00%	90.91%	0	96.31%	0
Kappa	0	0	0	0	0	0	0	0	0	0	0	0	0.943

Zone 9

Zone 9 Error Matrix (2022)										
Class Name	***S. alterniflora* short form**	***S. alterniflora* tall form**	***S. patens***	**Other Veg**	**Bare Soil**	**Creek/ Stream**	**Ponds**	**Total Checkpoints**	**User's Accuracy**	**Kappa**
***S. alterniflora* – short form**	213	0	6	0	0	0	1	220	96.82%	0
***S. alterniflora* – tall form**	2	8	0	0	0	0	0	10	80.00%	0
S. patens	0	1	54	0	0	0	0	55	98.18%	0
Other Veg	1	0	0	9	0	0	0	10	90.00%	0
Bare Soil	0	0	0	0	10	0	0	10	100.00%	0
Creek/Stream	0	0	0	0	0	12	0	12	100.00%	0
Ponds	0	0	0	0	0	1	52	53	98.11%	0
Total Checkpoints	216	9	60	9	10	13	53	370	0	0
Producer's Accuracy	98.61%	88.89%	90.00%	100.00%	100.00%	92.31%	98.11%	0	96.76%	0
Kappa	0	0	0	0	0	0	0	0	0	0.946

Zone 9 Error Matrix (2023)

Class Name	*S. alterniflora short form*	*S. alterniflora fall form*	*S. patens*	Other Veg	Bare Soil	Creek/ Stream	Ponds	Wrack	Total Checkpoints	User's Accuracy	Kappa
S. alterniflora* – *short form	245	0	6	0	0	0	1	0	252	97.22%	0
S. alterniflora* – *tall form	2	7	0	1	0	0	0	0	10	70.00%	0
S. patens	2	1	58	0	0	0	0	0	61	95.08%	0
Other Veg	0	0	0	9	0	0	0	1	10	90.00%	0
Bare Soil	1	0	0	0	9	0	0	0	10	90.00%	0
Creek/Stream	1	0	0	0	0	10	0	0	11	90.91%	0
Ponds	0	0	0	0	0	0	59	0	59	100.00%	0
Wrack	1	0	0	0	0	0	0	9	10	90.00%	0
Total Checkpoints	252	8	64	10	9	10	60	10	423	0	0
Producer's Accuracy	97.22%	87.50%	90.63%	90.00%	100.00%	100.00%	98.33%	90.00%	0	95.98%	0
Kappa	0	0	0	0	0	0	0	0	0	0	0.933

Zone 10

Zone 10 Error Matrix (2023)

Class Name	*S. alterniflora short form*	*S. alterniflora tall form*	*S. patens*	Bare Soil	Creek/ Stream	Ponds	Wrack	Total Checkpoints	User's Accuracy	Kappa
S. alterniflora – short form	225	0	2	8	0	0	0	235	95.74%	0
S. alterniflora – tall form	2	11	0	1	0	0	0	14	78.57%	0
S. patens	1	0	26	0	0	0	0	27	96.30%	0
Bare Soil	3	1	0	40	0	0	0	44	90.91%	0
Creek/Stream	0	0	0	1	9	0	0	10	90.00%	0
Ponds	0	0	0	0	0	29	0	29	100.00%	0
Wrack	0	0	0	1	0	0	9	10	90.00%	0
Total Checkpoints	231	12	28	51	9	29	9	369	0	0
Producer's Accuracy	97.40%	91.67%	92.86%	78.43%	100.00%	100.00%	100.00%	0	94.58%	0
Kappa	0	0	0	0	0	0	0	0	0	0.905

Appendix D: Evaluating the use of multispectral drones for delineation of low and high marsh communities: Plot Summary Results

Forsythe National Wildlife Refuge

2022 Data

Plot Summary Statistics - 2022
Forsythe National Wildlife Refuge
Normalized Difference Vegetation Index (NDVI)

Zone	Plot	Mean	Median	Standard Deviation	Minimum	Maximum	Range
2	5	0.087	0.103	0.121	-0.396	0.418	0.814
2	6	0.152	0.165	0.117	-0.334	0.494	0.828
2	7	0.319	0.322	0.097	-0.012	0.562	0.574
7	8	0.111	0.113	0.054	-0.145	0.313	0.458
7	9	-0.042	-0.040	0.065	-0.327	0.220	0.547
7	10	0.136	0.152	0.103	-0.266	0.402	0.668
7	11	0.077	0.075	0.093	-0.351	0.502	0.853
8	2	0.042	0.038	0.098	-0.310	0.464	0.774
8	3	0.029	0.031	0.100	-0.377	0.396	0.773
8	4	-0.028	-0.030	0.098	-0.402	0.355	0.757
8	5	-0.033	-0.022	0.093	-0.408	0.287	0.694
8	6	-0.005	-0.002	0.059	-0.274	0.191	0.465
8	7	0.076	0.077	0.047	-0.289	0.261	0.550
9	12	0.084	0.091	0.097	-0.515	0.399	0.913
9	13	-0.006	-0.005	0.102	-0.525	0.387	0.911
9	14	0.017	0.016	0.097	-0.284	0.370	0.654
9	15	-0.074	-0.010	0.199	-0.623	0.347	0.970
9	16	0.004	-0.003	0.089	-0.303	0.344	0.647
9	17	-0.185	-0.091	0.227	-0.647	0.230	0.877
9	18	-0.167	-0.093	0.205	-0.587	0.212	0.799

Plot Summary Statistics - 2022
Forsythe National Wildlife Refuge
Green Normalized Difference Index (GNDVI)

Zone	Plot	Mean	Median	Standard Deviation	Minimum	Maximum	Range
2	5	0.013	0.013	0.067	-0.253	0.292	0.545
2	6	0.012	0.007	0.068	-0.265	0.285	0.550
2	7	0.267	0.268	0.072	-0.045	0.476	0.520
7	8	0.086	0.088	0.033	-0.089	0.226	0.315
7	9	0.012	0.013	0.041	-0.201	0.193	0.394
7	10	0.016	0.017	0.064	-0.224	0.269	0.492
7	11	0.045	0.047	0.075	-0.359	0.331	0.690
8	2	-0.010	-0.015	0.060	-0.178	0.287	0.465
8	3	-0.038	-0.045	0.060	-0.239	0.259	0.498
8	4	-0.054	-0.058	0.050	-0.208	0.211	0.420
8	5	0.056	0.060	0.056	-0.249	0.258	0.507
8	6	0.048	0.050	0.039	-0.170	0.183	0.353
8	7	0.098	0.099	0.034	-0.155	0.237	0.392
9	12	0.065	0.071	0.072	-0.502	0.278	0.781
9	13	0.035	0.041	0.074	-0.461	0.249	0.711
9	14	0.012	0.008	0.068	-0.222	0.303	0.525
9	15	0.005	0.080	0.185	-0.537	0.310	0.847
9	16	0.037	0.038	0.056	-0.237	0.240	0.477
9	17	-0.079	0.037	0.237	-0.558	0.266	0.824
9	18	-0.098	0.005	0.216	-0.550	0.257	0.808

Plot Summary Statistics - 2022
Forsythe National Wildlife Refuge
Normalized Difference Red Edge Index (NDRE)

Zone	Plot	Mean	Median	Standard Deviation	Minimum	Maximum	Range
2	5	-0.007	-0.008	0.027	-0.119	0.139	0.258
2	6	-0.011	-0.015	0.030	-0.159	0.192	0.351
2	7	0.030	0.031	0.030	-0.093	0.137	0.230
7	8	0.030	0.029	0.028	-0.115	0.157	0.273
7	9	0.019	0.020	0.025	-0.131	0.140	0.271
7	10	-0.008	-0.010	0.040	-0.167	0.189	0.357
7	11	0.025	0.026	0.045	-0.228	0.200	0.428
8	2	-0.031	-0.034	0.024	-0.107	0.078	0.184
8	3	-0.032	-0.036	0.036	-0.206	0.258	0.464
8	4	-0.035	-0.036	0.045	-0.292	0.247	0.539
8	5	0.017	0.018	0.039	-0.206	0.203	0.409
8	6	0.019	0.019	0.017	-0.076	0.081	0.157
8	7	0.037	0.037	0.022	-0.102	0.138	0.240
9	12	0.031	0.035	0.047	-0.375	0.196	0.571
9	13	0.022	0.028	0.047	-0.323	0.144	0.466
9	14	0.009	0.008	0.036	-0.190	0.170	0.360
9	15	0.014	0.053	0.097	-0.263	0.169	0.432
9	16	0.018	0.017	0.028	-0.124	0.128	0.252
9	17	-0.023	0.024	0.096	-0.271	0.127	0.398
9	18	-0.041	0.008	0.100	-0.277	0.131	0.408

Plot Summary Statistics - 2022
Forsythe National Wildlife Refuge
Non-Photosynthetic Vegetation Index (NPV)

Zone	Plot	Mean	Median	Standard Deviation	Minimum	Maximum	Range
2	5	-0.055	-0.066	0.069	-0.240	0.336	0.576
2	6	-0.147	-0.158	0.076	-0.322	0.314	0.637
2	7	-0.099	-0.100	0.059	-0.294	0.183	0.477
7	8	-0.025	-0.026	0.036	-0.164	0.142	0.306
7	9	0.054	0.054	0.049	-0.148	0.272	0.420
7	10	-0.121	-0.131	0.060	-0.286	0.169	0.456
7	11	-0.032	-0.031	0.068	-0.340	0.312	0.652
8	2	-0.049	-0.057	0.065	-0.237	0.351	0.589
8	3	-0.052	-0.062	0.058	-0.208	0.242	0.450
8	4	-0.031	-0.034	0.059	-0.221	0.260	0.481
8	5	0.194	0.185	0.062	-0.076	0.407	0.484
8	6	0.046	0.045	0.054	-0.201	0.356	0.557
8	7	0.041	0.040	0.038	-0.101	0.313	0.415
9	12	-0.096	-0.098	0.048	-0.310	0.155	0.465
9	13	-0.037	-0.036	0.063	-0.280	0.298	0.578
9	14	-0.038	-0.046	0.062	-0.225	0.221	0.445
9	15	0.107	0.091	0.095	-0.154	0.404	0.558
9	16	0.006	0.000	0.083	-0.233	0.367	0.600
9	17	0.146	0.135	0.068	-0.089	0.390	0.479
9	18	0.097	0.096	0.076	-0.222	0.472	0.694

2023 Data

Plot Summary Statistics - 2023
Forsythe National Wildlife Refuge
Normalized Difference Vegetation Index (NDVI)

Zone	Plot	Plot Name	Mean	Median	Standard Deviation	Minimum	Maximum	Range
8	A	fu11a	0.079	0.082	0.083	-0.124	0.252	0.376
8	B	fu11b	0.006	0.003	0.067	-0.156	0.179	0.335
8	A	fu12a	0.065	0.067	0.064	-0.165	0.227	0.393
8	B	fu12b	0.054	0.047	0.069	-0.092	0.216	0.308
8	A	fu13a	0.125	0.113	0.068	-0.134	0.289	0.423
8	B	fu13b	0.051	0.058	0.094	-0.164	0.268	0.431
8	A	fu21a	0.094	0.091	0.120	-0.165	0.335	0.499
8	B	fu21b	0.087	0.083	0.074	-0.075	0.275	0.350
8	A	fu22a	0.152	0.161	0.104	-0.065	0.348	0.413
8	B	fu22b	0.123	0.120	0.094	-0.092	0.330	0.422
8	A	fu23a	0.116	0.116	0.064	-0.058	0.251	0.310
8	B	fu23b	0.181	0.172	0.069	0.036	0.358	0.321
8	A	fu31a	0.112	0.118	0.077	-0.071	0.284	0.354
8	B	fu31b	0.086	0.091	0.089	-0.132	0.255	0.387
8	A	fu32a	0.153	0.160	0.079	-0.046	0.325	0.371
8	B	fu32b	0.079	0.075	0.080	-0.145	0.326	0.471
8	B	fu33b	0.201	0.209	0.064	-0.056	0.315	0.370
8	A	fu34a	0.192	0.190	0.089	0.010	0.405	0.395
9	A	FD.11A	0.212	0.226	0.135	-0.094	0.464	0.558
9	B	FD.11B	0.176	0.201	0.110	-0.143	0.371	0.515
9	A	FD.12A	0.173	0.176	0.074	-0.031	0.308	0.340
9	B	FD.12B	0.243	0.263	0.080	0.020	0.374	0.354
9	A	FD.13A	0.219	0.220	0.104	-0.035	0.399	0.433
9	B	FD.13B	0.164	0.205	0.138	-0.219	0.367	0.586
9	A	FD.21A	0.069	0.062	0.082	-0.136	0.245	0.382
9	B	FD.21B	0.196	0.194	0.057	0.054	0.340	0.286
9	A	FD.22A	0.198	0.200	0.076	-0.032	0.328	0.359
9	B	FD.22B	0.192	0.213	0.074	-0.004	0.323	0.327

9	A	FD.23A	0.221	0.206	0.088	0.006	0.399	0.393
9	B	FD.23B	0.014	0.015	0.065	-0.110	0.206	0.316
9	A	FD.31A	0.111	0.112	0.073	-0.031	0.259	0.290
9	B	FD.31B	0.103	0.099	0.077	-0.050	0.262	0.312
9	A	FD.32A	0.344	0.353	0.099	0.089	0.516	0.428
9	B	FD.32B	0.076	0.078	0.088	-0.115	0.237	0.352
9	A	FD.33A	0.331	0.345	0.104	-0.006	0.497	0.503
9	B	FD.33B	0.342	0.336	0.093	0.150	0.500	0.351

Plot Summary Statistics - 2023
Forsythe National Wildlife Refuge
Green Normalized Difference Vegetation Index (GNDVI)

Zone	Plot	Plot Name	Mean	Median	Standard Deviation	Minimum	Maximum	Range
8	A	fu11a	0.034	0.034	0.032	-0.055	0.109	0.164
8	B	fu11b	0.002	0.000	0.029	-0.060	0.088	0.148
8	A	fu12a	0.056	0.056	0.030	-0.004	0.135	0.138
8	B	fu12b	0.041	0.035	0.037	-0.032	0.163	0.196
8	A	fu13a	0.104	0.096	0.043	0.016	0.220	0.204
8	B	fu13b	0.059	0.062	0.057	-0.073	0.193	0.265
8	A	fu21a	0.043	0.042	0.063	-0.115	0.251	0.366
8	B	fu21b	0.007	0.002	0.030	-0.107	0.099	0.206
8	A	fu22a	0.061	0.061	0.051	-0.045	0.165	0.210
8	B	fu22b	0.057	0.059	0.043	-0.051	0.158	0.210
8	A	fu23a	0.069	0.069	0.033	-0.012	0.173	0.185
8	B	fu23b	0.065	0.064	0.031	-0.014	0.194	0.208
8	A	fu31a	0.067	0.065	0.046	-0.021	0.233	0.254
8	B	fu31b	0.017	0.013	0.052	-0.106	0.117	0.224
8	A	fu32a	0.092	0.095	0.037	-0.003	0.172	0.175
8	B	fu32b	0.046	0.045	0.050	-0.080	0.155	0.235
8	B	fu33b	0.102	0.100	0.030	-0.006	0.184	0.190
8	A	fu34a	0.093	0.098	0.047	-0.005	0.210	0.214
9	A	FD.11A	0.109	0.093	0.073	-0.037	0.287	0.323
9	B	FD.11B	0.055	0.059	0.057	-0.093	0.173	0.266
9	A	FD.12A	0.049	0.051	0.043	-0.084	0.135	0.219
9	B	FD.12B	0.064	0.076	0.050	-0.062	0.165	0.227
9	A	FD.13A	0.085	0.073	0.069	-0.033	0.256	0.289
9	B	FD.13B	0.041	0.049	0.082	-0.207	0.188	0.395
9	A	FD.21A	0.030	0.021	0.047	-0.072	0.137	0.209
9	B	FD.21B	0.115	0.117	0.038	-0.043	0.227	0.270
9	A	FD.22A	0.065	0.068	0.038	-0.032	0.139	0.171
9	B	FD.22B	0.080	0.085	0.052	-0.095	0.173	0.269
9	A	FD.23A	0.095	0.086	0.055	-0.008	0.214	0.222
9	B	FD.23B	-0.028	-0.027	0.039	-0.126	0.079	0.205
9	A	FD.31A	0.050	0.052	0.043	-0.038	0.148	0.186

9	B	FD.31B	0.028	0.023	0.039	-0.039	0.114	0.154
9	A	FD.32A	0.140	0.135	0.049	0.042	0.269	0.227
9	B	FD.32B	0.007	0.002	0.053	-0.119	0.142	0.261
9	A	FD.33A	0.163	0.162	0.060	-0.093	0.270	0.363
9	B	FD.33B	0.140	0.130	0.066	-0.002	0.266	0.268

Plot Summary Statistics - 2023
Forsythe National Wildlife Refuge
Normalized Difference Red Edge Index (NDRE)

Zone	Plot	Plot Name	Mean	Median	Standard Deviation	Minimum	Maximum	Range
8	A	fu11a	-0.013	-0.013	0.010	-0.047	0.016	0.064
8	B	fu11b	-0.011	-0.012	0.009	-0.030	0.016	0.046
8	A	fu12a	-0.006	-0.005	0.011	-0.077	0.016	0.093
8	B	fu12b	-0.004	-0.005	0.009	-0.023	0.021	0.043
8	A	fu13a	0.001	0.001	0.010	-0.042	0.025	0.067
8	B	fu13b	0.005	0.004	0.015	-0.025	0.040	0.065
8	A	fu21a	0.001	-0.001	0.021	-0.050	0.059	0.109
8	B	fu21b	-0.013	-0.014	0.014	-0.064	0.030	0.095
8	A	fu22a	-0.001	-0.001	0.017	-0.049	0.040	0.090
8	B	fu22b	0.009	0.008	0.013	-0.024	0.042	0.067
8	A	fu23a	0.009	0.009	0.011	-0.021	0.037	0.058
8	B	fu23b	-0.003	-0.002	0.013	-0.048	0.025	0.072
8	A	fu31a	0.025	0.024	0.017	-0.014	0.072	0.086
8	B	fu31b	-0.007	-0.006	0.013	-0.046	0.019	0.066
8	A	fu32a	0.037	0.037	0.012	0.007	0.073	0.066
8	B	fu32b	0.010	0.010	0.012	-0.033	0.044	0.077
8	B	fu33b	0.008	0.009	0.013	-0.031	0.032	0.063
8	A	fu34a	0.011	0.012	0.020	-0.037	0.064	0.101
9	A	FD.11A	0.011	0.002	0.036	-0.077	0.101	0.177
9	B	FD.11B	-0.006	-0.010	0.021	-0.052	0.048	0.100
9	A	FD.12A	-0.004	-0.001	0.017	-0.048	0.032	0.080
9	B	FD.12B	-0.021	-0.021	0.021	-0.068	0.039	0.108
9	A	FD.13A	-0.002	-0.003	0.023	-0.064	0.049	0.112
9	B	FD.13B	-0.001	-0.002	0.029	-0.091	0.069	0.160
9	A	FD.21A	0.006	0.007	0.021	-0.052	0.055	0.107
9	B	FD.21B	0.025	0.026	0.019	-0.053	0.058	0.111
9	A	FD.22A	-0.010	-0.011	0.019	-0.054	0.043	0.097
9	B	FD.22B	0.004	0.007	0.029	-0.087	0.063	0.150
9	A	FD.23A	0.011	0.010	0.026	-0.037	0.059	0.096
9	B	FD.23B	-0.021	-0.021	0.021	-0.081	0.030	0.111
9	A	FD.31A	0.006	0.007	0.016	-0.034	0.048	0.081

9	B	FD.31B	-0.011	-0.012	0.013	-0.039	0.020	0.059
9	A	FD.32A	0.032	0.028	0.025	-0.018	0.099	0.117
9	B	FD.32B	-0.017	-0.017	0.022	-0.067	0.027	0.095
9	A	FD.33A	0.047	0.049	0.025	-0.019	0.106	0.125
9	B	FD.33B	0.018	0.020	0.026	-0.048	0.071	0.119

Plot Summary Statistics - 2023
Forsythe National Wildlife Refuge
Non-Photosynthetic Vegetation Index (NPV)

Zone	Plot	Plot Name	Mean	Median	Standard Deviation	Minimum	Maximum	Range
8	A	fu11a	-0.155	-0.151	0.064	-0.313	-0.033	0.280
8	B	fu11b	-0.109	-0.109	0.035	-0.199	-0.040	0.159
8	A	fu12a	-0.123	-0.124	0.027	-0.179	-0.046	0.133
8	B	fu12b	-0.116	-0.110	0.039	-0.238	-0.048	0.190
8	A	fu13a	-0.177	-0.171	0.049	-0.296	-0.008	0.288
8	B	fu13b	-0.066	-0.056	0.055	-0.245	0.035	0.280
8	A	fu21a	-0.088	-0.081	0.071	-0.239	0.065	0.304
8	B	fu21b	-0.150	-0.152	0.067	-0.328	-0.032	0.296
8	A	fu22a	-0.157	-0.161	0.061	-0.318	-0.017	0.301
8	B	fu22b	-0.118	-0.117	0.059	-0.266	0.006	0.273
8	A	fu23a	-0.118	-0.116	0.028	-0.230	-0.062	0.169
8	B	fu23b	-0.229	-0.235	0.053	-0.338	-0.103	0.235
8	A	fu31a	-0.095	-0.096	0.031	-0.192	-0.018	0.174
8	B	fu31b	-0.134	-0.132	0.058	-0.278	0.002	0.279
8	A	fu32a	-0.097	-0.092	0.035	-0.195	-0.023	0.171
8	B	fu32b	-0.082	-0.084	0.040	-0.272	0.017	0.289
8	B	fu33b	-0.213	-0.210	0.045	-0.316	-0.084	0.233
8	A	fu34a	-0.175	-0.180	0.042	-0.251	-0.079	0.172
9	A	FD.11A	-0.235	-0.244	0.055	-0.351	-0.037	0.314
9	B	FD.11B	-0.220	-0.219	0.051	-0.336	-0.109	0.227
9	A	FD.12A	-0.239	-0.246	0.037	-0.297	-0.113	0.184
9	B	FD.12B	-0.291	-0.292	0.034	-0.355	-0.186	0.169
9	A	FD.13A	-0.280	-0.283	0.059	-0.386	-0.162	0.223
9	B	FD.13B	-0.212	-0.229	0.069	-0.328	-0.025	0.302
9	A	FD.21A	-0.107	-0.107	0.023	-0.167	-0.014	0.152
9	B	FD.21B	-0.157	-0.145	0.035	-0.273	-0.092	0.181
9	A	FD.22A	-0.220	-0.219	0.041	-0.302	-0.134	0.168
9	B	FD.22B	-0.186	-0.188	0.041	-0.265	-0.067	0.198
9	A	FD.23A	-0.187	-0.183	0.043	-0.290	-0.050	0.239
9	B	FD.23B	-0.110	-0.107	0.032	-0.196	-0.037	0.159
9	A	FD.31A	-0.143	-0.139	0.024	-0.211	-0.100	0.111

9	B	FD.31B	-0.154	-0.150	0.039	-0.236	-0.045	0.190
9	A	FD.32A	-0.236	-0.250	0.040	-0.304	-0.116	0.188
9	B	FD.32B	-0.152	-0.153	0.045	-0.268	-0.052	0.216
9	A	FD.33A	-0.185	-0.188	0.051	-0.291	0.072	0.363
9	B	FD.33B	-0.256	-0.259	0.034	-0.329	-0.144	0.185

Great Bay Boulevard

2022 Data

Plot Summary Statistics - 2022
Great Bay Boulevard
Normalized Difference Vegetation Index (NDVI)

Zone	Plot	Mean	Median	Standard Deviation	Minimum	Maximum	Range
1	1	0.041	0.038	0.133	-0.299	0.449	0.747
1	2	0.049	0.054	0.129	-0.352	0.438	0.790
1	3	0.041	0.043	0.110	-0.346	0.358	0.704
1	4	0.035	0.030	0.115	-0.367	0.411	0.778
3	8	0.063	0.057	0.117	-0.270	0.412	0.682
3	9	0.131	0.138	0.112	-0.315	0.497	0.812
4	10	0.168	0.174	0.064	-0.156	0.358	0.514
4	11	0.066	0.109	0.162	-0.447	0.460	0.907
5	12	0.211	0.229	0.101	-0.239	0.504	0.744
5	13	0.120	0.115	0.086	-0.155	0.409	0.564
6	14	0.183	0.219	0.150	-0.282	0.504	0.786
6	15	0.190	0.191	0.049	0.017	0.409	0.392

Plot Summary Statistics - 2022
Great Bay Boulevard
Green Normalized Difference Index (GNDVI)

Zone	Plot	Mean	Median	Standard Deviation	Minimum	Maximum	Range
1	1	-0.021	-0.025	0.068	-0.233	0.249	0.482
1	2	-0.022	-0.024	0.070	-0.261	0.248	0.509
1	3	-0.055	-0.062	0.061	-0.233	0.180	0.413
1	4	-0.055	-0.063	0.063	-0.248	0.213	0.461
3	8	-0.001	-0.003	0.062	-0.184	0.221	0.405
3	9	0.153	0.174	0.104	-0.310	0.410	0.721
4	10	0.102	0.103	0.034	-0.109	0.226	0.335
4	11	0.054	0.100	0.138	-0.450	0.297	0.747
5	12	0.223	0.238	0.087	-0.269	0.422	0.690
5	13	0.084	0.083	0.052	-0.144	0.296	0.440
6	14	0.198	0.243	0.137	-0.298	0.431	0.729
6	15	0.193	0.193	0.036	-0.004	0.336	0.341

Plot Summary Statistics - 2022
Great Bay Boulevard
Normalized Difference Red Edge Index (NDRE)

Zone	Plot	Mean	Median	Standard Deviation	Minimum	Maximum	Range
1	1	-0.039	-0.042	0.025	-0.111	0.086	0.197
1	2	-0.041	-0.043	0.029	-0.140	0.095	0.236
1	3	-0.063	-0.067	0.025	-0.157	0.050	0.207
1	4	-0.067	-0.072	0.024	-0.130	0.044	0.174
3	8	-0.005	-0.007	0.028	-0.086	0.119	0.205
3	9	0.001	0.010	0.046	-0.358	0.181	0.539
4	10	0.016	0.017	0.023	-0.118	0.148	0.266
4	11	-0.003	0.010	0.047	-0.291	0.181	0.473
5	12	0.055	0.062	0.033	-0.159	0.153	0.312
5	13	0.020	0.020	0.023	-0.079	0.119	0.198
6	14	0.025	0.038	0.051	-0.205	0.146	0.351
6	15	0.054	0.053	0.020	-0.052	0.149	0.201

Plot Summary Statistics - 2022 Great Bay Boulevard Non-Photosynthetic Vegetation Index (NPV)							
Zone	Plot	Mean	Median	Standard Deviation	Minimum	Maximum	Range
1	1	-0.105	-0.117	0.066	-0.267	0.194	0.461
1	2	-0.101	-0.113	0.059	-0.230	0.214	0.444
1	3	-0.081	-0.092	0.048	-0.213	0.218	0.432
1	4	-0.080	-0.086	0.043	-0.234	0.210	0.444
3	8	-0.121	-0.128	0.072	-0.296	0.165	0.460
3	9	-0.112	-0.116	0.042	-0.280	0.141	0.421
4	10	-0.183	-0.185	0.045	-0.338	0.214	0.552
4	11	-0.184	-0.211	0.089	-0.382	0.213	0.596
5	12	-0.131	-0.133	0.039	-0.340	0.203	0.543
5	13	-0.069	-0.068	0.054	-0.248	0.184	0.432
6	14	-0.138	-0.151	0.057	-0.325	0.176	0.501
6	15	-0.110	-0.110	0.037	-0.290	0.140	0.430

2023 Data

Plot Summary Statistics - 2023 Great Bay Boulevard Normalized Difference Vegetation Index (NDVI)								
Zone	**Plot**	**Plot Name**	**Mean**	**Median**	**Standard Deviation**	**Minimum**	**Maximum**	**Range**
1	A	GD11A	0.027	0.030	0.082	-0.127	0.233	0.360
1	B	GD11B	0.050	0.073	0.090	-0.180	0.213	0.393
1	A	GD12A	-0.004	-0.014	0.067	-0.134	0.181	0.314
1	B	GD12B	0.142	0.169	0.086	-0.102	0.267	0.369
1	A	GD13A	-0.006	-0.007	0.075	-0.153	0.179	0.332
1	B	GD13B	-0.015	-0.005	0.085	-0.264	0.157	0.420
1	A	GD21A	0.045	0.038	0.061	-0.102	0.223	0.325
1	B	GD21B	0.010	0.039	0.121	-0.266	0.193	0.459
1	A	GD22A	-0.027	-0.031	0.082	-0.180	0.200	0.380
1	B	GD22B	-0.026	-0.035	0.084	-0.243	0.198	0.440
1	A	GD23A	0.058	0.058	0.036	-0.053	0.173	0.226
1	B	GD23B	0.018	0.010	0.085	-0.191	0.243	0.434
1	A	GD31A	0.176	0.193	0.081	-0.039	0.319	0.359
1	B	GD31B	0.114	0.155	0.144	-0.291	0.303	0.594
1	A	GD32A	0.400	0.429	0.107	0.138	0.539	0.401
1	B	GD32B	0.273	0.313	0.138	-0.086	0.473	0.558
1	A	GD33A	0.352	0.367	0.072	0.055	0.473	0.418
1	B	GD33B	0.304	0.322	0.099	0.046	0.449	0.403
10	A	GU11A	0.089	0.086	0.092	-0.147	0.279	0.426
10	B	GU11B	0.089	0.077	0.118	-0.146	0.331	0.477
10	A	GU12A	0.168	0.166	0.056	0.027	0.312	0.285
10	B	GU12B	0.069	0.071	0.071	-0.089	0.205	0.294
10	A	GU13A	0.027	0.023	0.059	-0.092	0.187	0.279
10	B	GU13B	-0.001	-0.014	0.071	-0.123	0.163	0.286
10	A	GU21A	0.122	0.116	0.059	0.004	0.328	0.324
10	B	GU21B	0.184	0.169	0.140	-0.190	0.478	0.668
10	A	GU22A	0.136	0.145	0.071	-0.107	0.282	0.389
10	B	GU22B	0.071	0.074	0.057	-0.105	0.197	0.302

10	A	GU23A	0.121	0.115	0.080	-0.047	0.349	0.396
10	B	GU23B	0.080	0.087	0.120	-0.181	0.373	0.554
10	A	GU31A	0.065	0.055	0.145	-0.193	0.401	0.594
10	B	GU31B	-0.063	-0.085	0.113	-0.270	0.241	0.511
10	A	GU32A	0.033	0.029	0.059	-0.088	0.177	0.265
10	B	GU32B	0.093	0.081	0.108	-0.154	0.361	0.515
10	A	GU33A	0.177	0.169	0.097	-0.031	0.350	0.381
10	B	GU33B	0.033	0.029	0.088	-0.139	0.249	0.388

Plot Summary Statistics - 2023
Great Bay Boulevard
Green Normalized Difference Vegetation Index (GNDVI)

Zone	Plot	Plot Name	Mean	Median	Standard Deviation	Minimum	Maximum	Range
1	A	GD11A	0.012	0.017	0.047	-0.111	0.113	0.224
1	B	GD11B	0.000	0.008	0.048	-0.106	0.099	0.205
1	A	GD12A	0.026	0.024	0.033	-0.058	0.129	0.187
1	B	GD12B	0.051	0.056	0.040	-0.157	0.131	0.287
1	A	GD13A	0.003	0.001	0.044	-0.102	0.105	0.207
1	B	GD13B	-0.007	-0.008	0.045	-0.112	0.083	0.196
1	A	GD21A	0.010	0.006	0.042	-0.101	0.118	0.219
1	B	GD21B	0.016	0.023	0.059	-0.167	0.117	0.284
1	A	GD22A	-0.003	-0.002	0.043	-0.132	0.088	0.220
1	B	GD22B	-0.032	-0.032	0.048	-0.185	0.089	0.274
1	A	GD23A	0.014	0.009	0.029	-0.053	0.106	0.160
1	B	GD23B	-0.024	-0.023	0.059	-0.158	0.143	0.301
1	A	GD31A	0.132	0.141	0.060	-0.019	0.235	0.254
1	B	GD31B	0.090	0.112	0.103	-0.210	0.239	0.449
1	A	GD32A	0.287	0.303	0.079	0.125	0.406	0.281
1	B	GD32B	0.218	0.241	0.114	-0.059	0.390	0.449
1	A	GD33A	0.273	0.278	0.044	0.090	0.352	0.262
1	B	GD33B	0.225	0.229	0.079	0.014	0.367	0.353
10	A	GU11A	0.015	0.011	0.045	-0.084	0.132	0.216
10	B	GU11B	-0.024	-0.033	0.073	-0.157	0.139	0.297
10	A	GU12A	0.010	0.007	0.047	-0.093	0.125	0.218
10	B	GU12B	-0.006	-0.015	0.042	-0.074	0.103	0.178
10	A	GU13A	-0.033	-0.038	0.034	-0.086	0.062	0.148
10	B	GU13B	-0.027	-0.029	0.043	-0.134	0.078	0.211
10	A	GU21A	0.082	0.083	0.047	-0.040	0.195	0.234
10	B	GU21B	0.035	0.020	0.082	-0.147	0.242	0.388
10	A	GU22A	0.051	0.056	0.050	-0.095	0.157	0.252
10	B	GU22B	-0.014	-0.017	0.030	-0.111	0.068	0.179
10	A	GU23A	-0.007	-0.017	0.056	-0.089	0.205	0.294
10	B	GU23B	-0.016	-0.022	0.053	-0.149	0.148	0.297
10	A	GU31A	0.034	0.048	0.087	-0.176	0.234	0.410

10	B	GU31B	-0.088	-0.087	0.044	-0.195	0.038	0.233
10	A	GU32A	-0.008	-0.006	0.039	-0.091	0.073	0.164
10	B	GU32B	-0.060	-0.070	0.048	-0.153	0.083	0.235
10	A	GU33A	0.042	0.027	0.063	-0.061	0.198	0.259
10	B	GU33B	0.005	0.009	0.058	-0.175	0.177	0.353

Plot Summary Statistics - 2023
Great Bay Boulevard
Normalized Difference Red Edge Index (NDRE)

Zone	Plot	Plot Name	Mean	Median	Standard Deviation	Minimum	Maximum	Range
1	A	GD11A	0.001	0.000	0.022	-0.044	0.084	0.128
1	B	GD11B	-0.015	-0.015	0.016	-0.054	0.019	0.073
1	A	GD12A	0.013	0.014	0.017	-0.038	0.057	0.095
1	B	GD12B	-0.005	-0.002	0.020	-0.101	0.035	0.136
1	A	GD13A	-0.014	-0.013	0.023	-0.084	0.037	0.120
1	B	GD13B	-0.005	-0.003	0.031	-0.098	0.066	0.164
1	A	GD21A	-0.013	-0.014	0.019	-0.063	0.029	0.091
1	B	GD21B	-0.003	-0.001	0.026	-0.074	0.061	0.135
1	A	GD22A	-0.008	-0.010	0.028	-0.091	0.065	0.156
1	B	GD22B	-0.019	-0.018	0.023	-0.084	0.039	0.123
1	A	GD23A	-0.014	-0.017	0.016	-0.047	0.035	0.082
1	B	GD23B	-0.018	-0.014	0.032	-0.113	0.066	0.179
1	A	GD31A	-0.005	-0.007	0.027	-0.061	0.055	0.116
1	B	GD31B	-0.010	-0.012	0.037	-0.083	0.064	0.147
1	A	GD32A	0.078	0.079	0.038	0.009	0.152	0.142
1	B	GD32B	0.059	0.057	0.050	-0.041	0.154	0.195
1	A	GD33A	0.076	0.077	0.019	0.017	0.120	0.103
1	B	GD33B	0.062	0.060	0.042	-0.048	0.153	0.201
10	A	GU11A	-0.005	-0.008	0.022	-0.064	0.063	0.128
10	B	GU11B	-0.031	-0.034	0.030	-0.081	0.052	0.132
10	A	GU12A	-0.020	-0.022	0.019	-0.055	0.032	0.087
10	B	GU12B	-0.011	-0.012	0.013	-0.041	0.026	0.067
10	A	GU13A	-0.018	-0.020	0.013	-0.039	0.028	0.067
10	B	GU13B	-0.014	-0.016	0.018	-0.063	0.034	0.097
10	A	GU21A	0.005	0.004	0.030	-0.065	0.075	0.140
10	B	GU21B	-0.009	-0.017	0.039	-0.100	0.118	0.218
10	A	GU22A	-0.010	-0.007	0.019	-0.083	0.029	0.112
10	B	GU22B	-0.023	-0.023	0.010	-0.053	0.000	0.053
10	A	GU23A	-0.021	-0.024	0.019	-0.046	0.052	0.099
10	B	GU23B	-0.028	-0.031	0.019	-0.062	0.045	0.107
10	A	GU31A	0.002	0.002	0.034	-0.094	0.098	0.192

10	B	GU31B	-0.033	-0.033	0.022	-0.095	0.024	0.120
10	A	GU32A	-0.007	-0.007	0.010	-0.031	0.019	0.050
10	B	GU32B	-0.040	-0.043	0.016	-0.073	0.009	0.081
10	A	GU33A	0.007	0.005	0.025	-0.033	0.090	0.123
10	B	GU33B	-0.007	-0.009	0.028	-0.070	0.078	0.148

Plot Summary Statistics - 2023 Great Bay Boulevard Non-Photosynthetic Vegetation Index (NPV)								
Zone	**Plot**	**Plot Name**	**Mean**	**Median**	**Standard Deviation**	**Minimum**	**Maximum**	**Range**
1	A	GD11A	-0.049	-0.058	0.065	-0.192	0.164	0.356
1	B	GD11B	-0.135	-0.137	0.043	-0.209	0.020	0.229
1	A	GD12A	0.013	0.009	0.046	-0.107	0.102	0.209
1	B	GD12B	-0.110	-0.125	0.058	-0.194	0.064	0.258
1	A	GD13A	-0.071	-0.080	0.051	-0.169	0.075	0.243
1	B	GD13B	-0.050	-0.059	0.076	-0.190	0.192	0.382
1	A	GD21A	-0.121	-0.122	0.042	-0.210	0.014	0.224
1	B	GD21B	-0.010	-0.043	0.087	-0.123	0.213	0.336
1	A	GD22A	-0.033	-0.036	0.077	-0.185	0.126	0.311
1	B	GD22B	-0.066	-0.071	0.053	-0.184	0.070	0.254
1	A	GD23A	-0.151	-0.156	0.029	-0.207	-0.054	0.153
1	B	GD23B	-0.111	-0.110	0.050	-0.211	0.016	0.227
1	A	GD31A	-0.056	-0.056	0.026	-0.105	0.037	0.143
1	B	GD31B	-0.027	-0.037	0.038	-0.084	0.101	0.185
1	A	GD32A	-0.136	-0.149	0.043	-0.207	-0.015	0.193
1	B	GD32B	-0.058	-0.050	0.047	-0.157	0.069	0.226
1	A	GD33A	-0.100	-0.101	0.033	-0.168	0.009	0.177
1	B	GD33B	-0.070	-0.075	0.033	-0.130	0.031	0.162
10	A	GU11A	-0.171	-0.165	0.074	-0.335	-0.032	0.303
10	B	GU11B	-0.198	-0.215	0.091	-0.317	0.282	0.599
10	A	GU12A	-0.272	-0.275	0.041	-0.345	-0.148	0.198
10	B	GU12B	-0.139	-0.140	0.057	-0.252	0.055	0.307
10	A	GU13A	-0.198	-0.200	0.043	-0.286	-0.085	0.201
10	B	GU13B	-0.066	-0.064	0.050	-0.171	0.018	0.189
10	A	GU21A	-0.203	-0.202	0.051	-0.341	-0.091	0.250
10	B	GU21B	-0.273	-0.301	0.123	-0.437	0.048	0.485
10	A	GU22A	-0.232	-0.244	0.054	-0.295	0.067	0.362
10	B	GU22B	-0.208	-0.215	0.061	-0.335	0.025	0.360
10	A	GU23A	-0.335	-0.341	0.053	-0.426	-0.145	0.281
10	B	GU23B	-0.190	-0.214	0.075	-0.280	0.173	0.453
10	A	GU31A	-0.234	-0.238	0.062	-0.365	-0.087	0.278

10	B	GU31B	-0.188	-0.163	0.099	-0.351	-0.003	0.348
10	A	GU32A	-0.148	-0.144	0.058	-0.277	-0.030	0.247
10	B	GU32B	-0.247	-0.259	0.052	-0.325	-0.068	0.258
10	A	GU33A	-0.295	-0.312	0.059	-0.377	-0.094	0.283
10	B	GU33B	-0.125	-0.119	0.071	-0.281	0.003	0.284

Appendix E: Evaluating the use of multispectral drones for delineation of low and high marsh communities: Subplot Summary Results

Forsythe National Wildlife Refuge

Subplot Summary Statistics - 2022
Forsythe National Wildlife Refuge
Normalized Difference Vegetation Index (NDVI)

Zone	Point ID	Mean	Median	Standard Deviation	Minimum	Maximum	Range
2	z2p5s2.01	0.191	0.206	0.101	-0.137	0.371	0.509
2	z2p5s3.01	-0.023	-0.031	0.121	-0.295	0.241	0.536
2	z2p5s4.01	0.167	0.175	0.125	-0.112	0.391	0.503
2	z2p5s6.01	0.147	0.149	0.070	-0.051	0.256	0.307
2	z2p6s1.01	0.120	0.124	0.091	-0.108	0.344	0.451
2	z2p6s2.01	0.155	0.163	0.082	-0.049	0.299	0.348
2	z2p6s3.01	0.232	0.214	0.075	0.053	0.401	0.348
2	z2p6s4.01	0.175	0.186	0.069	-0.054	0.306	0.360
2	z2p7s1.001	0.414	0.414	0.026	0.362	0.488	0.126
2	z2p7s2.01	0.405	0.410	0.048	0.205	0.505	0.300
2	z2p7s3.01	0.372	0.379	0.050	0.240	0.461	0.221
2	z2p7s4.01	0.216	0.218	0.054	0.094	0.340	0.246
7	Z7P10S1.01	0.139	0.156	0.074	-0.022	0.272	0.294
7	Z7P10S2.01	0.162	0.168	0.073	-0.015	0.319	0.334
7	Z7P10S3.01	0.178	0.176	0.074	0.006	0.348	0.342
7	Z7P10S4.01	0.084	0.092	0.060	-0.169	0.172	0.341
7	Z7P11S1.01	0.062	0.062	0.082	-0.148	0.247	0.395
7	Z7P11S2.01	0.023	0.024	0.068	-0.170	0.172	0.342
7	Z7P11S3.01	0.003	-0.003	0.084	-0.179	0.230	0.409
7	Z7P11S4.01	0.043	0.048	0.087	-0.169	0.241	0.411
7	Z7P8S1.01	0.126	0.127	0.050	0.009	0.295	0.287
7	Z7P8S2.01	0.079	0.083	0.056	-0.066	0.233	0.299
7	Z7P8S3.01	0.091	0.090	0.043	0.007	0.206	0.199
7	Z7P8S4.01	0.128	0.135	0.053	-0.035	0.264	0.299
7	Z7P9S1.01	-0.038	-0.036	0.060	-0.216	0.117	0.333
7	Z7P9S2.01	-0.035	-0.030	0.067	-0.209	0.120	0.330
7	Z7P9S3.01	-0.047	-0.051	0.043	-0.191	0.058	0.248
7	Z7P9S4.01	-0.025	-0.021	0.051	-0.167	0.094	0.261
8	Z8P2S1.01	0.055	0.056	0.073	-0.103	0.232	0.335
8	Z8P2S2.01	0.058	0.055	0.080	-0.149	0.220	0.369
8	Z8P2S3.01	-0.026	-0.025	0.074	-0.242	0.131	0.374

8	Z8P2S4.01	0.027	0.024	0.075	-0.147	0.257	0.403
8	Z8P3S1.01	0.081	0.071	0.063	-0.044	0.247	0.291
8	Z8P3S2.01	0.053	0.054	0.107	-0.174	0.236	0.410
8	Z8P3S3.01	-0.016	-0.028	0.077	-0.203	0.197	0.401
8	Z8P3S4.01	0.086	0.079	0.056	-0.062	0.260	0.322
8	Z8P4S1.01	0.046	0.032	0.102	-0.133	0.338	0.471
8	Z8P4S2.01	0.009	0.008	0.095	-0.198	0.259	0.456
8	Z8P4S3.01	0.005	0.019	0.078	-0.226	0.163	0.388
8	Z8P4S4.01	-0.071	-0.075	0.068	-0.217	0.105	0.321
8	Z8P5S1.01	-0.097	-0.089	0.091	-0.408	0.097	0.504
8	Z8P5S2.01	-0.045	-0.044	0.083	-0.275	0.132	0.407
8	Z8P5S3.01	0.025	0.024	0.069	-0.138	0.211	0.349
8	Z8P5S4.01	-0.042	-0.038	0.056	-0.183	0.079	0.262
8	Z8P6S1.01	-0.001	0.000	0.049	-0.111	0.134	0.245
8	Z8P6S2.01	-0.022	-0.016	0.046	-0.140	0.093	0.233
8	Z8P6S3.01	-0.016	-0.015	0.058	-0.198	0.151	0.348
8	Z8P6S4.01	0.046	0.045	0.038	-0.079	0.153	0.232
8	Z8P7S1.01	0.063	0.055	0.055	-0.103	0.213	0.315
8	Z8P7S2.01	0.068	0.066	0.035	-0.042	0.179	0.221
8	Z8P7S3.01	0.084	0.089	0.048	-0.192	0.169	0.361
8	Z8P7S4.01	0.090	0.092	0.069	-0.289	0.217	0.506
9	Z9P12S1.01	0.091	0.088	0.078	-0.077	0.285	0.361
9	Z9P12S2.01	0.013	-0.001	0.076	-0.122	0.236	0.358
9	Z9P12S3.01	0.069	0.074	0.064	-0.086	0.219	0.305
9	Z9P12S4.01	0.045	0.044	0.068	-0.154	0.245	0.400
9	Z9P13S1.01	0.012	0.006	0.070	-0.126	0.174	0.300
9	Z9P13S2.01	0.064	0.067	0.067	-0.140	0.201	0.341
9	Z9P13S3.01	-0.010	-0.001	0.070	-0.207	0.149	0.356
9	Z9P13S4.01	-0.038	-0.049	0.086	-0.203	0.248	0.451
9	Z9P14S1.01	0.050	0.044	0.097	-0.172	0.242	0.413
9	Z9P14S2.01	-0.062	-0.061	0.058	-0.221	0.089	0.310
9	Z9P14S3.01	0.089	0.077	0.081	-0.079	0.273	0.351
9	Z9P14S4.01	-0.034	-0.036	0.060	-0.161	0.139	0.300
9	Z9P15S1.01	0.068	0.076	0.092	-0.259	0.244	0.503
9	Z9P15S2.01	-0.042	-0.029	0.097	-0.332	0.122	0.454
9	Z9P15S3.01	0.004	0.004	0.071	-0.159	0.170	0.329
9	Z9P15S4.01	-0.021	-0.021	0.066	-0.206	0.150	0.356
9	Z9P16S1.01	-0.052	-0.043	0.050	-0.226	0.048	0.274
9	Z9P16S2.01	-0.055	-0.059	0.048	-0.179	0.089	0.268
9	Z9P16S3.01	0.098	0.100	0.058	-0.048	0.292	0.340
9	Z9P16S4.01	-0.031	-0.033	0.062	-0.174	0.108	0.282
9	Z9P17S1.01	-0.045	-0.040	0.072	-0.218	0.108	0.327
9	Z9P17S2.01	-0.098	-0.094	0.065	-0.263	0.034	0.297
9	Z9P17S3.01	-0.051	-0.054	0.065	-0.246	0.093	0.338

9	Z9P17S4.01	-0.003	0.009	0.067	-0.195	0.123	0.319
9	Z9P18S1.01	0.050	0.066	0.074	-0.149	0.187	0.336
9	Z9P18S2.01	-0.033	-0.020	0.057	-0.277	0.108	0.385
9	Z9P18S3.01	-0.036	-0.023	0.088	-0.262	0.131	0.393
9	Z9P18S4.01	-0.040	-0.028	0.092	-0.245	0.148	0.394

Subplot Summary Statistics - 2022
Forsythe National Wildlife Refuge
Green Normalized Difference Vegetation Index (GNDVI)

Zone	Point ID	Mean	Median	Standard Deviation	Minimum	Maximum	Range
2	z2p5s2.01	0.060	0.067	0.063	-0.089	0.241	0.329
2	z2p5s3.01	-0.043	-0.059	0.066	-0.151	0.108	0.259
2	z2p5s4.01	0.061	0.056	0.079	-0.069	0.221	0.290
2	z2p5s6.01	0.034	0.037	0.042	-0.070	0.111	0.181
2	z2p6s1.01	0.000	-0.009	0.057	-0.109	0.196	0.305
2	z2p6s2.01	0.033	0.028	0.044	-0.066	0.127	0.193
2	z2p6s3.01	0.060	0.043	0.065	-0.055	0.203	0.258
2	z2p6s4.01	0.004	0.008	0.041	-0.116	0.102	0.218
2	z2p7s1.001	0.336	0.331	0.031	0.273	0.447	0.174
2	z2p7s2.01	0.326	0.329	0.042	0.202	0.414	0.212
2	z2p7s3.01	0.304	0.308	0.051	0.145	0.428	0.283
2	z2p7s4.01	0.217	0.216	0.043	0.125	0.334	0.208
7	Z7P10S1.01	0.006	0.013	0.040	-0.111	0.100	0.211
7	Z7P10S2.01	0.007	0.005	0.045	-0.091	0.142	0.232
7	Z7P10S3.01	0.036	0.035	0.052	-0.075	0.155	0.230
7	Z7P10S4.01	0.004	0.005	0.032	-0.110	0.067	0.177
7	Z7P11S1.01	0.011	0.018	0.085	-0.221	0.179	0.400
7	Z7P11S2.01	0.022	0.019	0.079	-0.216	0.196	0.412
7	Z7P11S3.01	-0.002	-0.002	0.083	-0.240	0.177	0.417
7	Z7P11S4.01	0.022	0.021	0.074	-0.211	0.189	0.400
7	Z7P8S1.01	0.097	0.098	0.029	-0.007	0.162	0.169
7	Z7P8S2.01	0.073	0.072	0.030	-0.042	0.166	0.208
7	Z7P8S3.01	0.079	0.080	0.024	0.030	0.138	0.108
7	Z7P8S4.01	0.097	0.102	0.036	-0.067	0.184	0.251
7	Z7P9S1.01	0.012	0.014	0.042	-0.133	0.112	0.245
7	Z7P9S2.01	0.008	0.014	0.039	-0.114	0.101	0.215
7	Z7P9S3.01	0.016	0.013	0.028	-0.068	0.085	0.153
7	Z7P9S4.01	0.032	0.028	0.046	-0.087	0.139	0.226
8	Z8P2S1.01	-0.008	-0.010	0.040	-0.095	0.095	0.190
8	Z8P2S2.01	-0.010	-0.011	0.043	-0.113	0.096	0.209
8	Z8P2S3.01	-0.065	-0.070	0.038	-0.160	0.048	0.208
8	Z8P2S4.01	-0.011	-0.013	0.040	-0.111	0.088	0.199
8	Z8P3S1.01	-0.034	-0.041	0.050	-0.166	0.102	0.268
8	Z8P3S2.01	-0.037	-0.049	0.066	-0.148	0.094	0.242
8	Z8P3S3.01	-0.075	-0.087	0.044	-0.146	0.078	0.225
8	Z8P3S4.01	0.002	-0.003	0.048	-0.078	0.220	0.298
8	Z8P4S1.01	-0.024	-0.037	0.056	-0.117	0.168	0.285
8	Z8P4S2.01	-0.046	-0.051	0.047	-0.146	0.095	0.241

8	Z8P4S3.01	-0.020	-0.018	0.039	-0.123	0.077	0.199
8	Z8P4S4.01	-0.084	-0.083	0.037	-0.159	0.009	0.169
8	Z8P5S1.01	0.026	0.033	0.061	-0.249	0.180	0.429
8	Z8P5S2.01	0.058	0.066	0.059	-0.095	0.174	0.269
8	Z8P5S3.01	0.070	0.076	0.053	-0.143	0.212	0.355
8	Z8P5S4.01	0.038	0.043	0.039	-0.061	0.107	0.169
8	Z8P6S1.01	0.049	0.050	0.027	-0.048	0.107	0.155
8	Z8P6S2.01	0.042	0.044	0.043	-0.157	0.122	0.279
8	Z8P6S3.01	0.047	0.052	0.034	-0.056	0.145	0.201
8	Z8P6S4.01	0.106	0.108	0.029	-0.078	0.167	0.245
8	Z8P7S1.01	0.079	0.080	0.037	-0.048	0.181	0.229
8	Z8P7S2.01	0.099	0.099	0.026	-0.023	0.149	0.172
8	Z8P7S3.01	0.094	0.102	0.039	-0.073	0.164	0.237
8	Z8P7S4.01	0.107	0.110	0.044	-0.044	0.202	0.246
9	Z9P12S1.01	0.071	0.069	0.048	-0.037	0.196	0.233
9	Z9P12S2.01	0.035	0.035	0.048	-0.078	0.163	0.240
9	Z9P12S3.01	0.046	0.047	0.055	-0.099	0.166	0.265
9	Z9P12S4.01	0.050	0.048	0.053	-0.152	0.212	0.364
9	Z9P13S1.01	0.048	0.049	0.042	-0.055	0.143	0.198
9	Z9P13S2.01	0.081	0.084	0.042	-0.056	0.180	0.235
9	Z9P13S3.01	0.031	0.032	0.042	-0.127	0.130	0.258
9	Z9P13S4.01	0.027	0.025	0.053	-0.086	0.206	0.292
9	Z9P14S1.01	0.047	0.044	0.063	-0.180	0.206	0.386
9	Z9P14S2.01	-0.022	-0.025	0.061	-0.179	0.183	0.362
9	Z9P14S3.01	0.055	0.046	0.066	-0.080	0.236	0.317
9	Z9P14S4.01	-0.022	-0.027	0.053	-0.133	0.181	0.314
9	Z9P15S1.01	0.112	0.131	0.076	-0.192	0.220	0.412
9	Z9P15S2.01	0.048	0.077	0.094	-0.295	0.180	0.475
9	Z9P15S3.01	0.084	0.082	0.044	-0.036	0.180	0.216
9	Z9P15S4.01	0.087	0.085	0.035	-0.025	0.191	0.217
9	Z9P16S1.01	0.027	0.035	0.043	-0.183	0.108	0.291
9	Z9P16S2.01	0.033	0.037	0.040	-0.168	0.137	0.305
9	Z9P16S3.01	0.111	0.108	0.038	-0.007	0.220	0.227
9	Z9P16S4.01	0.028	0.030	0.042	-0.107	0.151	0.258
9	Z9P17S1.01	0.115	0.117	0.045	-0.017	0.266	0.283
9	Z9P17S2.01	0.042	0.046	0.050	-0.085	0.196	0.281
9	Z9P17S3.01	0.061	0.065	0.045	-0.079	0.198	0.277
9	Z9P17S4.01	0.072	0.070	0.039	-0.028	0.187	0.215
9	Z9P18S1.01	0.096	0.097	0.040	-0.019	0.192	0.211
9	Z9P18S2.01	0.061	0.066	0.038	-0.074	0.172	0.246
9	Z9P18S3.01	0.043	0.051	0.062	-0.150	0.165	0.316
9	Z9P18S4.01	0.054	0.057	0.055	-0.093	0.194	0.287

Subplot Summary Statistics - 2022
Forsythe National Wildlife Refuge
Normalized Difference Red Edge Index (NDRE)

Zone	Point ID	Mean	Median	Standard Deviation	Minimum	Maximum	Range
2	z2p5s2.01	0.009	0.008	0.026	-0.069	0.093	0.162
2	z2p5s3.01	-0.025	-0.031	0.027	-0.077	0.049	0.126
2	z2p5s4.01	0.008	0.013	0.038	-0.075	0.073	0.149
2	z2p5s6.01	-0.007	-0.007	0.020	-0.049	0.063	0.112
2	z2p6s1.01	-0.013	-0.018	0.023	-0.051	0.086	0.137
2	z2p6s2.01	-0.003	-0.005	0.017	-0.037	0.035	0.072
2	z2p6s3.01	0.007	0.002	0.035	-0.065	0.119	0.183
2	z2p6s4.01	-0.022	-0.022	0.016	-0.062	0.019	0.081
2	z2p7s1.001	0.051	0.052	0.017	0.020	0.100	0.081
2	z2p7s2.01	0.045	0.046	0.024	-0.023	0.101	0.123
2	z2p7s3.01	0.040	0.041	0.028	-0.034	0.108	0.141
2	z2p7s4.01	0.015	0.015	0.023	-0.053	0.067	0.120
7	Z7P10S1.01	-0.019	-0.021	0.026	-0.082	0.074	0.156
7	Z7P10S2.01	-0.012	-0.018	0.048	-0.104	0.143	0.246
7	Z7P10S3.01	0.000	-0.001	0.026	-0.065	0.060	0.125
7	Z7P10S4.01	-0.011	-0.012	0.021	-0.097	0.042	0.139
7	Z7P11S1.01	0.008	0.015	0.058	-0.148	0.152	0.299
7	Z7P11S2.01	0.016	0.011	0.053	-0.129	0.167	0.296
7	Z7P11S3.01	-0.002	-0.001	0.048	-0.118	0.126	0.245
7	Z7P11S4.01	0.015	0.021	0.041	-0.104	0.111	0.214
7	Z7P8S1.01	0.031	0.030	0.041	-0.060	0.142	0.202
7	Z7P8S2.01	0.023	0.021	0.036	-0.068	0.136	0.204
7	Z7P8S3.01	0.026	0.027	0.017	-0.020	0.068	0.089
7	Z7P8S4.01	0.033	0.036	0.025	-0.034	0.097	0.132
7	Z7P9S1.01	0.014	0.016	0.024	-0.065	0.070	0.135
7	Z7P9S2.01	0.012	0.014	0.030	-0.112	0.082	0.194
7	Z7P9S3.01	0.020	0.022	0.019	-0.035	0.071	0.106
7	Z7P9S4.01	0.022	0.023	0.027	-0.052	0.076	0.129
8	Z8P2S1.01	-0.032	-0.031	0.017	-0.069	0.018	0.087
8	Z8P2S2.01	-0.034	-0.033	0.018	-0.082	0.016	0.097
8	Z8P2S3.01	-0.052	-0.054	0.015	-0.099	-0.016	0.083
8	Z8P2S4.01	-0.037	-0.038	0.017	-0.095	0.016	0.111
8	Z8P3S1.01	-0.024	-0.028	0.050	-0.153	0.182	0.336
8	Z8P3S2.01	-0.034	-0.041	0.050	-0.131	0.114	0.245
8	Z8P3S3.01	-0.044	-0.048	0.018	-0.077	0.014	0.091
8	Z8P3S4.01	-0.026	-0.028	0.022	-0.076	0.029	0.104
8	Z8P4S1.01	-0.025	-0.033	0.034	-0.081	0.088	0.169
8	Z8P4S2.01	-0.031	-0.031	0.026	-0.105	0.031	0.137

8	Z8P4S3.01	-0.022	-0.026	0.034	-0.108	0.069	0.177
8	Z8P4S4.01	-0.050	-0.054	0.050	-0.157	0.119	0.276
8	Z8P5S1.01	0.015	0.013	0.042	-0.111	0.119	0.230
8	Z8P5S2.01	0.020	0.019	0.043	-0.094	0.134	0.228
8	Z8P5S3.01	0.015	0.019	0.050	-0.162	0.183	0.346
8	Z8P5S4.01	0.004	0.006	0.034	-0.077	0.078	0.155
8	Z8P6S1.01	0.015	0.016	0.016	-0.028	0.053	0.081
8	Z8P6S2.01	0.022	0.022	0.014	-0.018	0.052	0.070
8	Z8P6S3.01	0.030	0.032	0.016	-0.018	0.070	0.088
8	Z8P6S4.01	0.039	0.040	0.014	0.010	0.071	0.061
8	Z8P7S1.01	0.030	0.029	0.027	-0.045	0.103	0.148
8	Z8P7S2.01	0.036	0.038	0.020	-0.021	0.074	0.095
8	Z8P7S3.01	0.036	0.037	0.019	-0.023	0.085	0.108
8	Z8P7S4.01	0.039	0.039	0.029	-0.046	0.138	0.184
9	Z9P12S1.01	0.028	0.029	0.017	-0.011	0.069	0.080
9	Z9P12S2.01	0.023	0.025	0.025	-0.035	0.091	0.126
9	Z9P12S3.01	0.025	0.028	0.036	-0.084	0.110	0.194
9	Z9P12S4.01	0.022	0.024	0.045	-0.160	0.119	0.279
9	Z9P13S1.01	0.027	0.027	0.024	-0.052	0.082	0.134
9	Z9P13S2.01	0.036	0.040	0.025	-0.042	0.107	0.149
9	Z9P13S3.01	0.020	0.024	0.026	-0.057	0.103	0.159
9	Z9P13S4.01	0.021	0.021	0.024	-0.030	0.073	0.103
9	Z9P14S1.01	0.021	0.020	0.045	-0.190	0.170	0.360
9	Z9P14S2.01	0.008	0.006	0.045	-0.128	0.163	0.291
9	Z9P14S3.01	0.025	0.025	0.040	-0.094	0.122	0.216
9	Z9P14S4.01	0.004	0.006	0.032	-0.091	0.076	0.167
9	Z9P15S1.01	0.057	0.065	0.038	-0.070	0.123	0.193
9	Z9P15S2.01	0.043	0.049	0.039	-0.087	0.108	0.195
9	Z9P15S3.01	0.036	0.038	0.026	-0.032	0.089	0.120
9	Z9P15S4.01	0.047	0.048	0.023	-0.029	0.103	0.132
9	Z9P16S1.01	0.041	0.042	0.028	-0.055	0.101	0.156
9	Z9P16S2.01	0.035	0.035	0.022	-0.030	0.097	0.127
9	Z9P16S3.01	0.050	0.050	0.023	0.006	0.128	0.122
9	Z9P16S4.01	0.026	0.025	0.027	-0.042	0.097	0.139
9	Z9P17S1.01	0.035	0.035	0.024	-0.034	0.106	0.141
9	Z9P17S2.01	0.027	0.027	0.015	-0.012	0.061	0.073
9	Z9P17S3.01	0.041	0.041	0.015	-0.009	0.089	0.097
9	Z9P17S4.01	0.036	0.038	0.021	-0.025	0.079	0.105
9	Z9P18S1.01	0.035	0.037	0.019	-0.022	0.082	0.104
9	Z9P18S2.01	0.027	0.027	0.027	-0.057	0.082	0.139
9	Z9P18S3.01	0.024	0.023	0.026	-0.044	0.090	0.134
9	Z9P18S4.01	0.021	0.022	0.017	-0.019	0.068	0.087

Subplot Summary Statistics - 2022
Forsythe National Wildlife Refuge
Non-Photosynthetic Vegetation Index (NPV)

Zone	Point ID	Mean	Median	Standard Deviation	Minimum	Maximum	Range
2	z2p5s2.01	-0.075	-0.087	0.068	-0.210	0.137	0.347
2	z2p5s3.01	-0.039	-0.038	0.048	-0.140	0.078	0.218
2	z2p5s4.01	-0.086	-0.095	0.046	-0.164	0.084	0.248
2	z2p5s6.01	-0.102	-0.100	0.034	-0.175	-0.001	0.174
2	z2p6s1.01	-0.115	-0.117	0.043	-0.195	0.049	0.244
2	z2p6s2.01	-0.143	-0.154	0.051	-0.228	0.027	0.254
2	z2p6s3.01	-0.147	-0.160	0.075	-0.282	0.044	0.326
2	z2p6s4.01	-0.193	-0.200	0.047	-0.276	-0.034	0.242
2	z2p7s1.001	-0.149	-0.147	0.042	-0.245	-0.047	0.198
2	z2p7s2.01	-0.132	-0.131	0.043	-0.232	-0.044	0.189
2	z2p7s3.01	-0.125	-0.125	0.040	-0.221	-0.038	0.183
2	z2p7s4.01	-0.061	-0.060	0.035	-0.153	0.039	0.192
7	Z7P10S1.01	-0.134	-0.142	0.043	-0.233	-0.011	0.222
7	Z7P10S2.01	-0.155	-0.162	0.042	-0.260	-0.053	0.207
7	Z7P10S3.01	-0.143	-0.143	0.031	-0.214	-0.073	0.142
7	Z7P10S4.01	-0.080	-0.090	0.040	-0.144	0.060	0.203
7	Z7P11S1.01	-0.051	-0.050	0.072	-0.270	0.100	0.370
7	Z7P11S2.01	-0.001	-0.006	0.065	-0.146	0.188	0.334
7	Z7P11S3.01	-0.005	-0.006	0.060	-0.180	0.142	0.322
7	Z7P11S4.01	-0.021	-0.024	0.065	-0.196	0.159	0.355
7	Z7P8S1.01	-0.030	-0.032	0.036	-0.164	0.066	0.231
7	Z7P8S2.01	-0.006	-0.012	0.040	-0.115	0.108	0.223
7	Z7P8S3.01	-0.013	-0.010	0.031	-0.110	0.058	0.167
7	Z7P8S4.01	-0.032	-0.030	0.028	-0.098	0.077	0.174
7	Z7P9S1.01	0.050	0.045	0.043	-0.048	0.199	0.247
7	Z7P9S2.01	0.044	0.042	0.044	-0.069	0.155	0.224
7	Z7P9S3.01	0.063	0.061	0.033	-0.014	0.206	0.220
7	Z7P9S4.01	0.057	0.057	0.044	-0.055	0.203	0.258
8	Z8P2S1.01	-0.057	-0.060	0.047	-0.164	0.074	0.238
8	Z8P2S2.01	-0.066	-0.072	0.041	-0.161	0.053	0.214
8	Z8P2S3.01	-0.042	-0.047	0.041	-0.115	0.124	0.238
8	Z8P2S4.01	-0.048	-0.063	0.053	-0.149	0.150	0.300
8	Z8P3S1.01	-0.051	-0.057	0.044	-0.128	0.178	0.306
8	Z8P3S2.01	-0.069	-0.069	0.037	-0.155	0.062	0.217
8	Z8P3S3.01	-0.075	-0.082	0.030	-0.137	0.031	0.167
8	Z8P3S4.01	-0.087	-0.097	0.062	-0.189	0.092	0.281
8	Z8P4S1.01	-0.057	-0.067	0.056	-0.161	0.163	0.324
8	Z8P4S2.01	-0.047	-0.053	0.053	-0.148	0.107	0.255

8	Z8P4S3.01	-0.004	-0.006	0.039	-0.098	0.121	0.219
8	Z8P4S4.01	-0.029	-0.035	0.047	-0.111	0.109	0.221
8	Z8P5S1.01	0.230	0.235	0.050	0.092	0.388	0.296
8	Z8P5S2.01	0.204	0.202	0.054	0.077	0.330	0.252
8	Z8P5S3.01	0.201	0.186	0.071	0.048	0.395	0.348
8	Z8P5S4.01	0.191	0.189	0.053	0.070	0.322	0.252
8	Z8P6S1.01	0.031	0.032	0.037	-0.053	0.198	0.250
8	Z8P6S2.01	0.036	0.033	0.052	-0.119	0.167	0.286
8	Z8P6S3.01	0.089	0.082	0.061	-0.066	0.287	0.354
8	Z8P6S4.01	0.047	0.042	0.048	-0.124	0.297	0.421
8	Z8P7S1.01	0.042	0.042	0.035	-0.038	0.152	0.190
8	Z8P7S2.01	0.041	0.042	0.028	-0.048	0.106	0.154
8	Z8P7S3.01	0.042	0.040	0.036	-0.087	0.152	0.240
8	Z8P7S4.01	0.048	0.041	0.047	-0.038	0.291	0.330
9	Z9P12S1.01	-0.120	-0.115	0.049	-0.228	0.008	0.236
9	Z9P12S2.01	-0.074	-0.072	0.047	-0.231	0.026	0.257
9	Z9P12S3.01	-0.090	-0.091	0.046	-0.206	0.121	0.327
9	Z9P12S4.01	-0.098	-0.091	0.043	-0.231	0.003	0.235
9	Z9P13S1.01	-0.069	-0.069	0.038	-0.163	0.080	0.244
9	Z9P13S2.01	-0.066	-0.072	0.036	-0.135	0.037	0.172
9	Z9P13S3.01	-0.059	-0.059	0.054	-0.186	0.087	0.274
9	Z9P13S4.01	-0.032	-0.024	0.071	-0.245	0.156	0.401
9	Z9P14S1.01	-0.033	-0.041	0.071	-0.157	0.147	0.303
9	Z9P14S2.01	-0.015	-0.023	0.058	-0.122	0.160	0.283
9	Z9P14S3.01	-0.059	-0.065	0.054	-0.153	0.114	0.267
9	Z9P14S4.01	-0.043	-0.048	0.045	-0.138	0.079	0.217
9	Z9P15S1.01	0.037	0.029	0.053	-0.073	0.169	0.242
9	Z9P15S2.01	0.106	0.091	0.073	-0.042	0.318	0.359
9	Z9P15S3.01	-0.026	-0.022	0.042	-0.128	0.091	0.219
9	Z9P15S4.01	0.017	0.017	0.047	-0.141	0.236	0.377
9	Z9P16S1.01	0.073	0.074	0.058	-0.106	0.215	0.321
9	Z9P16S2.01	0.092	0.095	0.048	-0.064	0.245	0.310
9	Z9P16S3.01	0.011	0.008	0.061	-0.137	0.240	0.376
9	Z9P16S4.01	0.063	0.058	0.094	-0.170	0.346	0.516
9	Z9P17S1.01	0.103	0.106	0.033	0.005	0.176	0.171
9	Z9P17S2.01	0.143	0.141	0.043	0.048	0.261	0.214
9	Z9P17S3.01	0.114	0.114	0.033	0.041	0.215	0.175
9	Z9P17S4.01	0.057	0.054	0.047	-0.061	0.168	0.228
9	Z9P18S1.01	0.041	0.044	0.048	-0.093	0.175	0.268
9	Z9P18S2.01	0.076	0.070	0.052	-0.103	0.195	0.298
9	Z9P18S3.01	0.062	0.059	0.058	-0.075	0.213	0.288
9	Z9P18S4.01	0.055	0.059	0.066	-0.122	0.254	0.376

Great Bay Boulevard

Subplot Summary Statistics - 2022
Great Bay Boulevard
Normalized Difference Vegetation Index (NDVI)

Zone	Point ID	Mean	Median	Standard Deviation	Minimum	Maximum	Range
1	z1p1s2.01	0.114	0.105	0.117	-0.147	0.335	0.483
1	z1p1s3.01	0.193	0.217	0.102	-0.124	0.371	0.495
1	z1p1s4.01	-0.017	-0.004	0.077	-0.221	0.159	0.381
1	z1p1s5.01	0.152	0.166	0.139	-0.156	0.431	0.587
1	z1p2s1.01	0.106	0.100	0.127	-0.176	0.358	0.534
1	z1p2s2.01	0.094	0.117	0.111	-0.205	0.312	0.517
1	z1p2s5.01	0.032	0.041	0.069	-0.166	0.157	0.323
1	z1p2s6.01	0.146	0.152	0.125	-0.143	0.396	0.539
1	z1p3s2.01	0.034	0.015	0.082	-0.135	0.269	0.404
1	z1p3s3.01	0.015	0.017	0.089	-0.241	0.167	0.408
1	z1p3s4.01	0.093	0.079	0.101	-0.139	0.292	0.431
1	z1p3s5.01	0.033	0.032	0.059	-0.078	0.170	0.248
1	z1p4s1.01	0.094	0.093	0.094	-0.111	0.280	0.391
1	z1p4s3.01	0.096	0.099	0.096	-0.163	0.291	0.454
1	z1p4s4.01	-0.007	-0.011	0.054	-0.151	0.119	0.270
1	z1p4s5.01	-0.015	-0.023	0.063	-0.161	0.152	0.312
3	z3p8s1.01	-0.005	-0.015	0.064	-0.142	0.167	0.309
3	z3p8s2.01	0.044	0.042	0.073	-0.111	0.247	0.358
3	z3p8s3.01	0.067	0.065	0.125	-0.248	0.316	0.564
3	z3p8s6.01	0.007	-0.001	0.109	-0.213	0.213	0.427
3	z3p9s1.01	0.096	0.094	0.069	-0.042	0.243	0.286
3	z3p9s3.01	0.110	0.115	0.040	0.009	0.213	0.203
3	z3p9s5.01	0.114	0.152	0.133	-0.255	0.309	0.564
3	z3p9s6.01	0.034	0.004	0.132	-0.191	0.336	0.528
4	z4p10s2.01	0.162	0.167	0.034	0.027	0.240	0.213
4	z4p10s3.01	0.143	0.141	0.031	0.022	0.218	0.196
4	z4p10s5.01	0.199	0.201	0.059	-0.156	0.311	0.468
4	z4p10s6.01	0.224	0.227	0.029	0.098	0.293	0.195
4	z4p11s2.01	-0.042	-0.040	0.056	-0.224	0.070	0.294
4	z4p11s3.01	-0.044	-0.063	0.094	-0.298	0.155	0.453
4	z4p11s4.01	0.067	0.072	0.057	-0.176	0.183	0.359
4	z4p11s6.01	0.013	0.036	0.092	-0.250	0.176	0.426
5	z5p12s1.01	0.118	0.112	0.044	0.013	0.266	0.253
5	z5p12s2.01	0.066	0.072	0.082	-0.149	0.216	0.365
5	z5p12s3.01	0.175	0.173	0.039	0.087	0.286	0.199

5	z5p12s6.01	0.275	0.278	0.039	0.033	0.364	0.331
5	z5p13s1.01	0.118	0.130	0.062	-0.069	0.267	0.336
5	z5p13s2.01	0.106	0.108	0.046	-0.062	0.278	0.340
5	z5p13s5.01	0.113	0.112	0.055	-0.043	0.216	0.258
5	z5p13s6.01	0.157	0.155	0.045	0.060	0.276	0.217
6	z6p14s1.01	0.077	0.069	0.044	-0.009	0.202	0.211
6	z6p14s2.01	0.030	0.051	0.092	-0.252	0.158	0.410
6	z6p14s4.01	0.249	0.257	0.040	0.081	0.345	0.264
6	z6p14s6.01	0.216	0.231	0.064	-0.079	0.298	0.377
6	z6p15s1.01	0.196	0.184	0.057	0.043	0.323	0.281
6	z6p15s2.01	0.196	0.199	0.039	0.069	0.305	0.236
6	z6p15s4.01	0.197	0.202	0.037	0.090	0.289	0.199
6	z6p15s6.01	0.282	0.281	0.030	0.191	0.361	0.170

Subplot Summaries - 2022
Great Bay Boulevard
Green Normalized Difference Vegetation Index (GNDVI)

Zone	Point ID	Mean	Median	Standard Deviation	Minimum	Maximum	Range
1	z1p1s2.01	0.007	-0.010	0.056	-0.110	0.154	0.264
1	z1p1s3.01	0.048	0.056	0.055	-0.100	0.158	0.258
1	z1p1s4.01	-0.059	-0.057	0.034	-0.145	0.026	0.171
1	z1p1s5.01	0.029	0.034	0.078	-0.125	0.207	0.332
1	z1p2s1.01	0.012	0.012	0.071	-0.146	0.175	0.321
1	z1p2s2.01	0.010	0.009	0.051	-0.111	0.139	0.250
1	z1p2s5.01	-0.047	-0.042	0.035	-0.122	0.024	0.146
1	z1p2s6.01	0.024	0.022	0.082	-0.137	0.202	0.340
1	z1p3s1.01	-0.065	-0.064	0.043	-0.159	0.051	0.210
1	z1p3s2.01	-0.067	-0.075	0.049	-0.172	0.088	0.259
1	z1p3s4.01	-0.016	-0.022	0.065	-0.138	0.113	0.250
1	z1p3s5.01	-0.075	-0.077	0.034	-0.130	0.000	0.131
1	z1p4s1.01	-0.025	-0.032	0.053	-0.132	0.102	0.234
1	z1p4s3.01	-0.022	-0.029	0.052	-0.130	0.125	0.255
1	z1p4s4.01	-0.094	-0.097	0.024	-0.145	-0.027	0.118
1	z1p4s5.01	-0.094	-0.096	0.029	-0.162	-0.013	0.149
3	z3p8s1.01	0.019	0.014	0.037	-0.067	0.121	0.189
3	z3p8s2.01	0.033	0.029	0.038	-0.052	0.114	0.166
3	z3p8s3.01	0.013	0.012	0.057	-0.120	0.123	0.243
3	z3p8s6.01	-0.054	-0.054	0.047	-0.133	0.049	0.182
3	z3p9s1.01	0.161	0.168	0.050	0.014	0.257	0.243
3	z3p9s3.01	0.162	0.163	0.036	0.021	0.250	0.228
3	z3p9s5.01	0.123	0.171	0.133	-0.277	0.281	0.559
3	z3p9s6.01	0.034	0.018	0.107	-0.135	0.238	0.373
4	z4p10s2.01	0.101	0.101	0.027	-0.067	0.148	0.215
4	z4p10s3.01	0.080	0.081	0.029	-0.067	0.145	0.212
4	z4p10s5.01	0.091	0.090	0.029	-0.109	0.161	0.270
4	z4p10s6.01	0.120	0.124	0.027	-0.018	0.176	0.193
4	z4p11s2.01	0.016	0.013	0.050	-0.157	0.155	0.313
4	z4p11s3.01	0.025	0.045	0.069	-0.268	0.113	0.380
4	z4p11s4.01	0.066	0.085	0.064	-0.176	0.171	0.347
4	z4p11s6.01	0.063	0.079	0.067	-0.232	0.164	0.396
5	z5p12s1.01	0.203	0.205	0.042	0.066	0.334	0.268
5	z5p12s2.01	0.127	0.148	0.081	-0.063	0.252	0.315
5	z5p12s3.01	0.196	0.198	0.028	0.140	0.286	0.146
5	z5p12s6.01	0.300	0.308	0.048	-0.063	0.396	0.459
5	z5p13s1.01	0.057	0.053	0.049	-0.065	0.188	0.253
5	z5p13s2.01	0.070	0.072	0.039	-0.020	0.168	0.188

5	z5p13s5.01	0.078	0.079	0.033	-0.018	0.185	0.203
5	z5p13s6.01	0.103	0.102	0.033	0.013	0.185	0.172
6	z6p14s1.01	0.191	0.191	0.029	0.101	0.250	0.149
6	z6p14s2.01	0.137	0.180	0.123	-0.252	0.255	0.507
6	z6p14s4.01	0.286	0.293	0.029	0.141	0.332	0.191
6	z6p14s6.01	0.250	0.269	0.062	-0.004	0.306	0.310
6	z6p15s1.01	0.210	0.203	0.045	-0.004	0.315	0.319
6	z6p15s2.01	0.172	0.170	0.026	0.091	0.247	0.155
6	z6p15s4.01	0.198	0.202	0.029	0.110	0.288	0.178
6	z6p15s6.01	0.235	0.235	0.025	0.145	0.303	0.157

Subplot Summary Statistics - 2022
Great Bay Boulevard
Normalized Difference Red Edge Index (NDRE)

Zone	Point ID	Mean	Median	Standard Deviation	Minimum	Maximum	Range
1	z1p1s2.01	-0.032	-0.037	0.022	-0.072	0.023	0.095
1	z1p1s3.01	-0.018	-0.017	0.025	-0.068	0.051	0.119
1	z1p1s4.01	-0.056	-0.057	0.014	-0.088	-0.016	0.071
1	z1p1s5.01	-0.025	-0.027	0.027	-0.081	0.051	0.132
1	z1p2s1.01	-0.029	-0.034	0.028	-0.084	0.044	0.128
1	z1p2s2.01	-0.027	-0.028	0.018	-0.069	0.018	0.087
1	z1p2s5.01	-0.053	-0.052	0.019	-0.095	-0.013	0.082
1	z1p2s6.01	-0.024	-0.025	0.036	-0.099	0.062	0.161
1	z1p3s1.01	-0.068	-0.069	0.016	-0.108	-0.023	0.084
1	z1p3s2.01	-0.070	-0.073	0.022	-0.111	0.005	0.116
1	z1p3s4.01	-0.047	-0.043	0.031	-0.119	0.023	0.142
1	z1p3s5.01	-0.074	-0.075	0.015	-0.103	-0.025	0.078
1	z1p4s1.01	-0.055	-0.058	0.020	-0.086	0.002	0.088
1	z1p4s3.01	-0.056	-0.059	0.019	-0.088	0.008	0.096
1	z1p4s4.01	-0.084	-0.085	0.009	-0.103	-0.058	0.045
1	z1p4s5.01	-0.086	-0.086	0.010	-0.111	-0.061	0.050
3	z3p8s1.01	0.013	0.014	0.021	-0.047	0.074	0.120
3	z3p8s2.01	0.012	0.012	0.027	-0.047	0.093	0.141
3	z3p8s3.01	-0.005	-0.007	0.023	-0.071	0.069	0.140
3	z3p8s6.01	-0.021	-0.023	0.020	-0.079	0.030	0.109
3	z3p9s1.01	0.009	0.011	0.014	-0.029	0.031	0.060
3	z3p9s3.01	0.001	0.002	0.016	-0.044	0.040	0.083
3	z3p9s5.01	-0.038	-0.034	0.061	-0.234	0.071	0.305
3	z3p9s6.01	-0.069	-0.073	0.062	-0.202	0.060	0.262
4	z4p10s2.01	0.019	0.019	0.026	-0.067	0.123	0.191
4	z4p10s3.01	0.017	0.015	0.025	-0.041	0.090	0.130
4	z4p10s5.01	0.010	0.010	0.024	-0.059	0.074	0.133
4	z4p10s6.01	0.017	0.017	0.017	-0.023	0.058	0.081
4	z4p11s2.01	-0.017	-0.016	0.022	-0.082	0.041	0.124
4	z4p11s3.01	-0.011	-0.007	0.028	-0.124	0.040	0.164
4	z4p11s4.01	0.000	0.006	0.029	-0.099	0.062	0.161
4	z4p11s6.01	-0.004	0.003	0.028	-0.091	0.059	0.150
5	z5p12s1.01	0.043	0.044	0.022	-0.007	0.107	0.113
5	z5p12s2.01	0.019	0.019	0.032	-0.053	0.084	0.137
5	z5p12s3.01	0.044	0.045	0.016	0.004	0.084	0.080
5	z5p12s6.01	0.086	0.089	0.020	0.003	0.137	0.133
5	z5p13s1.01	0.010	0.011	0.021	-0.048	0.059	0.107
5	z5p13s2.01	0.012	0.012	0.020	-0.047	0.071	0.117

5	z5p13s5.01	0.017	0.018	0.021	-0.032	0.071	0.103
5	z5p13s6.01	0.025	0.026	0.020	-0.038	0.071	0.109
6	z6p14s1.01	0.012	0.011	0.014	-0.023	0.047	0.070
6	z6p14s2.01	-0.010	0.003	0.040	-0.127	0.052	0.179
6	z6p14s4.01	0.061	0.063	0.015	-0.008	0.092	0.101
6	z6p14s6.01	0.057	0.062	0.029	-0.063	0.097	0.160
6	z6p15s1.01	0.073	0.072	0.020	-0.023	0.118	0.141
6	z6p15s2.01	0.051	0.051	0.017	0.010	0.093	0.084
6	z6p15s4.01	0.055	0.055	0.019	-0.007	0.105	0.112
6	z6p15s6.01	0.063	0.061	0.011	0.037	0.095	0.058

Subplot Summary Statistics - 2022
Great Bay Boulevard
Non-Photosynthetic Vegetation Index (NPV)

Zone	Point ID	Mean	Median	Standard Deviation	Minimum	Maximum	Range
1	z1p1s2.01	-0.129	-0.136	0.045	-0.204	0.011	0.215
1	z1p1s3.01	-0.159	-0.159	0.032	-0.250	-0.048	0.201
1	z1p1s4.01	-0.103	-0.114	0.046	-0.184	0.032	0.216
1	z1p1s5.01	-0.147	-0.160	0.052	-0.267	0.077	0.344
1	z1p2s1.01	-0.108	-0.111	0.043	-0.194	-0.009	0.185
1	z1p2s2.01	-0.116	-0.125	0.042	-0.178	0.036	0.213
1	z1p2s5.01	-0.131	-0.140	0.030	-0.190	-0.056	0.135
1	z1p2s6.01	-0.146	-0.151	0.034	-0.227	-0.032	0.195
1	z1p3s1.01	-0.091	-0.097	0.030	-0.149	0.018	0.167
1	z1p3s2.01	-0.100	-0.107	0.030	-0.149	0.035	0.184
1	z1p3s4.01	-0.083	-0.090	0.038	-0.139	0.080	0.218
1	z1p3s5.01	-0.107	-0.109	0.018	-0.145	-0.032	0.112
1	z1p4s1.01	-0.083	-0.084	0.032	-0.141	0.020	0.161
1	z1p4s3.01	-0.084	-0.093	0.038	-0.145	0.061	0.206
1	z1p4s4.01	-0.093	-0.097	0.023	-0.149	-0.014	0.135
1	z1p4s5.01	-0.098	-0.096	0.029	-0.195	-0.015	0.180
3	z3p8s1.01	-0.044	-0.043	0.033	-0.129	0.019	0.148
3	z3p8s2.01	-0.070	-0.070	0.048	-0.186	0.135	0.321
3	z3p8s3.01	-0.120	-0.117	0.066	-0.253	0.023	0.276
3	z3p8s6.01	-0.115	-0.127	0.062	-0.209	0.052	0.261
3	z3p9s1.01	-0.116	-0.112	0.035	-0.230	-0.055	0.175
3	z3p9s3.01	-0.114	-0.112	0.018	-0.160	-0.049	0.111
3	z3p9s5.01	-0.118	-0.130	0.048	-0.190	0.085	0.275
3	z3p9s6.01	-0.106	-0.107	0.046	-0.218	0.021	0.239
4	z4p10s2.01	-0.183	-0.183	0.036	-0.310	0.002	0.312
4	z4p10s3.01	-0.166	-0.170	0.049	-0.267	0.197	0.464
4	z4p10s5.01	-0.213	-0.217	0.043	-0.327	0.011	0.338
4	z4p10s6.01	-0.217	-0.220	0.029	-0.306	-0.091	0.215
4	z4p11s2.01	-0.127	-0.129	0.044	-0.241	0.156	0.396
4	z4p11s3.01	-0.160	-0.159	0.044	-0.261	0.014	0.275
4	z4p11s4.01	-0.204	-0.213	0.041	-0.283	-0.009	0.274
4	z4p11s6.01	-0.203	-0.214	0.047	-0.280	-0.037	0.242
5	z5p12s1.01	-0.122	-0.124	0.022	-0.173	-0.059	0.114
5	z5p12s2.01	-0.101	-0.103	0.031	-0.159	0.000	0.159
5	z5p12s3.01	-0.130	-0.129	0.021	-0.173	-0.077	0.096
5	z5p12s6.01	-0.128	-0.126	0.033	-0.340	0.011	0.351
5	z5p13s1.01	-0.055	-0.054	0.049	-0.182	0.087	0.269
5	z5p13s2.01	-0.077	-0.070	0.046	-0.215	0.048	0.263

5	z5p13s5.01	-0.096	-0.093	0.043	-0.208	0.001	0.210
5	z5p13s6.01	-0.124	-0.126	0.048	-0.226	0.018	0.244
6	z6p14s1.01	-0.163	-0.163	0.024	-0.225	-0.078	0.146
6	z6p14s2.01	-0.150	-0.157	0.038	-0.227	-0.016	0.211
6	z6p14s4.01	-0.165	-0.169	0.022	-0.217	-0.042	0.176
6	z6p14s6.01	-0.138	-0.144	0.047	-0.258	0.074	0.332
6	z6p15s1.01	-0.100	-0.104	0.040	-0.179	0.140	0.319
6	z6p15s2.01	-0.139	-0.141	0.037	-0.242	-0.011	0.232
6	z6p15s4.01	-0.104	-0.106	0.036	-0.223	-0.006	0.217
6	z6p15s6.01	-0.140	-0.142	0.022	-0.211	-0.075	0.136

Appendix F: Supplementary Information for Chapter 5

Figures

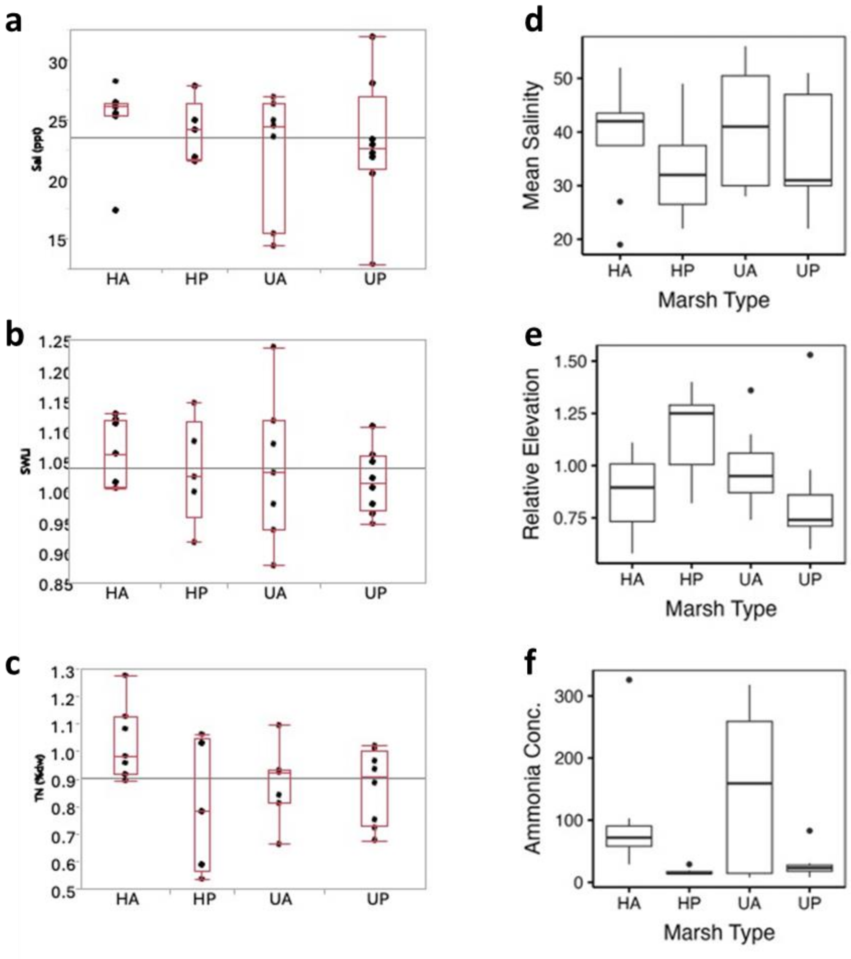

Figure 1. Box plots of diatom-based reconstructions of salinity (a), Surface Water Level Index (SWLI, b), and Total nitrogen (TN, c), and measured mean porewater salinity (d), marsh relative elevation (e) and porewater ammonia concentration (f) by marsh-type health category: HA = healthy *S. alterniflora,* HP = healthy *S. patens,* UA= unhealthy *S. alterniflora,* and UP = unhealthy *S. patens.* Bounds of box represent the 25% (bottom) and 75% (top)m interquartile range, center line indicates the median, whiskers depict the min and max values, and dots outside the min & max (d-f) denote outliers calculated as (min-(1.5*IQR) & max+(1.5*IQR)). IQR = Interquartile Range. Diatom reconstructions are based on 27 sites and measured variables on 33 sites.

Tables

Table 1. Diatom -based reconstructions of percent total nitrogen (TN) in dry sediment, Salinity, Tidal Exposure Index (TEI) and Surface Water Level Index (SWLI) and their respective errors of prediction (SEP). Wetland categories are: HA - healthy *Spartina alterniflora*; UA – unhealthy *Spartina alterniflora;* HP – healthy *Spartina patens*; and UP – unhealthy *Spartina patens*.

Sample	Plot Type	TN (%dw)	TN SEP	Sal (ppt)	Sal SEP	TEI (%)	TEI SEP	SWLI	SWLI SEP
Z1P1	UP	0.75	0.33	31.97	2.74	11.41	18.06	1.10	0.21
Z1P2	UP	0.72	0.32	28.06	2.55	17.86	18.04	0.90	0.19
Z2P5	HP	0.78	0.32	21.47	3.03	10.91	18.34	1.00	0.20
Z2P6	HP	0.54	0.32	24.19	2.76	19.67	18.62	0.90	0.20
Z3P8	UP	1.02	0.32	23.37	2.75	25.33	18.30	1.00	0.19
Z3P9	UA	0.84	0.32	26.88	2.64	7.53	17.97	1.10	0.19
Z4P10	HA	0.92	0.32	25.49	2.81	7.01	17.96	1.10	0.18
Z4P11	UA	0.92	0.32	23.54	2.93	6.61	18.07	1.10	0.19
Z5P12	UA	0.81	0.32	26.31	2.74	10.93	17.98	1.00	0.19
Z5P13	HA	1.13	0.34	26.04	2.85	7.15	18.04	1.00	0.19
Z6P14	UA	0.66	0.32	24.45	2.60	19.74	18.00	0.90	0.19
Z6P15	HA	0.90	0.32	25.32	2.82	9.26	17.96	1.00	0.19
Z7P10	HP	1.06	0.35	27.85	2.96	5.44	17.98	1.10	0.21
Z7P11	UP	0.94	0.32	20.49	2.82	14.04	18.01	1.00	0.19
Z7P8	HA	1.28	0.33	17.35	2.95	18.99	20.01	1.00	0.22
Z7P9	HA	0.96	0.32	26.43	2.79	7.91	18.10	1.10	0.18
Z8 P7	HA	1.08	0.33	28.21	3.07	3.95	18.11	1.10	0.19
Z8P2	UA	0.93	0.33	14.39	4.29	9.64	18.97	1.00	0.24
Z8P3	HP	0.59	0.32	24.99	2.61	10.33	18.10	1.00	0.19
Z8P4	HP	1.03	0.33	21.85	2.98	7.28	18.04	1.10	0.19
Z8P5	UA	1.10	0.33	24.95	3.02	5.79	18.30	1.20	0.19
Z8P6	HA	0.98	0.32	26.26	2.80	9.94	17.98	1.10	0.19
Z9 P16	UP	1.01	0.33	22.21	2.74	12.20	18.03	1.00	0.19
Z9P12	UP	0.97	0.32	21.87	2.72	18.68	18.29	1.00	0.19
Z9P14	UP	0.89	0.32	22.92	2.67	11.14	17.96	1.10	0.19
Z9P15	UP	0.68	0.40	12.84	4.23	5.45	19.46	1.10	0.23
Z9P17	UA	0.93	0.34	15.41	3.18	27.84	19.50	0.90	0.21

Appendix G: Presentation Abstracts

Conference: Atlantic Estuarine Research Society 2023 Spring Meeting

Title: Assessing salt marsh health through soil and pore water chemistry

Authors: Kriish Hate (presenter), Brittany Wilburn, Metthea Yepsen, Kirk Raper, Lori Lester, Mihaela Enache, Joe Smith, Andrea Habeck, Gregg Sakowicz, and Charles Schutte

Abstract: Salt marshes are invaluable to coastal communities due to ecosystem services they provide, such as shoreline protection and water filtration. New Jersey salt marshes are threatened by sea-level rise, highlighting the need for preservation and restoration. However, restoration is expensive and should be targeted to areas with the greatest need, which is difficult to assess. Here, we report initial findings from a project to develop new methods for salt marsh health assessment using drone-based multispectral imaging and on-the-ground measurements. We show that soil and porewater chemistry vary between plant species and between plots qualitatively grouped into healthy and unhealthy categories.

Conference: Society of Wetland Scientists 2023 annual meeting

Title: Linking soil and porewater chemistry with aboveground measurements to assess coastal wetland health

Authors: Charles Schutte (presenter), Kriish Hate, Brittany Wilburn, Metthea Yepsen, Kirk Raper, Lori Lester, Mihaela Enache, Joe Smith, Andrea Habeck, and Gregg Sakowicz

Abstract: Coastal wetlands like salt marshes provide myriad ecosystem services, including habitat provenance, shoreline protection, carbon burial, and nitrogen removal. Coastal development and sea-level rise have resulted in past and ongoing salt marsh degradation and loss. New and improved preservation and restoration practices are required to maintain this important ecosystem and the services it provides. However, restoration is expensive and should be targeted to areas with the greatest need, something that is difficult to assess. Here, we report initial findings from a project to develop new standardized methods for salt marsh health assessment using drone-based multispectral imaging and on-the-ground measurements. We show that soil and porewater chemistry vary between plant species and between plots qualitatively grouped into healthy and unhealthy categories. For example, *Spartina alterniflora*-dominated marshes tend to have relatively high soil pH and low ORP, while healthy *Spartina patens* marshes have relatively low soil pH and high ORP. *Spartina patens*-dominated marshes that were assessed to be unhealthy had soil pH and ORP values that spanned the range between healthy *Spartina patens* and *Spartina alterniflora* marshes. Through ongoing data synthesis, we will attempt to link metrics of soil and porewater chemistry with assessments of aboveground plant health and spectral indices acquired from drone-based multispectral imaging.

Conference: Fall Northeast Arc Users Group meeting 2023

Title: Developing a Protocol for Using Multispectral Drone Imagery to Study Salt Marsh Vegetation

Authors: Kevin Blythe (presenter), Brittany Wilburn, Metthea Yepsen, Josh Moody, William Smith, Steven Jacobus, Molly VanWieren, Kirk Raper, David DuMont

Abstract: New Jersey has over 200,000 acres of tidal wetlands, most of which are owned and managed by the state. These areas provide numerous environmental services. Traditional field methods for assessing tidal wetland condition are time- and resource-intensive. While remotely sensed multispectral imagery has been used for many years to study vegetation, the introduction of low-cost drones fitted with multispectral cameras has enabled the collection of higher resolution imagery more suited for studying the health of individual wetland plant communities. New Jersey Fish and Wildlife along with the New Jersey Department of Environmental Protection's Division of Science and Research and Bureau of GIS are conducting research at 9 sites in two salt marshes along the New Jersey coast with the goal of developing a protocol for multispectral drone imagery to assess tidal wetland health. In year one, we calculated several vegetation indices for each site, classified each site, and conducted accuracy assessments of our classifications supported by traditional field methods. In year two, we are focused specifically on *Spartina patens*, a high marsh species that is sensitive to inundation. We are comparing unstable, ditched sites shown to be subject to rapid pond expansion to more stable unditched sites. If we can see a correlation between our plot-based metrics and the imagery, we may be able to use the multispectral imagery to show early signs of marsh drowning and future habitat loss.

Conference: CERF 2023 27th Biennial Conference

Title: Assessing salt marsh health through potential denitrification rates and drone multispectral imagery

Authors: Kriish Hate, Charles Schutte, Brittany Wilburn, and Joshua Moody

Abstract: Salt marshes are invaluable to coastal communities due to the ecosystem services they provide, such as shoreline protection and water filtration. New Jersey's salt marshes are threatened by sea-level rise and other compounding factors like climate change and land use and coverage changes, highlighting the need for protection and restoration. However, identifying and prioritizing spatial hierarchical restoration needs across New Jersey's 200,000 acres of coastal wetlands can be difficult. Drones can ease the burden of salt marsh health assessments if observable salt marsh qualities align with known indicators of impaired functionality. As a part of a multi-year evaluation of the use of drone-based multispectral imagery to identify salt marsh impairment, measurements of vegetation condition, soil and porewater parameters, denitrification rates, and vegetation multispectral indices were collected across four salt marsh areas varying in platform stability and tidal inundation. Eighteen vegetation, soil, and porewater sampling plots were established at each of the four sites: two of each in the Forsythe Wildlife Refuge and Tuckerton Peninsula areas that varied in tidal range. Within each of the areas, two sites were selected: one with ponds that had stable borders since 1950 and one with expanding pond borders and mosquito ditching. In each of the respective sites, three ponds were selected around which six samples were collected: three within 5m and three between 11-20m of the pond edge (n=18 site^{-1}). Each of the samples from the respective ponds were homogenized and made into two composite samples according to their respective distance bands (three within 5m and three between 11-20m of the pond edge). Soil incubations were then conducted in the lab using the acetylene block assay. Potential Denitrification rate data will be evaluated at the varying factor levels independently and with data related to vegetation density and sediment bearing capacity. Here, we report preliminary findings regarding spatial variability in denitrification rates across the various factor levels. If relationships exist between salt marsh qualities observable from drones and their health conditions, this approach would ease the effort required for preliminary assessment of the marshes' functional condition across large spatial scales.

Conference: 10th Delaware Wetlands Conference 2024

Title: Investigating the use of multispectral drones for identifying salt marsh condition

Authors: Brittany Wilburn, Joshua Moody, Charles Schutte, Kevin Blythe, William Smith, and Metthea Yepsen

Abstract: New Jersey has ~165,000 acres of salt marshes. Appropriate protection and restoration efforts require understanding their spatial and temporal vulnerability. Field-based evaluation methods can be costly and time-consuming. Drones represent an opportunity to assess large areas efficiently. This project develops a methodology to use multispectral drone imagery to identify conditions that can lead to high marsh pond expansion and vegetation loss by evaluating relationships between soil and porewater chemistry, vegetation, and multispectral indices.

Conference: Atlantic Estuarine Research Society 2024 Spring Meeting

Title: Ditching creates increased oxidation reduction potential in salt marshes

Authors: Omar Selim, Joshua Moody, Brittany Wilburn, and Charles Schutte

Abstract: There is little published research on how pond expansion changes soil and porewater chemistry in salt marshes. In this study, we attempted to determine whether the chemical properties of the environment are different in locations that contain expanding ponds in a ditched marsh, as compared to sites that do not have expanding ponds and are unditched. We gathered samples atop the plant species *Spartina Patens* at two distances from known pond conditions. Preliminary results indicate that soil oxidation reduction potential is significantly higher in ditched sites as compared to unditched sites. This is likely due to increased drainage from ditching.